

**AFRL-RV-PS-
TR-2016-0130
Vol. 1**

**AFRL-RV-PS-
TR-2016-0130
Vol. I**

A DESIGNER FLUID FOR ALUMINUM PHASE CHANGE DEVICES

**Volume I of III
General Inorganic Aqueous Solution (IAS) Chemistry**

Qi Yao and Ivan Catton

**University of California, Los Angeles
420 Westwood Plaza, Room 43-132
Los Angeles, CA 90095-1597**

17 Nov 2016

Final Report

APPROVED FOR PUBLIC RELEASE; DISTRIBUTION IS UNLIMITED.



**AIR FORCE RESEARCH LABORATORY
Space Vehicles Directorate
3550 Aberdeen Ave SE
AIR FORCE MATERIEL COMMAND
KIRTLAND AIR FORCE BASE, NM 87117-5776**

DTIC COPY NOTICE AND SIGNATURE PAGE

Using Government drawings, specifications, or other data included in this document for any purpose other than Government procurement does not in any way obligate the U.S. Government. The fact that the Government formulated or supplied the drawings, specifications, or other data does not license the holder or any other person or corporation; or convey any rights or permission to manufacture, use, or sell any patented invention that may relate to them.

This report is the result of contracted fundamental research deemed exempt from public affairs security and policy review in accordance with SAF/AQR memorandum dated 10 Dec 08 and AFRL/CA policy clarification memorandum dated 16 Jan 09. This report is available to the general public, including foreign nationals. Copies may be obtained from the Defense Technical Information Center (DTIC) (<http://www.dtic.mil>).

AFRL-RV-PS-TR-2016-0130, Vol. I HAS BEEN REVIEWED AND IS APPROVED FOR PUBLICATION IN ACCORDANCE WITH ASSIGNED DISTRIBUTION STATEMENT.

//SIGNED//
ANDREW WILLIAMS
Program Manager

//SIGNED//
PAUL HAUSGEN, Ph.D.
Technical Advisor, Spacecraft Component Technology

//SIGNED//
JOHN BEAUCHEMIN
Chief Engineer, Spacecraft Technology Division
Space Vehicles Directorate

This report is published in the interest of scientific and technical information exchange, and its publication does not constitute the Government's approval or disapproval of its ideas or findings.

Approved for public release; distribution is unlimited.

REPORT DOCUMENTATION PAGE

Form Approved
OMB No. 0704-0188

Public reporting burden for this collection of information is estimated to average 1 hour per response, including the time for reviewing instructions, searching existing data sources, gathering and maintaining the data needed, and completing and reviewing this collection of information. Send comments regarding this burden estimate or any other aspect of this collection of information, including suggestions for reducing this burden to Department of Defense, Washington Headquarters Services, Directorate for Information Operations and Reports (0704-0188), 1215 Jefferson Davis Highway, Suite 1204, Arlington, VA 22202-4302. Respondents should be aware that notwithstanding any other provision of law, no person shall be subject to any penalty for failing to comply with a collection of information if it does not display a currently valid OMB control number. **PLEASE DO NOT RETURN YOUR FORM TO THE ABOVE ADDRESS.**

1. REPORT DATE (DD-MM-YY) 17-11-16		2. REPORT TYPE Final Report		3. DATES COVERED 29 June 2015 - 26 Sept 2016	
4. TITLE AND SUBTITLE A DESIGNER FLUID FOR ALUMINUM PHASE CHANGE DEVICES, Vol. I of III General Inorganic Aqueous Solution (IAS) Chemistry				5a. CONTRACT NUMBER FA9453-15-1-0318	
				5b. GRANT NUMBER	
				5c. PROGRAM ELEMENT NUMBER 62601F	
6. AUTHOR(S) Qi Yao and Ivan Catton				5d. PROJECT NUMBER 628809	
				5e. TASK NUMBER PPM00020770	
				5f. WORK UNIT NUMBER EF126504	
7. PERFORMING ORGANIZATION NAME(S) AND ADDRESS(ES) University of California, Los Angeles 420 Westwood Plaza room 43-132 Los Angeles, CA 90095-1597				8. PERFORMING ORGANIZATION REPORT NUMBER	
9. SPONSORING / MONITORING AGENCY NAME(S) AND ADDRESS(ES) Air Force Research Laboratory Space Vehicles Directorate 3550 Aberdeen Ave SE Kirtland AFB, NM 87117-5776				10. SPONSOR/MONITOR'S ACRONYM(S) AFRL/RVSV	
				11. SPONSOR/MONITOR'S REPORT NUMBER(S) AFRL-RV-PS-TR-2016-0130, Vol I	
12. DISTRIBUTION / AVAILABILITY STATEMENT Approved for public release; distribution is unlimited.					
13. SUPPLEMENTARY NOTES					
14. ABSTRACT Research with the goal of understanding the chemistry of an Inorganic Aqueous Solution (IAS) used as a working fluid in copper and aluminum phase change heat transfer devices, finding the advantages and limits of IAS in various heat transfer applications, and providing a general guideline of how to correctly use IAS for performance enhancement and surface passivation purposes was performed.					
15. SUBJECT TERMS inorganic aqueous solution <and> heat pipe					
16. SECURITY CLASSIFICATION OF:			17. LIMITATION OF ABSTRACT	18. NUMBER OF PAGES	19a. NAME OF RESPONSIBLE PERSON Andrew Williams
a. REPORT	b. ABSTRACT	c. THIS PAGE			
Unclassified	Unclassified	Unclassified	Unlimited	242	19b. TELEPHONE NUMBER (include area code)

(This page intentionally left blank)

Approved for public release; distribution is unlimited.

Table of Contents

LIST OF FIGURES	v
LIST OF TABLES	xiii
1. SUMMARY.....	1
2. INTRODUCTION.....	2
2.1. Basic Mechanics and Operating Limitations	5
2.1.1. Viscous limit.....	6
2.1.2. Sonic limit.....	6
2.1.3. Entrainment limit	7
2.1.4. Capillary limit.....	7
2.1.5. Boiling limit.....	9
2.2. How to Choose a Working Fluid?.....	10
2.3. Thermal Resistances in Thermo-Syphons and Heat Pipes.....	13
2.4. Wettability and Evaporation.....	15
2.5. Motivation	18
2.5.1. Past UCLA experience.....	20
2.5.2. Objective.....	25
2.6. Background	28

Approved for public release; distribution is unlimited.

2.6.1.	SRI Qu tube report.....	29
2.6.2.	TAMU Qu technology report.....	30
2.6.3.	University of Alabama Tests	31
2.6.4.	Summary	31
3.	METHODS, ASSUMPTIONS, AND PROCEDURES (WHAT IS IAS).....	33
3.1.	IAS Reproduction.....	34
3.1.1.	Chemical constituents of IAS	34
3.1.2.	Reproduce IAS.....	41
3.2.	Physical Analysis	45
3.3.	Chemical Analysis.....	51
3.3.1.	Water self-ionization.....	52
3.3.2.	Chromium (VI) balance	52
3.3.3.	Oxidation.....	55
3.3.4.	Hydrophilic coatings.....	73
3.3.5.	Silver effect.....	83
3.3.6.	Disassociation during storage	83
3.4.	Coating study.....	84
3.5.	Conclusion.....	94
4.	USING IAS IN COPPER DEVICES	97

Approved for public release; distribution is unlimited.

4.1.	Related Chemicals and Reactions	98
4.2.	Diffusion Model	99
4.2.1.	Thermal fluid model	101
4.2.2.	Calculation progress.....	104
4.2.3.	Results and Discussion	108
4.3.	Capillary Tests.....	114
4.4.	Charging Station.....	127
4.5.	Thermo-syphon Tests.....	135
4.5.1.	Experiment setup	135
4.5.2.	Test results	141
4.5.3.	Results and Discussion	150
4.6.	Comparison Tests in Other Applications	155
4.6.1.	Flat heat pipe test	155
4.6.2.	Sintered heat pipe test.....	157
4.7.	Conclusion.....	163
5.	USING IAS IN ALUMINUM DEVICES	166
5.1.	Aluminum Passivation Theory.....	166
5.2.	Passivation in Phase Change Heat Transfer Devices	170
5.2.1.	Electrochemical cycle in aluminum passivation.....	173

Approved for public release; distribution is unlimited.

5.2.2.	Aluminum thermo-syphon test	174
5.2.3.	Silver effect.....	179
5.3.	Importance of a Continuous Liquid Back Flow	180
5.3.1.	Aluminum thermo-syphon test with a natural convention cooling.....	182
5.3.2.	Results and Discussion	185
5.4.	Conclusion.....	190
5.5.	Discussion of Using IAS in Steel Devices	190
6.	CONCLUSIONS	192
6.1.	Main Contributions	192
6.2.	What is IAS	193
6.3.	IAS and copper	194
6.4.	IAS and aluminum.....	196
7.	RECOMMENDATIONS.....	197
7.1.	Chemical optimization	197
7.2.	Design of heat transfer applications.....	198
	REFERENCES	200
	APPENDIX: Coding of 1-D Diffusion Model.....	205
	List of Symbols, Abbreviations, and Acronyms.....	217

Approved for public release; distribution is unlimited.

List of Figures

Figure 1: Thermo-syphon and heat pipe	4
Figure 2: Three common used wicks: screen, axial groove, and sintered metal	5
Figure 3: Usage limitations of a heat pipe	6
Figure 4: Diagram of an operating heat pipe	8
Figure 5: Merit number of commonly used working fluids.....	12
Figure 6: Thermal resistances of a thermo-syphon.....	13
Figure 7: Thermal resistances of a sintered heat pipe.....	14
Figure 8: Evaporating thin film and coordinate system.....	16
Figure 9: Force balance at the intersection of three phases	17
Figure 10: Wall temperatures as a function of heat flux as well as nano-particle concentration .	18
Figure 11: Pool boiling characteristic of nano-fluids on the smoother and roughened heater	19
Figure 12: The effect of NCG generation to a thermo-syphon.....	20
Figure 13: Vapor chamber test setup and bi-porous wick structure	21
Figure 14: Performance comparison between water and IAS in a vapor chamber.....	22
Figure 15: SEM results of a copper wick: clean vs coated by IAS.....	22
Figure 16: Schematic of aluminum thermo-syphon test and locations of thermocouples.....	23
Figure 17: First week, aluminum/IAS thermo-syphon lifetime testing	24
Figure 18: Second week, aluminum/IAS thermo-syphon lifetime testing.....	25
Figure 19: Schematic of the three solid layers in QuTech's Heat Pipe.....	28
Figure 20: Black suspension in IAS fluid.....	33
Figure 21: IAS fluid, before and after use	33

Approved for public release; distribution is unlimited.

Figure 22: E-pH diagram of manganese vs Standard Hydrogen Electrode (SHE).....	37
Figure 23: Vapor pressure test results.....	48
Figure 24: (a) fresh IAS; (b) used IAS; (c) condensed liquid from the vapor of IAS	49
Figure 25: Contact angle comparison between smooth and IAS treated metal surfaces	50
Figure 26: Chromium balance in UCLA IAS #1 at 25°C	54
Figure 27: Concentrations of chromium (VI) at different temperatures.....	55
Figure 28: Relation between reacted permanganate and pH number in UCLA IAS #1	59
Figure 29: Pourbaix diagram of copper vs SHE at 25°C, calculated by OLI with UCLA IAS #1 as the inflow	60
Figure 30: Copper surface pre-treated by UCLA IAS #1	61
Figure 31: Pourbaix diagram of manganese vs SHE at 25°C, calculated by OLI with IAS as the inflow	62
Figure 32: Pourbaix diagram of chromium vs SHE at 25°C, calculated by OLI with IAS as the inflow	63
Figure 33: Relation between pH number and percentage of the chromium (VI) reacted in UCLA IAS #1	64
Figure 34: Comparison between fresh and used IAS.....	65
Figure 35: Mirror like copper surfaces cooked by: DI-water, potassium permanganate solution, potassium dichromate solution adjusted to pH=6.22.....	67
Figure 36: Existence of manganese (IV) oxide in the product	68
Figure 37: Black solid on IAS/copper thermo-syphon and IAS/aluminum flat heat pipe.....	69

Approved for public release; distribution is unlimited.

Figure 38: Used UCLA IAS #1, collected from (a) IAS/copper thermo-syphon, (b) IAS/aluminum thermo-syphon	69
Figure 39: Pourbaix diagram of aluminum vs SHE at 25°C, calculated by OLI with UCLA IAS #1 as the inflow	70
Figure 40: Pourbaix diagram of iron vs SHE at 25°C, calculated by OLI with UCLA IAS #1 as the inflow	72
Figure 41: How hydrophilic coating works	77
Figure 42: Relation between calcium chromate and evaporated liquid at different temperatures	77
Figure 43: Relation between strontium chromate and evaporated liquid at different temperatures	79
Figure 44: Relation between potassium dichromate/chromate and evaporated liquid at different temperatures	80
Figure 45: The effects of temperature and pH number to the hydrophilic coating generation.....	81
Figure 46: DI-water on mirror like copper surface	85
Figure 47: DI-water on mirror like copper surface cooked by potassium permanganate: (a) pre-treated, (b) rinsed by DI-water	86
Figure 48: SEM image of a copper surface pre-treated by potassium permanganate	87
Figure 49: SEM image of a copper surface pre-treated by potassium permanganate and then rinsed by DI-water	87
Figure 50: DI-water on mirror like copper surface cooked by calcium chromate	88
Figure 51: SEM image of a copper surface pre-treated by calcium chromate	88
Figure 52: DI-water on mirror like copper surface cooked by strontium chromate	89

Approved for public release; distribution is unlimited.

Figure 53: SEM image of a copper surface pre-treated by strontium chromate.....	89
Figure 54: DI-water on mirror like copper surface cooked by potassium chromate	90
Figure 55: SEM image of a copper surface pre-treated by potassium chromate	90
Figure 56: Copper surface pre-treated by sodium chromate, 2 hours after the pretreatment	91
Figure 57: SEM image of a copper surface pre-treated by IAS.....	91
Figure 58: Copper surfaces cooked by IAS or potassium permanganate with the plate temperature 135°C.....	92
Figure 59: Initially wetted region vs coated region	93
Figure 60: 1-D diffusion model	99
Figure 61: Thermal fluid model of condensation and evaporation within a thermo-syphon.....	102
Figure 62: Simplified thermal fluid model of condensation and evaporation within a thermo- syphon.....	102
Figure 63: Diagram of thermo-syphon	105
Figure 64: Diffusion coefficients of related ions	106
Figure 65: Film thickness of the liquid back flow along the thermo-syphon.....	109
Figure 66: Velocity of the liquid back flow along the thermo-syphon.....	110
Figure 67: Concentration profile of calcium ion along thermo-syphon, without considering the solubility limit.....	111
Figure 68: Concentration profile of chromate ion along thermo-syphon, without considering the solubility limit.....	111
Figure 69: Concentration profile of potassium ion along thermo-syphon, without considering the solubility limit.....	112

Approved for public release; distribution is unlimited.

Figure 70: Concentration profiles of calcium ion, chromate ion, and potassium ion along thermo-syphon, with considering solubility	114
Figure 71: Picture of capillary test.....	115
Figure 72: Schematic of capillary test	115
Figure 73: Example capillary test image	116
Figure 74: Test results of water/clean mirror like copper surface	117
Figure 75: Test results of UCLA Yellow #1/clean mirror like copper surface	119
Figure 76: Diagram of how chromate salts deposit on smooth copper surface	120
Figure 77: Sample surface coated by potassium chromate in the coating study test.....	121
Figure 78: Test results of potassium permanganate solution/clean mirror like copper surface..	123
Figure 79: Test results of UCLA Yellow #1/mirror like copper surface pretreated by potassium solution and then rinsed by DI-water.....	125
Figure 80: Diagram of how chromate salts deposit on copper surface pretreated by potassium permanganate	126
Figure 81: Difference between water and IAS while being dried out	126
Figure 82: Degassing chamber and magnetic stirrer.....	128
Figure 83: Charging station with degassing feather	129
Figure 84: Schematic diagram of the new charging station.....	132
Figure 85: Swagelok bellows-sealed valve.....	133
Figure 86: The sealed end of thermo-syphon	136
Figure 87: Filling end of thermo-syphon: (a) before charge, (b) sealed by cold welder, (c) protected by J-B weld adhesive	137

Approved for public release; distribution is unlimited.

Figure 88: Cold welder	137
Figure 89: Schematic diagram of the set-up of the thermo-syphon experiment.....	138
Figure 90: Locations of thermocouples in thermo-syphon test	139
Figure 91: Thermo-syphon test.....	140
Figure 92: Overview of a cut open IAS/copper thermo-syphon.....	143
Figure 93: Test results of thermo-syphon with 1.47g water at inclination angle 90°	144
Figure 94: Performance comparison between water/copper and IAS/copper thermo-syphons at inclination angle 90°	145
Figure 95: Performance comparison between water/copper and IAS/copper thermo-syphons at inclination angle 30°	146
Figure 96: Performance comparison between water/copper and IAS/copper thermo-syphons at inclination angles of 3° and 5°	148
Figure 97: Performance comparison between water/copper, yellow/copper, and IAS/copper thermo-syphons at inclination angles 10°	149
Figure 98: Performance comparison between water/copper, yellow/copper, and IAS/copper thermo-syphons at inclination angles 20°	150
Figure 99: Meniscus regions in vertical IAS/copper and water/copper thermo-syphons, without liquid back flow	151
Figure 100: Working regions of a thermo-syphon.....	152
Figure 101: Meniscus regions in vertical IAS/copper and water/copper thermo-syphons, with liquid back flow	153
Figure 102: Meniscus regions in an inclined thermo-syphon, with liquid back flow.....	154

Approved for public release; distribution is unlimited.

Figure 103: Flat heat pipe test results	156
Figure 104: Difference between water and IAS in grooved flat heat pipe, evaporating region .	157
Figure 105: Original Enertron heat pipe and recharged heat pipe	158
Figure 106: Schematic and thermocouple locations of heat pipe test.....	159
Figure 107: Heat pipe test results.....	160
Figure 108: Schematic of the evaporating region of a heat pipe, with IAS as working fluid.....	162
Figure 109: Comparison between water and IAS in sintered wicks	163
Figure 110: E-pH diagram for pure Al at 25°C in aqueous solution.....	169
Figure 111: Cut open aluminum/IAS thermo-syphon: (a) condensing region; (b) evaporating region	171
Figure 112: DI-water after used to rinse (a) condensing region; (b) evaporating region	172
Figure 113: Electrochemical cycle in aluminum passivation	173
Figure 114: Schematic of the aluminum thermo-syphon test	175
Figure 115: Thermocouple locations in the aluminum thermo-syphon experiment.....	176
Figure 116: Performance comparison between water and IAS in aluminum thermo-syphons, temperatures at condensing, adiabatic, and evaporating regions	177
Figure 117: Performance comparison between copper/water and aluminum/IAS thermo-syphons, temperature difference of the evaporating temperature and the condensing temperature	178
Figure 118: Effect of silver in electrochemistry circle and SEM result of aluminum surface cooked by IAS fluid with Mag=504X.....	179
Figure 119: Test result of IAS 2.1 in aluminum thermo-syphon: temperatures of evaporating, adiabatic, and condensing regions	180

Approved for public release; distribution is unlimited.

Figure 120: Discontinuous liquid back flow in a thermo-syphon.....	181
Figure 121: Comparison of thermo-syphons cooled by different methods	182
Figure 122: Aluminum thermo-syphon experiment setup	183
Figure 123: Thermocouple locations	184
Figure 124: Test results of 6-foot thermo-syphon	185
Figure 125: Test results of 3-foot thermo-syphon	186
Figure 126: Test results of 2-foot thermo-syphon	187
Figure 127: Test results of 1-foot thermo-syphon	188
Figure 128: Test results of 6-foot thermo-syphon with 2.6ml three times concentrated IAS	189

Approved for public release; distribution is unlimited.

List of Tables

Table 1: Useful operating temperature range of heat pipe working fluids	11
Table 2: Comparative values of thermal resistances for a heat pipe.....	15
Table 3: Composition by ICP-OES analysis of the original IAS fluid.....	35
Table 4: Anion scan detection.....	35
Table 5: Possible ions in an IAS fluid	36
Table 6: Standard formation Gibbs free energy of related chemicals	38
Table 7: Positive and negative ions in an IAS fluid.....	41
Table 8: Chemicals needed to produce 1 liter IAS fluid.....	42
Table 9: Mass and mole of chemicals in the original IAS and UCLA IAS #1	43
Table 10: Aimed chemical concentrations in IAS	44
Table 11: Required chemicals to produce IAS	45
Table 12: Physical properties of water and the original IAS	46
Table 13: Thermal conductivity of solutions similar to IAS	47
Table 14: Specific heat of solutions similar to IAS	47
Table 15: Chemical equilibrium constants for chromium balance at 25°C	53
Table 16: Standard electrode potentials in H ₂ O at 25°C and 1 bar.....	56
Table 17: Concentrations of oxidizers in UCLA IAS #1 at 25°C.....	57
Table 18: Electrode potentials of oxidizers in UCLA IAS #1 at 25°C	58
Table 19: pH number of fluids from used IAS/copper thermo-syphons	66
Table 20: pH numbers of used IAS, collected from aluminum phase change heat transfer devices	71

Approved for public release; distribution is unlimited.

Table 21: K_{sp} of related insoluble compounds at 18-25°C.....	74
Table 22: Solubility of calcium chromate in water.....	76
Table 23: Solubility of strontium chromate in water.....	76
Table 24: Generation conditions of hydrophilic coatings.....	82
Table 25: Solutions used in coating study on copper surfaces.....	84
Table 26: Chemical constituents in UCLA IAS #1.....	94
Table 27: Tube geometry of the copper thermo-syphon used in thermo-syphon tests.....	103
Table 28: Test results of a IAS/copper thermo-syphon.....	104
Table 29: Diffusion coefficients of related ions.....	105
Table 30: Peclet numbers of the related ions at different input powers.....	113
Table 31: Percentage of chemicals coming out as solid chromate salts.....	113
Table 32: Parts information in the charging station.....	130
Table 33: Information of Enertron heat pipe.....	157
Table 34: Ion roles for IAS and aluminum.....	167

Approved for public release; distribution is unlimited.

ACKNOWLEDGMENTS

This material is based on research sponsored by Air Force Research Laboratory under agreement number FA9453-15-1-0318. The U.S. Government is authorized to reproduce and distribute reprints for Governmental purposes notwithstanding any copyright notation thereon.

DISCLAIMER

The views and conclusions contained herein are those of the authors and should not be interpreted as necessarily representing the official policies or endorsements, either expressed or implied, of Air Force Research Laboratory or the U.S. Government.

Approved for public release; distribution is unlimited.

(This page intentionally left blank)

Approved for public release; distribution is unlimited.

1. SUMMARY

The objectives of this research include: understanding the chemistry of an Inorganic Aqueous Solution (IAS) used as a working fluid in copper and aluminum phase change heat transfer devices, finding the advantages and limits of IAS in various heat transfer applications, and providing a general guideline of how to correctly use IAS for performance enhancement and surface passivation purposes.

First, a comparison between IAS and water is done both physically and chemically of being used as a working fluid in phase change heat transfer devices. Above all, the chemical constituents in an IAS fluid are investigated, and a method is given to produce it. Afterwards, the physical properties of IAS are measured and compared to those of water. Moreover, a chemical analysis is performed, and the chemical reactions involved between IAS and the surfaces of copper or aluminum made devices where it is to be used are listed and categorized by their contributions to the heat transfer performance or the surface passivation. In addition, OLI software, commercial software to simulate electrolytes, is used to estimate the amount of the solid products, generated by redox reactions or temperature increases, at different temperatures and ratios of being concentrated. At the end, a coating study is performed to understand how each chemical coats the surface and how it contributes to the surface wettability. The positive and negative effects of each coating are discussed and demonstrated by data from scanning electron microscope (SEM) observations and contact angle tests.

Second, using IAS in copper made phase change heat transfer devices is discussed, and the main focus is how IAS improves the heat transfer performance by a smaller thermal resistance and

Approved for public release; distribution is unlimited.

a larger critical heat flux. At the beginning, a 1-D diffusion model is built and used to estimate the concentration profiles of chemicals along the liquid flow path and the location where each coating begins to be deposited. Next, a capillary rise test is performed to show how each chemical contributes to the improvement of the surface wettability. The heat transfer performance of water and IAS are compared for a thermo-syphon test at different inclination angles, a grooved flat heat pipe test, and a sintered heat pipe test. The test results validate the conclusions of the diffusion model and the capillary rise test. Based on the results of the comparison tests, the advantages and limits of using IAS, for performance enhancement purposes in various heat transfer applications, are discussed.

Last, an investigation of the aluminum passivation, with IAS being used as the working fluid in aluminum made phase change heat transfer devices, is done, and the key factors that lead to failures, are discussed. Initially, an electrochemical theory of aluminum passivation is introduced, and the existence of an electrochemical cycle is demonstrated by an aluminum thermo-syphon test. Afterwards, the importance of a continuous liquid back flow to aluminum passivation is pointed out, and a vertical thermo-syphon test with natural convection cooling is used to demonstrate that a discontinuous liquid back flow is the main reason of the failures. At the end, using IAS in steel or stainless steel phase change heat transfer devices is discussed.

2. INTRODUCTION

Nowadays, with the rapid development of science and technology, the production and consumption of power has been increasing rapidly. As a result, thermal management has become a significant obstacle in almost every industry, such as electronics cooling of digital devices, waste

Approved for public release; distribution is unlimited.

heat recovery in large power systems, and nuclear power generation. The world market for thermal management products is predicted to grow from about \$8.8 billion in 2013 to \$15.56 billion by 2018, reported by IRAP Inc.[1]. Innovative thermal solutions are demanded to keep the systems running at a peak efficiency and with a high reliability.

Phase change heat transfer devices have been a popular method of transferring heat for decades, and they are widely used to spread the large heat flux generated by various devices. A phase change heat transfer device usually has an evacuated internal space which has been charged with a small quantity of working fluid before it is sealed. Because of the low internal pressure, the working fluid evaporates and condenses at a much lower temperature compared to what it would be in the open air. When heat is added to the heating section (evaporator), the working fluid evaporates and takes away the heat, flows through the vapor space because of the pressure difference resulting from a lower temperature at the cooled section, and condenses and releases the heat to the cooling section (condenser). Because the latent heat of evaporation is large, heat can be transported with a very small temperature difference between the evaporator and the condenser, which results in a high effective thermal conductance.

A thermo-syphon or Perkins tube [2], as shown in Figure 1 (a), is one of the simplest versions of phase change heat transfer devices. A tube with a smooth internal surface is located vertically, and heat is added at the bottom and removed at the top. Because of the gravity, the condensed working fluid flows back to the evaporator forming a circuit. As a result, the evaporating region of a thermo-syphon is always situated at the lowest point.

Approved for public release; distribution is unlimited.

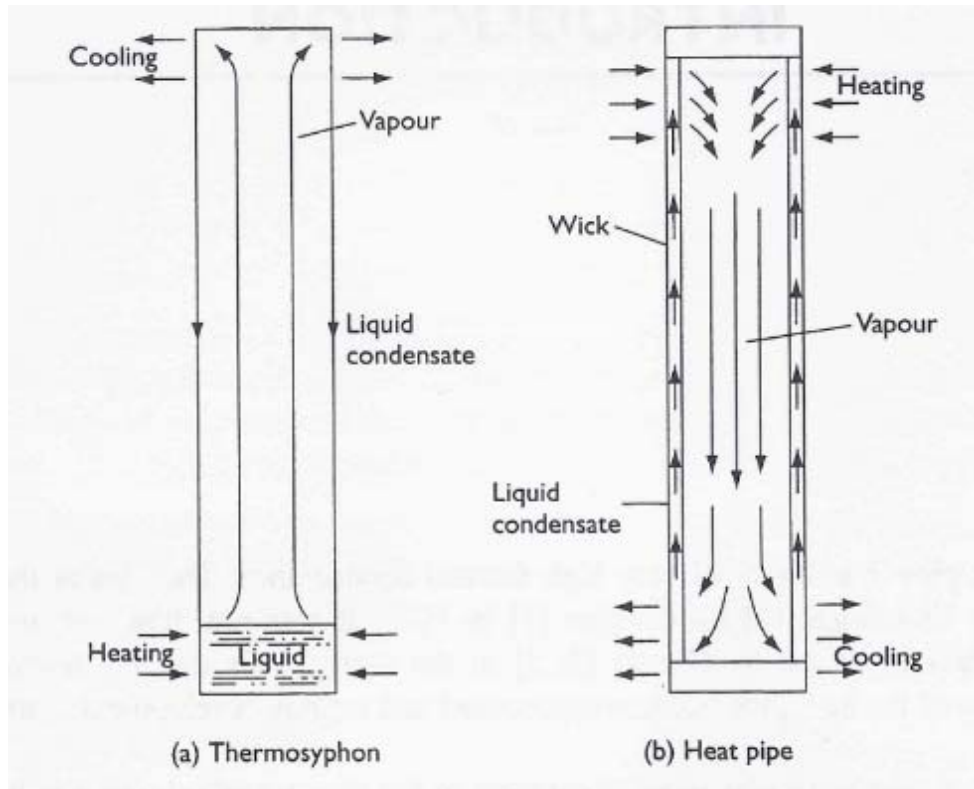


Figure 1: Thermo-syphon and heat pipe

Gaugler [3] first reported the idea of the heat pipe to remove the directional limitation of a thermo-syphon in 1942, see Figure 1 (b), and Grover [4][5] independently invented it in early 1960s. The main difference between a heat pipe and a thermo-syphon is that a wick is added to the inside surface of the heat pipe, and the capillary forces transport the condensed working fluid back to the evaporator. The three most used wicks are screens, axial grooves, and sintered metals, as shown in Figure 2.

Approved for public release; distribution is unlimited.



Screen

Axial Groove

Sintered Metal

Figure 2: Three common used wicks: screen, axial groove, and sintered metal

Because the wick increases the effective surface area and improves the surface wettability of the evaporating region, to transfer the same amount of heat, the temperature difference between the evaporator and the condenser is further reduced. In addition, the dry-out point is delayed which means that heat pipes can handle larger heat fluxes than thermo-syphons.

2.1. Basic Mechanics and Operating Limitations

When using heat pipes to transfer heat, there are several limitations which prevent them from reaching high heat fluxes: viscous limit, sonic limit, entrainment limit, capillary limit, and boiling limit, as shown in Figure 3 [6].

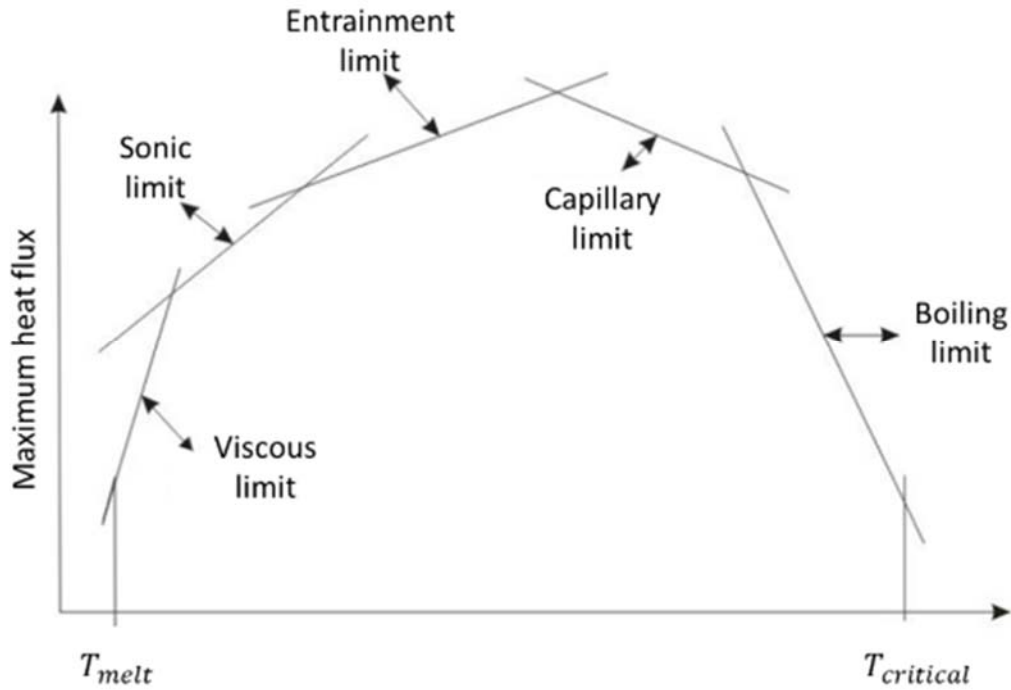


Figure 3: Usage limitations of a heat pipe

2.1.1. Viscous limit

At very low operating temperatures, the vapor pressure difference between the evaporating and condensing regions will be very small, in which case, the viscous forces on the vapor will be larger than the pressure gradients caused by the temperature difference. As a result, the pressure gradient will not be large enough to generate a vapor flow which brings the heat to the condenser. This vapor stagnation condition is called the viscous limit [7].

2.1.2. Sonic limit

Cotter [9] points out that compressible flow in a constant cross section duct with mass addition and removal, such as a heat pipe, and constant mass flow in a converging-diverging nozzle share some common properties. For some cases in heat pipes, with the thermal load increasing, the vapor velocity reaches the velocity of sound at the end of the evaporator. Because the flow reaches

Approved for public release; distribution is unlimited.

sonic flow, lower the pressure of the condenser will not further increase the mass flow rate. As the result, the thermal load reaches a limit and will not be able to be increased. This sonic flow condition is called the sonic limit.

2.1.3. Entrainment limit

Peterson and Bage [10] find that, in operating heat pipes and thermo-syphons, the liquid and vapor flow in opposite directions, and the shear forces occur at the counter-flow interface. The shear forces may inhibit the return of liquid to the evaporator, which may make the vapor-liquid interface be unstable or lead to the flooding limit. This case is called the entrainment limit.

2.1.4. Capillary limit

In an operating heat pipe, heat is added to the evaporator section, and the liquid evaporates and takes away the heat, which causes the meniscus to recede into the wick. The vapor flows through the vapor space because of the pressure difference, resulting from a lower temperature at the cooled section, condenses and releases the heat in the condenser section, which causes flooding. The combined effect of this vaporization and condensation results in a meniscus radius of curvature that varies along the axial length of the heat pipe, as shown in Figure 4.

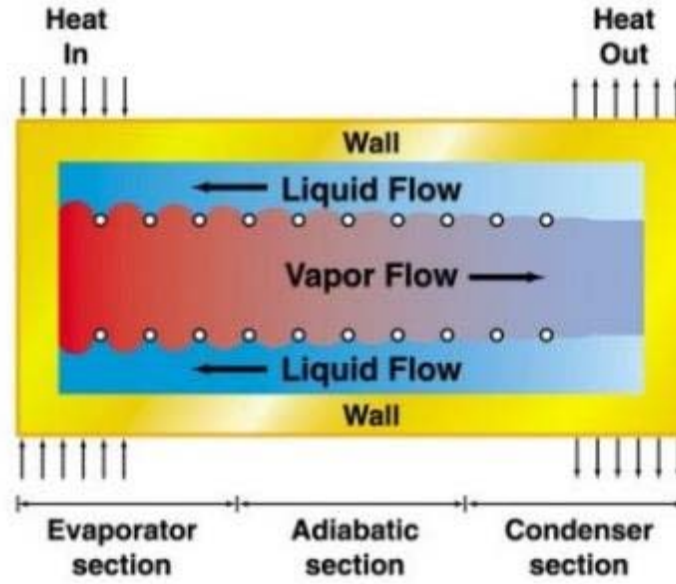


Figure 4: Diagram of an operating heat pipe

With the heat load increasing, the meniscus in the evaporator recedes more and more. When the point in the evaporator, at which the meniscus has a minimum radius of curvature, is out of liquid, the heat load will not be able to be further increased, and the heat pipe or thermo-syphon reaches dry-out. This condition is called the capillary limit. For a heat pipe to function properly, the net capillary pressure difference between the wet and dry points must be greater than the summation of all the pressure losses throughout both the liquid and vapor flow paths [7].

$$(\Delta P_c)_m \geq \int_{L_{eff}} \frac{\partial P_v}{\partial x} dx + \int_{L_{eff}} \frac{\partial P_l}{\partial x} dx + \Delta P_{ph,e} + \Delta P_{ph,c} + \Delta P_+ + \Delta P_{\square} \quad (1)$$

where:

$(\Delta P_c)_m$ = maximum capillary pressure difference generated within capillary wicking structure between wet and dry points

Approved for public release; distribution is unlimited.

$\int_{L_{eff}} \frac{\partial P_v}{\partial x} dx$ = sum of inertial and viscous pressure drops occurring in vapor phase

$\int_{L_{eff}} \frac{\partial P_l}{\partial x} dx$ = sum of inertial and viscous pressure drops occurring in liquid phase

$\Delta P_{ph,e}$ = pressure gradient across phase transition in evaporator

$\Delta P_{ph,c}$ = pressure gradient across phase transition in condenser

ΔP_+ = normal hydrostatic pressure drop

$\Delta P_{||}$ = axial hydrostatic pressure drop

2.1.5. Boiling limit

When the input heat flux is sufficient, nucleate boiling occurs in the wick of the evaporator, and bubbles will be trapped in the wick, which prevents the liquid return and cause dry out. This phenomenon is call the boiling limit. Marcus [8] derived the following relationship for calculating the critical superheat of the boiling limit.

$$\Delta T_{cr} = \left(\frac{T_{sat}}{\lambda \rho_v} \right) \left(\frac{2\sigma}{r_n} - \Delta P_{i,m} \right) \quad (2)$$

An expression for the heat flux beyond which the bubble growth will occur developed by Chi [12] is

$$q_{b,e} = \left(\frac{2\pi L_e k_{eff} T_v}{\lambda \rho_v \ln(r_i / r_o)} \right) \left(\frac{2\sigma}{r_n} - \Delta P_{c,m} \right) \quad (3)$$

Approved for public release; distribution is unlimited.

2.2. How to Choose a Working Fluid?

Heat pipes transfer heat by the vaporization and condensation of the working fluid, so choosing a suitable working fluid is the most important part of the design and manufacture process.

The prime requirements are as follows:

- 1) Compatibility with wick and wall materials
- 2) Good thermal stability
- 3) Wettability of wick and wall materials
- 4) Vapor pressure not too high or low over the operating temperature range
- 5) High latent heat
- 6) High thermal conductivity
- 7) Low liquid and vapor viscosities
- 8) High surface tension
- 9) Acceptable freezing or pour point

Table 1 gives the useful operating temperature range of heat pipe working fluids [11].

Table 1: Useful operating temperature range of heat pipe working fluids

Medium	Melting point (°C)	Boiling point at 1 atm. (°C)	Useful range (°C)
Helium	-271	-261	-271 to -269
Nitrogen	-210	-196	-203 to -160
Ammonia	-78	-33	-60 to 100
Pentane	-130	28	-20 to 120
Acetone	-95	57	0 to 120
Methanol	-98	64	10 to 130
Flutec PP2	-50	76	10 to 160
Ethanol	-112	78	0 to 130
Heptane	-90	98	0 to 150
Water	0	100	30 to 200
Toluene	-95	110	50 to 200
Flutec PP9	-70	160	0 to 225
Thermex	12	257	150 to 350
Mercury	-39	361	250 to 650
Caesium	29	670	450 to 900
Potassium	62	774	500 to 1000
Sodium	98	892	600 to 1200
Lithium	179	1340	1000 to 1800
Silver	960	2212	1800 to 2300

Focusing on the performance, the characteristics of a good working fluid are a high latent heat of vaporization, a high surface tension, a high liquid density, and a low liquid viscosity. Chi [12] combined these properties in the form of Merit number for evaluating of working fluids. The Merit number is

$$N_l = \frac{\rho_l \sigma h_{fg}}{\mu_l} \quad (4)$$

Approved for public release; distribution is unlimited.

Figure 5 developed by ACT^a gives the merit number for commonly used working fluids. Sodium is good for high temperatures. For electronic cooling, 250K – 375K, water is the best above 280K, and ammonia is a better choice for temperatures below 280K.

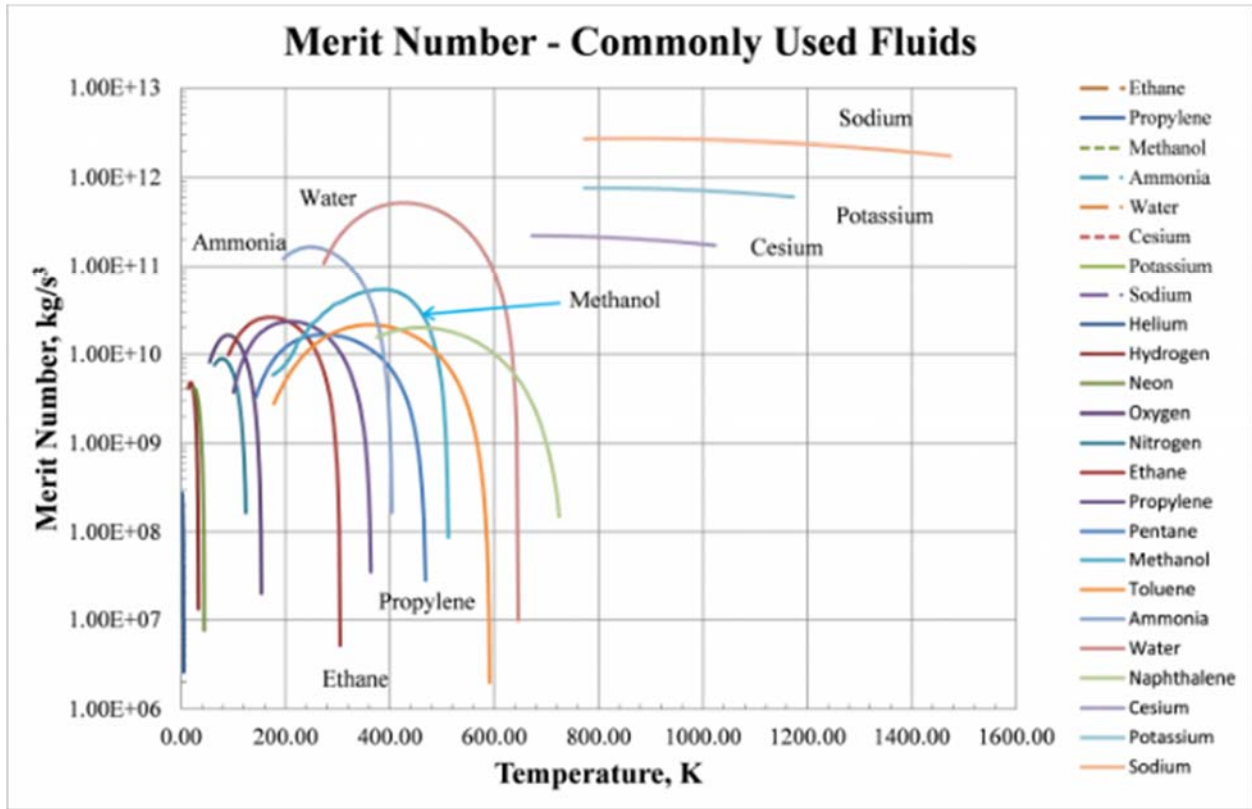


Figure 5: Merit number of commonly used working fluids

^a ACT website, <http://www.1-act.com/merit-number-and-fluid-selection/>.

Approved for public release; distribution is unlimited.

2.3. Thermal Resistances in Thermo-Syphons and Heat Pipes

Figure 6 shows the thermal resistances needed for an analysis of a thermo-syphon. These thermal resistances are the thermal resistances through the tube walls (R_1 , R_7) and the liquid films (R_2 , R_6) in the evaporator and the condenser, the thermal resistances of evaporation (R_3) and condensation (R_5) on the liquid surfaces, the thermal resistances of axially conducting heat along the tube (R_9) and the liquid back flow (R_8), and the thermal resistance due to the temperature drop along the vapor column (R_4).

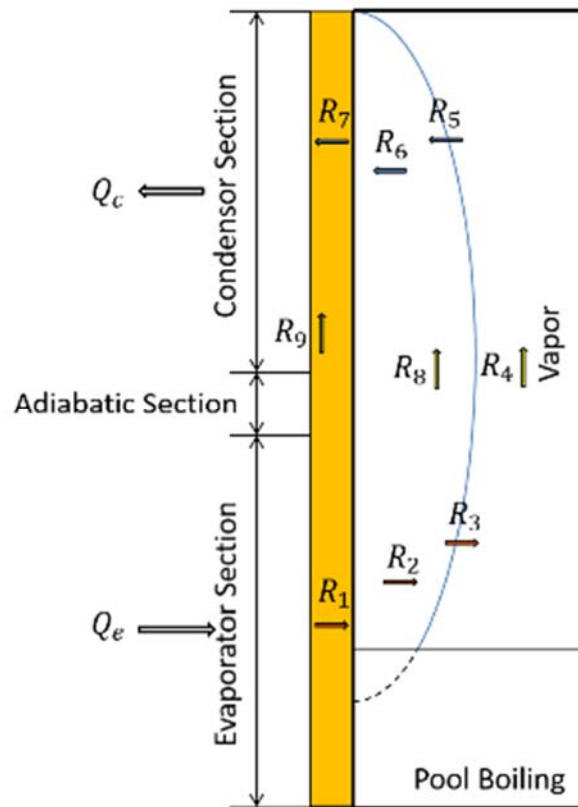


Figure 6: Thermal resistances of a thermo-syphon

The thermal resistances needed for an analysis of a sintered heat pipe are shown in Figure 7. The needed resistances include the thermal resistances through the tube walls (R_1 , R_7) and the

Approved for public release; distribution is unlimited.

wicks, saturated with the working fluid, (R_2, R_6) in the evaporator and the condenser, the thermal resistances of evaporation (R_3) and condensation (R_5) on the liquid surfaces, the thermal resistances of axial conduction of energy along the tube (R_9) and the wick (R_8), and the thermal resistance due to the temperature drop along the vapor column (R_4).

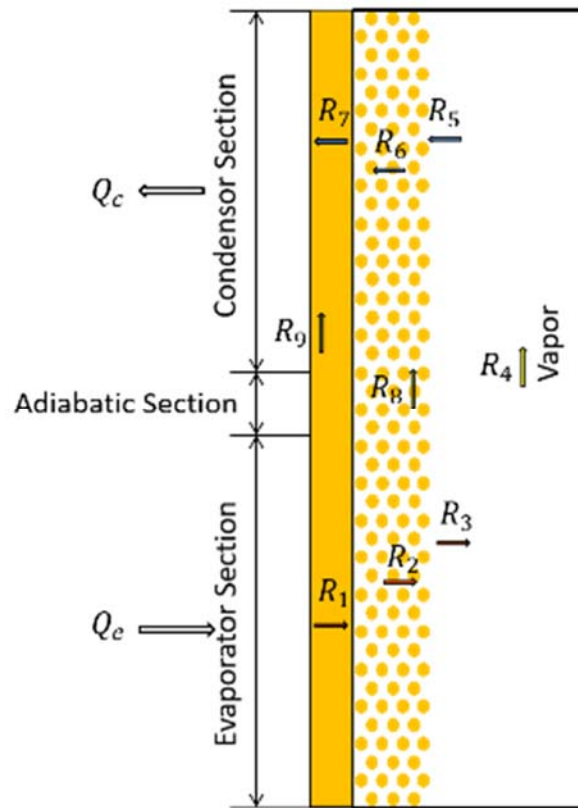


Figure 7: Thermal resistances of a sintered heat pipe

Table 2 presents values of the thermal resistances within a heat pipe. Compared to the heat transferred by evaporation, condensation, and radial thermal conduction, the heat transferred axially by thermal conduction along the tube and the liquid/wick can be neglected. In addition, among the remaining thermal resistances, the thermal resistances of radial conduction through the wick, saturated with the working fluid, in the evaporator and the condenser are dominant. As a

Approved for public release; distribution is unlimited.

result, in order to improve the heat transfer performance of a thermo-syphon or a heat pipe, a decrement of R_2 or R_6 is required. The effects of the other thermal resistances are not obvious.

Table 2: Comparative values of thermal resistances for a heat pipe

Resistance	K/W
R_1, R_7	$\sim 10^{-1}$
R_2, R_6	$\sim 10^{+1}$
R_3, R_5	$\sim 10^{-5}$
R_4	$\sim 10^{-8}$
R_8	$\sim 10^{+4}$
R_9	$\sim 10^{+2}$

The only difference between a thermo-syphon and a heat pipe is that the R_2 , R_6 , and R_8 of a thermo-syphon varies with the liquid film thickness, and the thickness is a function of the heat flux and the surface wettability. However, the R_2 , R_6 , and R_8 of a heat pipe is only a function of the wick thickness, which is fixed. As a result, increasing surface wettability can decrease the thermal resistance of a thermo-syphon but has little effect to the one of a heat pipe.

2.4. Wettability and Evaporation

Phase change heat transfer devices use evaporation and condensation of the working fluid to transfer heat, so the efficiency of evaporation and condensation determines the performance of heat transfer devices. For evaporation, most of the heat is transferred in the interline region, see Figure 8. The evaporating thin film can be divided into three regions: Equilibrium film region I, Evaporating film region II, and Intrinsic meniscus III. The equilibrium film region is the top zone of the meniscus. The liquid film thickness is very small, and the adhesive force between liquid and surface is dominant preventing liquid from evaporating. As a result, there is no heat removed in region I. In region II (1), adhesive forces become smaller, and evaporation appears. However, the

Approved for public release; distribution is unlimited.

adhesive force is not negligible limiting the heat removed in this region. In both regions II (2) and III, adhesive forces can be neglected. Region II (2) has a much thinner film thickness than region III, so the evaporation is much greater in region II (2). Therefore, the length of the region II (2) is the key to determining how rapid the evaporation will be.

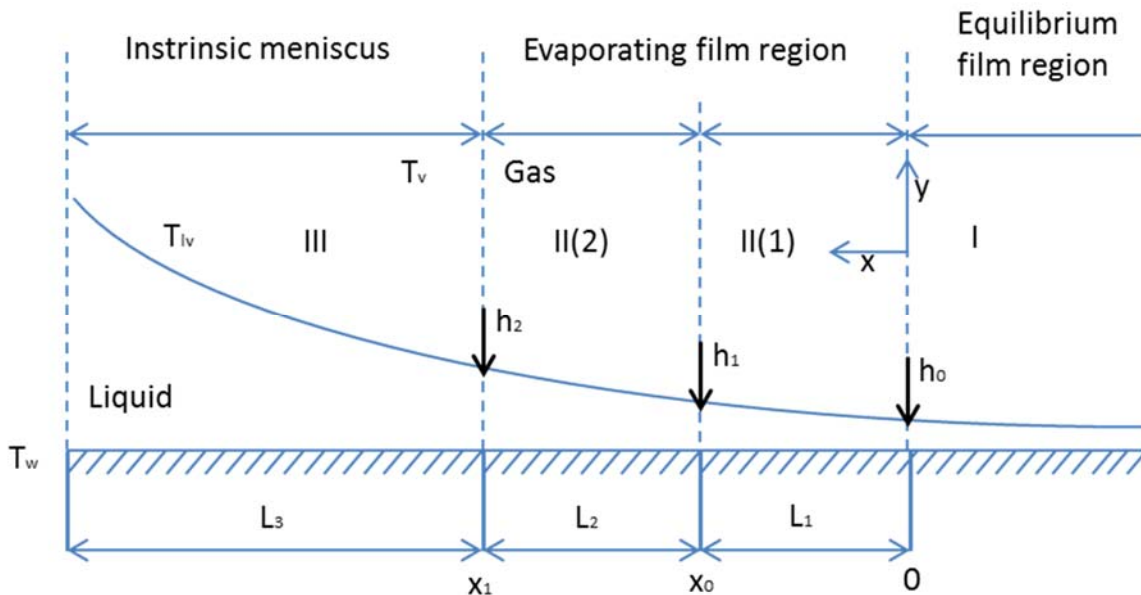


Figure 8: Evaporating thin film and coordinate system

Wayner and Kao [13] discussed the interline heat transfer coefficients of an evaporating wetting film. Solovyev and Kovalev [14] studied the mechanisms associated with the evaporation of a liquid film from a porous surface. Ibrahim and etc. [15], using an experimental method, found that the local heat fluxes at the interline region were about 5.4 - 6.5 times higher than the mean input heat fluxes. Miao and Wang [16] analyzed the evaporation heat transfer for the thin liquid film in a capillary of equilateral triangular cross-section, shown in Figure 8. In addition, Miao and Wang [16] derived the following expression for L_2 :

Approved for public release; distribution is unlimited.

$$L_2 = \frac{125}{6} \frac{v_l k_l}{H_{lv} \sigma_l} \left(\frac{0.8}{\tan \theta} \right)^5 - \left(\frac{6}{125} \frac{H_{lv} \sigma_l}{v_l k_l} h_1^5 \right)^{\frac{1}{4}} \quad (5)$$

where $h_1 = \left(\frac{1}{a} \right)^{\frac{1}{b}}$, with a and b being constants.

Based on equation (5), for a given liquid, increasing the liquid thermal conductivity, decreasing the liquid surface tension, or decreasing the contact angle is a method to obtain a larger L_2 , which leads to the evaporation enhancement. Figure 9 shows a force balance at the point where three phases meet. The contact angle is given by equation (6).

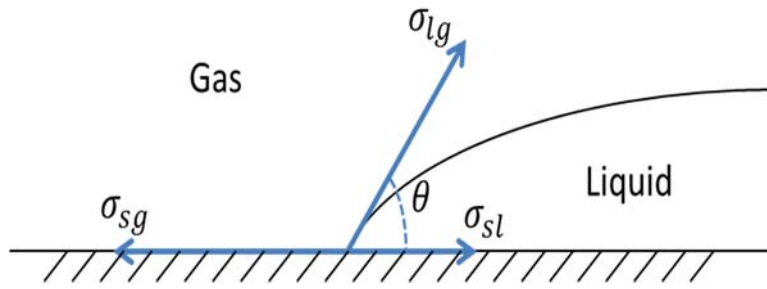


Figure 9: Force balance at the intersection of three phases

$$\theta = \arccos \frac{\sigma_{sg} - \sigma_{sl}}{\sigma_{lg}} \quad (6)$$

In order to obtain a smaller contact angle, a smaller σ_{lg} or a larger $\sigma_{sg} - \sigma_{sl}$ is required. σ_{lg} is determined by the liquid, and $\sigma_{sg} - \sigma_{sl}$ is determined by both the liquid and the surface. However, for wicked devices, a small σ_{lg} harms capillarity which leads to an early dry out, so a large $\sigma_{sg} - \sigma_{sl}$ is always welcomed. Therefore, a good combination of fluid and device material is the key to obtain a peak heat transfer performance.

Approved for public release; distribution is unlimited.

2.5. Motivation

Water is one of the most popular working fluids used for the electronic cooling because of its large latent heat of evaporation. However, the performance of water cannot fulfill the needs of the rapid developments of science and technology, leading researchers to keep looking for methods of improving it. Wasekar [17] added anionic surfactants to the working fluid to augment bubble incipience and increase the heat transfer coefficient. However, adding surfactants harms capillarity which leads to an early dry out in wicked phase change heat transfer devices. Wen [18] used nanoparticle suspensions to successfully increase the boiling heat transfer coefficient, as shown in Figure 10.

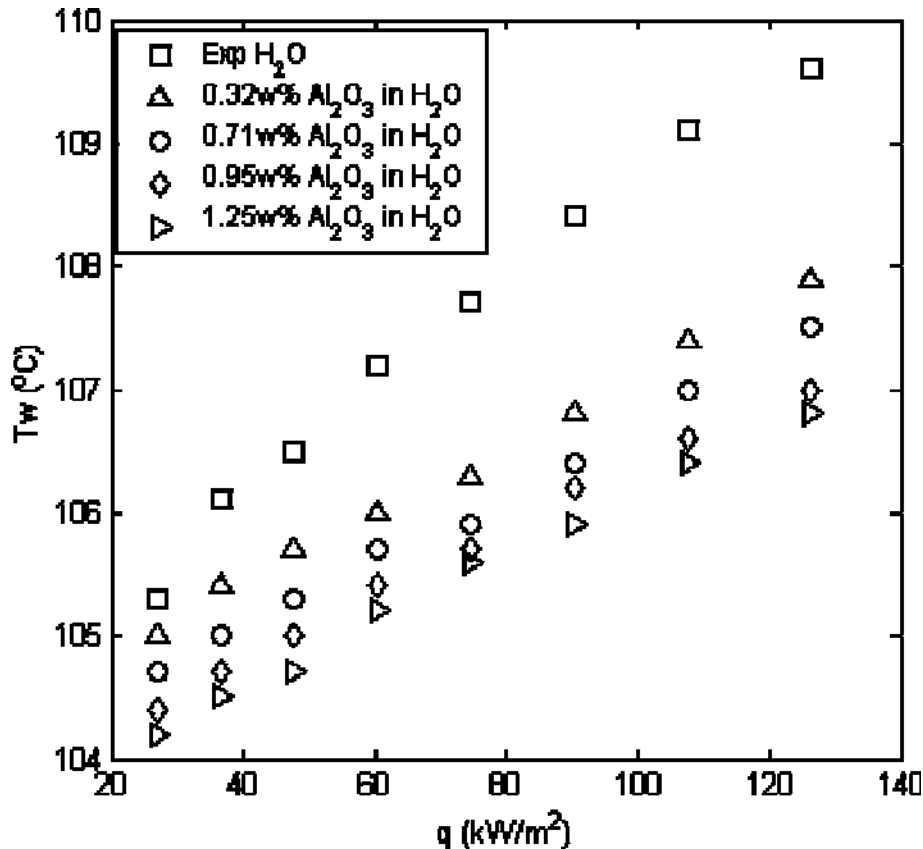


Figure 10: Wall temperatures as a function of heat flux as well as nano-particle concentration

Approved for public release; distribution is unlimited.

However, it was found that overloading the solution with nano-scale particles can negatively impact the boiling performance, see Das [19]. Figure 11 indicates that, with the nano-particle concentration increasing, the boiling performance decreases. As a result, nano-particles cannot be used in phase change heat transfer devices because they sink in the evaporator and will decrease the performance.

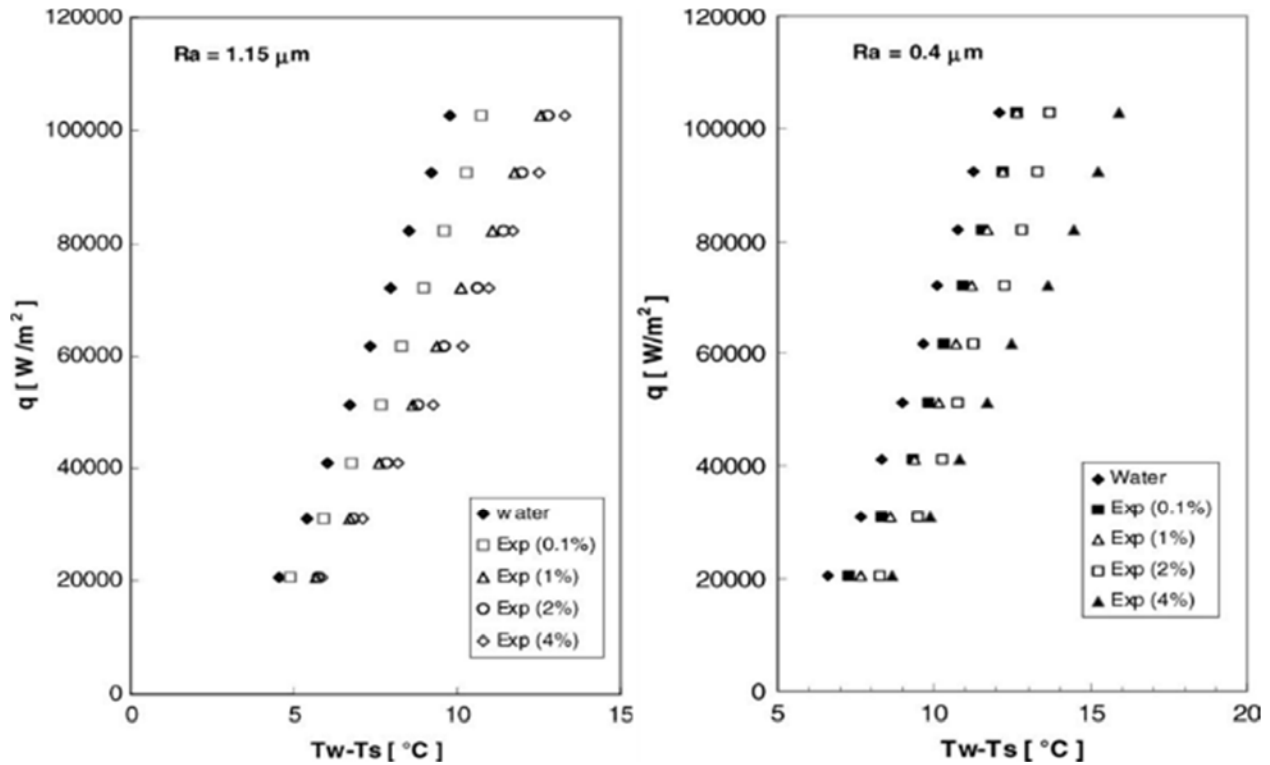


Figure 11: Pool boiling characteristic of nano-fluids on the smoother and roughened heater

Moreover, a major limitation of water is that it is not compatible with some high chemically reactive materials, such as aluminum, because hydrogen gas, a non-condensable gas (NCG) will be generated. It will be accumulated in the condenser, obstruct the heat transfer, and eventually fail the heat transfer device, see Figure 12.

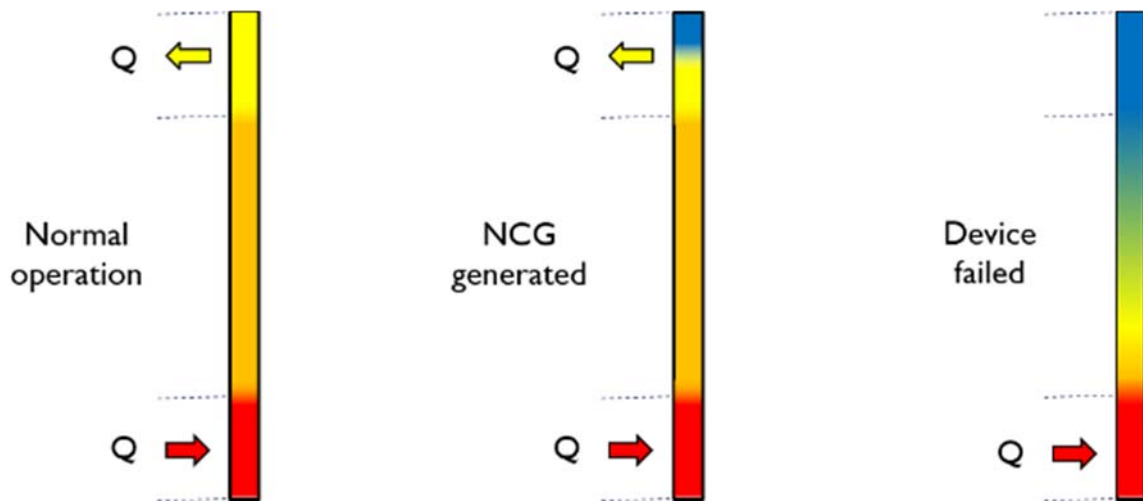


Figure 12: The effect of NCG generation to a thermo-syphon

Therefore, in some weight limited projects, water is replaced with ammonia. There have, as a result, been methods proposed to passivate aluminum surfaces. Chromate passivation schemes are popular when used with aluminum alloys. Kendig [20], and Rocco [21] compared two methods of chromate coatings on Al/Zn alloys and concluded that increasing corrosion resistance allowed water to be in contact with an aluminum surface and actively resisted oxidation. Most, however, failed when there was heat transfer presented.

2.5.1. Past UCLA experience

University of California, Los Angeles (UCLA) tested IAS in a vapor chamber with a copper bi-porous target and in an aluminum thermo-syphon separately. It was found that IAS fluid had a smaller thermal resistance and a later dry out compared to water in the vapor chamber test. In addition, IAS showed its compatibility with aluminum in the thermo-syphon test with NCG generated after two months of operation.

Approved for public release; distribution is unlimited.

2.5.1.1. Vapor chamber test

A comparison of the performances of water and IAS was done by Reilly [22] in a vapor chamber test. A copper bi-porous wick was tested with water and IAS as the working fluid separately. Figure 13 indicates the setup of the vapor chamber test and the wick structure.

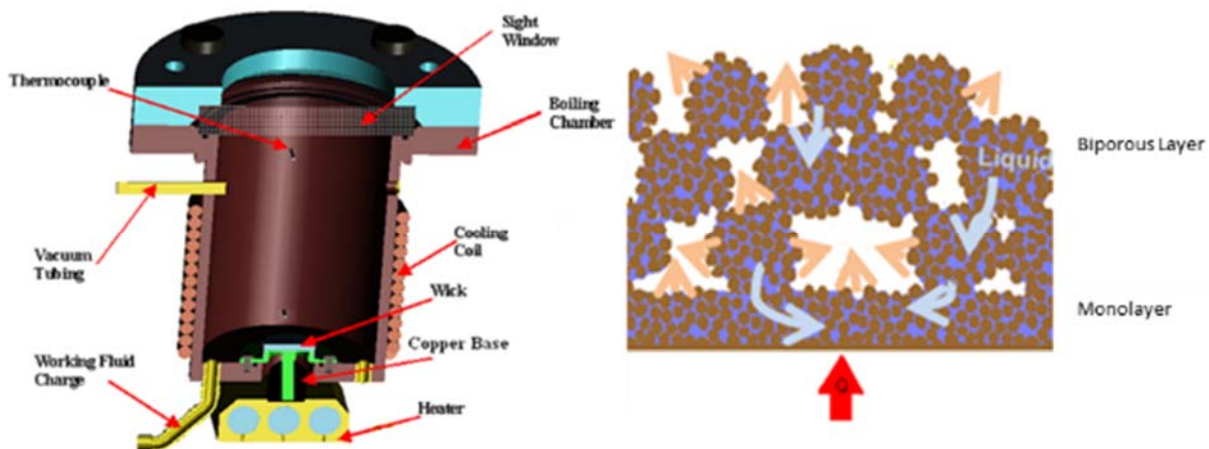


Figure 13: Vapor chamber test setup and bi-porous wick structure

Figure 14 shows the results of the comparison between water and IAS. Compared to water, IAS has a larger superheat at low heat fluxes, low evaporating temperatures. However, with increased heat flux, the superheat of IAS decreases and remains steady with having a much smaller superheat than water. In addition, the dry-out of IAS is greatly delayed.

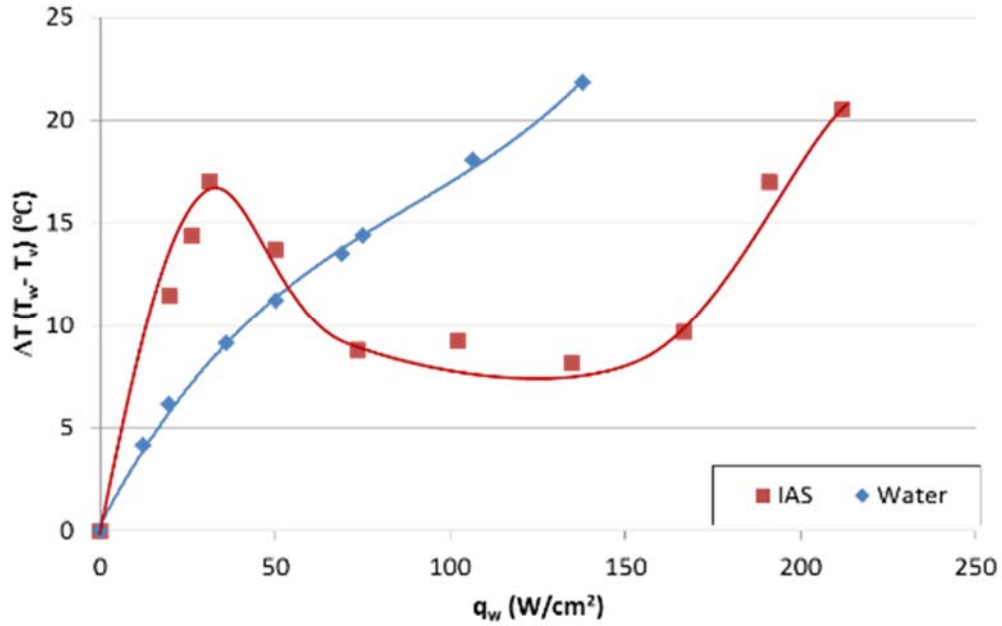


Figure 14: Performance comparison between water and IAS in a vapor chamber

Figure 15 shows SEM images of a copper wick obtained from the vapor chamber test. The left is a clean wick, and the right is one coated by IAS. A thin and smaller scale porous coating can be seen on copper particles. This could be the reason why heat transfer performance is improved.

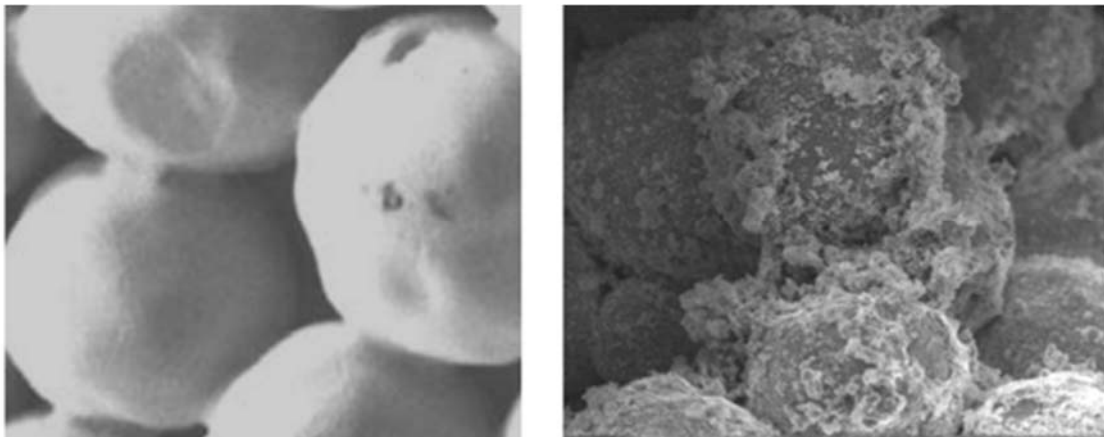


Figure 15: SEM results of a copper wick: clean vs coated by IAS

Approved for public release; distribution is unlimited.

2.5.1.2. Aluminum thermo-syphon lifetime test

An aluminum thermo-syphon charged with IAS was tested by Reilly et al [23]. Figure 16 shows the schematic of the test set up and the locations of thermocouples.

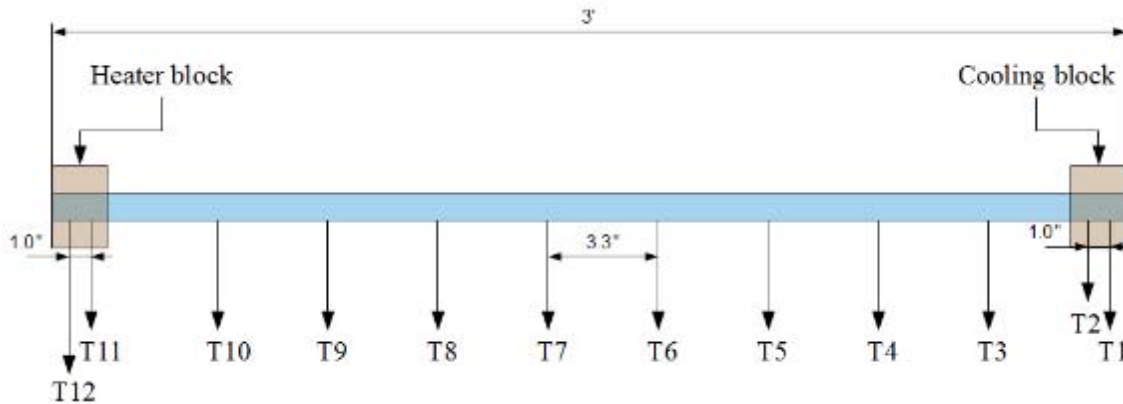


Figure 16: Schematic of aluminum thermo-syphon test and locations of thermocouples

The tube was located with an inclination angle of 10 degrees from the horizontal, and the evaporator was at the bottom. In addition, the test was initiated with an input power of 140 watts and then gradually increased to 200 watts in the first week, see Figure 17. Afterwards, the input power was kept at 200 watts in the second week, see Figure 18. The performance was very stable, and there was no NCG generated. Further, another IAS/aluminum thermo-syphon was tested by Stubblebine et al [24]. It was run for two months without non-condensable gas being detected.

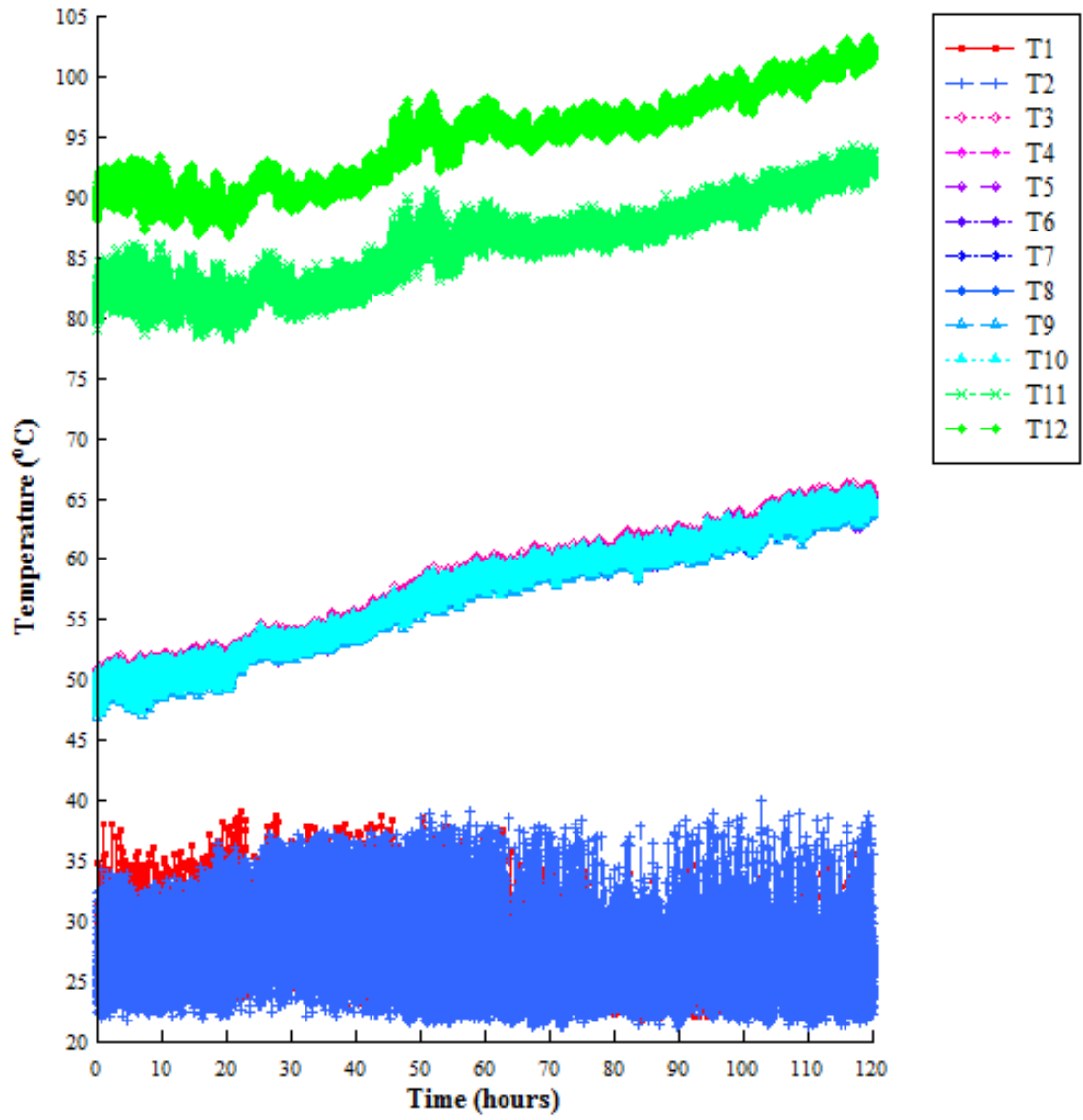
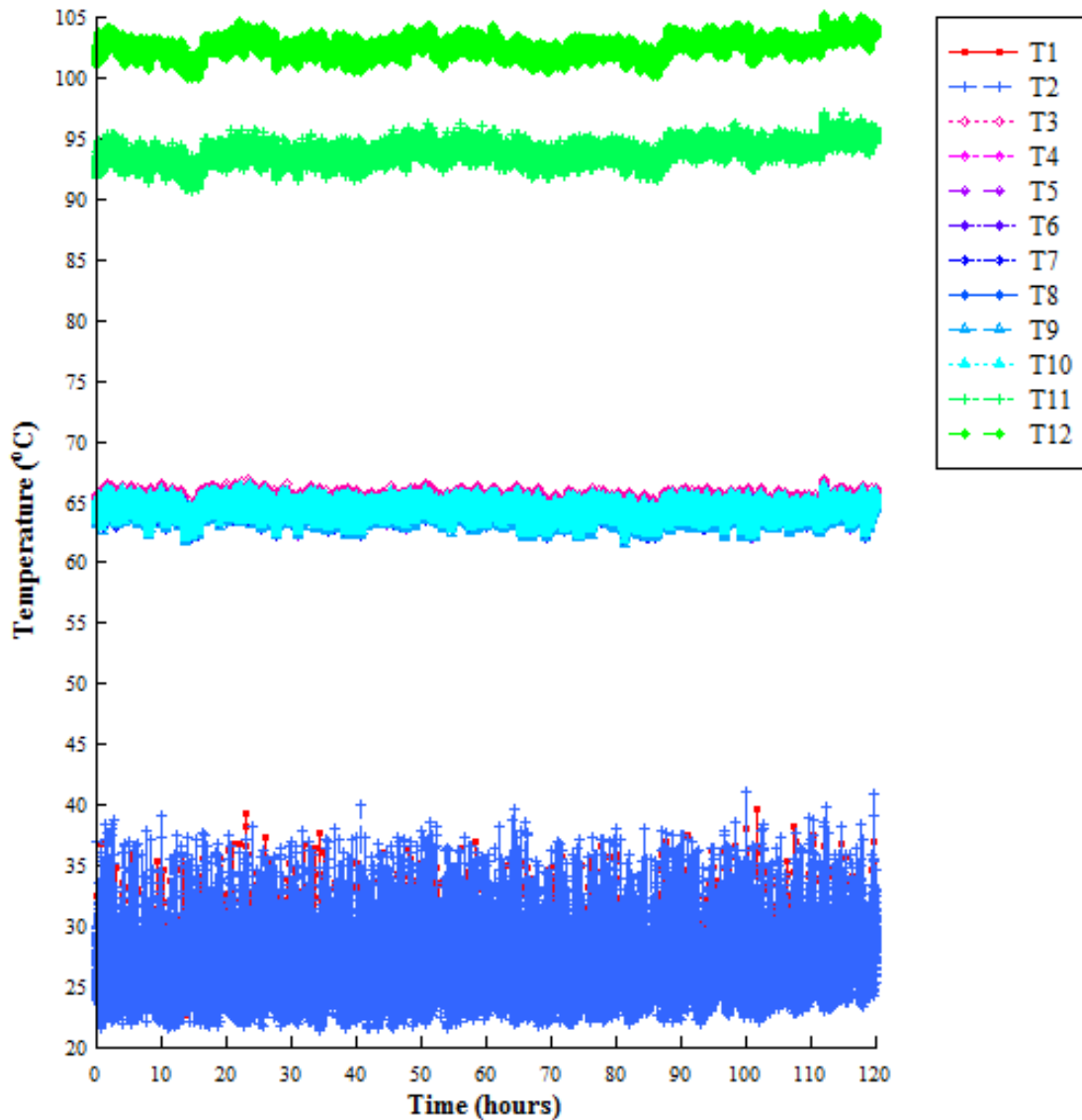


Figure 17: First week, aluminum/IAS thermo-syphon lifetime testing

Approved for public release; distribution is unlimited.



al10252010-02-allID.grf

Figure 18: Second week, aluminum/IAS thermo-syphon lifetime testing

2.5.2. Objective

The results of the tests done by UCLA show that IAS has a smaller thermal resistance and a later dry out point compared to water when used in copper phase change heat transfer devices. In addition, IAS is compatible with aluminum and can be used in aluminum phase change heat

Approved for public release; distribution is unlimited.

transfer devices, while water is not. However, IAS is a mystery, and all of its advantages do not have convincing explanations. Even the original developer of IAS does not know how IAS works.

The objective of this report is to uncover the mystery of IAS. This objective will be accomplished in three steps: 1) determine what IAS is, 2) explain the phenomena associated with the use of IAS in copper made phase change heat transfer devices, and 3) in aluminum made phase change heat transfer devices. The three steps become the basic three tasks of this report.

2.5.2.1. Task 1: what is IAS?

Task 1 aims to understand what IAS is and how it works while being used in different material heat transfer devices. Above all, the chemical constituents in an IAS fluid will be investigated, and a method will be given to produce it. Afterwards, the physical properties of IAS will be measured and compared to those of water. A chemical analysis will be performed, and the chemical reactions involved between IAS and the surfaces of copper or aluminum made devices, where it is to be used, will be listed and categorized by their contributions to the heat transfer performance or the surface passivation. In addition, OLI software, commercial software to simulate electrolytes, will be used to estimate the amount of solid products, generated by redox reactions or temperature increases, at different temperatures and concentration ratios. Lastly, a coating study will be performed to understand how each chemical coats the surface and how it contributes to the surface wettability. The positive and negative effects of each coating will be discussed and demonstrated by data from SEM observations and contact angle tests.

Approved for public release; distribution is unlimited.

2.5.2.2. Task 2: using IAS in copper devices

Task 2 is the main part of the report. The performance enhancement effects of IAS when used in copper made phase change heat transfer devices will be studied. To begin, a 1-D diffusion model will be built and used to estimate the concentration profiles of the chemicals along the liquid flow path and the location where deposition of each coating begins. Next, a capillary rise test will be performed to show how each chemical contributes to the improvement of the surface wettability. The heat transfer performances of water and IAS will be compared using a thermo-syphon test at different inclination angles, a grooved flat heat pipe test, and a sintered heat pipe test. The test results will validate the conclusions of the diffusion model and the capillary rise tests. Based on the comparison results, the advantages and limits of using IAS, for performance enhancement purposes, in various heat transfer applications will be discussed.

2.5.2.3. Task 3: using IAS in aluminum devices

Task 3 aims to give an explanation of the compatibility between IAS and aluminum and discuss the key factors that will lead to failures. Initially, an electrochemical theory of aluminum passivation will be introduced, and the existence of an electrochemical cycle will be demonstrated by an aluminum thermo-syphon test. Afterwards, the importance of a continuous liquid back flow to aluminum passivation will be pointed out, and a vertical thermo-syphon test with natural convection cooling will be used to demonstrate that a discontinuous liquid back flow is the main reason of the failures. At the end, using IAS in steel or stainless steel phase change heat transfer devices will be discussed.

2.6. Background

The original IAS fluid was used to prepare what is often called a Qu tube. The Qu tube, sometimes called “Super tube,” was invented by Yuzhi Qu [25] in 1997. It was claimed to be a solid state super conductive heat pipe and use resonance waves to transfer heat. There are three layers of chemical compounds coat the Qu tube: anti-corrosion layer, active heat transfer layer, and black powder layer. The original IAS was used to prepare one of the three layers, and Figure 19^b shows the three solid layers in Qu tube which is claimed in US Patent 6132823.



Figure 19: Schematic of the three solid layers in QuTech's Heat Pipe

The Qu tube is advertised to have the following features on a Chinese website^c:

- 1) Qu tube is a solid state super conductive heat pipe and uses resonance waves to transfer heat. As a result, Qu tube can transfer heat without the effect of the gravity.
- 2) Qu tube is super thermally conductive, and the thermal conductivity can reach $14MW/m \cdot K$, which equals to thirty-two thousand times that of the one of silver. The

^b Non-public report: Lee, S., Marotta, E., and Lau, S. C., 2007, “Investigation of Heat Transfer Mechanism and Performance of QuTech™ Superconducting Technology,” Final Report on the QuTech™ Superconducting Tube to INTEL Corporation.

^c http://baike.baidu.com/link?url=P-0iWqJAMdGOc9K9fYDOMAw7KAIY2PeQb_uV3Qi2JbkHkfu7zLG-38q4TF8MQrwUhht1nee_F9HEWOHYJnkQ1q.

Approved for public release; distribution is unlimited.

maximum axial heat flux can reach $27.2MW/m^2$, and the maximum radial heat flux can reach $158kW/m^2$.

- 3) The heat transfer efficiency of Qu tube can reach 171%^d. In addition, Qu tube can transfer heat from a low temperature to a high temperature without any extra loss^e.
- 4) The media can be used in temperatures ranging from $-30^{\circ}C$ to $1100^{\circ}C$, and the applications can be used from $-30^{\circ}C$ to $350^{\circ}C$.
- 5) It has lower internal pressures while working compared to the conventional phase change heat transfer devices, and will not lead to explosion at high temperatures.
- 6) The media does not react with common metal materials and prevents the generation of hydrogen gas and oxygen gas. It has a long lifetime and can work stably for 110,000 hours.
- 7) Based on the test results of Stanford Research Institute (SRI), the Qu tube is nontoxic, pollution-free, and non-corrosive. The intensity of radioactivity is $1.4 \times 10^{-1}Bq/g$, β $1.7 \times 10^{-1}Bq/g$ (like wood), which is harmless to human.

2.6.1. SRI Qu tube report

Stanford Research Institute (SRI) was the first to test the performance of Qu tubes in 1999^f. However, their test was designed based on the description given by the inventor that the Qu tube was a thermal conducting tube, and the measurement errors of the test were large. All the above

^d http://blog.sina.com.cn/s/blog_4bb17e9d0102e29r.html

^e <http://www.q-t-g.com/14.-electrical-potential-measurement-of-qit-medium.html>

^f Non-public report: McKubre, M. C. H. and Tanzella, F. L., 1999, "Thermal Property Analysis of the Qu Supertube, Part I: Thermal Conduction Studies," SRI International.

Approved for public release; distribution is unlimited.

led them to make some inaccurate conclusions, such as a 102% heat transfer efficiency^g, a sinusoidal wave temperature distribution along the tube, and an effective thermal conductivity 100-1000 times greater than silver^h.

2.6.2. TAMU Qu technology report

In 2007, Leeⁱ from Texas A&M University (TAMU) tested the heat transfer performance of a QuTechTM superconducting tube at different inclination angles and compared it to the one of a copper/water thermo-syphon with a similar outside diameter (OD). The test results of the QuTechTM tube showed that the gravity was one of the main factors that determined the heat transfer performance of QuTechTM tubes. In addition, the performance comparison indicated that the QuTechTM tube had similar thermal conductance as the copper/water thermo-syphon, but it dried out earlier.

Moreover, Lee cut open several QuTechTM tubes and found that the QuTechTM tube was a sintered heat pipe with a strong basic yellow water base solution as the working fluid, and the wick was coated by a layer of black solid compounds, which was found to be a hydrates mixture with fourteen chemical elements. He guessed that the hydrates might help improving the heat transfer performance by adding an extra energy of dehydrating to the potential heat of evaporation, while it did not seem to be correct.

^g Non-public report: McKubre, M. C. H. and Tanzella, F. L., 1999, “*Thermal Property Analysis of the Qu Supertube, Part II: Mass Flow Calorimetry*,” SRI International.

^h Non-public report: McKubre, M. C. H. and Tanzella, F. L., 2000, “*Thermal Property Analysis of the Qu Supertube, Part II: Studies*,” SRI International

ⁱ Non-public report: Lee, S., Marotta, E., and Lau, S. C., 2007, “*Investigation of Heat Transfer Mechanism and Performance of QuTechTM Superconducting Technology*,” Final Report on the QuTechTM Superconducting Tube to Intel Corporation.

Approved for public release; distribution is unlimited.

2.6.3. University of Alabama Tests

In 2008, Entekin [26] from the University of Alabama in Huntsville finished his M.S. report by testing a ten feet long Qu tube at different inclination angles and comparing the performances with those of a copper rod and a copper tube separately, both of which had the same OD as the Qu tube. He used the same test design as the one in SRI reports, but the instruments were well calibrated and more accurate.

Entekin's test results again demonstrated that the heat transfer performance of the Qu tube was affected a lot by the gravity. The Qu tube did not work while located horizontally or the evaporator was higher than the condenser. This meant that the Qu tube was a thermo-syphon. In addition, the sinusoidal temperature distribution was not found in Entekin's tests.

Moreover, in 2009, Rao [27] from the University of Alabama in Huntsville finished his M.S. report by testing Qu tubes and calculating the critical axial and radial heat fluxes. He found that the critical axial and radial heat fluxes of the Qu tube were much larger than found for off the shelf similar size heat pipes. In addition, the test results showed that the behavior of Qu tube at onset, an increase in input power, and in failure process mimiced the behavior of a thermo-syphon.

2.6.4. Summary

To sum up, all the previous tests had demonstrated that Qu tube was actually a conventional heat pipe or thermo-syphon instead of a super thermal conducting tube. The difference was that the internal surface was coated by a layer of black solid compounds, and a strong basic aqueous solution was used as the working fluid instead of water.

Approved for public release; distribution is unlimited.

The inventor used his technology in different phase change heat transfer applications. For example, the QuTech™ tube tested by TAMU was a sintered heat pipe, but the Qu tube tested by the University of Alabama was probably a thermo-syphon based on the test results. The Qu tube, the thermo-syphon one, had much larger critical axial and radial heat fluxes than the similar size water heat pipes in the market, but the heat transfer performance of the QuTech™ tube, the sintered heat pipe one, was not significantly improved.

However, at this time, nobody has compared the heat transfer performance of a Qu tube to a water heat pipe that has the identical geometries. No research has been done to investigate if and how the black solid coating and the basic yellow liquid can help improving the heat transfer performance. Moreover, no explanation has been given about why the thermo-syphon Qu tube and the heat pipe QuTech™ tube have such different heat transfer performances. All these questions will be answered in this report.

Approved for public release; distribution is unlimited.

3. METHODS, ASSUMPTIONS, AND PROCEDURES (WHAT IS IAS)

The original IAS fluid is a dark red aqueous solution with black suspensions, see Figure 20, and it has an initial pH number of 6.22. After being used in copper, aluminum, or stainless steel phase change heat transfer devices, it becomes transparent, and the color turns to light yellow, as shown in Figure 21.

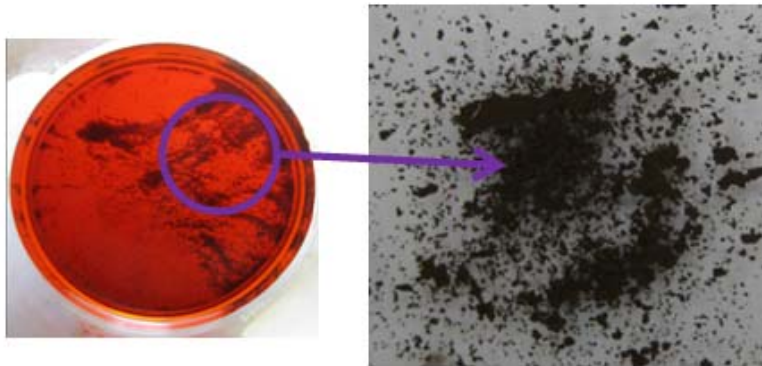


Figure 20: Black suspension in IAS fluid

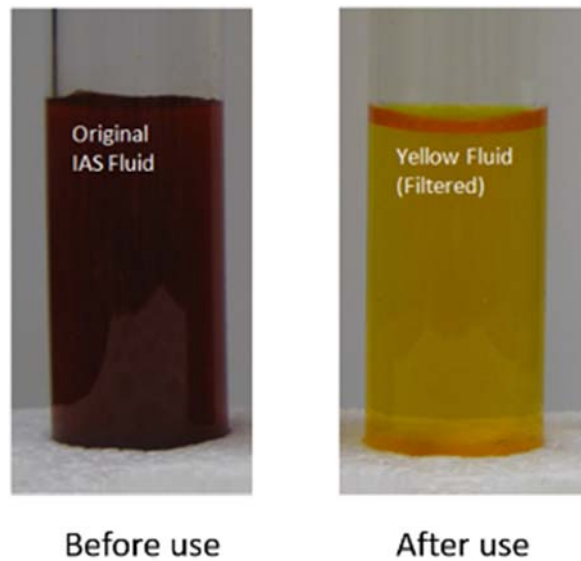


Figure 21: IAS fluid, before and after use

Approved for public release; distribution is unlimited.

This chapter focuses on studying what IAS is both physically and chemically. Above all, the chemical constituents in an IAS fluid are investigated, and a method is given to produce it. Afterwards, the physical properties of IAS are measured and compared to those of water. Moreover, a chemical analysis is performed, and the chemical reactions involved between IAS and the surfaces of copper or aluminum made devices where it is to be used are listed and categorized by their contributions to the heat transfer performance or the surface passivation. In addition, OLI, commercial software to simulate electrolytes, is used to estimate the amount of solid products, generated by the redox reactions or the temperature increases, at different temperatures and solution molarities. At the end, a coating study is performed to understand how each chemical coats the surface and how it contributes to the surface wettability. The positive and negative effects of each coating are discussed and demonstrated by the data from SEM observations and contact angle tests.

3.1. IAS Reproduction

In order to study how IAS works, understanding what IAS is made of and how to reproduce it are very important. This section aims to find out what the chemical constituents of IAS are and how to produce IAS with different chemical concentrations.

3.1.1. Chemical constituents of IAS

The original IAS fluid was tested by the Naval Research Lab (NRL)^j, and eight chemical elements were detected in the fluid using an Inductively Coupled Plasma – Optical Emission

^j Non-public report: Naval Research Lab, “*Chemical Analysis of Posnett International Company Inc. Heat Pipe Solution, Generation 2.5*”.

Spectrometry (ICP-OES) analysis, as shown in Table 3. In the NRL report, the mass of 200ml IAS fluid was measured to be 25.17 grams, so the density of the original IAS fluid was 1.0068kg/L.

Table 3: Composition by ICP-OES analysis of the original IAS fluid

Element	Concentration	
	mg/kg	mmol/L
Sodium	154	6.74
Potassium	2380	61.28
Magnesium	14	0.58
Calcium	527	13.24
Strontium	75	0.86
Silver	7	0.065
Chromium	4010	77.64
Manganese	153	2.80

Moreover, a High-Performance Liquid Chromatography (HPLC) type test was done to find that there were chromate and permanganate in the liquid. Small amounts of chloride and sulfate were found, but they were below the detection limit, see Table 4.

Table 4: Anion scan detection

Chloride	3mg/kg
Sulfate	3mg/kg

Based on the chemical elements listed in Table 3, the possible positive and negative ions, which could be in an aqueous solution at a pH number of 6.22, are listed in Table 5.

Approved for public release; distribution is unlimited.

Table 5: Possible ions in an IAS fluid

Possible ions	Existence
Na^+	Only possibility, exist
K^+	Only possibility, exist
Mg^{2+}	Only possibility, exist
Ca^{2+}	Only possibility, exist
Sr^{2+}	Only possibility, exist
Ag^+	Only possibility, exist
Cr^{2+}	May not coexist with permanganate
Cr^{3+}	May not coexist with permanganate
Mn^{2+}	May not coexist with permanganate
MnO_4^{2-}	Not stable at pH 6.22, not exist
MnO_4^-	Exist
CrO_4^{2-}	Exist, have a balance with $Cr_2O_7^{2-}$, $HCrO_4^-$, and H_2CrO_4

Figure 22 is an E-pH diagram, which is also called the Pourbaix diagram, of manganese at 25°C. It shows that at the pH number of 6.22, there are only two forms of manganese in aqueous solutions, permanganate ion and manganese (II) ion. Manganate ion is only stable at strong basic conditions, so it will not exist in an IAS solution.

Approved for public release; distribution is unlimited.

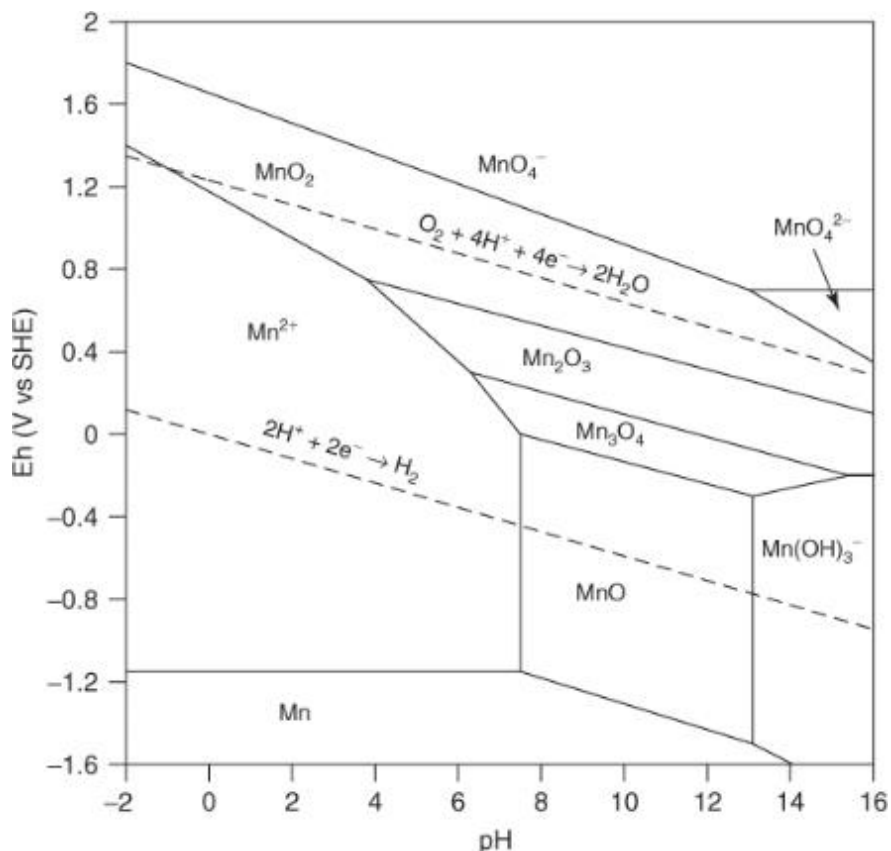
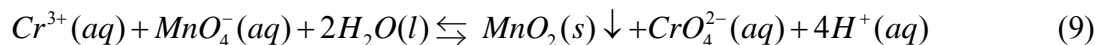
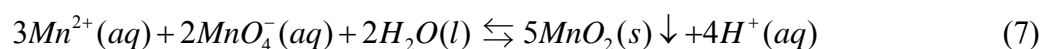


Figure 22: E-pH diagram of manganese vs Standard Hydrogen Electrode (SHE)

Manganese (II), chromium (II), and chromium (III) ions can be oxidized by permanganate, and the reactions are shown separately in equations (7), (8), and (9).



The chemical equilibrium constants at standard condition of these reactions can be calculated using equations (10) and (11).

Approved for public release; distribution is unlimited.

$$\Delta_r G_m^\theta = -RT \ln K^\theta \quad (10)$$

$$\Delta_r G_m^\theta = \sum_{\text{products}} \Delta_f G_m^\theta - \sum_{\text{reactants}} \Delta_f G_m^\theta \quad (11)$$

Table 6 shows the needed standard formation Gibbs free energy of the related chemicals [28].

Table 6: Standard formation Gibbs free energy of related chemicals

Chemical constituents	$\Delta_f G_m^\theta, kJ/mol$
H^+	0
Cr^{2+}	-176.1
Cr^{3+}	-215.5
Mn^{2+}	-224.4
MnO_4^-	-425.1
CrO_4^{2-}	-736.8
H_2O (liquid)	-237.19
MnO_2	-466.1

For Mn^{2+} ,

$$[Mn^{2+}] + [MnO_4^-] = [Mn]_{total} \quad (12)$$

$$\Delta_r G_m^\theta = -332.72 kJ / mol \quad \text{for reaction (7)}$$

and

$$K^\theta = \frac{[H^+]^4}{[Mn^{2+}]^3 \cdot [MnO_4^-]^2} \cdot c_0^{3+2-4} = 1.14 \quad (13)$$

Approved for public release; distribution is unlimited.

Because the pH number is 6.22,

$$\left\{ \begin{array}{l} [Mn^{2+}] = 2.68 \times 10^{-7} \text{ mol / L} \\ [MnO_4^-] = 2.80 \times 10^{-3} \text{ mol / L} \end{array} \right. \text{ or } \left\{ \begin{array}{l} [Mn^{2+}] = 2.80 \times 10^{-3} \text{ mol / L} \\ [MnO_4^-] = 2.62 \times 10^{-9} \text{ mol / L} \end{array} \right. \quad (14)$$

The result shows that manganese (II) ions do not coexist with permanganate ions. Permanganate ions have been detected, so manganese (II) ions do not exist in a IAS fluid.

For Cr^{2+} ,

$$\Delta_r G_m^\theta = -733.34 \text{ kJ / mol} \quad \text{for reaction (8)}$$

$$K^\theta = \frac{[H^+]^8 \cdot [CrO_4^{2-}]^3}{[Cr^{2+}]^3 \cdot [MnO_4^-]^4} \cdot c_0^{3+4-8-3} = 1.34 \quad (15)$$

Because the pH number is 6.22,

$$[Cr^{2+}] = 5.94 \times 10^{-14} \cdot [CrO_4^{2-}] \quad (16)$$

When all the chromium exists as chromate, the concentration of the chromium (II) ion has the maximum value.

$$[Cr^{2+}]_{\max} = 4.61 \times 10^{-15} \text{ mol / L} \quad (17)$$

As a result, chromium (II) ions do not exist in a IAS fluid.

Similarly, for Cr^{3+} ,

Approved for public release; distribution is unlimited.

$$\Delta_r G_m^\theta = -562.3 \text{ kJ / mol} \quad \text{for reaction (9)}$$

$$K^\theta = \frac{[H^+]^{-4} \cdot [CrO_4^{2-}]}{[Cr^{3+}] \cdot [MnO_4^-]} \cdot c_0^{1+1-4-1} = 1.25 \quad (18)$$

Because the pH number is 6.22,

$$[Cr^{3+}] = 3.75 \times 10^{-23} \cdot [CrO_4^{2-}] \quad (19)$$

When all the chromium exists as chromate, the concentration of the chromium (III) ion has the maximum value.

$$[Cr^{3+}]_{\max} = 2.91 \times 10^{-24} \text{ mol / L} \quad (20)$$

As a result, chromium (III) ions do not exist in a IAS fluid.

In addition, based on the results of an X-Ray Diffraction (XRD), SEM test and an Energy-Dispersive X-ray Spectroscopy (EDS) test, the small amount of suspension in the original IAS fluid was found to be mostly manganese (IV) oxide 0 with some potassium, chromium, calcium, and strontium, which should come from the residual of the solution.

Therefore, the original IAS fluid should be a dilute aqueous solution with a small amount of manganese (IV) oxide suspension, with sodium (I) ion, potassium (I) ion, magnesium (II) ion, calcium (II) ion, strontium (II) ion, silver (I) ion, chromium (VI) ions, and permanganate ion in the solution.

Approved for public release; distribution is unlimited.

3.1.2. Reproduce IAS

Table 7 shows the positive and negative ions in the IAS fluid. Manganese (IV) oxide suspension will not be considered in this section. The reason of the generation of manganese (IV) oxide will be discussed in Section 3.3.6.

Table 7: Positive and negative ions in an IAS fluid

Positive ions	Negative ions
Na^+	CrO_4^{2-}
K^+	
Ag^+	$HCrO_4^- \leftrightarrow Cr_2O_7^{2-}$
Mg^{2+}	
Ca^{2+}	MnO_4^-
Sr^{2+}	
H^+	OH^-

In order to reproduce the IAS fluid, any chemical compound which is a combination of the ions in Table 7 can be used as the source chemical. For example, sodium chromate, silver dichromate, magnesium chromate, sodium permanganate, potassium hydroxide, and many others are all good. However, the chemical compounds of some combinations are expensive, unstable, hard to find, or even non-existent on the earth.

A method of reproducing an IAS fluid is given, and the required chemicals are listed in Table 8. All the chemicals are easily obtained in chemistry stores, such as Sigma-Aldrich. They all have good purities, and the prices are fairly low.

Approved for public release; distribution is unlimited.

Table 8: Chemicals needed to produce 1 liter IAS fluid

Chemicals	Amount (mmol/L)	Mole Weight (g/mol)	Weight (g)
$KMnO_4$	2.80	158.034	0.44
$K_2Cr_2O_7$	29.24	294.185	8.60
CrO_3	19.13	99.99	1.91
Ag_2CrO_4	0.033	331.73	0.011
$Sr(OH)_2$	0.86	121.63	0.10
$Ca(OH)_2$	13.24	74.093	0.98
$Mg(OH)_2$	0.58	58.3197	0.034
NaOH	6.74/14.59	39.997	0.27/0.58

Simply putting chemicals in DI-water with overnight stirring will be sufficient. There is no redox reaction during the production process. Moreover, acidic chemicals should be added first because insoluble chromate salts will be generated at basic conditions and will not be re-dissolved easily.

There are two numbers for the sodium hydroxide in Table 8. Because of the measurement errors, for the required concentration of sodium ion (6.74mmol/L), the final pH number is only 6.02. In order to obtain a pH number of 6.22, a total of 0.58g sodium hydroxide is required. This calculation is done with the help of OLI. The pH number is more important in later analysis, so the concentration of sodium ion will be changed to 14.59mmol/L . The IAS fluid made by this method will be called **UCLA IAS #1**, and the procedure is shown below:

- Dissolve 0.44g $KMnO_4$ in about 700ml DI-water with stirring.
- Add 8.60g $K_2Cr_2O_7$ to the solution. Keep stirring till everything is dissolved.
- Add 1.91g CrO_3 to the solution with stirring. CrO_3 is easily hydrated, so the weighing process should be done as soon as possible. The dissolving process will generate a little amount of heat.

Approved for public release; distribution is unlimited.

- Add 0.011g $Ag_2Cr_2O_7$, 0.10g $Sr(OH)_2$, 0.98g $Ca(OH)_2$, 0.034g $Mg(OH)_2$, and 0.58g $NaOH$ to the solution with stirring. Not all of the chemicals will be dissolved at this time.
- Keep stirring the solution over night until all the suspensions disappear.
- Dilute the solution to 950ml and move the solution to a volumetric flask, and then dilute it to 1L.
- The fresh IAS solution should be clear with a dark red color.

All the steps should be done in a fume hood, and the operator should wear a goggle, gloves, and a mask for protection.

Table 9 shows the masses and moles of the chemicals in the original IAS fluid and the UCLA IAS #1. Hydrogen and hydroxide ions are not counted, and all the chromium (VI) ions will be counted as chromate ions.

Table 9: Mass and mole of chemicals in the original IAS and UCLA IAS #1

	Original IAS		UCLA IAS #1	
	Mole (mmol/L)	Mass (g/L)	Mole (mmol/L)	Mass (g/L)
Na^+	6.74	0.16	14.59	0.34
K^+	61.28	2.40	61.28	2.40
Mg^{2+}	0.58	0.014	0.58	0.014
Ca^{2+}	13.24	0.53	13.24	0.53
Sr^{2+}	0.86	0.076	0.86	0.076
Ag^+	0.065	0.007	0.065	0.007
MnO_4^-	2.80	0.33	2.80	0.33
CrO_4^{2-}	77.64	9.01	77.64	9.01
Total	163.22	12.52	171.06	12.70
Fraction	0.29%	1.25%	0.31%	1.27%

The main role of potassium ions and sodium ions is balancing the electrons, and the heat transfer performance of IAS is not sensitive to their concentrations. This will be discussed in

Approved for public release; distribution is unlimited.

Section 3.3. Therefore, a general method to produce IAS fluid with different chemical concentrations is given below.

In case if one liter IAS fluid with the main chemical concentrations shown in Table 10 is required to be made, a general procedure and the amount of chemicals are shown in Table 11.

Table 10: Aimed chemical concentrations in IAS

Ions	Concentrations (mmol/L)
Mg^{2+}	c_1
Ca^{2+}	c_2
Sr^{2+}	c_3
Ag^+	c_4
MnO_4^-	c_5
$Cr(VI)$	c_6
H^+	pH_{goal}

As shown in Table 11, the required amount of potassium permanganate, silver chromate, magnesium hydroxide, calcium hydroxide, and strontium hydroxide can be calculated easily. Based on the required total amount of chromium (VI) and the goal pH number, the required amounts of potassium dichromate and chromium (VI) oxide can be calculated by OLI except the following two cases: When all the extra chromium (VI), except silver chromate, comes from chromium (VI) trioxide, but the calculated pH number is larger than the desired pH number, it is a bad design, and the total amount of chromium (VI) should be increased. When all the extra chromium (VI) comes from potassium dichromate, but the calculated pH number is still smaller than the goal pH number, sodium hydroxide is required to balance the pH number.

Approved for public release; distribution is unlimited.

Table 11: Required chemicals to produce IAS

Chemicals	Amount (mmol/L)
$KMnO_4$	c_5
Ag_2CrO_4	$c_4/2$
$Mg(OH)_2$	c_1
$Ca(OH)_2$	c_2
$Sr(OH)_2$	c_3
OLI calculation to make $pH = pH_{goal}$	
$K_2Cr_2O_7$	x_1 , to be calculated, and $0 \leq x_1 \leq \frac{c_6}{2} - \frac{c_4}{4}$
CrO_3	$c_6 - \frac{c_4}{2} - 2x_1$
Case 1: if a result of x_1 can be found in range $\left[0, \frac{c_6}{2} - \frac{c_4}{4}\right]$, follow the concentrations above	
Case 2: if $x_1 = 0$, but $pH > pH_{goal}$	
Bad design, the total amount of chromium (VI), c_6 , should be increased.	
Case 3: if $x_1 = \frac{c_6}{2} - \frac{c_4}{4}$, but $pH < pH_{goal}$	
$NaOH$ is required	x_2 , calculated by using OLI

3.2. Physical Analysis

The physical properties of the original IAS fluid at room temperature were measured and compared to those of water by NRL 0 and by UCLA separately. Table 12 is the summary of the comparison results.

Approved for public release; distribution is unlimited.

Table 12: Physical properties of water and the original IAS

Properties	Water	Original IAS	
		NRL	UCLA
Mass fraction	0%	1.25%	1.27%
Mole fraction	0%	0.29%	0.31%
Density	$997.5\text{kg}/\text{m}^3$ @23°C	$1006.8\text{kg}/\text{m}^3$ measured @23°C	$1005.6\text{kg}/\text{m}^3$ measured @23°C
Boiling Point	100°C	100.1°C	N/A
Freezing Point	0°C	-0.3°C	N/A
Thermal Conductivity	$0.604\text{W}/\text{m} \cdot \text{K}$ @23°C	mole fraction 0.29% thermal conductivity change should be small by Ivan D. Zaytsev [29]	
Contact Angle	100° on smooth copper	N/A	98° on smooth copper
Surface Tension	$0.072\text{N}/\text{m}$ measured @23°C	$0.066\text{N}/\text{m}$ measured @23°C	$0.069\text{N}/\text{m}$ measured @23°C
Viscosity	$9.32 \times 10^{-4}\text{N} \cdot \text{s}/\text{m}^2$ @23°C	Same	$9.60 \times 10^{-4}\text{N} \cdot \text{s}/\text{m}^2$ measured @23°C
Potential Heat of Evaporation	$2355.5\text{kJ}/\text{kg}$ Average value from 70°C to 100°C	Same vapor pressure	$2350.0\text{kJ}/\text{kg}$ Average value from 70°C to 100°C
Specific Heat (C_p)	$4.18\text{kJ}/\text{kg} \cdot \text{K}$ @23°C	mole fraction is 0.29% specific heat difference should be small by Ivan D. Zaytsev [29]	

The density, boiling point, freezing point, surface tension, and viscosity of IAS are measured to be close to those of water.

Further, IAS is a very dilute aqueous solution. The mass and mole fractions of the chemicals are 1.25% and 0.29% separately. Potassium ion, sodium ion, calcium ion, and chromate ion have the largest concentrations in IAS. Table 13 and Table 14 [29] show the thermal

Approved for public release; distribution is unlimited.

conductivities and specific heats of the solutions that are similar to IAS. The mole fraction is 2% or 5% which is larger than the one of IAS, but the changes of the thermal conductivity and the specific heat are small. Therefore, a conclusion can be reached that the thermal conductivity and specific heat of IAS should be very close to those of water.

Table 13: Thermal conductivity of solutions similar to IAS

Chemical	C%	Thermal conductivity, $W/m \cdot K$	Difference with water
$CaCrO_4$	2	0.605	-0.3%
$CaCr_2O_7$	5	0.603	-0.7%
K_2CrO_4	2	0.605	-0.3%
$K_2Cr_2O_7$	2	0.604	-0.5%
$MgCrO_4$	2	0.607	Same
Na_2CrO_4	2	0.607	Same
$Na_2Cr_2O_7$	2	0.615	+1.3%

Table 14: Specific heat of solutions similar to IAS

Chemical	C%	Specific heat, $kJ/kg \cdot K$	Difference with water
$CaCrO_4$	2	4.076	-2.5%
K_2CrO_4	2	4.065	-2.8%
$K_2Cr_2O_7$	2	4.080	-2.4%
$MgCrO_4$	2	4.076	-2.5%
Na_2CrO_4	2	3.994	-4.5%
$Na_2Cr_2O_7$	2	4.094	-2.1%

The vapor pressure of DI-water and IAS was measured separately in the vapor chamber, which was mentioned in Section 2.5.1.1. The test results were compared to the theoretical vapor pressure of pure water, as seen in Figure 23.

Approved for public release; distribution is unlimited.

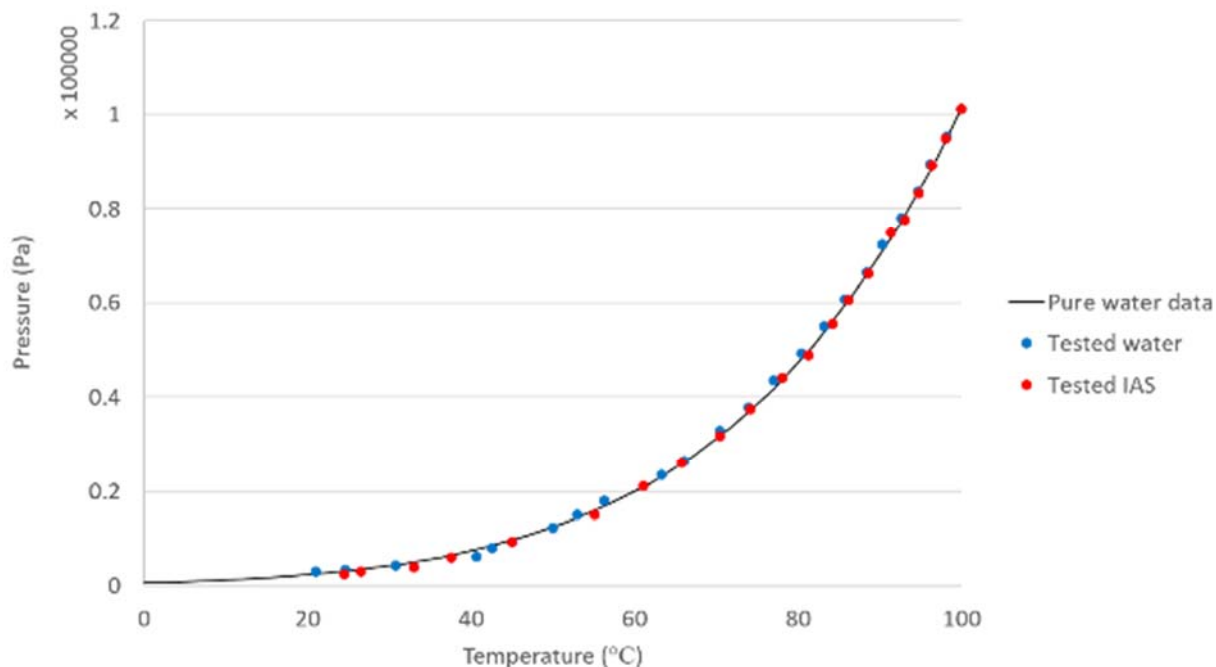


Figure 23: Vapor pressure test results

The results given in Figure 23 show that IAS has almost the same vapor pressure as water, which can be explained theoretically. The vapor pressure of IAS can be calculated by equation (21). The chemicals in IAS are all inorganic and have much larger boiling points, above 400°C, than water. As a result, at low temperatures, below 200°C, their vapor pressures are almost zero. In addition, IAS is a dilute solution with a mole fraction of only 0.29%, so the mole fraction of water is almost 1. Therefore, the vapor of IAS is only water vapor, and the vapor pressure of IAS is the same as that of water.

$$P_{v,IAS} = x_w \cdot P_{v,w} + \sum_{i=1}^n x_i \cdot P_{v,i} \quad (21)$$

Figure 24 (c) shows the condensed liquid from the vapor of IAS. It is completely transparent and has no color. It demonstrates that the vapor of IAS is pure water vapor.

Approved for public release; distribution is unlimited.

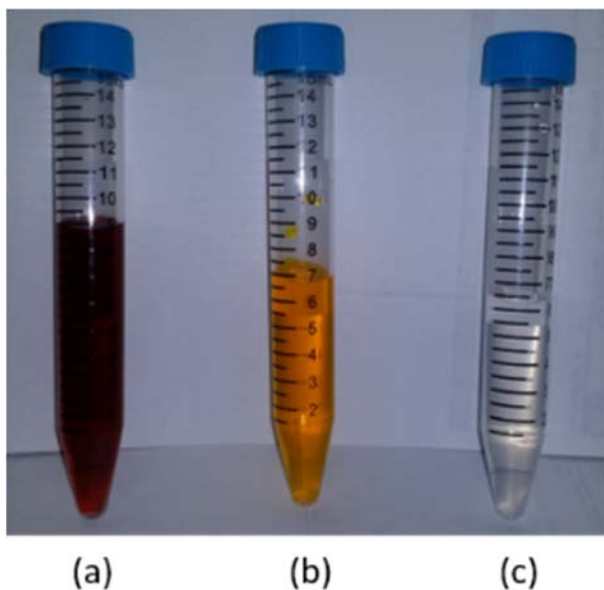


Figure 24: (a) fresh IAS; (b) used IAS; (c) condensed liquid from the vapor of IAS

The Clausius-Clapeyron equation, Eqn. (22) can be used to calculate the potential heat of evaporation. For the temperature range of 70°C to 100°C, the evaporation potential heat of water is 2355.5kJ/kg, and that of IAS is 2350.0kJ/kg.

$$\left(\frac{d \ln P}{dT} \right)_{sat} = \frac{h_{fg}}{RT^2} \quad (22)$$

At room temperature, IAS has almost the same contact angle on a smooth copper surface as water. However, with temperature increasing, IAS generates a layer of coating on the surface. Part of the coating will be re-dissolved after the surface is cooled down, but part of it will not. Even after being rinsed by DI-water for hours, there is still a layer of black coating left on the

Approved for public release; distribution is unlimited.

copper surface. Contact angle of DI-water was measured on IAS pretreated surfaces at different cases, see Figure 25^k.

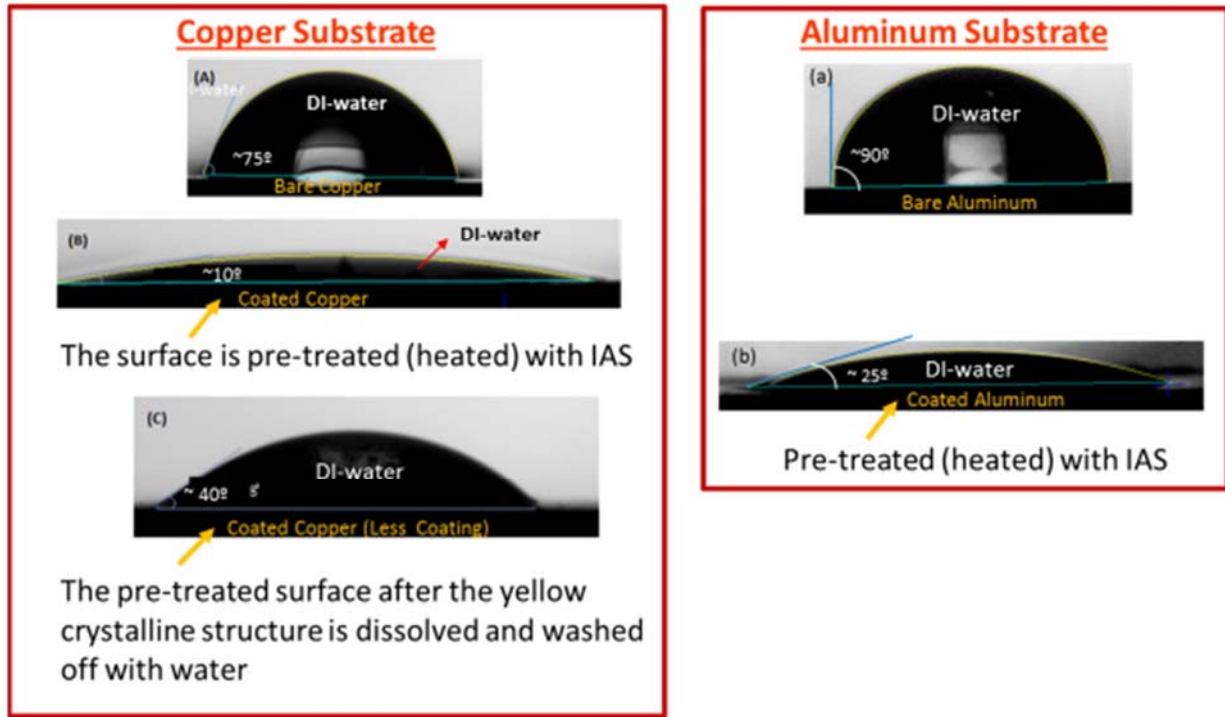


Figure 25: Contact angle comparison between smooth and IAS treated metal surfaces

As shown in Figure 25, DI-water has a much smaller contact angle on IAS-treated copper and aluminum surfaces. In addition, even though the soluble part of the coating is washed off by DI-water, the surface still has a better wettability than the original smooth surface.

To sum up, the good heat transfer performance of IAS is not a result of changes of any bulk physical properties. The reactions between the chemicals in IAS and the metal surface change the

^k Non-public report: Amouzegar, L., 2014, "A Multi-Scale Study of Inorganic Aqueous Solution for Use in Advanced Heat Pipe Applications," Ph.D. thesis prospectus.

surface wettability, and this should be the reason of the performance enhancement. Therefore, a chemical analysis of the surface should be performed to understand how IAS works chemically.

3.3. Chemical Analysis

In order to understand how IAS works chemically, understanding what type of chemicals there are in IAS is important. The chemicals in IAS can be classified into four groups:

- 1) MnO_4^- , $Cr(VI)$
- 2) Na^+ , K^+
- 3) Mg^{2+} , Ca^{2+} , Sr^{2+}
- 4) Ag^+

Permanganate and chromium (VI) are strong oxidizers. They may react with metal surfaces based on the reduction ability of the surface material.

Sodium ion and potassium ion are chemically stable and will not participate in any chemical reactions unless in super strong reductive conditions, which is impossible in aqueous solutions. In addition, their salts usually have large solubility. Unless the surface is close to being dried out or completely dried out, they will not come out as solid coatings.

Magnesium, calcium, and strontium belong to the same chemical group. Their chromate salts have small solubility. With the temperature increasing, the chromate salts will be generated and coat the surface, and when the temperature decreases, they will be slowly dissolved again.

Approved for public release; distribution is unlimited.

Silver was believed to play an important role in aluminum passivation in the NRL report¹.

Based on the classification above, a completely investigation of the involved reactions is done in this section.

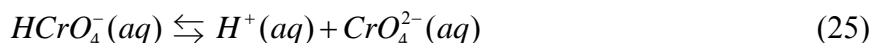
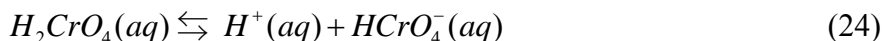
3.3.1. Water self-ionization

Water molecules can auto-dissociate and become hydrogen ions and hydroxide ions until an equilibrium is reached as shown by reaction (23). The standard chemical equilibrium constant is 10^{-14} at 25°C, but varies with temperature.



3.3.2. Chromium (VI) balance

Chromium (VI) exists as four forms in aqueous solutions: chromate acid, hydrogen chromate ion, chromate ion, and dichromate ion. With the pH number changing, the composition will become different, see reactions (24), (25), and (26).



¹ Non-public report: Naval Research Lab, "Chemical Analysis of Posnett International Company Inc. Heat Pipe Solution, Generation 2.5".

Table 15 shows the related chemical equilibrium constants for the chromium balance at 25°C [30], but they vary with temperature.

Table 15: Chemical equilibrium constants for chromium balance at 25°C

Reaction	K
$H_2CrO_4 \leftrightarrow H^+ + HCrO_4^-$	1.8×10^{-1}
$HCrO_4^- \leftrightarrow H^+ + CrO_4^{2-}$	3.2×10^{-7}
$2HCrO_4^- \leftrightarrow Cr_2O_7^{2-} + H_2O$	9.8×10^1

The concentrations of the four forms of chromium (VI) at different pH numbers were calculated using Visual C++. Figure 26 shows the relationship between the pH number and chromium (VI) concentrations in UCLA IAS #1. The existence of chromate acid can be neglected (<0.03%), when the pH number is larger than 4. Between the pH values of 6 and 8, there is a concentration jump for the chromate ion. The initial pH number of the IAS fluid is 6.22, so a small incremental increase in the pH number will lead to a large augmentation of the concentration of the chromate ion.

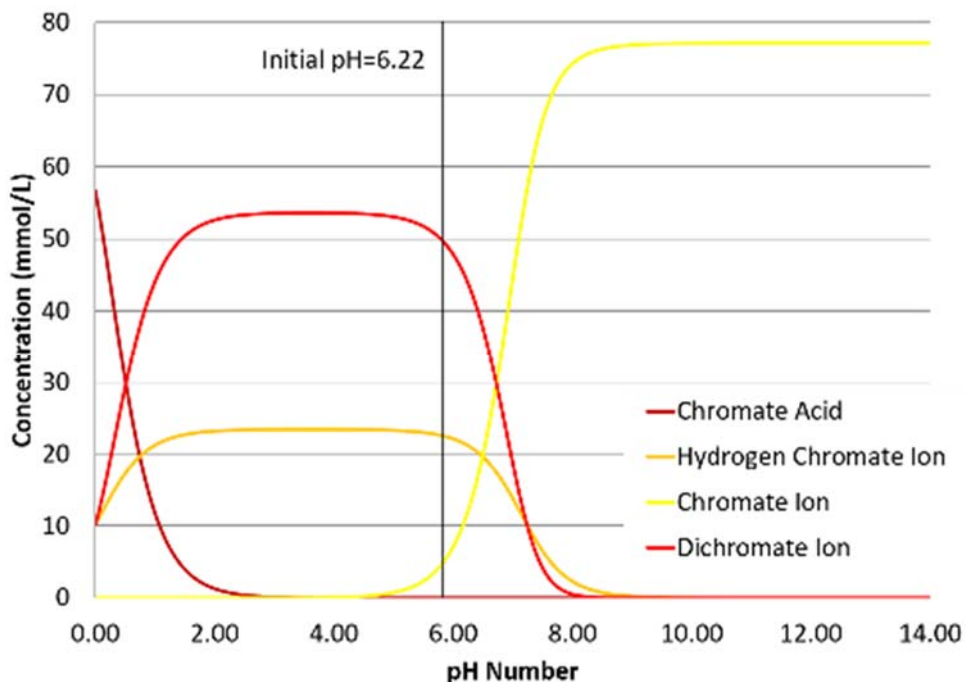


Figure 26: Chromium balance in UCLA IAS #1 at 25°C

For a solution with a given initial pH number of 6.22 and a given total amount of chromium (VI), which is the same as UCLA IAS #1, the concentrations of chromium (VI) at different temperatures are calculated with the help of OLI, see Figure 27. With the temperature increasing, the concentration of dichromate ion decreases, but the concentration of hydrogen chromate ion increases. However, the concentration of chromate ion will not be affected by temperature.

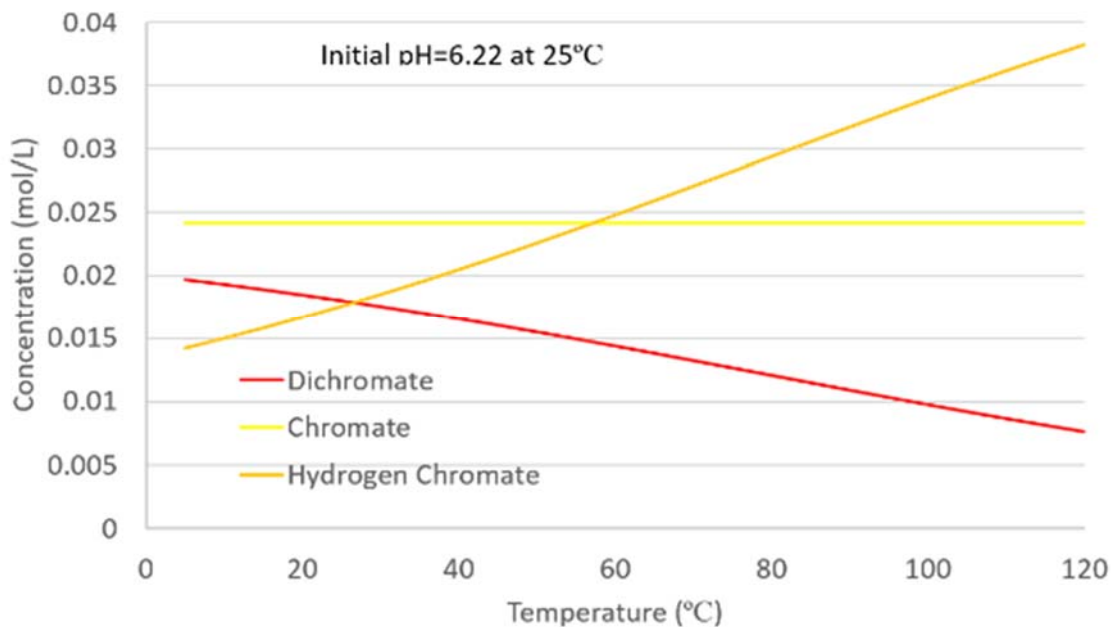


Figure 27: Concentrations of chromium (VI) at different temperatures

3.3.3. Oxidation

There are two oxidizers in the IAS fluid: permanganate and chromium (VI). They may react with the metal surface based on the reductive ability of the surface material. Permanganate is a much stronger oxidizer than chromium (VI), so it can be seen to react with the surface first. Based on the strength of the surface as a reducer, chromium (VI) may or may not work as an oxidizer. For example, permanganate is the only oxidizer for copper surfaces, but both permanganate and chromium (VI) work as oxidizers on aluminum or iron surfaces.

Table 16 shows the standard electrode potentials of related chemicals in H_2O at 25°C and 1atm [30]. Standard condition means that all the concentrations of the ions in half-cell reactions are 1mol/L.

Approved for public release; distribution is unlimited.

Table 16: Standard electrode potentials in H₂O at 25°C and 1 bar

Half-cell reaction	φ^θ/V
$K^+ + e^- \rightarrow K$	-2.936
$Sr^{2+} + 2e^- \rightarrow Sr$	-2.89
$Ca^{2+} + 2e^- \rightarrow Ca$	-2.868
$Na^+ + e^- \rightarrow Na$	-2.714
$Mg^{2+} + 2e^- \rightarrow Mg$	-2.360
$Al^{3+} + 3e^- \rightarrow Al$	-1.677
$Zn^{2+} + 2e^- \rightarrow Zn$	-0.762
$Fe^{2+} + 2e^- \rightarrow Fe$	-0.44
$Sn^{2+} + 2e^- \rightarrow Sn$ (white)	-0.141
$CrO_4^{2-} + 4H_2O + 3e^- \rightarrow Cr(OH)_3 + 5OH^-$	-0.13
$Pb^{2+} + 2e^- \rightarrow Pb$	-0.126
$Fe^{3+} + 3e^- \rightarrow Fe$	-0.04
$2H^+ + 2e^- \rightarrow H_2$	0
$Cu^{2+} + 2e^- \rightarrow Cu$	0.339
$Cu^+ + e^- \rightarrow Cu$	0.518
$Fe^{3+} + e^- \rightarrow Fe^{2+}$	0.771
$Ag^+ + e^- \rightarrow Ag$	0.7992
$HCrO_4^- + 7H^+ + 3e^- \rightarrow Cr^{3+} + 4H_2O$	1.195
$O_2(g) + 4H^+ + 4e^- \rightarrow 2H_2O$	1.229
$MnO_2 + 4H^+ + 2e^- \rightarrow Mn^{2+} + 2H_2O$	1.23
$Cr_2O_7^{2-} + 14H^+ + 6e^- \rightarrow 2Cr^{3+} + 7H_2O$	1.33
$Ce^{4+} + e^- \rightarrow Ce^{3+}$	1.61
$MnO_4^- + 4H^+ + 3e^- \rightarrow MnO_2 + 2H_2O$	1.69
$Co^{3+} + e^- \rightarrow Co^{2+}$	1.95

Positive values mean that the half reactions tend to go from right to left, and the negative values mean that the half reactions tend to go from left to right. It can be seen that metal potassium, strontium, calcium, sodium, and magnesium are very strong reducers, so their ions will not be reduced by copper, aluminum, or iron. In addition, potassium ion, strontium ion, calcium ion, sodium ion, and magnesium ion are already at their highest chemical valences, so they will not be further oxidized either. Therefore, potassium ion, strontium ion, calcium ion, sodium ion, and magnesium ion are chemically stable, and they will not be oxidized or reduced in an operating heat pipe, regardless of the surface material.

Approved for public release; distribution is unlimited.

Aluminum and iron are better reducers than hydrogen gas, so they can reduce the hydrogen ions in water and generate hydrogen gas, which is NCG. Aluminum is a much stronger reducer than iron, so it reacts with water faster. That is why water cannot be used as the working fluid in aluminum phase change heat transfer devices. Iron reacts with water much slower than aluminum, so water can be used in steel or stainless steel devices. However, there will be a ~10% performance decay per year. All of these issues will be discussed in detail in Chapter 5. Copper is a weaker reducer than hydrogen gas, so water is safe in copper phase change heat transfer devices.

Permanganate is the strongest oxidizer in IAS. At standard condition, it can be reduced to manganese (II) ion by aluminum, iron, or even copper. However, in the real case, the pH number of IAS is only 6.22, which means that the concentration of hydrogen ion is much smaller. This makes the oxidation ability of permanganate weaker, and so are manganese (IV) oxide and chromium (VI). Equation (27) shows the relation between the electrode potential and the standard electrode potential.

$$\varphi = \varphi^\theta - \frac{RT}{nF} \ln \frac{\alpha_{prod.}}{\alpha_{react.}} \quad (27)$$

The concentrations of permanganate and chromium (VI) in UCLA IAS #1 at 25°C are calculated by OLI, as given in Table 17.

Table 17: Concentrations of oxidizers in UCLA IAS #1 at 25°C

Oxidizer	Concentration
MnO_4^-	2.80×10^{-3}
$HCrO_4^-$	1.76×10^{-2}
$Cr_2O_7^{2-}$	1.80×10^{-2}
CrO_4^{2-}	2.42×10^{-2}

Approved for public release; distribution is unlimited.

Table 18 shows the electrode potentials of the oxidizers in UCLA IAS #1 at 25°C. For reactions occurring or chemicals existing, the concentrations of manganese (II) ion, chromium (III) ion, aluminum (III) ion, iron (II) ion, iron (III) ion, and copper (II) ion are set to be 10^{-6} mol/L .

Table 18: Electrode potentials of oxidizers in UCLA IAS #1 at 25°C

Electrode	Electrode potential φ (V)
$\varphi_{MnO_4^-/MnO_2}$	1.15
$\varphi_{MnO_2/Mn^{2+}}$	0.67
$\varphi_{HCrO_4^-/Cr^{3+}}$	0.42
$\varphi_{Cr_2O_7^{2-}/Cr^{3+}}$	0.57
$\varphi_{CrO_4^{2-}/Cr(OH)_3}$	0.61
$\varphi_{Al^{3+}/Al}$	-1.80
$\varphi_{Fe^{3+}/Fe}$	-0.16
$\varphi_{Fe^{2+}/Fe}$	-0.62
$\varphi_{Cu^{2+}/Cu}$	0.16

Based on the calculation results given in Table 18, aluminum, iron, and copper can reduce manganese (VII) to manganese (II) and reduce chromium (VI) to chromium (III). However, this is just the thermal physical conclusion. Kinematically, how long it takes for the reactions to be completed is unknown, maybe minutes to hours, or maybe months to years. Therefore, extra tests are required.

It can be seen from Table 18 that permanganate is still the strongest oxidizer in IAS. Therefore, it can be assumed that permanganate reacts with metal surfaces first and is reduced to manganese (IV) oxide. The manganese (IV) oxide is a similar oxidizer to chromium (VI), and they can be assumed to react with metal surfaces at the same time.

Each permanganate ion consumes one hydrogen ion while reacting with the metal surface, see equation (28). Copper is used here as an example. Therefore, with permanganate being consumed, the pH number of the solution increases.

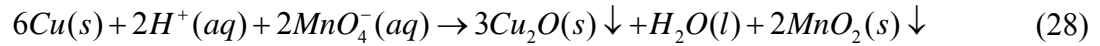


Figure 28 shows the relation between the pH number and the percentage of the permanganate reacted in UCLA IAS #1. When all the permanganate is reduced to manganese (IV) oxide, the pH number of UCLA IAS #1 will move up to 6.28.

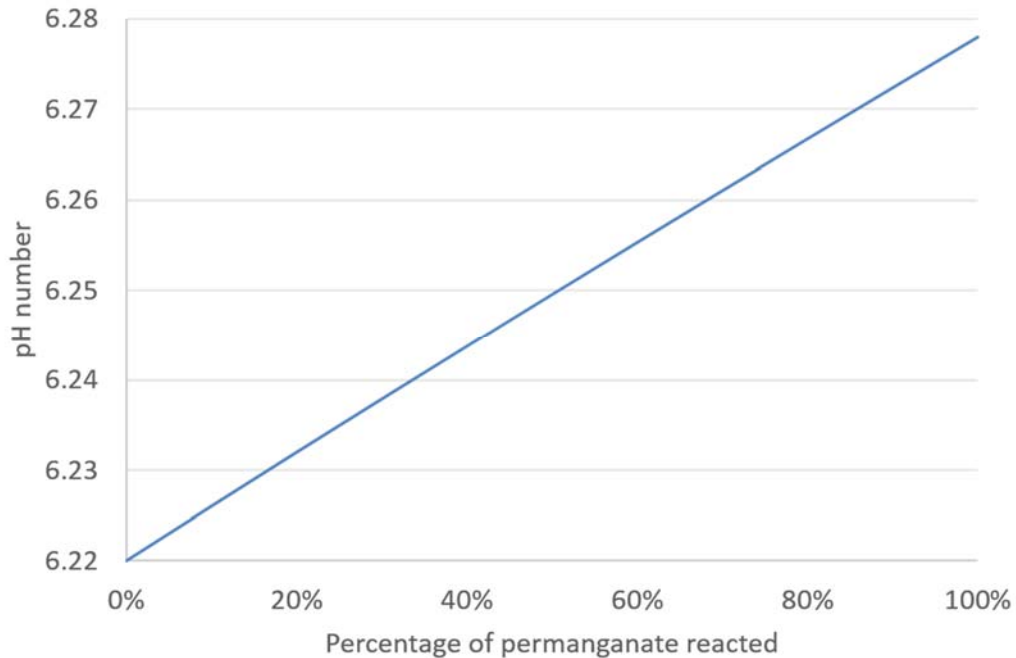


Figure 28: Relation between reacted permanganate and pH number in UCLA IAS #1

Figure 29 is a Pourbaix diagram of copper calculated by OLI with UCLA IAS #1 as the inflow. The natural pH line has a pH number of 6.28, at which permanganate is completely reacted out. It can be seen that at the time permanganate is completely reacted out, copper should be

Approved for public release; distribution is unlimited.

oxidized to copper (I) oxide or copper (II) ion. However, based on the pH number and the solubility product constant (K_{sp}) of copper (II) hydroxide, see Table 21, copper (II) ion will not exist with a concentration higher than $6.06 \times 10^{-8} \text{ mol/L}$. Therefore, copper should be oxidized to copper (I) oxide.

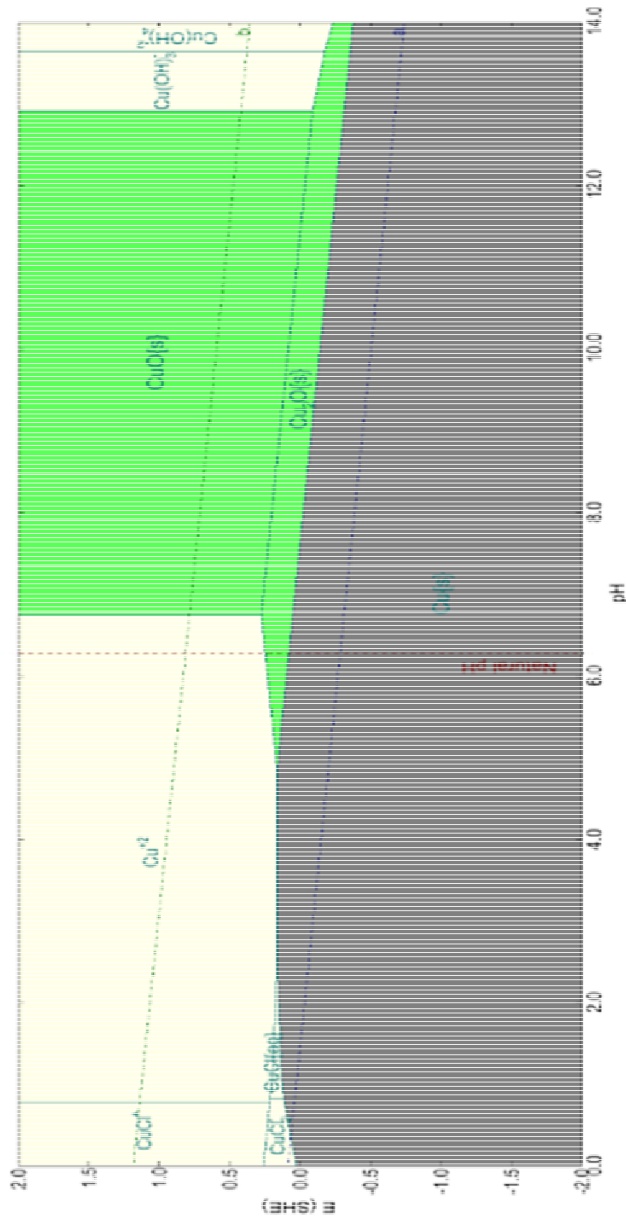


Figure 29: Pourbaix diagram of copper vs SHE at 25°C, calculated by OLI with UCLA IAS #1 as the inflow

Approved for public release; distribution is unlimited.

Figure 30 shows a mirror like copper surface, which was heated up to 120°C with a IAS droplet completely dried on it. Afterwards, it was rinsed by DI-water for 5 minutes to remove all the soluble chemicals. A layer of brownish-red coating was left on the surface, which matched the color of copper (I) oxide. In addition, Lee detected Cu_2O , by using a XRD test, in the solid coating in the QuTech™ tube.



Figure 30: Copper surface pre-treated by UCLA IAS #1

Figure 31 is a Pourbaix diagram of manganese calculated by OLI with UCLA IAS #1 as the inflow. The natural pH line has a pH number of 6.28, and the intersection point of the natural pH line and the boundary of manganese (IV) oxide and manganese (III) oxide has a E value of 0.60V. Figure 32 is a Pourbaix diagram of chromium calculated by OLI with UCLA IAS #1 as the inflow. The natural pH line has a pH number of 6.28, and the intersection point of the natural pH line and the boundary of hydrogen chromate and chromium (III) oxide has a E value of 0.71V. This means that manganese (IV) oxide will not be further reduced unless chromium (VI) is largely reacted.

Approved for public release; distribution is unlimited.

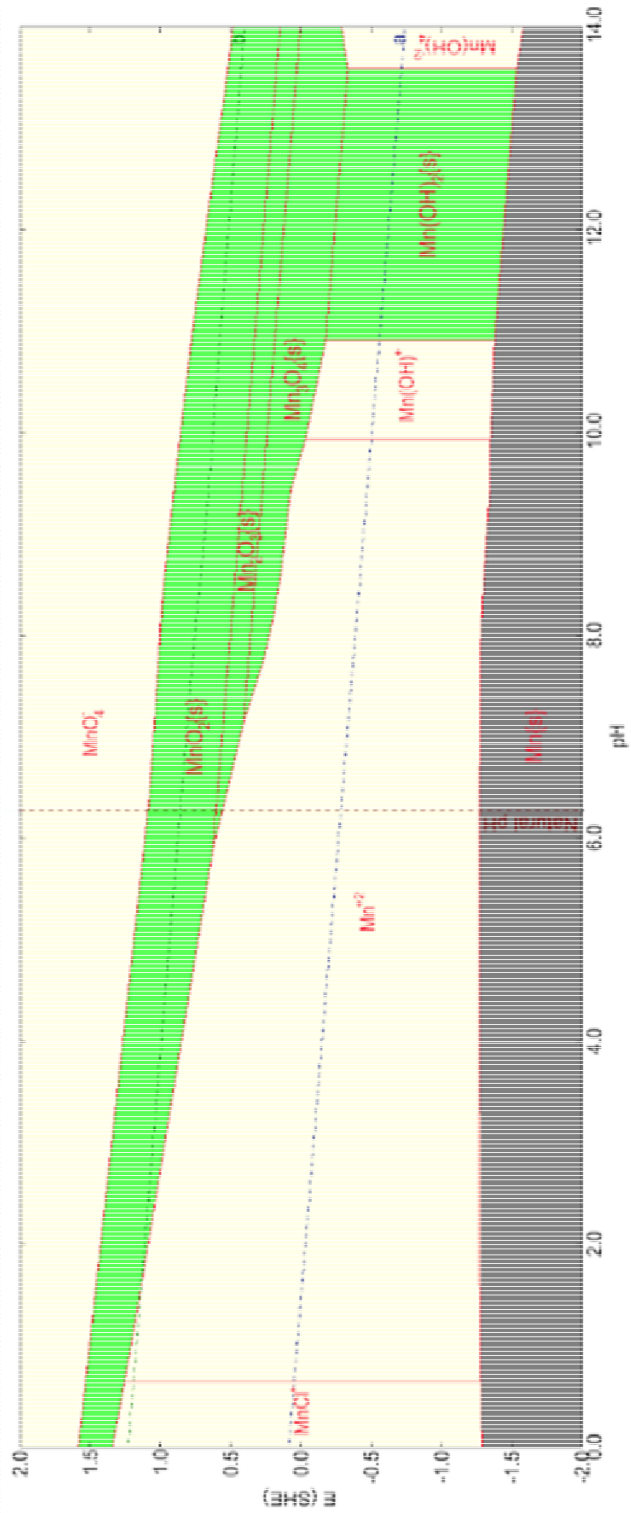


Figure 31: Pourbaix diagram of manganese vs SHE at 25°C, calculated by OLI with IAS as the inflow

Approved for public release; distribution is unlimited.

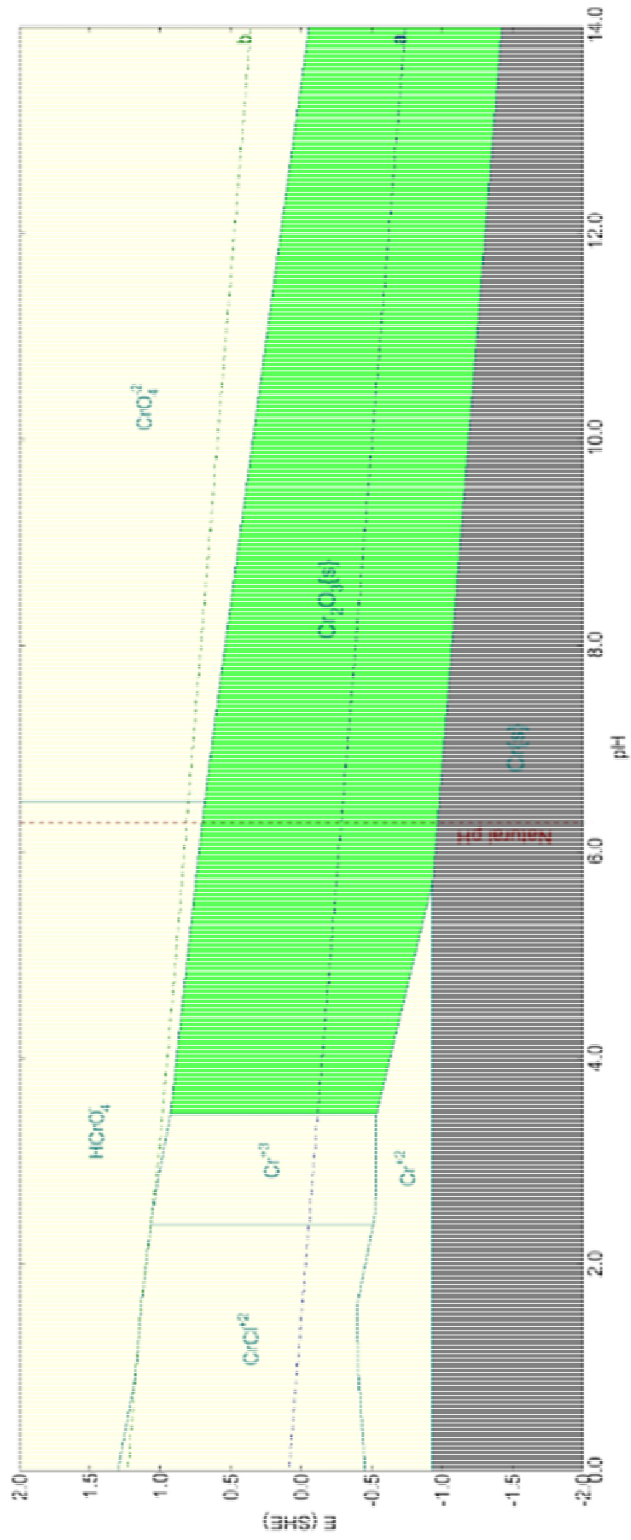


Figure 32: Pourbaix diagram of chromium vs SHE at 25°C, calculated by OLI with IAS as the inflow

Approved for public release; distribution is unlimited.

Moreover, the reaction between chromium (VI) and the copper surface also consumes hydrogen ions, as seen in reaction (29). The chromate ion is used here to represent chromium (VI), and each chromate ion consumes two hydrogen ions. The reaction between chromate ion and the copper surface can only increase the pH number and decrease the electrode potential, so chromium (III) oxide should be the product of the chromium (VI) being reduced. For the same reason, copper (I) oxide should be the product if copper can be oxidized.



Figure 33 shows the relation between the pH number and the percentage of the chromium (VI) reacted in UCLA IAS #1. With chromium (VI) being consumed, the pH number increases and can eventually reach 12.78.

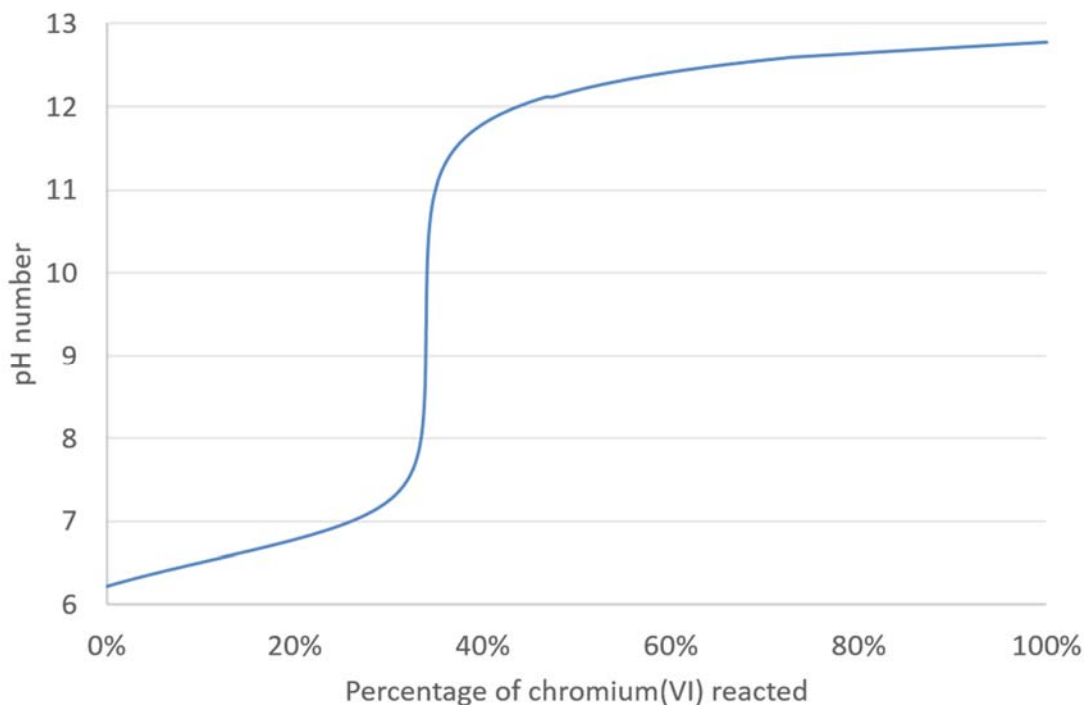


Figure 33: Relation between pH number and percentage of the chromium (VI) reacted in UCLA IAS #1

Approved for public release; distribution is unlimited.

As a result, measuring the pH number of the working fluid from a used IAS/copper phase change heat transfer device can tell us which oxidizer reacts with the surface and how much it is reacted. Figure 34 shows the comparison between a fresh IAS fluid and used IAS fluids.



Figure 34: Comparison between fresh and used IAS

The liquid in the bottle on the left in Figure 34 is fresh UCLA IAS #1, which has a dark red color and a pH number of 6.22. The one in the middle was collected from a IAS/copper thermo-syphon after being charged for two days and a four-hour test. It has an orange-yellow color, and the pH number is 6.26. The one on the right was collected from a IAS/copper thermo-syphon which was charged almost two years ago. It has an orange-yellow color, and the pH number is 6.28. Table 19 shows the pH number of the fluids collected from six used IAS/copper thermo-syphons. The measurement error of the pH meter is ± 0.01 .

Approved for public release; distribution is unlimited.

Table 19: pH number of fluids from used IAS/copper thermo-syphons

Tube #	Charged time	pH
1	2 days	6.26
2	1 week	6.24
3	3 weeks	6.25
4	2 months	6.27
5	5 months	6.26
6	2 years	6.28

The permanganate ions have a dark purple color. Dichromate ions and hydrogen chromate ions have an orange-red color, and chromate ions have a light yellow color. Fresh IAS has a combination color of all of the above, so it is dark red. Used IAS is orange-yellow, indicating that the permanganate ions must be completely reacted out. In addition, the pH number of it is about 6.27, which means that chromium (VI) is not reacted yet. Therefore, manganese (IV) should be the product of the permanganate being reduced.

More tests were done to demonstrate these conclusions. Three mirror like copper surfaces were cooked using a DI-water, a potassium permanganate solution, and a potassium dichromate solution with the pH number adjusted to 6.22 by potassium hydroxide, see Figure 35.

Approved for public release; distribution is unlimited.

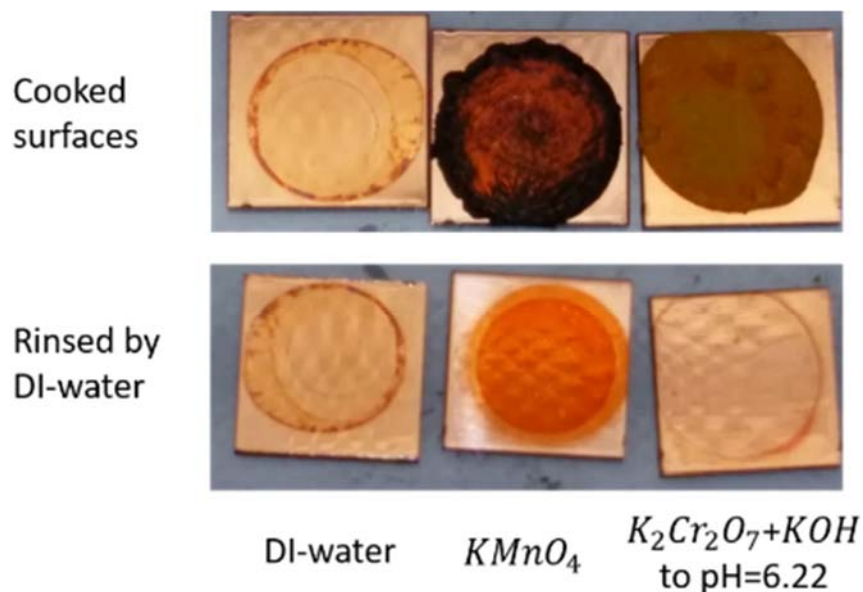


Figure 35: Mirror like copper surfaces cooked by: DI-water, potassium permanganate solution, potassium dichromate solution adjusted to pH=6.22

The surfaces were heated up to 120°C until the solution droplets were completely dried out. Afterwards, the cooked surfaces were rinsed by DI-water for five minutes. DI-water and the chromium (VI) solution only left a ring mark in the meniscus region because the copper surface was oxidized by the oxygen in the air. However, the permanganate solution coated the entire wetted region uniformly, and the coating can only be washed off by acids. It satisfies the previous conclusion that permanganate reacts with copper, but chromium (VI) does not. In addition, a chromium (VI) only IAS, UCLA Yellow #1, was charged into a copper thermo-syphon. After being tested, the thermo-syphon was cut open, and the copper surface was as shiny as a clean one. This is another evidence that chromium (VI) in IAS will not react with a copper surface. For the details, please see Section 4.5.

A glass beaker with IAS and a piece of copper surface in it was heated up till the color of IAS turned to yellow, as shown in Figure 36. The black solid generated by the reaction was

Approved for public release; distribution is unlimited.

collected, and a few droplets of 2mol/L KOH solution were added to it. It was left in the open air for a few minutes. The solution turned to dark green/blue because manganese (IV) oxide can be oxidized to potassium manganate by the oxygen in the air in a strong basic potassium hydroxide solution, see reaction (30). The solution of potassium manganate has a dark green color.

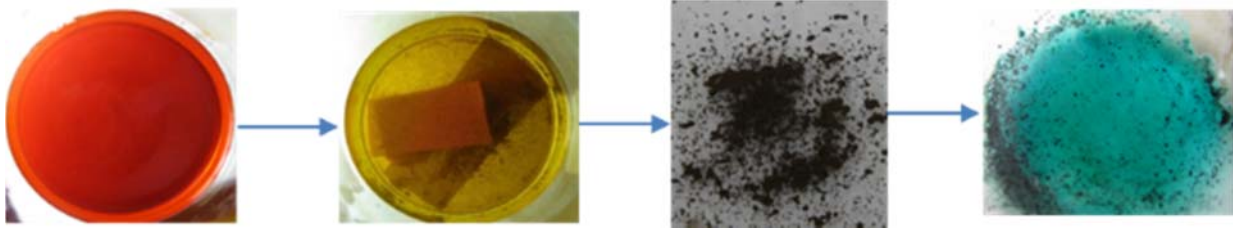


Figure 36: Existence of manganese (IV) oxide in the product



The same black solid can be seen on the internal surface of a IAS/copper thermo-syphon and an aluminum flat heat pipe, see Figure 37, and it can also be seen in the used IAS solutions collected from IAS/copper and IAS/aluminum thermo-syphons, see Figure 38.

Approved for public release; distribution is unlimited.

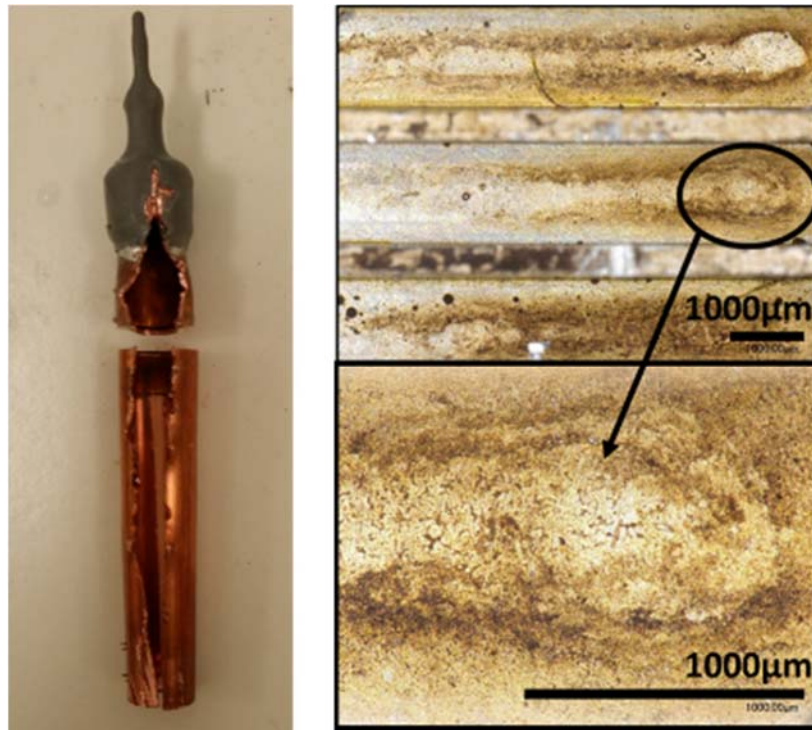


Figure 37: Black solid on IAS/copper thermo-syphon and IAS/aluminum flat heat pipe

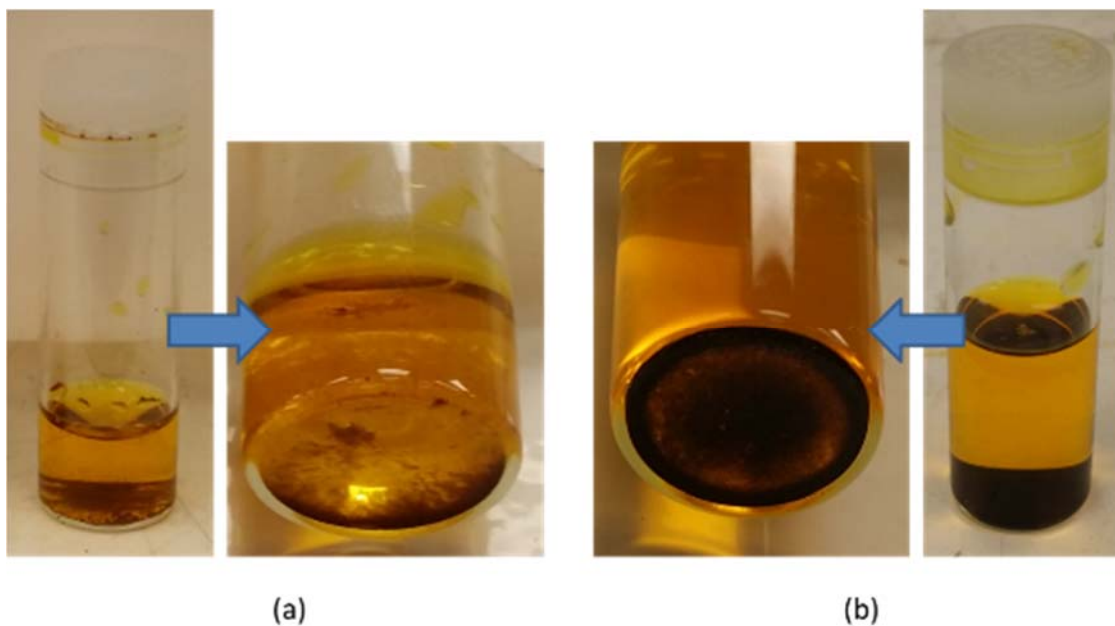


Figure 38: Used UCLA IAS #1, collected from (a) IAS/copper thermo-syphon, (b) IAS/aluminum thermo-syphon

Approved for public release; distribution is unlimited.

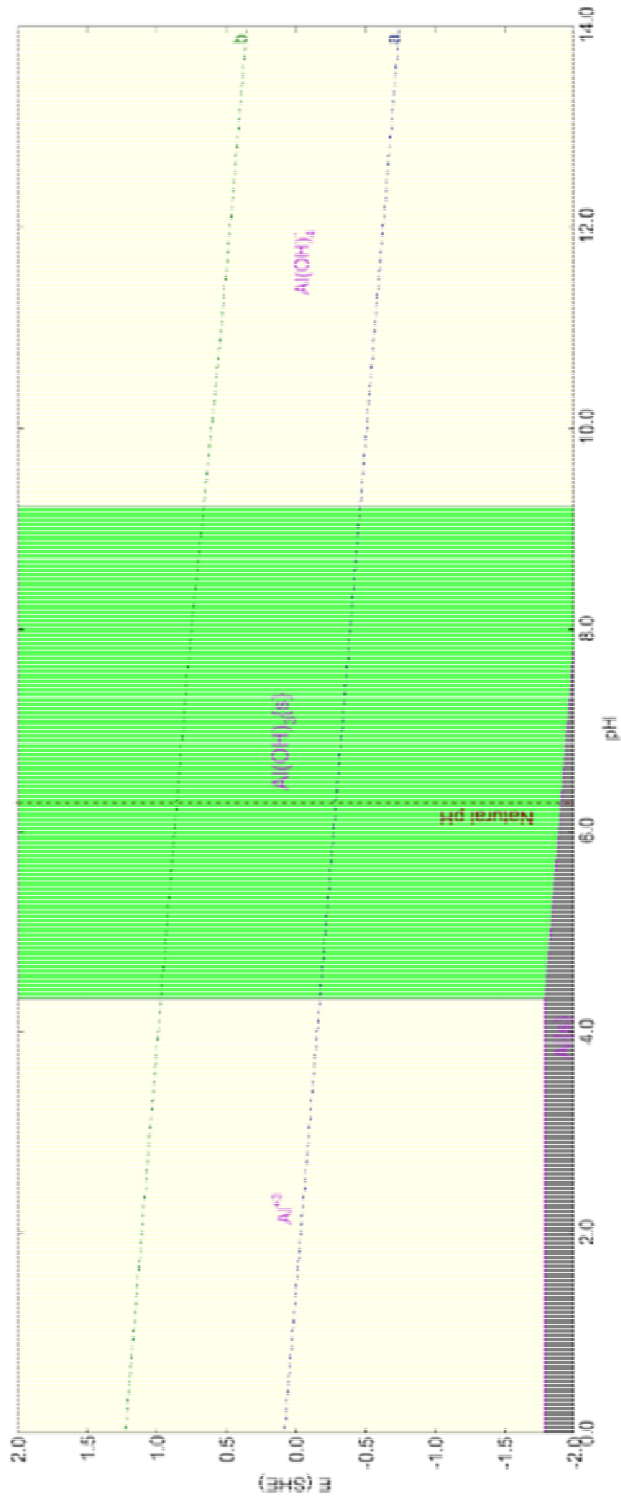


Figure 39: Pourbaix diagram of aluminum vs SHE at 25°C, calculated by OLI with UCLA IAS #1 as the inflow

Approved for public release; distribution is unlimited.

Figure 39 is a Pourbaix diagram of aluminum calculated by OLI with UCLA IAS #1 as the inflow, and the natural pH line has a pH number of 6.28. It can be seen that if the pH number is not larger than 9.2, aluminum should be oxidized to aluminum (III) hydroxide.

Table 20 indicates the pH numbers of the used IAS which were collected from aluminum thermo-syphon tests and aluminum flat heat pipe tests. It shows that the difference between the initial and final pH numbers is larger than the IAS fluids from IAS/copper devices. In addition, as the time after being charged increases, the final pH number becomes larger. However, the final pH number is much smaller than the theoretical one, at which all the chromium (VI) is completely reacted. Therefore, for IAS/aluminum devices, both permanganate and chromium (VI) react with aluminum surface, but only part of chromium (VI) will be reacted, which is a result of the passivation effect of IAS slowing down the reaction rate of aluminum and chromium (VI).

Table 20: pH numbers of used IAS, collected from aluminum phase change heat transfer devices

IAS	Test	Initial pH	Final pH
UCLA #1	Al thermo-syphon	6.18	6.65
UCLA #1 batch 2	Al FHP	6.31	6.71
UCLA #1 batch 2	Al FHP	6.31	6.87
UCLA #1	Al thermo-syphon	6.18	7.03 (2yrs)

Iron is not the main focus of this report, so it will only be discussed theoretically. As a reducer, iron is weaker than aluminum, but stronger than copper. It reacts with water and the oxidizers in IAS, but the reaction rate is very slow. Figure 40 is a Pourbaix diagram of iron calculated by OLI with UCLA IAS #1 as the inflow. The natural pH line has a pH number of 6.28. As a result, within the possible pH number range of IAS, iron can only be oxidized to iron (III) oxide.

Approved for public release; distribution is unlimited.

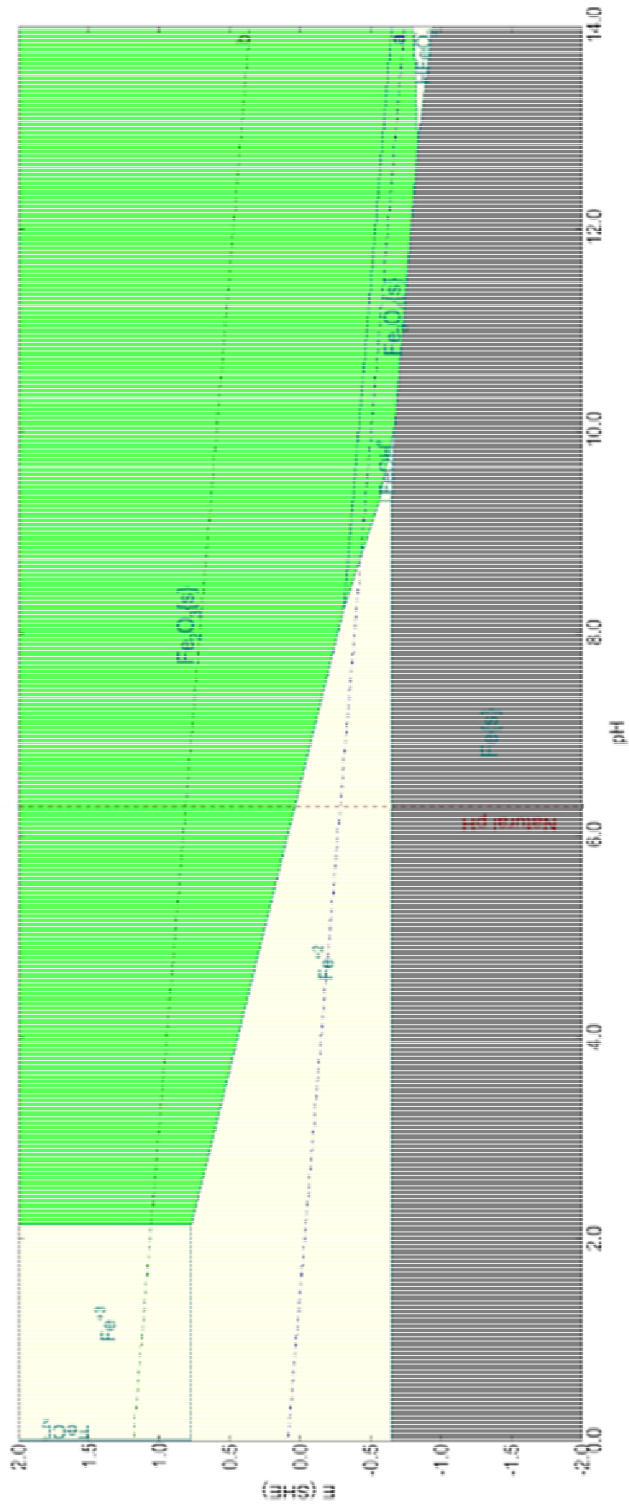


Figure 40: Pourbaix diagram of iron vs SHE at 25°C, calculated by OLI with UCLA IAS #1 as the inflow

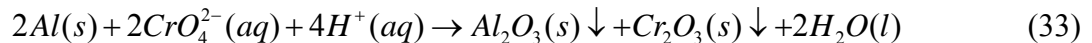
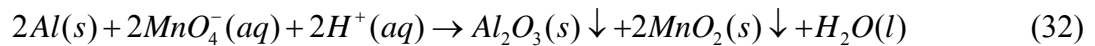
Approved for public release; distribution is unlimited.

To summarize, for different surface materials, the redox reactions between the oxidizers in IAS and metal surfaces are listed below:

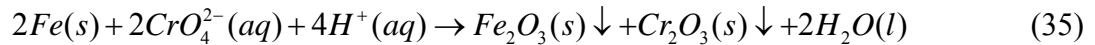
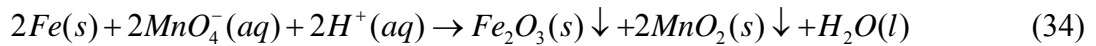
For copper,



For aluminum,



For steel or stainless steel,



Permanganate will finish reacting with metal surfaces in several hours, and the reaction can be accelerated by being heated up. Chromium (VI) only plays a role of oxidizer when IAS is used in aluminum or iron heat transfer devices. Because of the passivation effect of IAS, the reaction between chromium (VI) and aluminum or iron is slowed down sharply, and only part of the chromium (VI) will be reacted during the lifetime.

3.3.4. Hydrophilic coatings

In an operating heat pipe, water evaporates in the evaporator and is condensed in the condenser. In addition, the vapor of IAS has been demonstrated to be pure water vapor, so when

Approved for public release; distribution is unlimited.

IAS is used as the working fluid, the local concentrations of chemicals in the evaporator will be larger than the initial bulk ones because of the evaporation. Moreover, with the temperature increasing, the solubility of some compounds in IAS decreases. The result will be coatings of surfaces in the evaporating region.

Table 21 shows the solubility product constants of the related insoluble compounds at 18~25°C [30].^{m, n}

Table 21: K_{sp} of related insoluble compounds at 18-25°C

Chemical	K_{sp}
$Al(OH)_3$	1.3×10^{-33}
Ag_2CrO_4	2.0×10^{-12}
$AgOH$	2.0×10^{-8}
$CaCrO_4$	7.1×10^{-4}
$Ca(OH)_2$	5.5×10^{-6}
$Cu(OH)_2$	2.2×10^{-20}
$Fe(OH)_2$	8.0×10^{-16}
$Fe(OH)_3$	4.0×10^{-38}
$MgCrO_4$	4.2×10^{-6}
$Mg(OH)_2$	1.8×10^{-11}
$Mn(OH)_2$	1.9×10^{-13}
$SrCrO_4$	2.2×10^{-5}

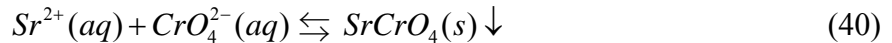
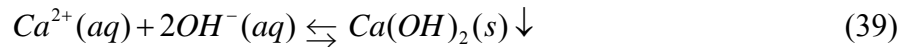
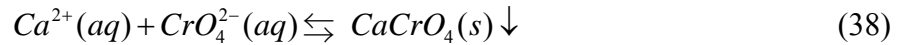
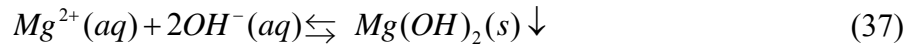
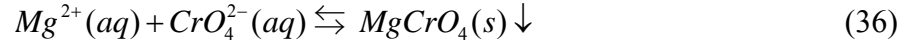
The solubility product constants of the products from the oxidation reactions are much smaller than the other ones. As a result, when pH number is at 6.22 or larger, the products from the oxidation reactions can be seen as completely insoluble, and they build up the first irremovable coating layer on the surface. Afterwards, with the temperature increasing, the second coating layer will be generated because of the constituents reaching the solubility limits. Once the temperature

^m <http://www.aqion.de/site/16>

ⁿ http://www4.ncsu.edu/~franzen/public_html/CH201/data/Solubility_Product_Constants.pdf

Approved for public release; distribution is unlimited.

decreases, they will be re-dissolved. Reactions (36), (37), (38), (39), and (40) show the five possible coatings which might be generated because of reaching the solubility limits.



Magnesium hydroxide and calcium hydroxide will only be generated instead of magnesium chromate and calcium chromate when the pH number is larger than 11, which will never be reached in an operating heat transfer device charged with IAS. Therefore, magnesium hydroxide and calcium hydroxide will not be considered.

The amount of magnesium (II) ions in IAS is very small. A new solution, **UCLA IAS #3.2**, was made with no silver or magnesium, and all the other chemicals had the same concentrations as UCLA IAS #1. It was tested in the copper thermo-syphon test, which will be introduced in Section 4.5, and the heat transfer performance was identical to that of UCLA IAS #1. Therefore, magnesium is not necessary in IAS. The original IAS might be made by some hard water, such as tap water, because the concentration of magnesium in the original IAS is 14mg/kg, which is very close to that in the tap water of China, 10-15mg/kg.

Approved for public release; distribution is unlimited.

Table 22 [31] and Table 23 [32] show the solubility of calcium chromate and strontium chromate in water. It shows that the solubility of calcium chromate and strontium chromate decreases with the temperature increasing. As a result, these chemicals will automatically coat the hottest place, the evaporator, in the device. Once the evaporating region is changed to another place, such as the other end of a heat pipe or another location on a TGP, the previously formed coating will be washed off by the condensed pure water, and the chemicals will be brought back to the new evaporator, by the liquid back flow, and form a new coating.

Table 22: Solubility of calcium chromate in water

Solubility (g/kg Water)			
25°C	20.49	80°C	6.88
35°C	17.04	110°C	3.47
45°C	13.96	120°C	2.99
50°C	12.25	130°C	2.37
55°C	11.29	150°C	1.86
60°C	10.73	160°C	1.62
70°C	7.98	170°C	1.48

Table 23: Solubility of strontium chromate in water

Solubility (g/kg Water)	
25°C	0.96
50°C	0.9
75°C	0.8

Moreover, these salts will coat the surface with a porous structure, see Figure 41, and the salts are hydrophilic. The porous hydrophilic coating is the main reason of the improvement of the heat transfer performance.

Approved for public release; distribution is unlimited.

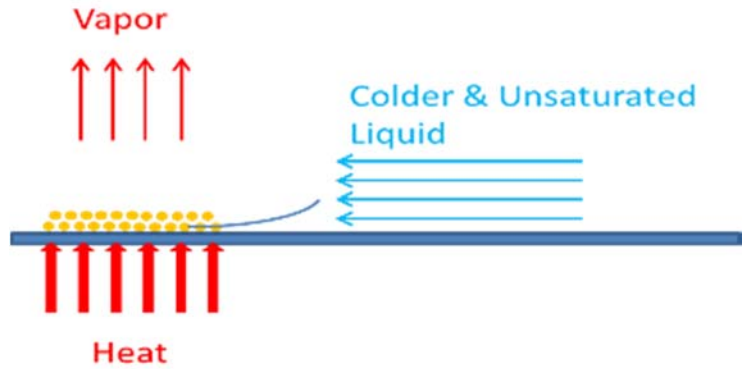


Figure 41: How hydrophilic coating works

A higher evaporating temperature is usually associated with a larger heat flux, a higher vapor pressure, and more vapor and back flow of water in the adiabatic and condensing regions. Therefore, compared to the initial IAS, a higher evaporating temperature makes the liquid in the evaporating region be condensed more.

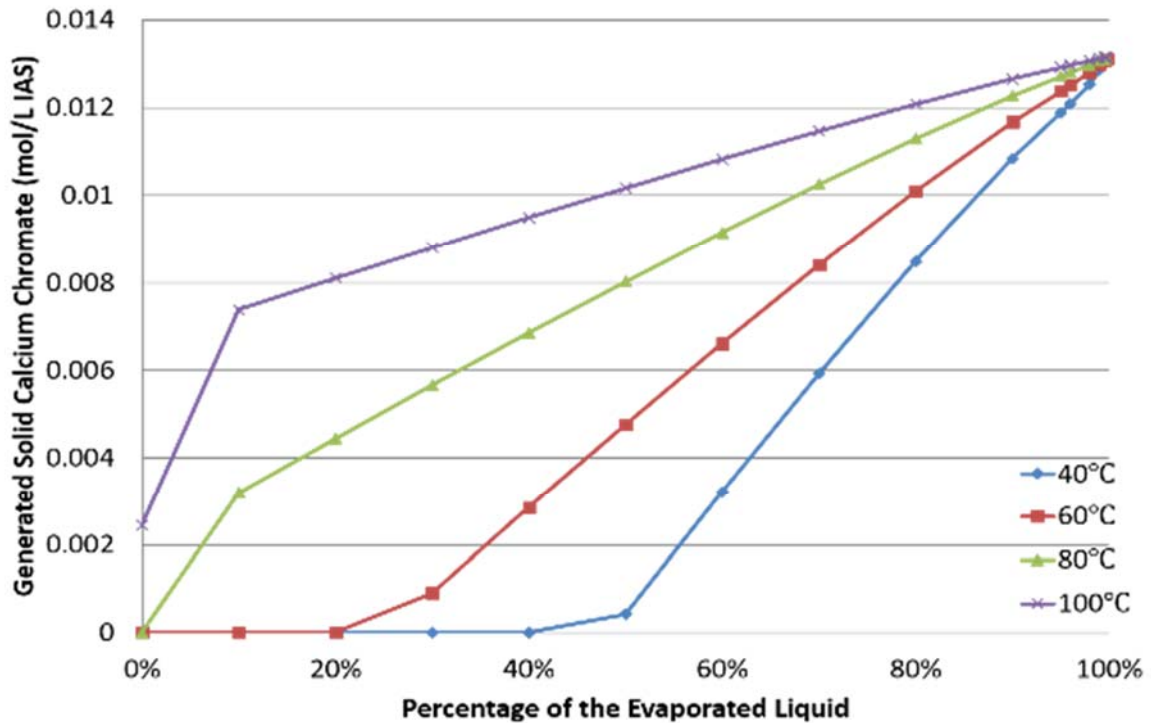


Figure 42: Relation between calcium chromate and evaporated liquid at different temperatures

Approved for public release; distribution is unlimited.

Calcium chromate is the main component of the hydrophilic coating. As shown in Figure 42, with the temperature increasing or the liquid evaporating, the amount of the generated calcium chromate increases. However, at low evaporating temperatures, calcium chromate will not be generated in large amounts, so the recommended evaporating temperature for calcium chromate will be no lower than 80°C for UCLA IAS #1. In addition, by changing the total concentration of the calcium ion in IAS, the amount of the generated calcium chromate at different temperatures can be controlled.

Strontium chromate works the same way as calcium chromate, see Figure 43. However, compared to calcium chromate, strontium chromate has a larger molecule size, which leads to a larger particle size. Therefore, strontium chromate might be used to change the structure of the hydrophilic coating. In addition, strontium chromate has a smaller solubility compared to calcium chromate, so it can be used to generate coating at low temperatures.

Approved for public release; distribution is unlimited.

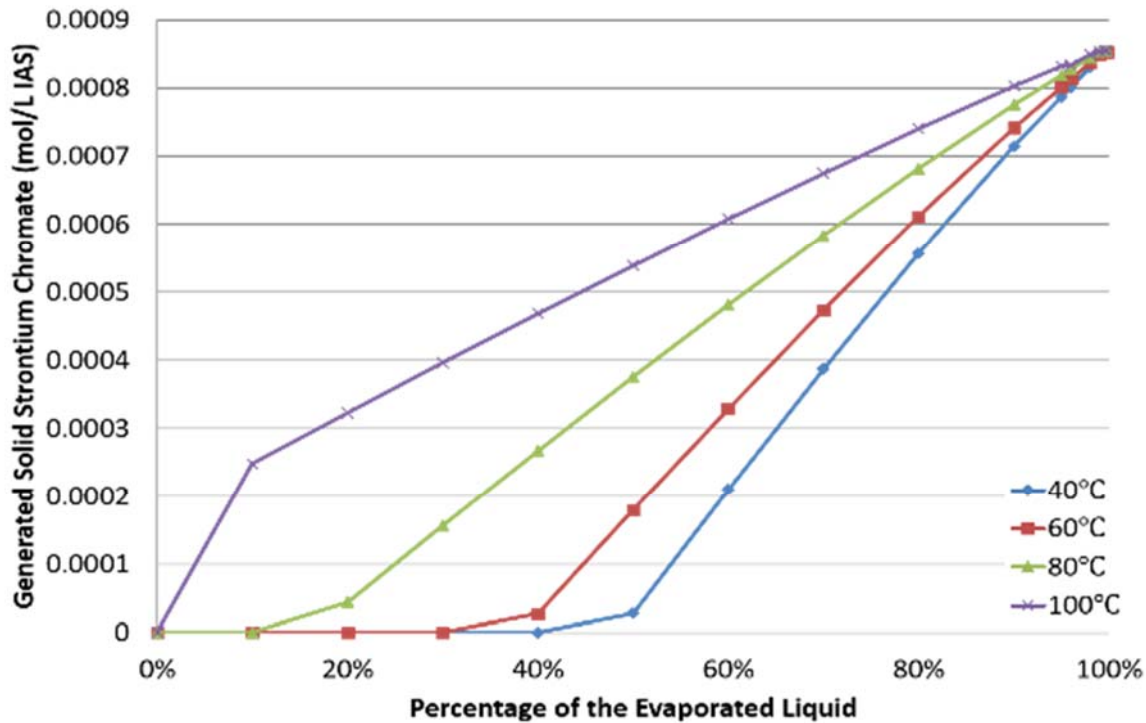
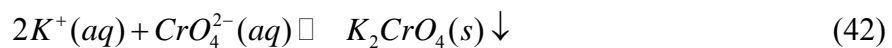
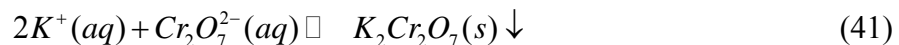


Figure 43: Relation between strontium chromate and evaporated liquid at different temperatures

As stated above, calcium chromate and strontium chromate generate a porous structured hydrophilic coating in the evaporating region. However, it is not the only reason of which IAS has a performance superior to water. In the meniscus region, once the surface is close to dry-out, a thin layer of potassium dichromate or potassium chromate will be generated and coat the surface, outside of the hydrophilic coating, see reactions (41) and (42).



Approved for public release; distribution is unlimited.

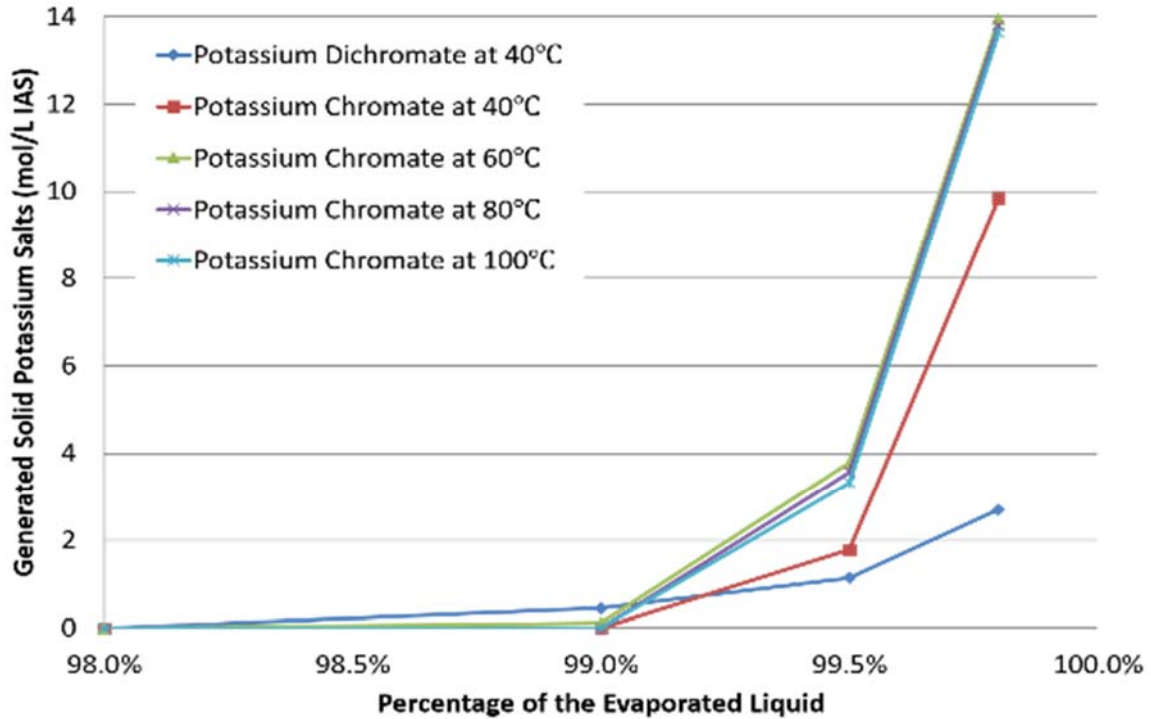


Figure 44: Relation between potassium dichromate/chromate and evaporated liquid at different temperatures

As shown in Figure 44, if over 99% of the water is evaporated, solid potassium dichromate or potassium chromate, which depends on the evaporating temperature, will be generated and coat the surface. If the evaporating temperature is 40°C or lower, both potassium dichromate and potassium will be generated, but only potassium chromate will be generated if it is above 40°C. Both potassium dichromate and potassium chromate have large solubility in water, and that makes the re-wetting process easier and faster. However, in an operating water base heat pipe or thermosyphon, the evaporating temperature will not be lower than 40°C at dry out. Therefore, potassium chromate should be the one left on the surface when it is locally dried out.

In addition, sodium chromate is a hygroscopic salt, and it absorbs water vapor from the air to become a solution, see Figure 56 in Section 3.4. Based on OLI simulations, there is no solid sodium chromate generated until the water is completely evaporated out. Because of the strong

bonding force between sodium chromate and water, it will be very difficult for the surface to dry out. As a result, the surface is super hydrophilic during the operation, and the meniscus retreating, dry-out, is largely delayed. This is an important part of the heat transfer enhancement.

Further, the pH number affects the on-set temperature of the hydrophilic coatings being generated. Calcium chromate is the main component of the hydrophilic coating. Figure 45 shows the OLI simulation result for the effect of the evaporating temperature and the final pH number of the solution on the generation of calcium chromate. It shows that, with the temperature rising, the amount of calcium chromate increases, and a larger pH number can make the process occur earlier at lower temperatures.

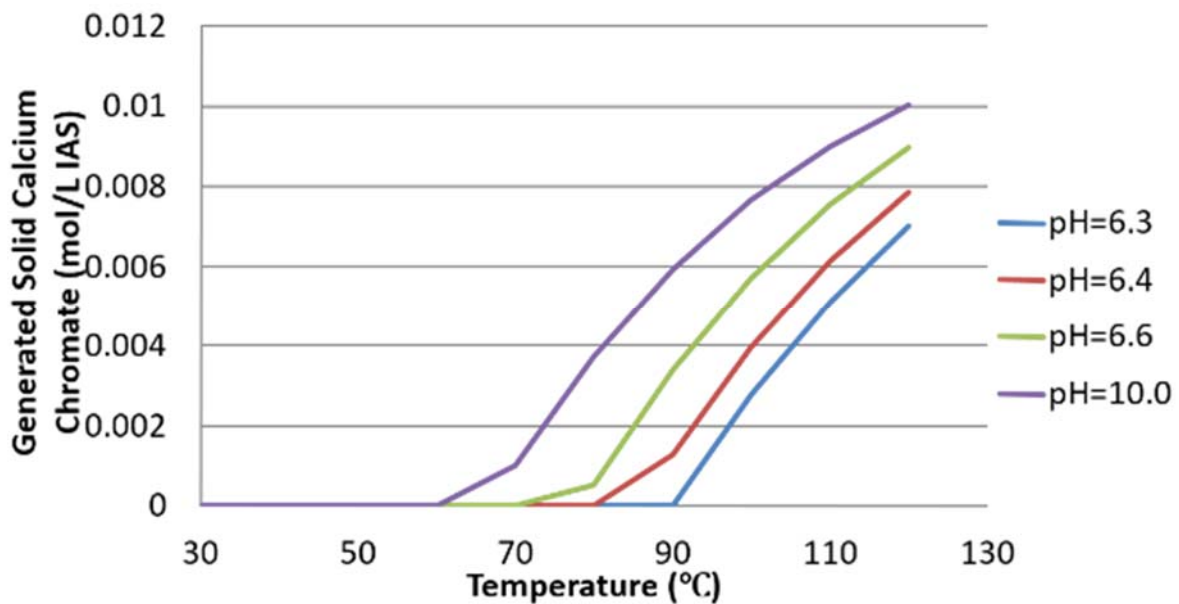


Figure 45: The effects of temperature and pH number to the hydrophilic coating generation

In order to obtain a higher final pH number, there are two methods can be used. The first one is increasing the initial pH number with bases such as sodium hydroxide, but this will weaken the oxidation ability of the oxidizers. The other is increasing the amount of permanganate, but this

Approved for public release; distribution is unlimited.

will bring in more manganese (IV) oxide, which might clog the wick. A correct initial pH number and amount of permanganate is important.

The right thickness of the hydrophilic coating can improve the surface wettability, increase the effective surface area, enhance the heat transfer performance, and delay the dry out point, but excessive coating will lower the thermal conductance from the device surface to the working liquid and eventually clog the vapor space of the wicked devices. Therefore, optimization needs to be done to find the thickness range for the best performance, the lowest effective thermal resistance.

To sum up, the hydrophilic coatings (chromate salts) will be generated under the conditions seen Table 24.

Table 24: Generation conditions of hydrophilic coatings

Coating chemicals	Generated conditions
$CaCrO_4$	Generated at higher temperatures
$SrCrO_4$	Generated at lower temperatures
K_2CrO_4	Generated when closed to dry out and $T \geq 40^\circ C$
$Na_2CrO_4 \cdot nH_2O$	Generated when the surface is completely dried out

All above show what will happen if a static IAS fluid is in contact with a hot metal surface. However, in an operating phase change heat transfer device, there is a liquid back flow, which is almost pure water, entering the evaporator. Because of the advection, all the chemicals will be pushed towards the meniscus region, at where the evaporation takes place. As a result, an analysis of advection against diffusion is required to estimate where solid chromate salts start to be generated in an operating phase change heat transfer device, see Section 4.2.

3.3.5. Silver effect

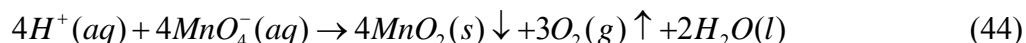
Based on the NRL report^o, the silver ions in IAS were assumed to play a role in aluminum passivation. When IAS is used as the working fluid in an aluminum heat pipe or thermo-syphon, the silver ion is easily reduced by aluminum and becomes silver metal, as shown in reaction (43). The silver metal might work as a bridge in the electrochemistry process of aluminum passivation.



However, the amount of silver in IAS is tiny, and it is almost below the detection limit of the ICP-OES tests. Therefore, more experimental tests are required to justify if silver is necessary in IAS. More tests details will be discussed in Section 5.2.3. The test results show that silver is not necessary in IAS, and, as a result, will be eliminated from the future IAS and will not be considered in copper studies reported in Chapter 4.

3.3.6. Disassociation during storage

During a long term storage, some suspensions will appear in an IAS fluid. One reason is that small magnesium chromate particles group into large ones and sink. The other reason is because of the permanganate disassociation shown in the reaction (44).



In the disassociation reaction, each permanganate ion consumes the same amount of hydrogen ions as the one that reacts with surface materials in reactions (31), (32), and (34).

^o Non-public report: Naval Research Lab, "Chemical Analysis of Posnett International Company Inc. Heat Pipe Solution, Generation 2.5".

Therefore, the amount of the hydrophilic coating generated by an old IAS fluid remains the same, but its ability to oxidize the surfaces becomes weaker.

However, this disassociation reaction is very slow at the room temperature. The pH number of a two years old UCLA IAS #1 was measured to be 6.23, and the solid suspension sunk in the bottle was much less than that in the original IAS. The original IAS must have been stored for a long time, or it was in contact with some reductive materials, such as rubber plug or some other organic materials.

3.4. Coating study

The porous structure created by the oxides and chromates could be the main reason for the enhancement of heat transfer. For this reason, a study of the effect of each coating on contact angle and structure is performed and compared to those generated by the complete IAS.

Five groups of solutions, each of which generates only one chemical coating, will be made and used to cook a mirror like copper surface. Table 25 shows the initial chemical concentrations and the generated coating constituents of the solutions. The resulting treated surfaces will be undergoing contact angle tests and SEM observations.

Table 25: Solutions used in coating study on copper surfaces

Chemical	Initial Concentration	Coating
$KMnO_4$	same [Mn] as it in UCLA IAS #1	$Cu_2O + MnO_2$
$K_2Cr_2O_7 + KOH$ (1:2)	same [Cr] as it in UCLA IAS #1	K_2CrO_4
$CrO_3 + NaOH$ (1:2)	same [Cr] as it in UCLA IAS #1	Na_2CrO_4
$Ca(OH)_2 + CrO_3$ (1: 1)	same [Ca] as it in UCLA IAS #1	$CaCrO_4$
$Sr(OH)_2 + CrO_3$ (1: 1)	Same [Sr] as it in UCLA IAS #1	$SrCrO_4$

Figure 46 is a DI-water droplet on a mirror like copper surface. The contact angle is a little larger than 90 degrees, so a smooth copper surface is somewhat hydrophobic.

Approved for public release; distribution is unlimited.



Figure 46: DI-water on mirror like copper surface

Figure 47 is a mirror like copper surface cooked with a potassium permanganate solution. For surface cooking, a mirror like copper surface was heated up to 120°C, and then 4 droplets potassium permanganate solution, about 0.2ml, were dropped on it. The solution amount was calculated to have the same ratio of solution volume and surface area as the thermo-syphon test in Chapter 4. The surface was heated for 5 minutes to reach a chemical equilibrium and then dried out. During the heating, DI-water was added to keep the surface wet.

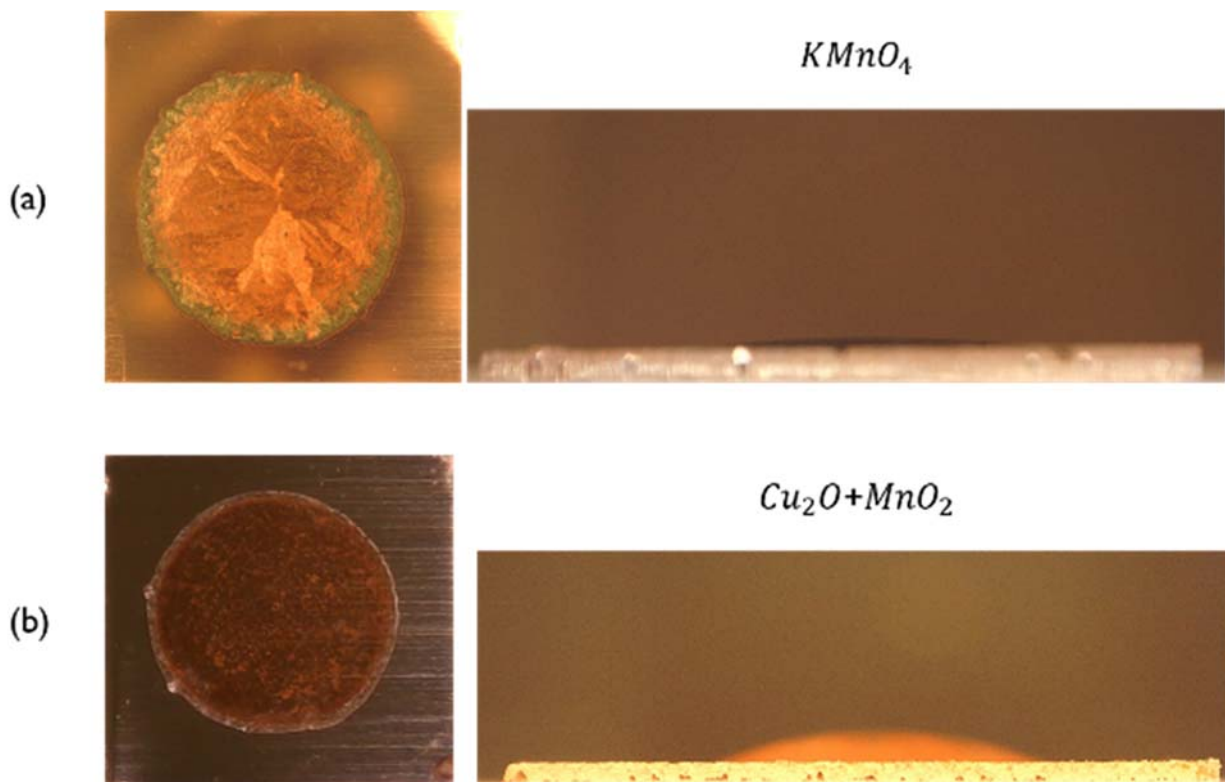


Figure 47: DI-water on mirror like copper surface cooked by potassium permanganate: (a) pre-treated, (b) rinsed by DI-water

Figure 47 (a) is a surface just treated by potassium permanganate. The amount of permanganate is more than the need of reacting with the wetted copper surface, so there is permanganate left on the surface. When a water droplet is added to the coating, it immediately spreads throughout the coated area because potassium permanganate is a soluble compound. Another potassium permanganate treated surface is rinsed by DI-water for five minutes, and then dried out by air convection, see Figure 47 (b). There is no soluble chemical compound anymore, and the surface is still more hydrophilic than a clean copper surface.

Figure 48 is the SEM image of the surface pre-treated by potassium permanganate, and Figure 49 is the SEM image of the surface after being rinsed by DI-water. After being rinsed by DI-water, all the soluble chemical compounds should be gone, and the coating left should be oxides

Approved for public release; distribution is unlimited.

of copper and manganese. It can be seen that the coating structure in Figure 49 is similar to the one observed in the vapor chamber test, see Section 2.5.1.1. Therefore, the coating left on the boiling target in the vapor chamber test should mainly be the oxides of copper and manganese.

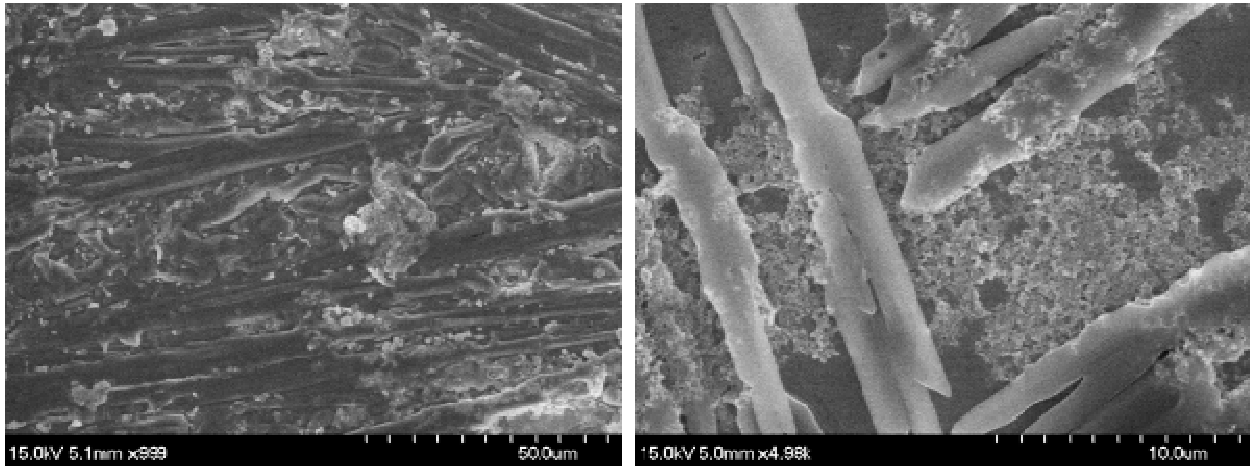


Figure 48: SEM image of a copper surface pre-treated by potassium permanganate

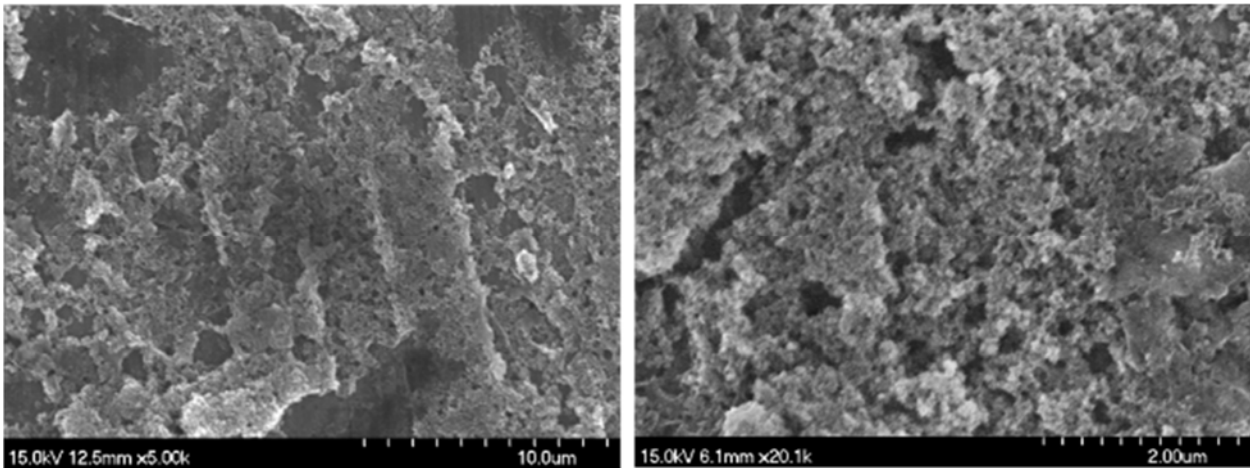


Figure 49: SEM image of a copper surface pre-treated by potassium permanganate and then rinsed by DI-water

Figure 50 is a copper surface pre-treated by calcium chromate. When water is added on the coating, it is sucked into the coating, just like a porous wick. The extra water is left outside and forms a dome shape, but it does not cover the whole coating region. Figure 51 is the SEM image of the surface pre-treated by calcium chromate.

Approved for public release; distribution is unlimited.



Figure 50: DI-water on mirror like copper surface cooked by calcium chromate

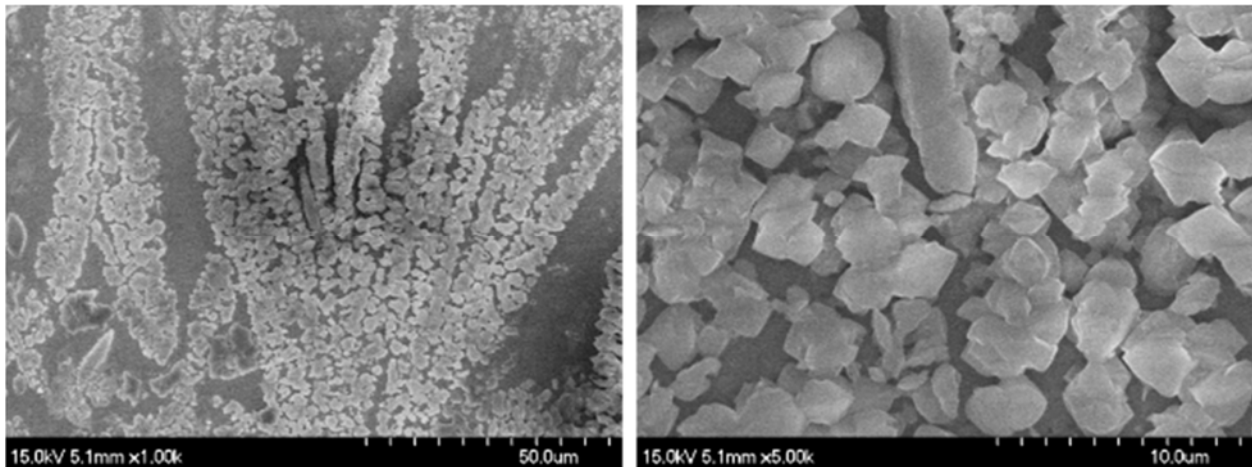


Figure 51: SEM image of a copper surface pre-treated by calcium chromate

Figure 52 is a copper surface pre-treated by strontium chromate. The amount of strontium in IAS is small, so it does not contribute a lot to the coating or contact angle. In case if there is a larger amount of strontium chromate coating the surface, it should be similar to calcium chromate. Figure 53 is the SEM image of the copper surface pre-treated by strontium chromate.

Approved for public release; distribution is unlimited.

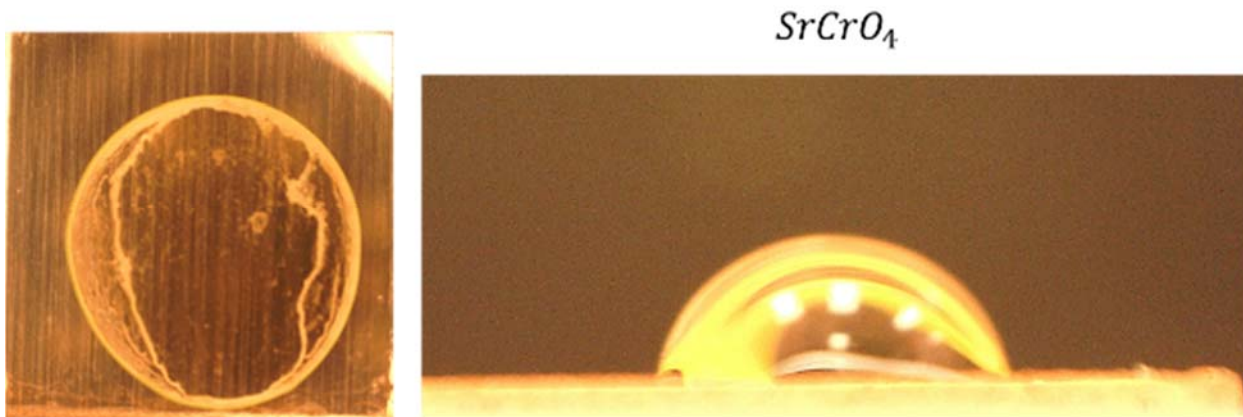


Figure 52: DI-water on mirror like copper surface cooked by strontium chromate

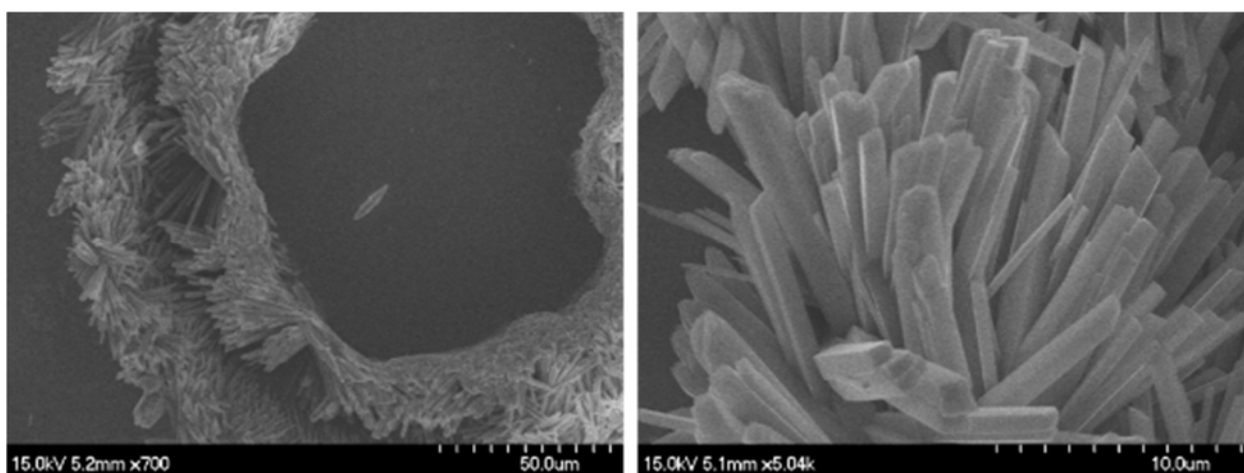


Figure 53: SEM image of a copper surface pre-treated by strontium chromate

Figure 54 is a copper surface pre-treated by potassium chromate. When water is added on the coating, the coating is dissolved into the water immediately, and the solution covers the whole coated region. With more water added, all the coating will be dissolved completely, and the copper is as shiny as a clean one. Figure 55 is the SEM image of the copper surface pre-treated by potassium chromate.

Approved for public release; distribution is unlimited.

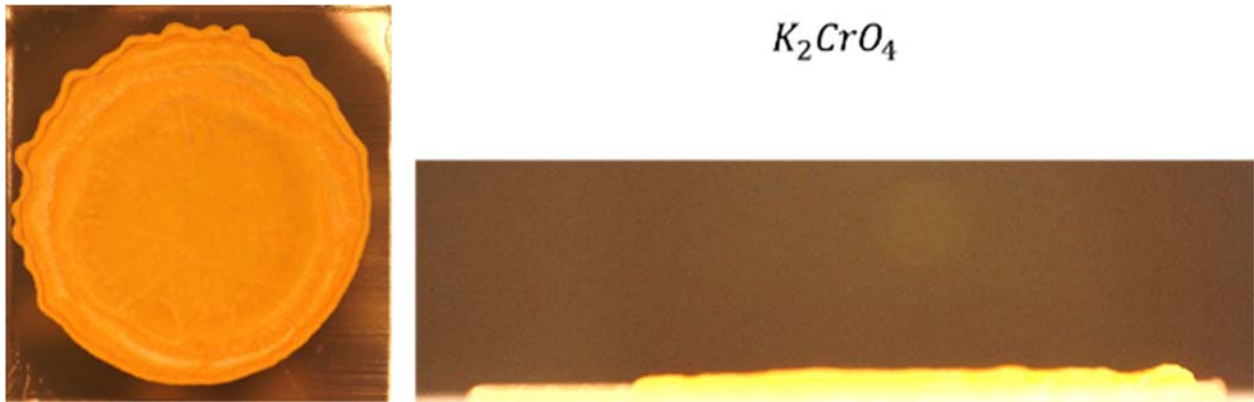


Figure 54: DI-water on mirror like copper surface cooked by potassium chromate

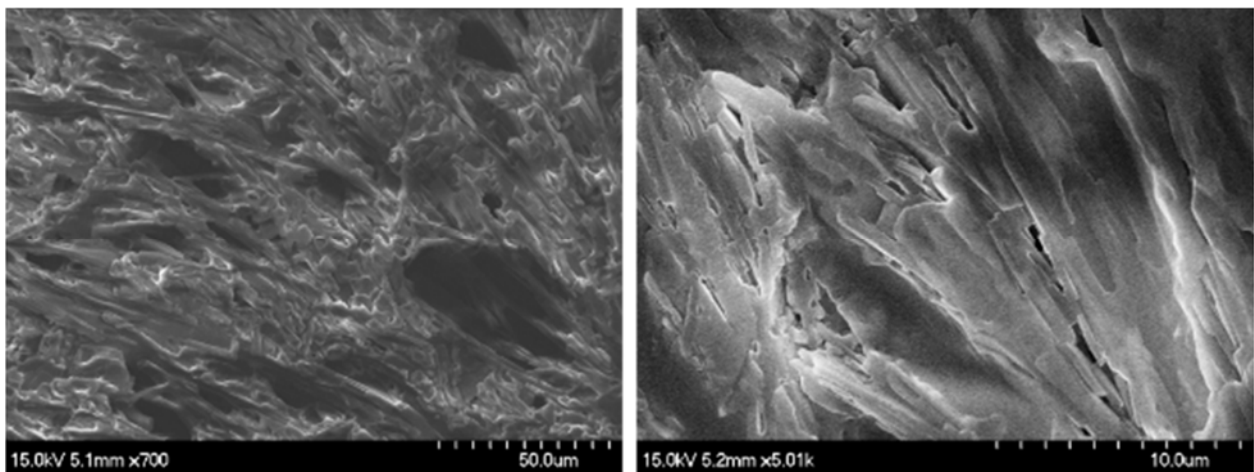


Figure 55: SEM image of a copper surface pre-treated by potassium chromate

Five mirror like copper surfaces were pre-treated by sodium chromate. However, one to two hours later, the solid coatings all became solutions, as seen in Figure 56. It is because the sodium chromate is hygroscopic, and it absorbs water vapor from the air. Therefore, no SEM test or contact angle test was done for sodium chromate.

Approved for public release; distribution is unlimited.

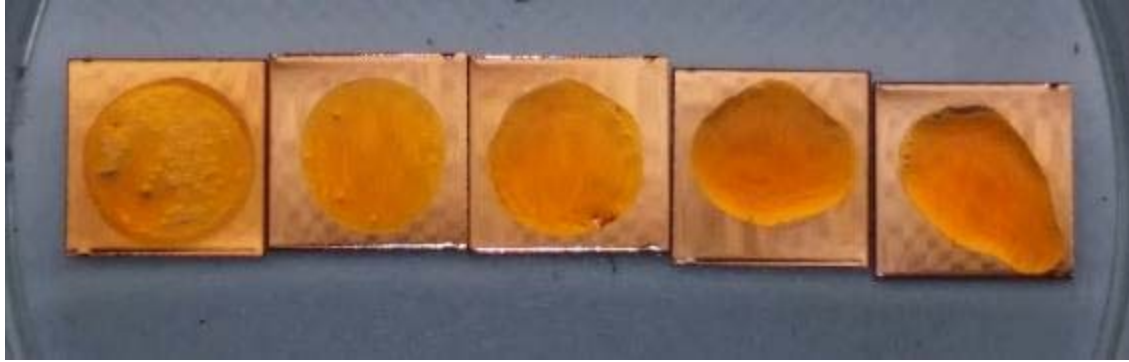


Figure 56: Copper surface pre-treated by sodium chromate, 2 hours after the pretreatment

To sum up, all the coatings help by improving the surface wettability. However, only the oxides coatings generated by potassium permanganate are fixed on the copper surface, and cannot be washed off by DI-water. None of the chromate coatings has a strong bonding force with copper surfaces. They are deposited on the copper surface and can be easily wrapped off.

Unfortunately, the coating structure of IAS does not look like any of the individual coatings above, see Figure 57. When all the coatings are generated at the same time, it forms a new structure which is completely different with the one of each chemical above.

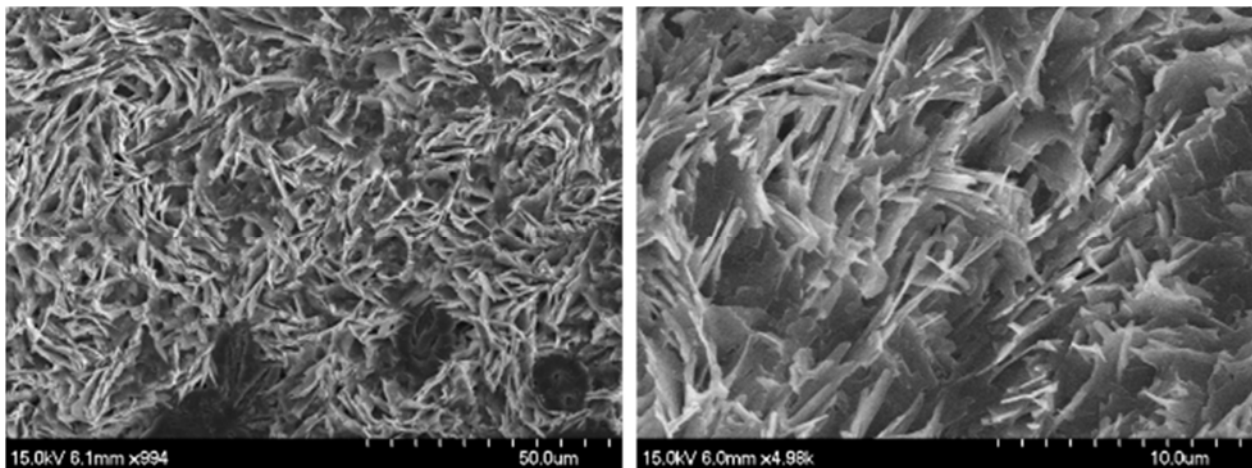


Figure 57: SEM image of a copper surface pre-treated by IAS

Approved for public release; distribution is unlimited.

In conclusion, the coating structure of IAS will not be predicted by the amount of any individual chemical. Some other methods are needed to investigate the performance enhancement effect of IAS.

An interesting phenomenon was detected while cooking copper surfaces with potassium permanganate solutions or IAS solutions, see Figure 58. When the plate temperature is adjusted to higher values, in this case 135°C, the coatings generated by the solutions of chromate salts are still within the initially wetted region. However, the ones on the copper surfaces cooked by IAS or potassium chromate were not anymore. The meniscus started to creep, and the wetted region expanded.

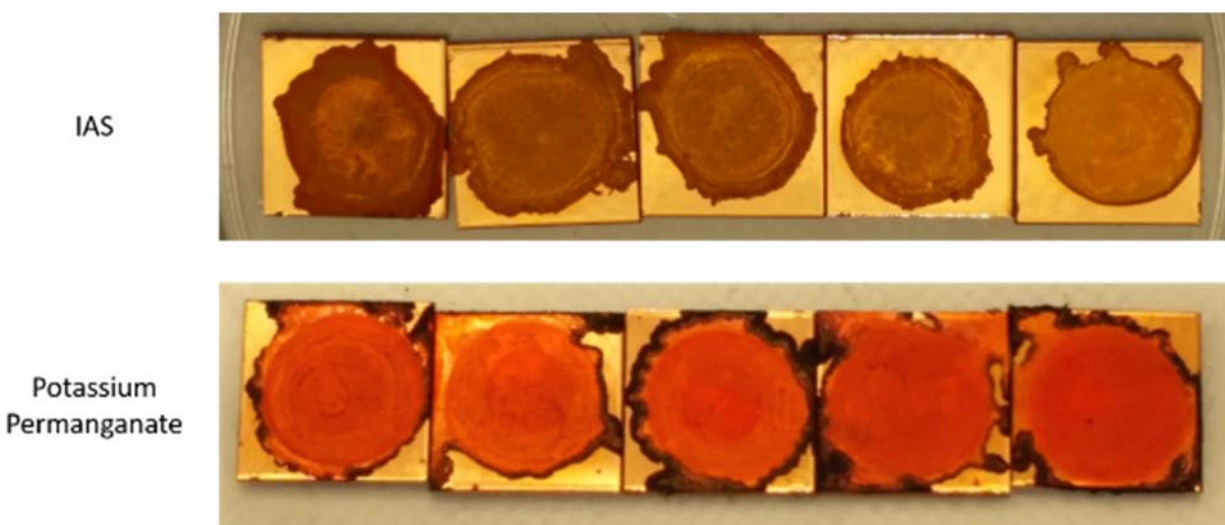


Figure 58: Copper surfaces cooked by IAS or potassium permanganate with the plate temperature 135°C

Figure 59 shows the coated regions compared to the initially wetted regions for IAS, potassium permanganate, and potassium chromate. The black circles are the initially wetted regions. It can be seen that all the solid potassium chromate only coats within the initially wetted

region. However, the wetted regions of potassium permanganate and IAS expand during the heating, and the final coated regions are much larger than the initially wetted regions.

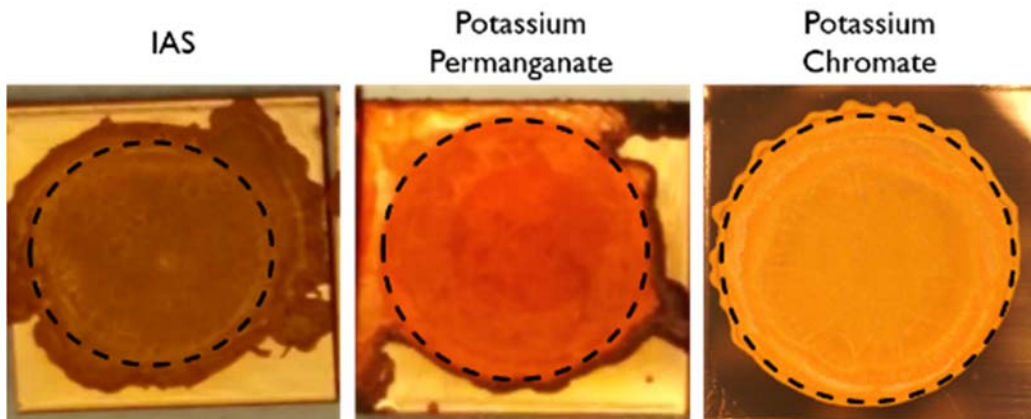


Figure 59: Initially wetted region vs coated region

This phenomenon can be explained by the reaction between the permanganate ion and the copper surface. When the surface is reactive to the solution, the surface tension between the surface and the liquid (σ_{sl}) becomes smaller, and this makes the contact angle be smaller than the one on the surface that is not. Therefore, increasing the plate temperature accelerates the reaction rate between the permanganate ion and the copper surface, which makes the contact angle further decrease and leads to the expanding of the wetted region on the copper surface. However, for chromate solutions, their contact angles on clean copper surfaces are large and do not change with temperature increasing, so solid chromate salts are generated in the initial meniscus region and form a ring.

In fact, the redox reaction between the permanganate ion and the copper surface completes a few hours after the heat transfer device is charged. It should not cause meniscus creeping during operation. However, it opens the door to investigating the performance enhancement of IAS. A guess can be made that something happens to smaller the surface tension between the liquid and

Approved for public release; distribution is unlimited.

the surface (σ_{sl}) with the temperature increasing, and it improves the surface wettability, thinner the liquid film thickness, and enhances the heat transfer performance. A capillary test will be done in Section 4.3 to show what is happening in an operating phase change heat transfer device.

3.5. Conclusion

IAS is demonstrated to be a dilute aqueous solution with eight inorganic chemical constituents: potassium (I) ion, sodium (I) ion, silver (I) ion, magnesium (II) ion, calcium (II) ion, strontium (II) ion, permanganate ion, and chromium (VI) ions.

Magnesium (II) ion and silver (I) ion are in very small amounts and have been demonstrated to be useless in IAS. Therefore, they are eliminated from the list, and the new IAS should be a dilute aqueous solution with six inorganic chemicals in it, potassium (I) ion, sodium (I) ion, calcium (II) ion, strontium (II) ion, permanganate ion, and chromium (VI) ions, see Table 26.

Table 26: Chemical constituents in UCLA IAS #1

Positive ions	Negative ions
K^+	MnO_4^-
Na^+	$HCrO_4^-$
Ca^{2+}	$Cr_2O_7^{2-}$
Sr^{2+}	CrO_4^{2-}

Potassium permanganate, potassium dichromate, chromium trioxide, calcium hydroxide, strontium hydroxide, and sodium hydroxide can be used to produce an IAS solution.

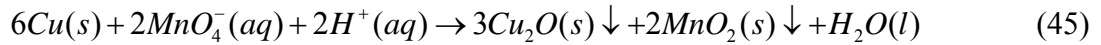
The bulk physical properties of IAS are identical to those of water, and the vapor of IAS is pure water vapor with no other chemical constituents in it. Therefore, the performance

Approved for public release; distribution is unlimited.

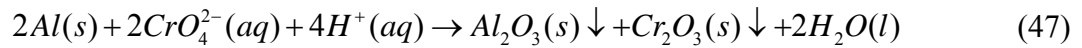
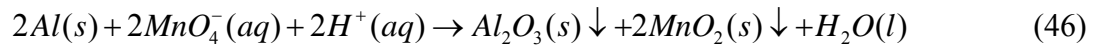
enhancement of heat transfer of using IAS as the working fluid is not a result of the changes of bulk physical properties.

The heat transfer performance enhancement effect of IAS should be a result of a series of chemical reactions as follows:

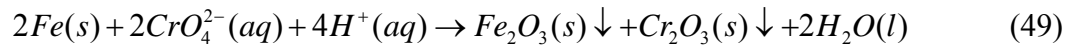
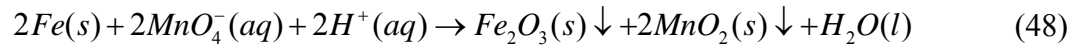
For copper,



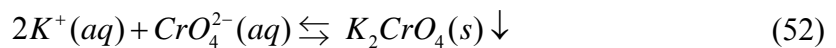
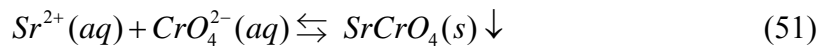
For aluminum,



For steel or stainless steel,



Hydrophilic coatings,



Approved for public release; distribution is unlimited.

The oxidizers in IAS, permanganate and chromium (VI), have been demonstrated to react with metal surfaces and coat them with a layer of insoluble oxides. In addition, with the temperature increasing, some solid chromate salts come out of the solution because their solubility limits are reached, and coat the surface with a layer of porous structured hydrophilic coating. All of the above improve the surface wettability and enhance the heat transfer performance.

In addition, a guess is made that the generated oxide coating and the chromate solution decrease the surface tension between the surface and the liquid, and this makes the contact angle smaller and improves the surface wettability. This guess requires additional tests in Chapter 4 to demonstrate.

Approved for public release; distribution is unlimited.

4. USING IAS IN COPPER DEVICES

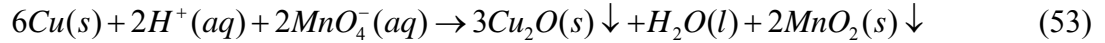
The results of an investigation of the performance enhancement effect of IAS when used in copper phase change heat transfer devices are presented in this chapter. Copper is a stable material when used with water, so it does not lead to the generation of NCGs. As a result, enhancing the heat transfer performance, such as a smaller effective thermal resistance or a larger critical heat flux of dry out, is the only concern. When IAS is used as the working fluid in copper phase change heat transfer devices, one or both of the two goals can be reached depending on the type of wicking used in the device. In this chapter, how IAS decreases the effective thermal resistance and delays the dry out will be addressed, and the limitations of using IAS in different type of copper applications will be discussed.

At the beginning, a 1-D diffusion model is built and used to estimate the concentration profiles of chemicals along the liquid flow path and the location where each coating begins to be deposited. Next, a capillary rise test is performed to show how each chemical contributes to the improvement of the surface wettability. The heat transfer performances of water and IAS are compared using a thermo-syphon test at different inclination angles, a grooved flat heat pipe test, and a sintered heat pipe test. The test results are used to validate the conclusions of the diffusion model and the capillary rise test. Based on the results of the comparison tests, the advantages and limits of using IAS for performance enhancement purposes in various heat transfer applications are discussed.

Approved for public release; distribution is unlimited.

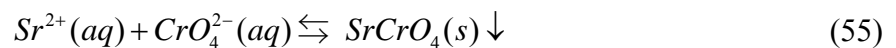
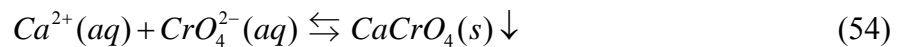
4.1. Related Chemicals and Reactions

When using IAS as the working fluid in a copper heat transfer device, permanganate is the only oxidizer. It starts to react and roughen the copper surface immediately after exposure to IAS. The chemical equation for this is

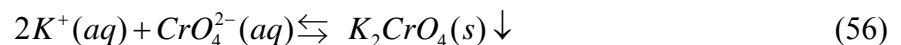


Depending on the ratio of the liquid volume and the surface area, this reaction will take minutes to hours and will advance until permanganate is completely reacted out. Heating will accelerate the reaction. The products, copper (I) oxide and manganese (IV) oxide, will uniformly coat the surface that is exposed to IAS. In addition, the surface coating is stable during the operation. If UCLA IAS #1 is used, the theoretical final pH number will be 6.28.

During the operation, with the temperature increasing, calcium chromate and strontium chromate will be generated because their solubility limits are reached, and they will coat the surfaces in the evaporating region according to the chemical reactions



When the surface is close to being dried out, potassium chromate will be generated and coat the surface according to the reaction



Approved for public release; distribution is unlimited.

Sodium chromate will not be generated until the surface is completely dried out. When the dry out limit is reached is of interest, but chemical processes beyond this point are not.

4.2. Diffusion Model

It has been demonstrated that the vapor of IAS is pure water vapor, so the condensed liquid in the condensing and adiabatic regions and the liquid back flow entering the evaporating region will be pure water. As a result, all the chemicals in the evaporating region will be pushed toward the meniscus region because most of the evaporation occurs there. As a result, the chemical concentrations in the meniscus region will be much larger than the initial bulk values, and coatings begin to be deposited.

A 1-D diffusion model is built to estimate the chemical concentration profiles along the liquid flow path and the location where each coating starts to be generated, see Figure 60.

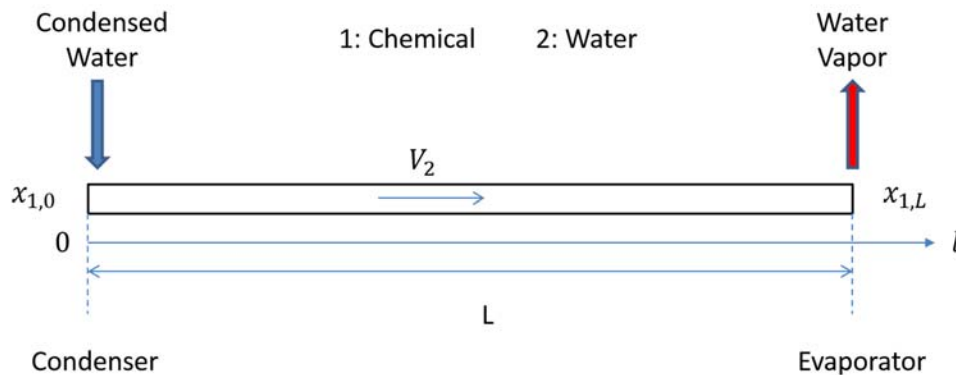


Figure 60: 1-D diffusion model

Specie 1 is a chemical, and specie 2 is water. The left side is the condenser, and the right side is the evaporator. The length of the pathway is L . Liquid flows from the condenser ($l = 0$

Approved for public release; distribution is unlimited.

side) back to the evaporator ($l = L$ side). At the end of the evaporator ($l = L$), the solubility limit applies. Fick's law for a binary system can be used, see [33], is

$$N_1 = x_1 \cdot (N_1 + N_2) - cD_{12}\nabla x_1 \quad (57)$$

where N is the molar flux ($mol/m^2 \cdot s$), x is the mole fraction, c is the mole density (mol/m^3), and D is the diffusion coefficient (m^2/s).

At steady state, the local concentration of the chemical is not changing, so the mole flux of the chemical should be 0 at all locations

$$N_1 = 0$$

Fick's law can be simplified to

$$\frac{N_2}{cD_{12}} = \frac{1}{x_1} \cdot \frac{dx_1}{dl} \quad (58)$$

And the mathematical solutions are given by

$$\frac{N_2}{c \cdot D_{12}}(l - L) = \ln\left(\frac{x_1[l]}{x_1[L]}\right) \quad (59)$$

and

$$\frac{N_2}{c \cdot D_{12}}l = \ln\left(\frac{x_1[l]}{x_1[0]}\right) \quad (60)$$

Approved for public release; distribution is unlimited.

For dilute solutions,

$$N_2 \approx V \cdot c \quad (61)$$

$$\rho \cdot V \cdot A_c = \dot{m} = \frac{\dot{Q}}{h_{fg}} \quad (62)$$

where V is the flow velocity (m/s), ρ is the density of the solution, A_c is the cross section area of the liquid back flow, \dot{m} is the mass flow rate, \dot{Q} is the power load, and h_{fg} is the potential heat of evaporation.

The Peclet number

$$Pe_L = \frac{LV}{D} \quad (63)$$

Is used to compare the advective transport rate to the diffusive transport rate. If advection is dominant, $Pe_L > 100$, all the chemical will be pushed to the end of the evaporator, the meniscus region.

4.2.1. Thermal fluid model

A copper thermo-syphon will be the subject investigated. In order to calculate the chemical concentration profile along an operating thermo-syphon, the velocity and the cross section area of the liquid back flow are necessary. A thermal fluid model can be used to calculate the film thickness, see Figure 61 [34], and the flow velocity can be calculated using

$$V = \frac{4\dot{Q}}{\pi\rho h_{fg} \left[D_i^2 - (D_i - 2\delta)^2 \right]} \quad (64)$$

Approved for public release; distribution is unlimited.

Figure 61 is a thermal fluid model of a general operating thermo-syphon. In order to simplify the calculation, the pool part can be ignored, and a simplified thermal fluid model is shown in Figure 62.

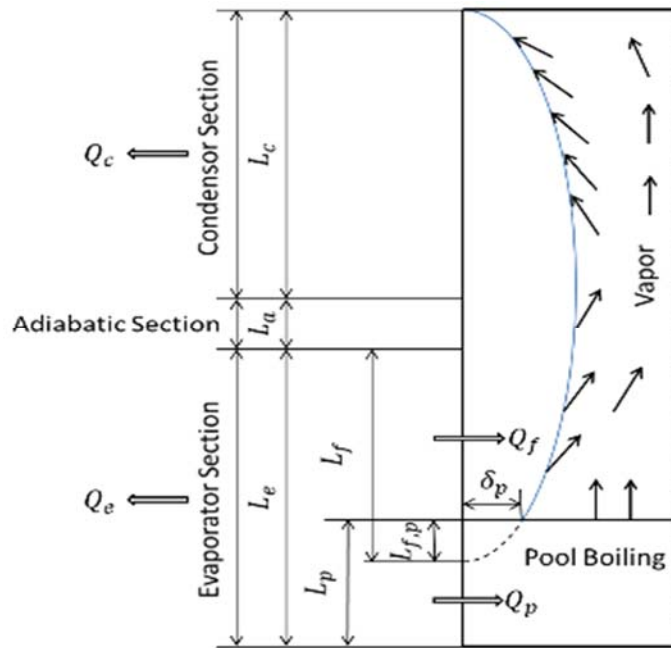


Figure 61: Thermal fluid model of condensation and evaporation within a thermo-syphon

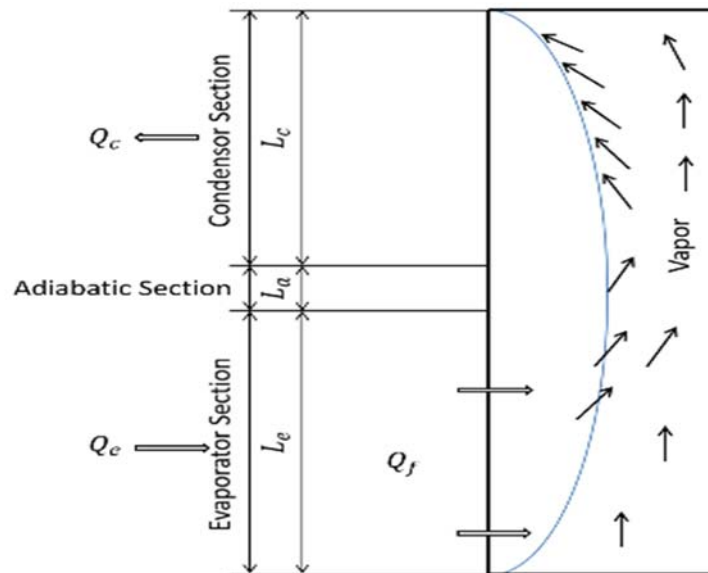


Figure 62: Simplified thermal fluid model of condensation and evaporation within a thermo-syphon

Approved for public release; distribution is unlimited.

The mathematic solutions for the simplified model are

$$\delta_c = \left[\frac{4k\mu_l (T_{w,e} - T_{w,c}) L_e z_c}{\rho_l^2 g h_{fg} (L_c + L_e)} \right]^{\frac{1}{4}} \quad (65)$$

$$\delta_a = \left[\frac{4k\mu_l (T_{w,e} - T_{w,c}) L_e L_c}{\rho_l^2 g h_{fg} (L_c + L_e)} \right]^{\frac{1}{4}} \quad (66)$$

$$\delta_e = \left[\frac{4k\mu_l (T_{w,e} - T_{w,c}) L_c z_e}{\rho_l^2 g h_{fg} (L_c + L_e)} \right]^{\frac{1}{4}} \quad (67)$$

$$(T_{w,e} - T_{w,c}) = \left(\frac{L_c + L_e}{L_c L_e} \right) \left[\left(\frac{3Q}{4\pi D} \right)^4 \left(\frac{4\mu_l}{h_{fg} \rho_l^2 g k^3} \right) \right]^{\frac{1}{3}}$$

$$\mathbb{V}_t = \left[\frac{4}{5} (L_c + L_e) + L_a \right] \cdot \left[\frac{3Q\mu_l (\pi D)^2}{\rho_l^2 g h_{fg}} \right]^{\frac{1}{3}} \quad (68)$$

Table 27 gives the geometry of the copper thermo-syphon used in Section 4.5, and Table 28 presents the test results of the heat transfer performance for the thermo-syphon charged with IAS.

Table 27: Tube geometry of the copper thermo-syphon used in thermo-syphon tests

ID (cm)	L_e (cm)	L_a (cm)	L_c (cm)
0.79	5	35	5

Approved for public release; distribution is unlimited.

Table 28: Test results of a IAS/copper thermo-syphon

Q (watt)	$T_{w,e}$ (°C)	$T_{w,c}$ (°C)
120.86	62.37	40.28
140.86	68.99	43.76
161.55	75.11	46.24
182.32	81.68	49.37
201.53	87.65	52.05
221.69	93.12	54.63
241.28	103.69	57.81
260.09	110.06	60.14
281.27	116.48	62.97
300.98	122.20	65.90
323.14	128.32	68.48

The data in Table 28 can be used to estimate the velocity of the liquid back flow in the evaporating region.

4.2.2. Calculation progress

If the thermo-syphon is equally divided into N sections as shown in Figure 63, solution (59) is given by

$$\frac{V_{i+\frac{1}{2}}}{D_{12}} \cdot \Delta l = \ln \left(\frac{x_1 [l_{i+1}]}{x_1 [l_i]} \right) \quad (69)$$

where

$$V_{i+\frac{1}{2}} = \frac{V_i + V_{i+1}}{2} \quad (70)$$

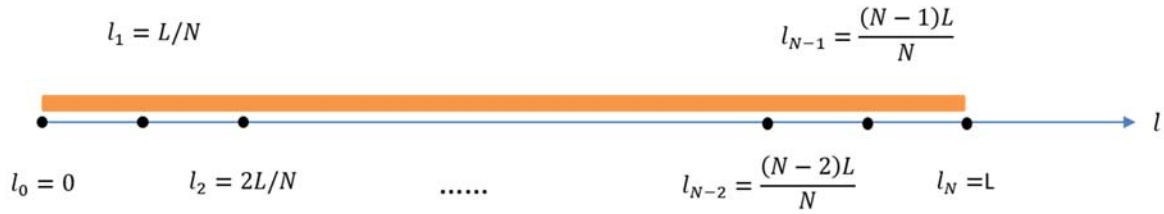


Figure 63: Diagram of thermo-syphon

When IAS is used in copper thermo-syphons, the oxides can be seen to coat the wetted evaporating region uniformly. The amount of strontium chromate is much smaller than calcium chromate and potassium chromate. Sodium chromate will not be generated until the surface is completely dried out. Therefore, calcium chromate and potassium chromate are the main coatings that will be effected by the advection of the liquid back flow.

The diffusion coefficients of the related ions at different temperatures [35] are presented in Table 29, and the data are shown on Figure 64. It can be assumed that the diffusion coefficient increases linearly with the temperature.

Table 29: Diffusion coefficients of related ions

Ion	$D_{12}(10^{-10}m^2/s)$		
	0°C	18°C	25°C
K^+	9.86	16.7	19.6
Ca^{2+}	3.73	6.73	7.93
CrO_4^{2-}	5.12	9.36	11.2

Approved for public release; distribution is unlimited.

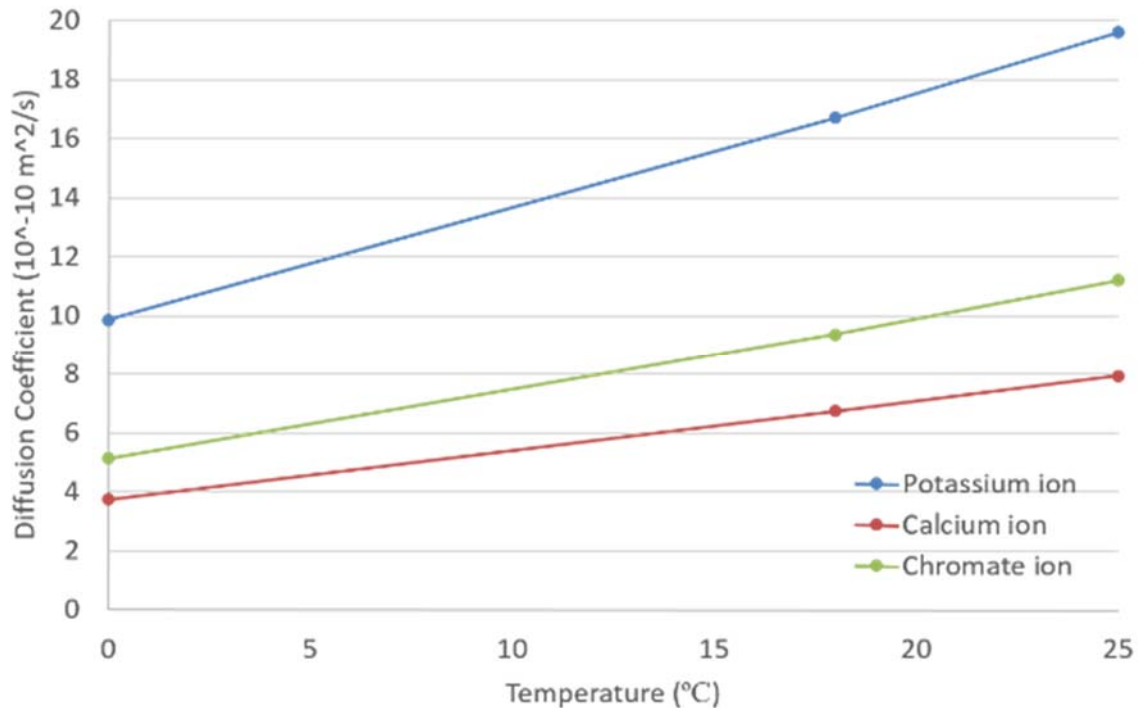


Figure 64: Diffusion coefficients of related ions

Before beginning the calculation, the following assumptions are made to simplify the calculation:

- 1) The diffusion coefficient changes linearly with the temperature.
- 2) The heat fluxes in the condenser and the evaporator are individually uniform.
- 3) The physical properties of water are determined by the average value of the wall temperatures in the evaporator and the condenser.
- 4) The liquid back flow velocity and chemical concentrations in each section change linearly.
- 5) The total amount of chromate ion is calculated based on the initial bulk concentration of chromium (VI) and pH number, and the chromium balance is ignored during the calculation.

Approved for public release; distribution is unlimited.

Calculations are done using the following iterative procedure:

- 1) Initial values are given: number of sections, input power, wall temperatures in evaporator and condenser, and total amount of potassium ion, calcium ion, and chromate ion.
- 2) Calculate liquid film thickness and velocity of the liquid back flow at all locations.
- 3) Give initial coating amounts, zero, for both calcium chromate and potassium chromate.
- 4) Start iteration loop 1.
- 5) Calculate the total amount of potassium ion, calcium ion, and chromate ion in aqueous solution.
- 6) Give initial local mole fraction of potassium ion at l_N , $x_K[l_N]$, and start sub-iteration loop 1.1.
- 7) Calculate local mole fraction of potassium ion at all locations and calculate the total amount of potassium ion.
- 8) Judge loop 1.1, compare the calculated total amount of potassium ion to the one in step 5), if the calculated result is larger, smaller $x_K[l_N]$; smaller, larger $x_K[l_N]$; equal stop loop 1.1.
- 9) Give initial local mole fraction of calcium ion at l_N , $x_{Ca}[l_N]$, and start sub-iteration loop 1.2.
- 10) Calculate local mole fraction of calcium ion at all locations and calculate the total amount of calcium ion.

Approved for public release; distribution is unlimited.

- 11) Judge loop 1.2, compare the calculated total amount of calcium ion to the one in step 5), if the calculated result is larger, smaller $x_{Ca}[l_N]$; smaller, larger $x_{Ca}[l_N]$; equal stop loop 1.2.
- 12) Give initial local mole fraction of chromate ion at l_N , $x_{Cr}[l_N]$, and start sub-iteration loop 1.3.
- 13) Calculate local mole fraction of chromate ion at all locations and calculate the total amount of chromate ion.
- 14) Judge loop 1.3, compare the calculated total amount of chromate ion to the one in step 5), if the calculated result is larger, smaller $x_{Cr}[l_N]$; smaller, larger $x_{Cr}[l_N]$; equal stop loop 1.3.
- 15) Calculate concentration product of calcium chromate and potassium chromate at all locations.
- 16) Judge loop 1, compare the maximum values from step 15) to the solubility product constants of calcium chromate and potassium chromate. If maximum values are larger, larger coating amounts; smaller, smaller coating amounts; equal, or smaller but coating amounts are zeros, stop loop 1.

4.2.3. Results and Discussion

Based on the model, the liquid film thickness, the flow velocity, and the chemical concentration profiles are calculated by using a Visual C++ computer code, see Appendix 0. Figure 65 shows the thickness of the liquid film in the thermo-syphon at different input powers, and Figure 66 shows the velocity of the liquid film along the thermo-syphon at different input powers. The condenser starts at $l = 0\text{cm}$ and ends at $l = 5\text{cm}$, and the evaporation begins at $l = 40\text{cm}$ and

Approved for public release; distribution is unlimited.

ends at $l = 45\text{cm}$. Both film thickness and flow velocity increase in the condensing region, reach maximum in the adiabatic region, and decrease in the evaporating region.

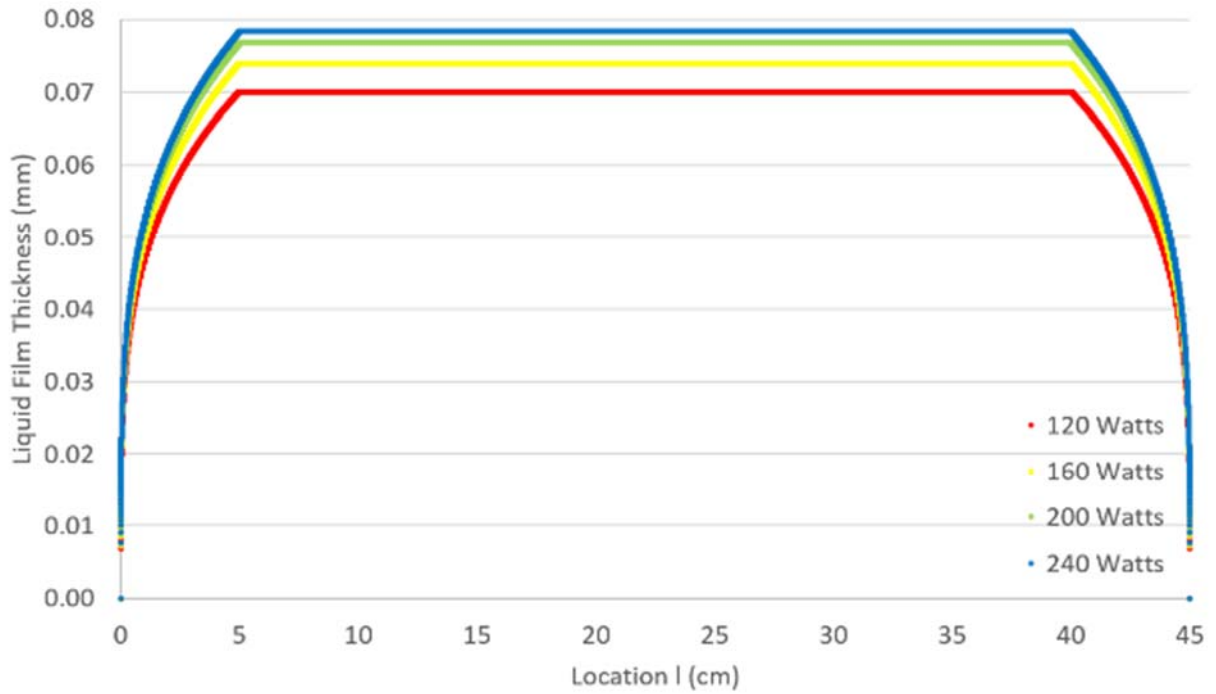


Figure 65: Film thickness of the liquid back flow along the thermo-syphon

Approved for public release; distribution is unlimited.

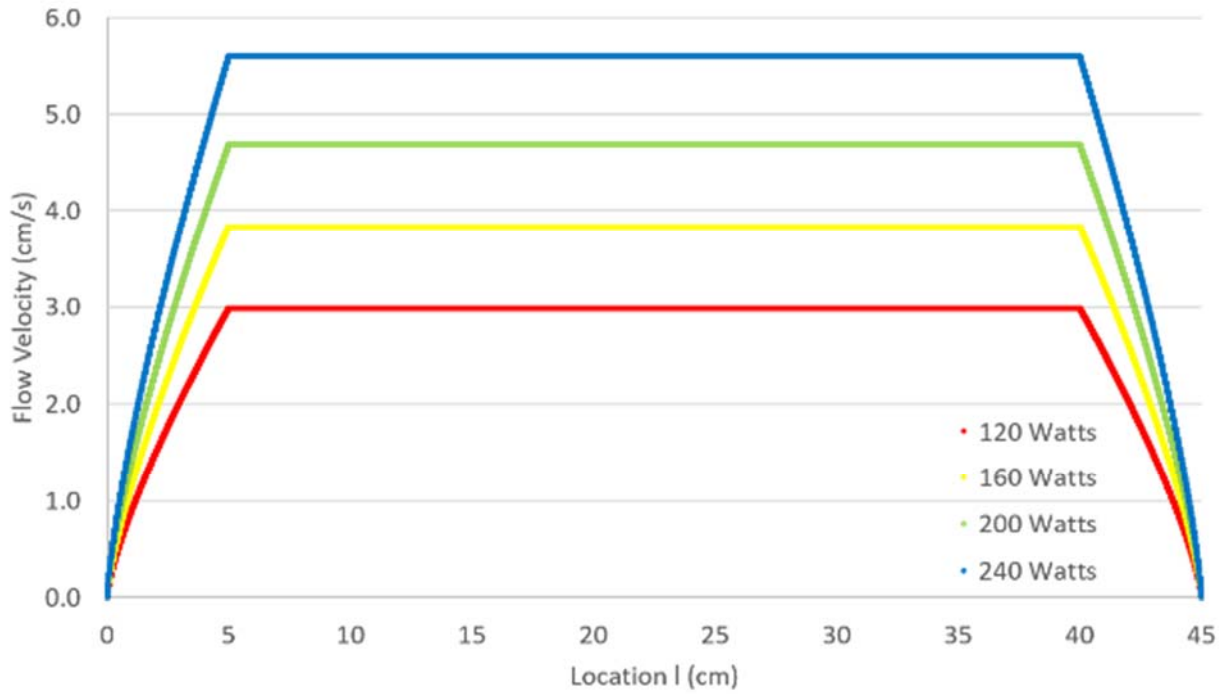


Figure 66: Velocity of the liquid back flow along the thermo-syphon

If the solubility limit is not considered, the concentration profiles of calcium ions, chromate ions, and potassium ions are shown in Figure 67, Figure 68, and Figure 69.

Approved for public release; distribution is unlimited.

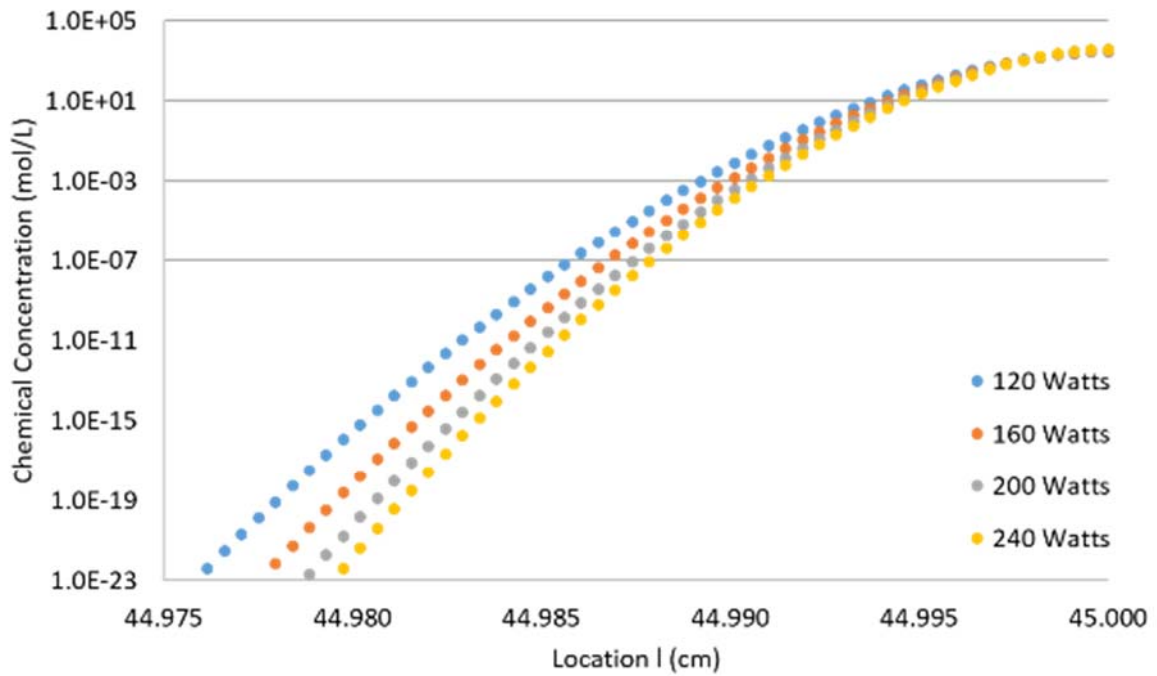


Figure 67: Concentration profile of calcium ion along thermo-syphon, without considering the solubility limit

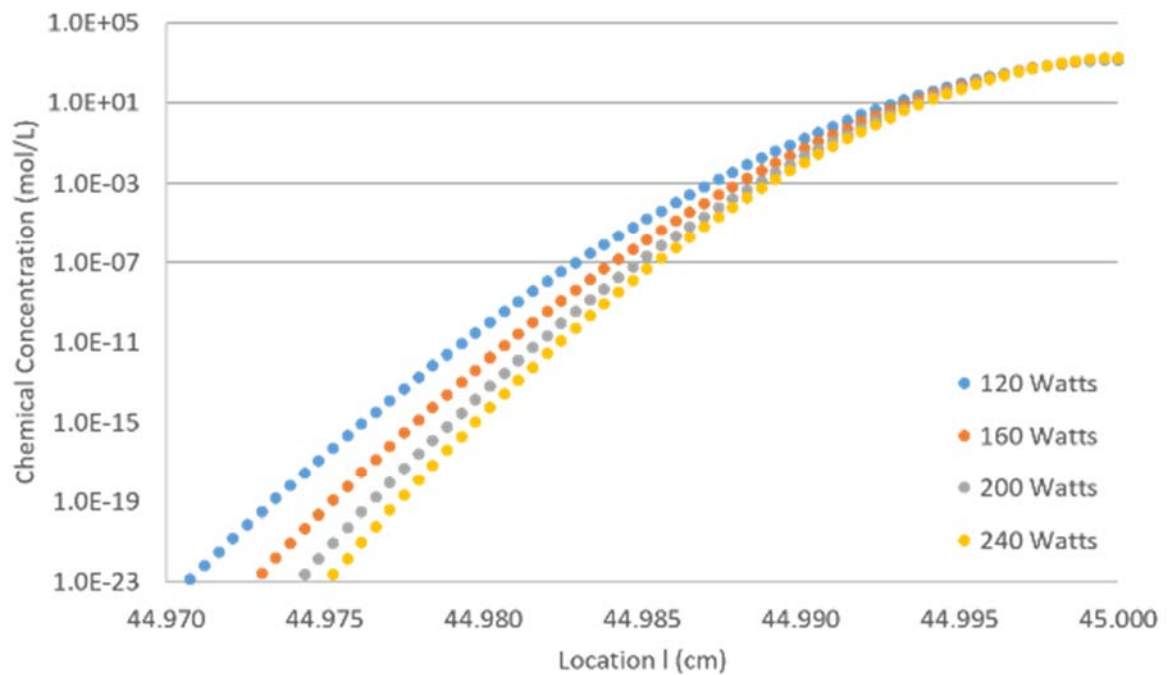


Figure 68: Concentration profile of chromate ion along thermo-syphon, without considering the solubility limit

Approved for public release; distribution is unlimited.

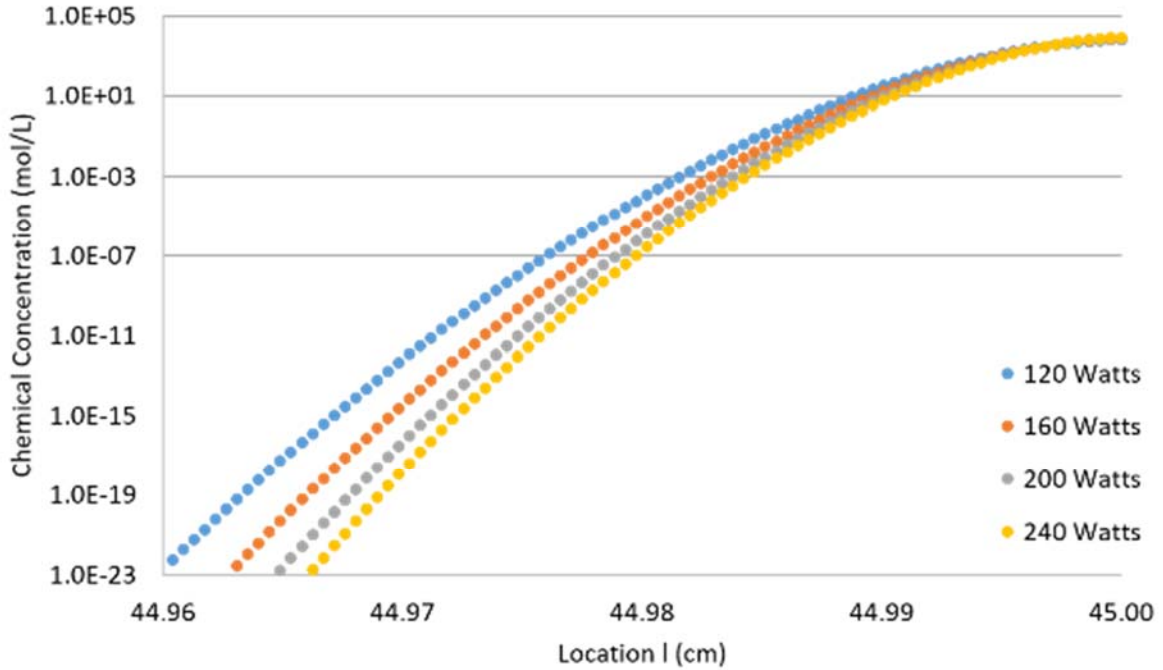


Figure 69: Concentration profile of potassium ion along thermo-syphon, without considering the solubility limit

It can be seen that all the chemicals are pushed to a very small region at the end of the evaporator, which would be the meniscus region in the real case. It is because of the advection dominates the diffusion. Table 30 shows the Peclet numbers

$$Pe_L = \frac{L \cdot V}{D_{12}} \quad (71)$$

of the related ions at different input powers. All of them are very large numbers, so the advection is dominant in the thermo-syphon. As a result, all the soluble chemicals will be pushed to the meniscus region, and all the solid chromate salts will be generated at the meniscus region.

Approved for public release; distribution is unlimited.

Table 30: Peclet numbers of the related ions at different input powers

		Chemicals		
		Ca^{2+}	CrO_4^{2-}	K^+
Input power (Watt)	120	1.09E+07	7.68E+06	4.52E+06
	140	1.17E+07	8.20E+06	4.85E+06
	160	1.24E+07	8.74E+06	5.18E+06
	180	1.31E+07	9.20E+06	5.46E+06
	200	1.37E+07	9.60E+06	5.71E+06
	220	1.43E+07	1.00E+07	5.97E+06
	240	1.46E+07	1.02E+07	6.12E+06

Table 31 shows the percentage of each chemical coming out as its solid chromate salt, and Figure 70 shows the final concentration profiles of calcium ion, chromate ion, and potassium ion after the solid chromate salts are generated in the meniscus region. As a result, all the chemicals will be pushed to the meniscus region and come out as solids.

Table 31: Percentage of chemicals coming out as solid chromate salts

	120 Watts	180 Watts	240 Watts
Potassium	99.99%	100%	100%
Calcium	100%	100%	100%

Approved for public release; distribution is unlimited.

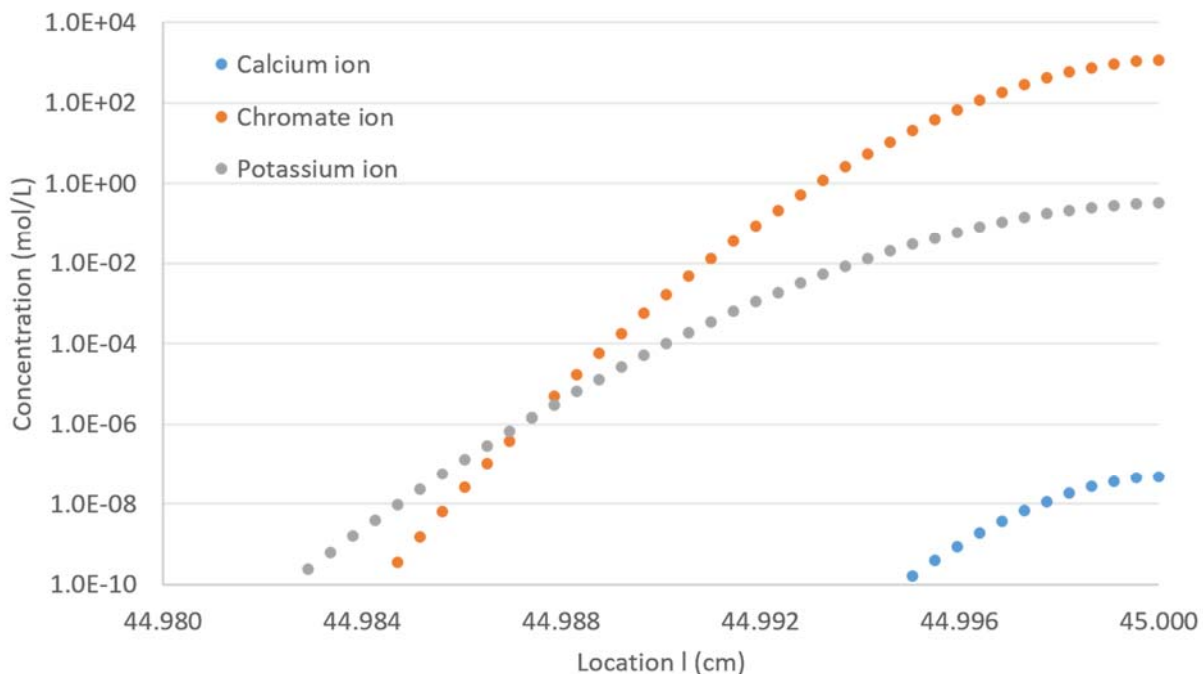


Figure 70: Concentration profiles of calcium ion, chromate ion, and potassium ion along thermo-syphon, with considering solubility

Therefore, the previous assumption that hydrophilic coatings will coat the entire evaporating region uniformly is not correct. Instead, all the soluble chemicals will be pushed to the meniscus region, and all the hydrophilic coatings will only play a role in the meniscus region. How hydrophilic coatings contribute to the surface wettability will require further tests.

4.3. Capillary Tests

In order to understand how each type of coating contributes to the surface wettability, a capillary test was performed. This is only a visual test to show what happens in an operating phase change heat transfer device, and it is not designed for the purpose of heat transfer demonstration. Figure 71 is a photograph of the experimental apparatus, and Figure 72 is a schematic of the capillary test. One end of a mirror like copper surface, $1.5\text{cm} \times 1.5\text{cm}$, was sandwiched by a

cartridge heater block and a stainless steel plate, with the mirror like side facing up. The opposite end of the surface was put into the liquid in a reservoir, and the angle between the surface and the horizontal is 45 degrees. A digital microscope was used to monitor the capillary raise on the mirror like side of the copper surface.

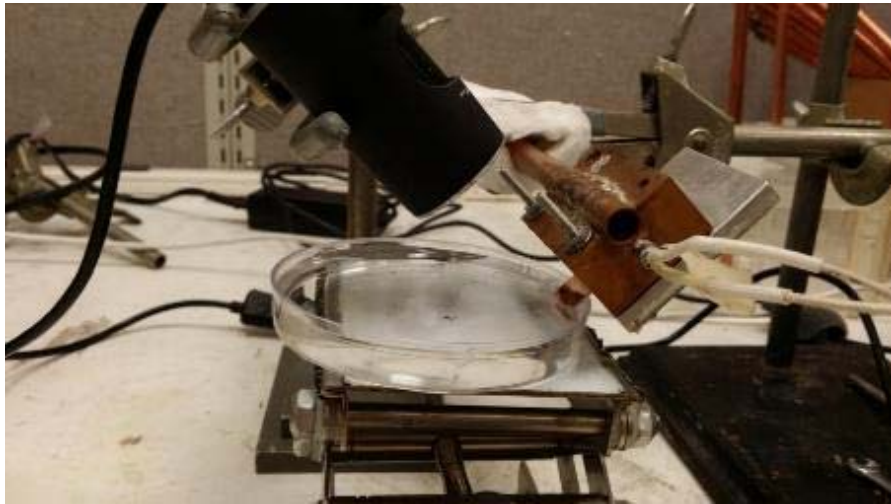


Figure 71: Picture of capillary test

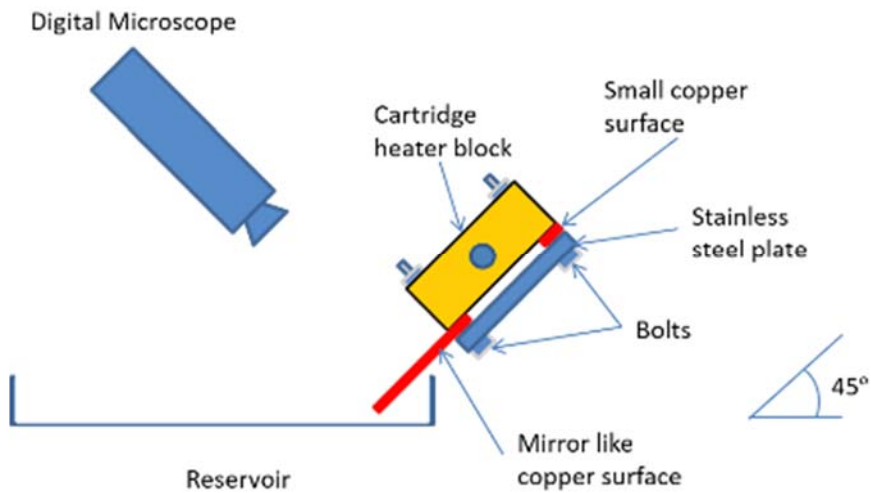


Figure 72: Schematic of capillary test

Four tests were done, and the solutions and surfaces used were listed below:

Approved for public release; distribution is unlimited.

- 1) DI-water and a clean mirror like copper surface
- 2) UCLA IAS Yellow #1 and a clean mirror like copper surface
- 3) Potassium permanganate solution, with the same amount of manganese as UCLA IAS #1, and a mirror like copper surface
- 4) UCLA IAS Yellow #1 and a mirror like copper surface pre-treated by the potassium permanganate solution used in test 3) and then rinsed by DI-water

During the test, 50 watts was applied to the cartridge heater, and the temperature of the surface would reach about 105 – 110°C after 3 minutes. Figure 73 is an example capillary test image, which is what will be seen from the digital microscope. Approximately one quarter of the top of the copper surface is sandwiched between the heater block and the stainless-steel plate, and another quarter of the surface at the bottom is submerged in the solution. The center half, about 0.75mm, of the copper surface is exposed.

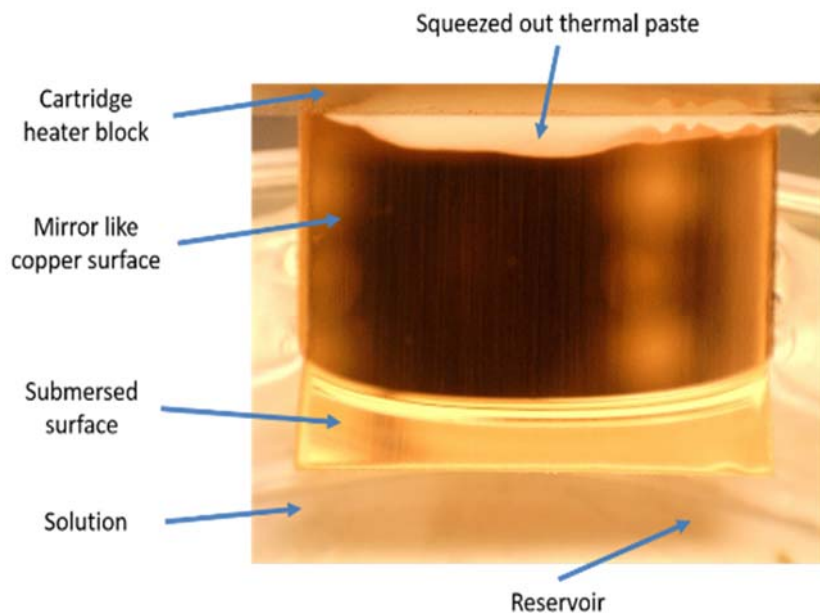


Figure 73: Example capillary test image

Approved for public release; distribution is unlimited.

Figure 74 shows the test results of water and a clean mirror like copper surface. The source light was adjusted to have a reflection on the meniscus. If the reflected light disappeared, it meant that the contact angle decreased. With the temperature increasing, bubbling occurred uniformly on the submerged copper surface, and the bubbles were large. The meniscus did not rise, and the contact angle did not change significantly during the test and as a result the reflection of the source light could still be seen.

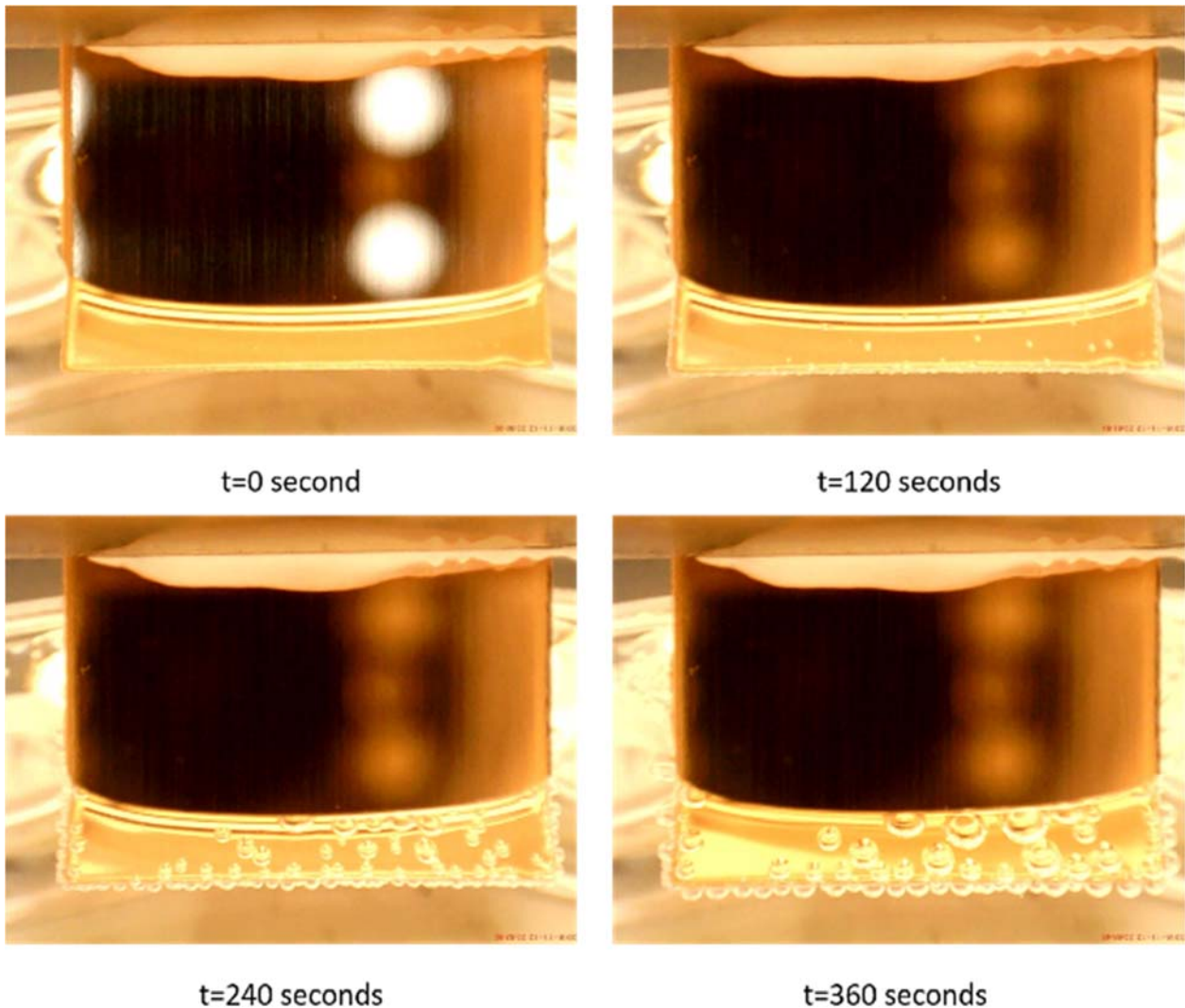
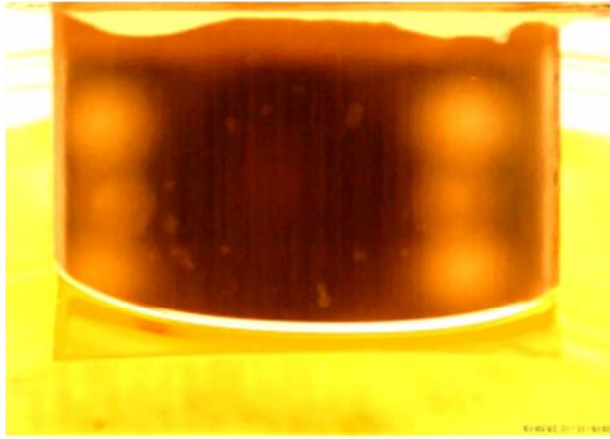


Figure 74: Test results of water/clean mirror like copper surface

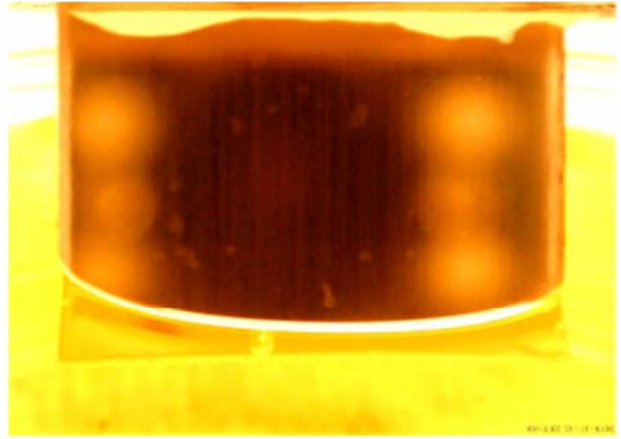
Approved for public release; distribution is unlimited.

Figure 75 shows the test results of UCLA Yellow #1 and a clean mirror like copper surface. With the temperature increasing, most of the bubbling occurred in the meniscus region, and the bubbles were much smaller than those seen in the test of water and the clean copper surface. Based on the conclusions from Section 4.2, chromate salts will come out as solids in the meniscus region because the solubility limits were reached.

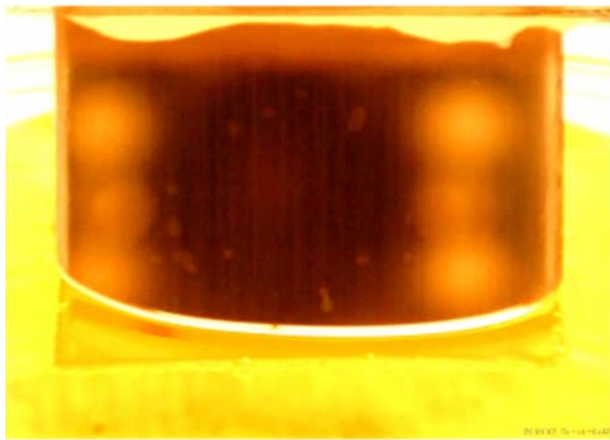
Approved for public release; distribution is unlimited.



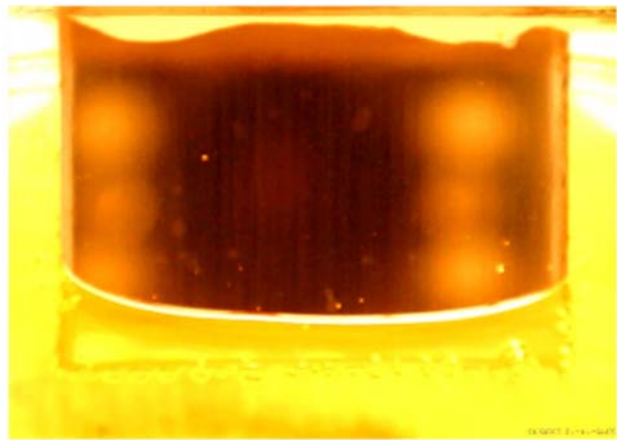
t=90 seconds



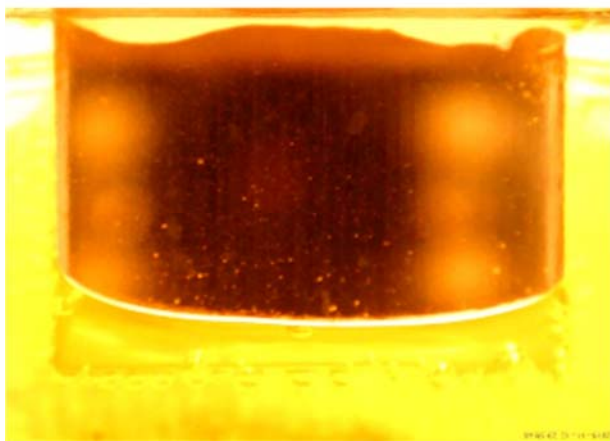
t=210 seconds



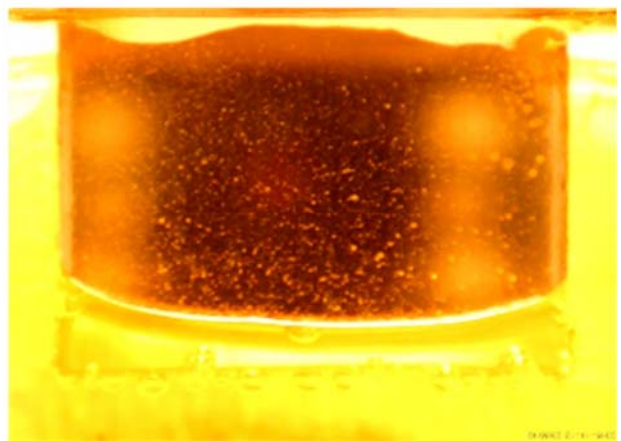
t=330 seconds



t=450 seconds



t=490 seconds



t=530 seconds

Figure 75: Test results of UCLA Yellow #1/clean mirror like copper surface

Approved for public release; distribution is unlimited.

Solid chromate salts were generated from the liquid/vapor interface because it was where evaporation took place and had the largest chemical concentrations. In addition, as was mentioned in Section 3.4 that chromate solutions did not have good wettability on smooth copper surfaces, and the contact angle did not change much as temperature increasing. Therefore, solid chromate salts would be generated and pile up in the meniscus, see Figure 76. With time, more and more solid chromate salts were generated in the meniscus region, and eventually lifted the meniscus away from the heated surface. Figure 77 is a photo of a sample copper surface coated by potassium chromate in the coating study section. In this case, the new meniscus was at the intersection of the liquid and chromate salts, which was not directly heated except by the conduction through the solid coatings. However, the thermal conductivity of the coating was much smaller than copper, so little heat could be transferred through the coating. As a result, the liquid was mainly heated by the copper surface. That became more like a pool boiling, and the bubbling caused splashes.



Figure 76: Diagram of how chromate salts deposit on smooth copper surface

Approved for public release; distribution is unlimited.



Figure 77: Sample surface coated by potassium chromate in the coating study test

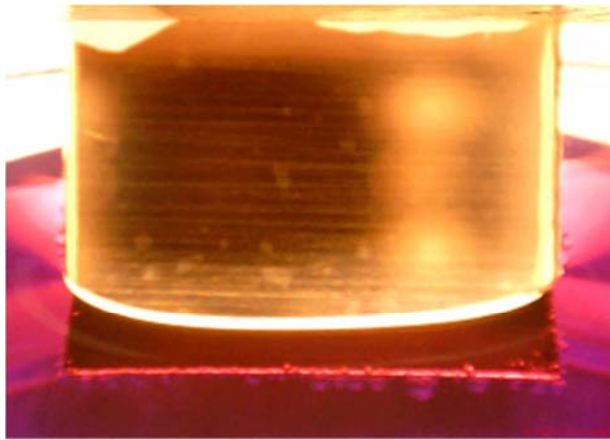
Figure 78 shows the test results of the potassium permanganate solution and a clean mirror like copper surface. Bubbling occurred uniformly on the submerged surface, which was similar to the case of water and the clean copper surface, and there was no splashing during bubbling, which was different with UCLA yellow #1. For this case, copper (I) oxide and manganese (IV) oxide were generated and coat the surface. Because the oxides were the products of the reaction between permanganate and the copper surface, they were generated at the interface of the liquid and the surface. In addition, the oxides were insoluble and had a strong bonding force with the copper surface, so they would not be washed off by the liquid flow. As a result, the oxides would coat the surface uniformly and be stable on the surface.

Moreover, with the temperature increasing, the reflection of the source light started disappearing after 330 seconds, and it completely disappeared at 490 seconds. It was a result of the reaction between permanganate and the copper surface. The reactive surface made the contact

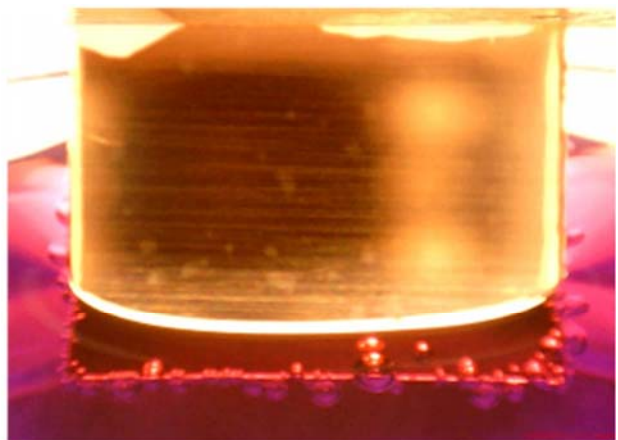
Approved for public release; distribution is unlimited.

angle smaller and pulled up the meniscus. However, the capillarity caused by this was limited, and the meniscus ceased rising up after 490 seconds.

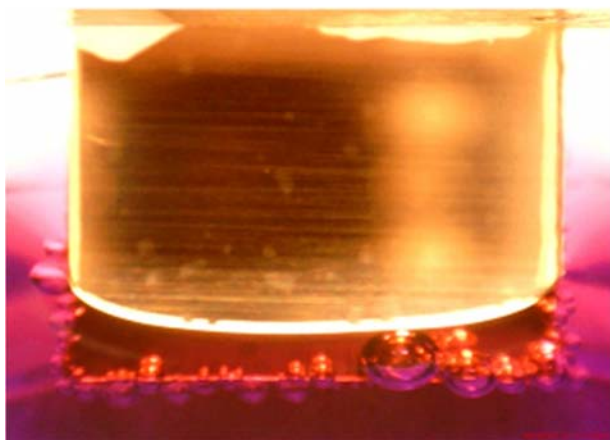
Approved for public release; distribution is unlimited.



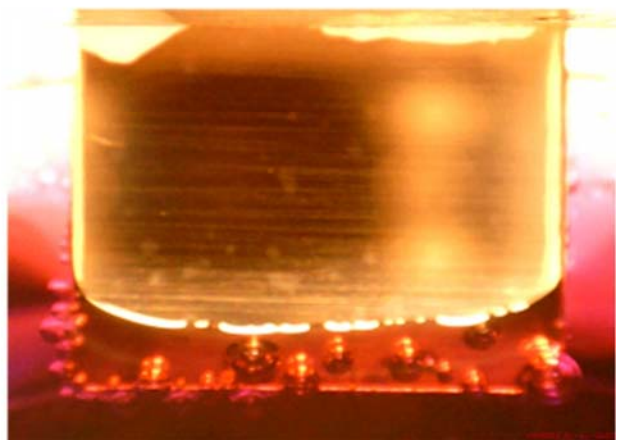
t=90 seconds



t=210 seconds



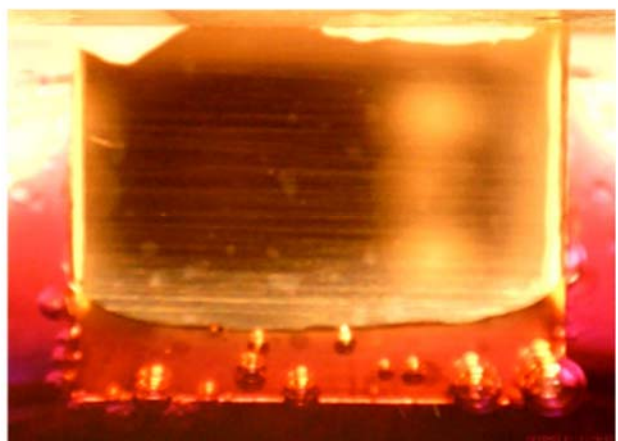
t=330 seconds



t=450 seconds



t=490 seconds



t=530 seconds

Figure 78: Test results of potassium permanganate solution/clean mirror like copper surface

Approved for public release; distribution is unlimited.

Figure 79 shows the test results of UCLA Yellow #1 and the mirror like copper surface which was pretreated by the potassium permanganate solution and then rinsed by DI-water for 5 minutes. After the pretreatment, the copper surface could be seen to have the oxides coating only, and all the soluble chemicals had been washed off. Therefore, the surface wettability will not be affected by the soluble chemicals.

The reflection of the source light was not from the meniscus region, so UCLA Yellow #1 had a smaller contact angle, a better wettability, on the oxide coated copper surface. With the temperature increasing, there was not a lot of bubbling on the submerged copper surface or in the meniscus region. However, when the temperature was above 80°C, the meniscus started climbing up the copper surface. It climbed up along the edges at the beginning, which could be seen at 210 seconds. At 270 seconds, the same phenomena occurred at the center of the surface.

The climbing of the meniscus was not the result simply of a rougher surface because it did not happen at low temperatures. Moreover, the solution used was UCLA Yellow #1, and there was no splashing during the test. As a result, the chromate salts were not piled up as what in Figure 76. In addition to the climbing phenomena, the chromate salts were deposited on the surface at the edge of the meniscus, see Figure 80, and extend the wetted region.

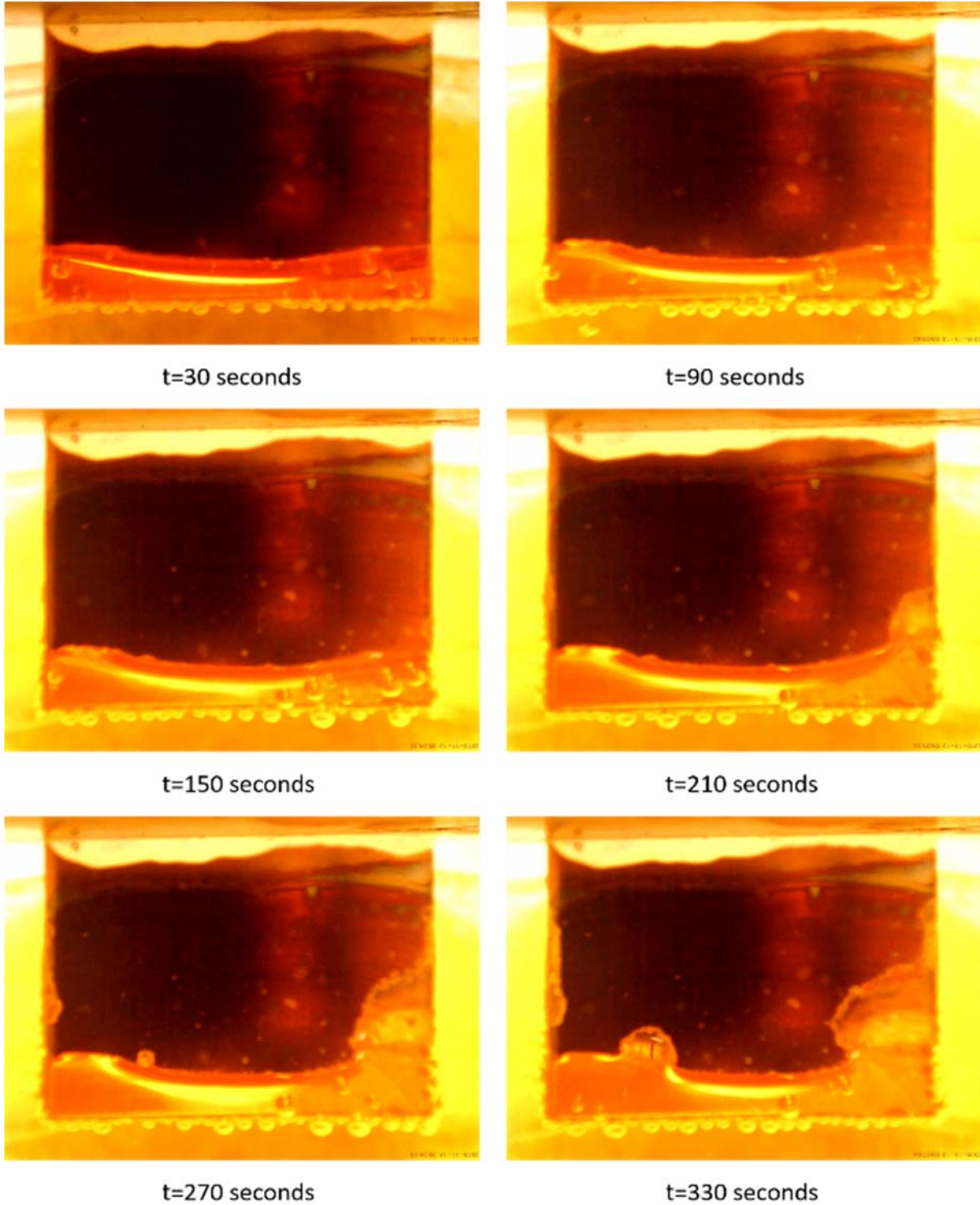


Figure 79: Test results of UCLA Yellow #1/mirror like copper surface pretreated by potassium solution and then rinsed by DI-water

Approved for public release; distribution is unlimited.

Chromate solutions have smaller contact angles on oxide coated surfaces than those on clean copper surfaces, and their contact angles decrease as the concentrations increasing. Because of the evaporation, the chemical concentrations in the meniscus region increase, so the contact angle decreases. This causes the climbing up. In addition, because of reaching solubility limits, solid chromate salts start being generated in the meniscus region and increase the film thickness of the meniscus, which makes the meniscus further extend, see Figure 80. The solid chromate salts, which are further away from the meniscus region, are re-dissolved in the liquid, and the new solid chromate salts are generated in the meniscus region and keep pushing the meniscus to extend until an equilibrium is reached.



Figure 80: Diagram of how chromate salts deposit on copper surface pretreated by potassium permanganate

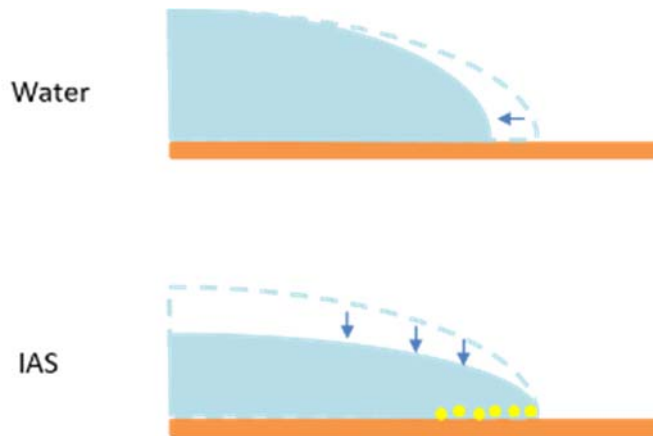


Figure 81: Difference between water and IAS while being dried out

Figure 81 shows the difference between water and IAS working fluids when the surfaces are close to being dried out. For water, when the surface is close to being dried out, the meniscus

Approved for public release; distribution is unlimited.

retreats, and surface is no longer cooled by evaporation, which leads to dry out. However, for IAS, the meniscus does not retreat because the solid chromate salts provide extra capillary forces to pump the liquid to the meniscus region. Therefore, dry out is significantly delayed, and the liquid film just becomes thinner and results in an enhanced cooling.

In conclusion, it has been demonstrated that the combination effects of permanganate and chromate is the key to improve the heat transfer performance. The chromate solution has much better wettability on the surface pretreated by permanganate, and it will delay dry out and keep the device operating at higher heat fluxes. However, for lower heat fluxes, at which both water and IAS work normally, IAS might have a larger temperature difference, between the evaporator and the condenser, because the coatings cause an extra thermal resistance.

4.4. Charging Station

In order to verify the conclusions reached by chemical analysis and capillary tests, testing the heat transfer performance of IAS in a real phase change heat transfer application is required. However, the heat transfer performance of a phase change heat transfer device is very sensitive to the amount of NCG and the amount of working liquid. As a result, the usual boil-off method, used in industries, will not be used. A charging station that can hold high vacuum and guarantee high precision in charging is required. To meet this need, a charging station has been built with a degassing section, as shown in Figure 83.

The degassing and charging sections on the right are made of stainless steel in order to reach and maintain a better vacuum. The other section on the left is made of PFA in order to release

the stress to the glass parts. A magnetic stirrer is used to agitate water, increasing the interface area between water and gas, in order to accelerate the degassing.



Figure 82: Degassing chamber and magnetic stirrer

Approved for public release; distribution is unlimited.



Figure 83: Charging station with degassing feather

Approved for public release; distribution is unlimited.

Table 32 is a tabulation of the important parts of the charging station. Two vacuum pumps are used in the charging station. One is used for degassing and pre-drying the charging station. The second one is used to completely dry out and create a vacuum for the charging of a heat transfer device.

The McMaster vacuum gauge is used for the general pressure monitoring. The Omega gauge, which is more accurate and has a smaller range, is used to determine if there is any water left, detecting leakages, and measuring the pressure before charging.

Table 32: Parts information in the charging station

Category	Vendor	Part #	Description
Pressure Gauge	McMaster Carr	3840K8	Digital Vacuum Gauge, Polycarbonate Case, 29.9”Hg-0
	Omega	PX409-005AV	5 Psi High Accuracy Transducer, mV/V Output, Cable Connection
Valve	Swagelok	SS-6BK	Stainless Steel Bellows-Sealed Valve, Gasketed, PCTFE Stem Tip, 3/8 in. Swagelok Tube Fitting, SC-11 Cleaned
		SS-2H	Stainless Steel Bellows-Sealed Valve, Welded, SS Stem Tip, 1/8 in. Swagelok Tube Fitting
		PFA-4RPS6	PFA Needle Valve, 3/8 in. Swagelok Tube Fitting
	Ideal Vacuum	P103568	Ball Valve, Manual, ISO-KF Interface, NW-16 Vacuum Fittings, Stainless Steel
Vacuum Pump	Ideal Vacuum	P102308	Old Alcatel Adixen 2005SD Dual Stage Rotary Vane Vacuum Pump, Ultimate Total Pressure 2×10^{-3} mbar, Pump Speed $5.4m^3/h$
		P102295	New Varian DS302 Dual Stage Rotary Vane Vacuum Pump, Ultimate Total Pressure 2×10^{-3} mbar, Pump Speed $11.6m^3/h$

Three types of valves are used in the charging station. The PFA valves are used in the PFA section because of their light weight. IAS fluid is strongly corrosive requiring the use of ball valves

Approved for public release; distribution is unlimited.

where there is direct contact with the strongly corrosive IAS to have a long lifetime. Bellows-sealed valves are required at the locations where the flow rate controlling is important.

Figure 84 is a schematic diagram of the new charging station. IAS fluid is strongly corrosive, so the bellows part of the bellows-sealed valve must not be kept in contact with IAS during the degassing process. The liquid must flow in the direction shown in Figure 85. For valve #5, the arrow should point down because there will be IAS liquid in the chamber for hours during the degassing process. For valve #14, the arrow should point up in order to obtain a more accurate charge, in which case, the liquid in the bellows will not affect the total charge amount. If the arrow is pointing down, liquid will be stuck in the bellows, and the amount is unpredictable. However, both valves #5 and #14 are still in danger. During the charging process, both valves must be open to let the IAS liquid fill the bellows and pass through them. It is very difficult to wash IAS off the bellows, so both valve #5 and #14 have to be replaced with new ones every three or four months because they begin to leak.

When a heat transfer device is connected to the charging station, the charging related section, enclosed by valves #5, #6, #7, #11, #13, and the heat transfer device, can hold high vacuum. It can be vacuumed to 2×10^{-3} mbar, which is the ultimate total pressure reached by the Varian pump, and it takes 24 hours for the pressure to reach 7 mbar, 0.1 psi, because of leaking.

Approved for public release; distribution is unlimited.

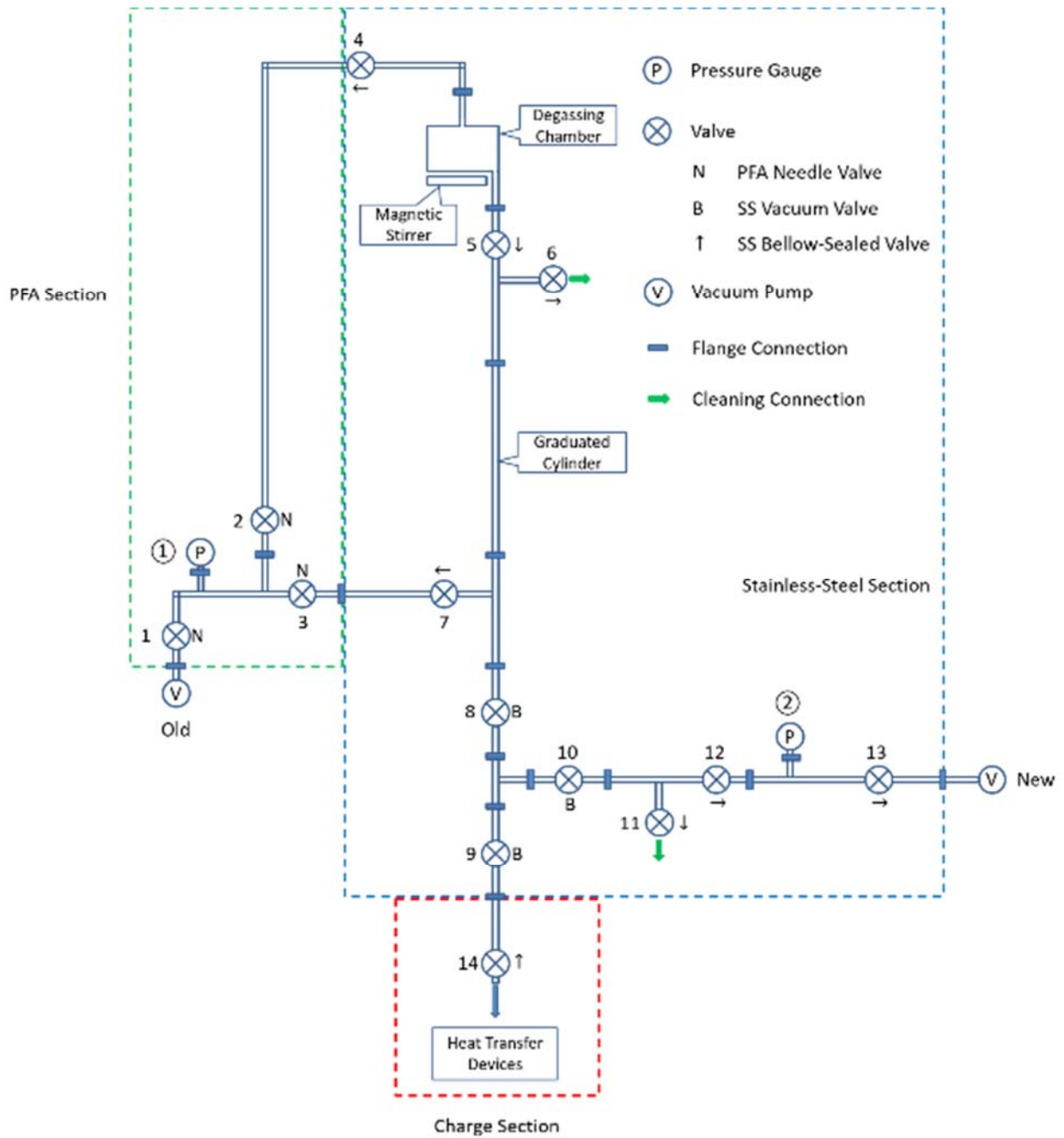


Figure 84: Schematic diagram of the new charging station

Approved for public release; distribution is unlimited.

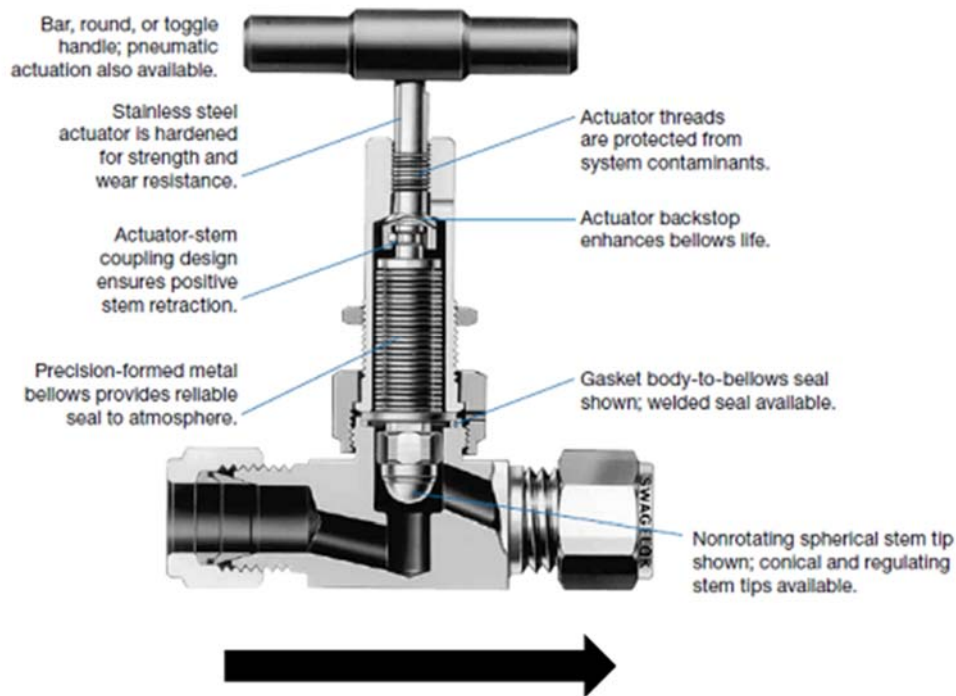


Figure 85: Swagelok bellows-sealed valve

Below is the operational procedure for the charging station:

- 1) **DEGASSING.** Add liquid to the chamber and connect the parts correctly.
- 2) Close all the valves and turn on the magnetic stirrer.
- 3) Turn on the Alcatel vacuum pump and then open valves #1, #2, and #4.
- 4) Wait until no large bubbles are generated from the liquid and then close valves #2 and #4. Turn off the Alcatel pump.
- 5) Keep stirring for 6 hours to degas. During the degassing, repeat steps 3) and 4) every hour to improve the degassing.
- 6) **PRE-DRYING OUT.** Keep valves #4, #5, #6, #11, and #13 closed, and open all the other valves. Valves #8, #9, and #10 should be half open.
- 7) Turn on the Alcatel pump to dry out the charging station and the heat transfer device.

Approved for public release; distribution is unlimited.

- 8) Wait until the output of the pressure gauge #2 is 1mV, close valves #7, #4, and #1. Turn off the Alcatel pump.
- 9) Turn on the Varian pump and open the valve #13.
- 10) Wait until the output of the pressure gauge #2 is stable at approximately -0.461mV, it varies with the room temperature, completely open valves #8, #9, and #10.
- 11) Close valves #14, #10, #12, and #13 in orders. Turn off the Varian pump.
- 12) **CHARGING.** Open the valve #5 to release the liquid. Wait until the liquid level is approximately at the 7ml mark on the graduated cylinder, close the valve #5.
- 13) Wait until no droplets are falling down, record the initial mark and open the valve #14 to charge.
- 14) After the required amount of the liquid has been charged into the heat transfer device, close the valve #14, seal the heat transfer device, and disconnect it from the charging station.
- 15) **CLEANING.** Open valves #6 and #14 to release the extra liquid, and then connect the valve #6 to the cleaning peristaltic pump. Water goes into the valve #6 and comes out from the valve #14.
- 16) Close the valve #6 and open the valve #11. Connect the valve #11 to the cleaning pump. Water goes into the valve #11 and comes out from the valve #14.

The charging uncertainty is ± 0.1 ml because of the accuracy of the graduated cylinder. In addition, the heat transfer device is connected to the charging station by a fill tube with 1/8 inch OD and 0.061 inch ID. A cold welding method is used to seal the device, so a part of the fill tube,

Approved for public release; distribution is unlimited.

about 3-4 cm, will be chopped off. There will be some liquid left in the chopped off fill tube, the maximum amount of being about 0.08 ml. Therefore, the total charging error is -0.18 ml to +0.1 ml.

4.5. Thermo-syphon Tests

In order to verify the conclusions in Section 4.3, a thermo-syphon test was developed to test the heat transfer performance of IAS at different inclination angles, and the results were compared to those of water. Copper thermo-syphons charged with DI-water, UCLA Yellow #1, and UCLA IAS #3.2 were tested at five inclination angles: 90°(vertical), 30°, 10°, 5°, and 3°.

4.5.1. Experiment setup

The copper thermo-syphon is made of a 45cm-long copper tube, with 3/8 inch OD and 0.311 inch inside diameter (ID). The tube is cleaned by fragment free wipes to remove dust and machine oil, and then pretreated by a 2mol/L chloride acid solution to remove oxides. One end of the tube is sealed with a copper joint end cap and a 1/8 inch OD copper fill tube by soldering, see Figure 87 (a). A 6-millimeter length copper rod, with 5/16 inch OD, is punched into the other end of the tube and sealed by soldering, see Figure 86.

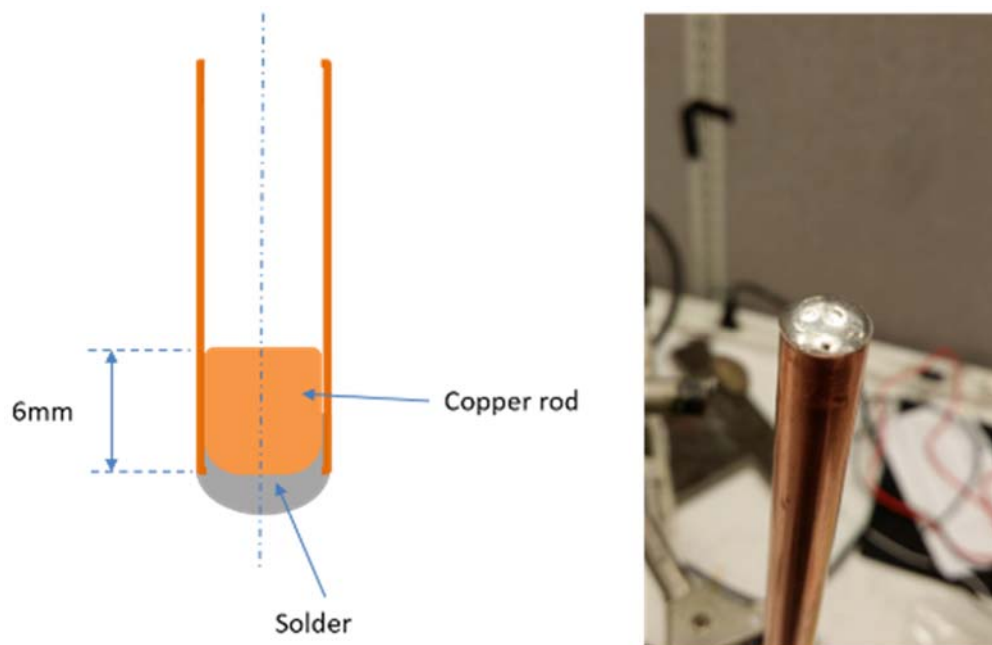


Figure 86: The sealed end of thermo-syphon

Before charging, the thermo-syphon is pretreated by the 2mol/L chloride acid solution again in order to remove the oxide generated during the soldering, and then rinsed by DI-water ten times. After being charged, the fill tube is sealed by cold welding, see Figure 87 (b), and Figure 88 is the cold welder. After being weighed, the sealing seam is protected by a J-B weld adhesive, see Figure 87 (c).

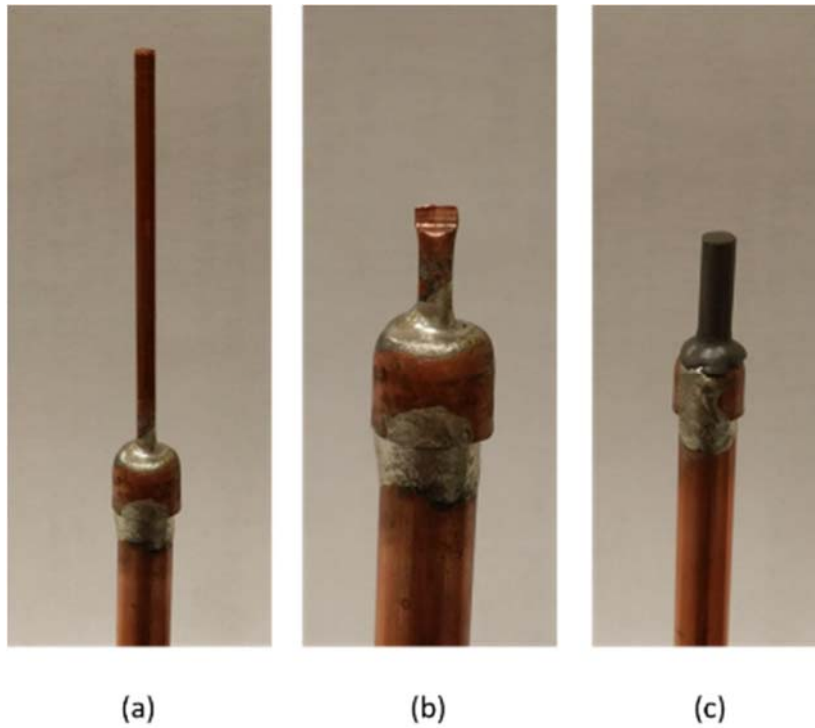


Figure 87: Filling end of thermo-syphon: (a) before charge, (b) sealed by cold welder, (c) protected by J-B weld adhesive



Figure 88: Cold welder

During the test, the thermo-syphon is heated by a cartridge heater block and cooled by a water cooling block with tap water about 20°C, see Figure 89. The tap water is pumped through the cooling block by a fixed-flow chemical metering pump, with the flow rate 18.26gal/day.

Approved for public release; distribution is unlimited.

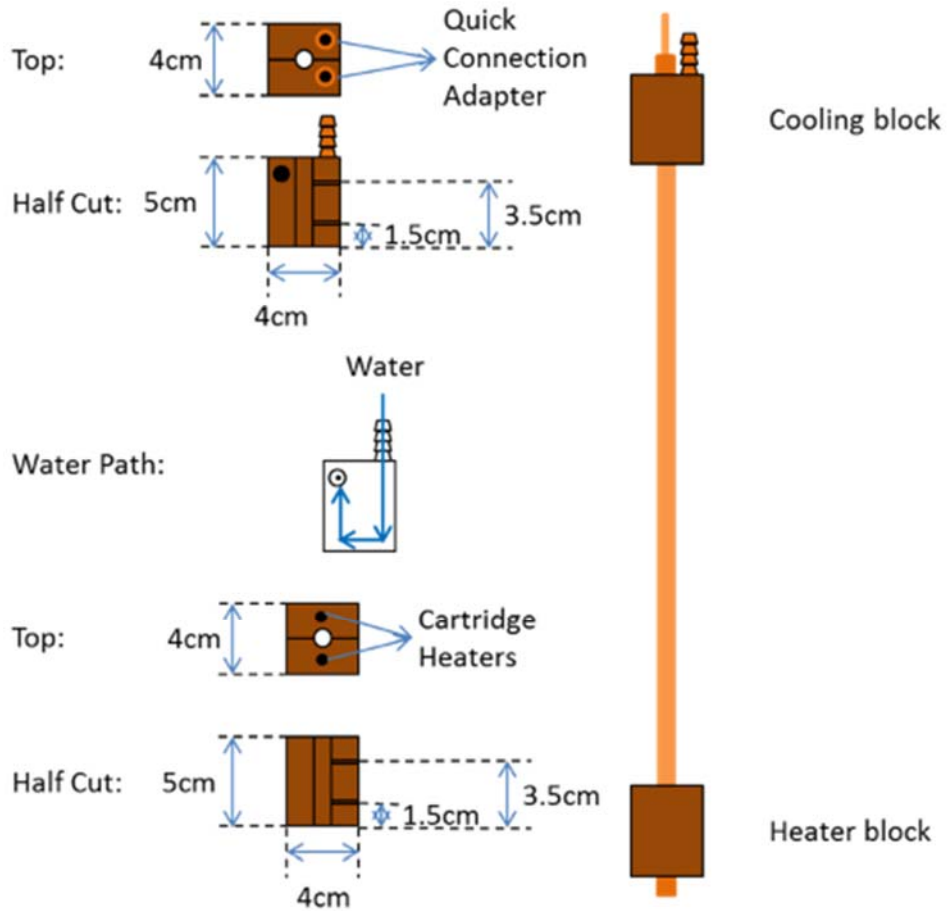


Figure 89: Schematic diagram of the set-up of the thermo-syphon experiment

Ten thermocouples are located on the outer surface of the tube: two in the evaporating region, two in the condensing region, and the other six in the adiabatic region, see Figure 90. The temperatures data is collected by a PC with DASyLab. Figure 91 is the picture of the thermo-syphon test.

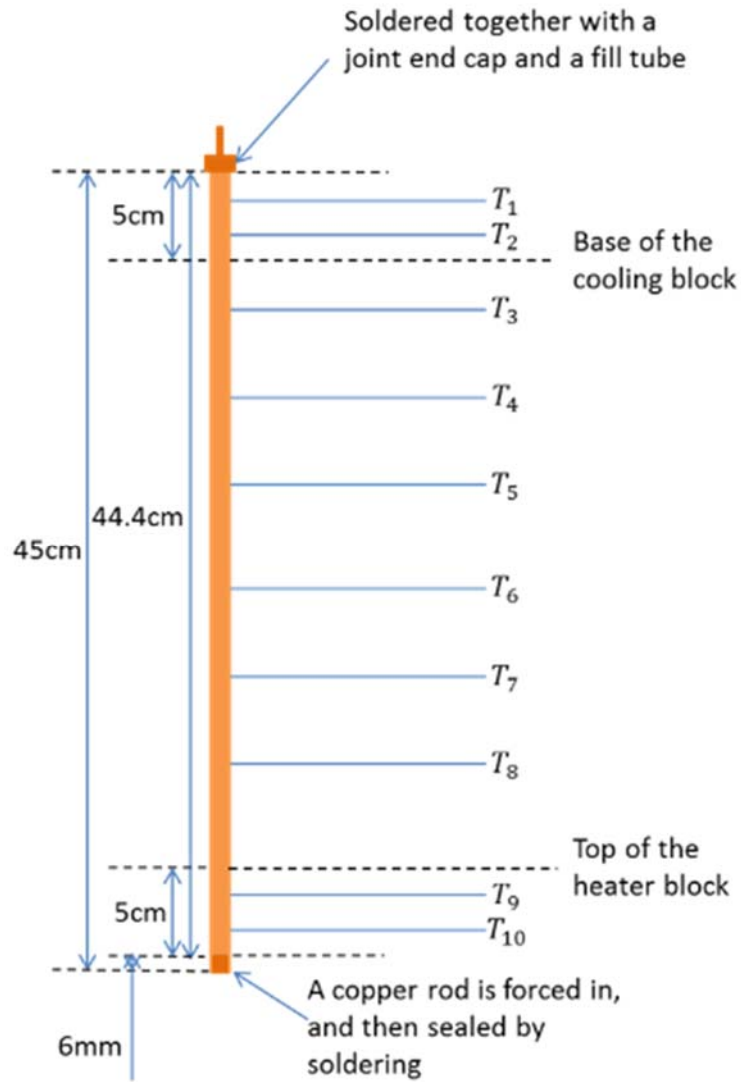


Figure 90: Locations of thermocouples in thermo-syphon test

Approved for public release; distribution is unlimited.

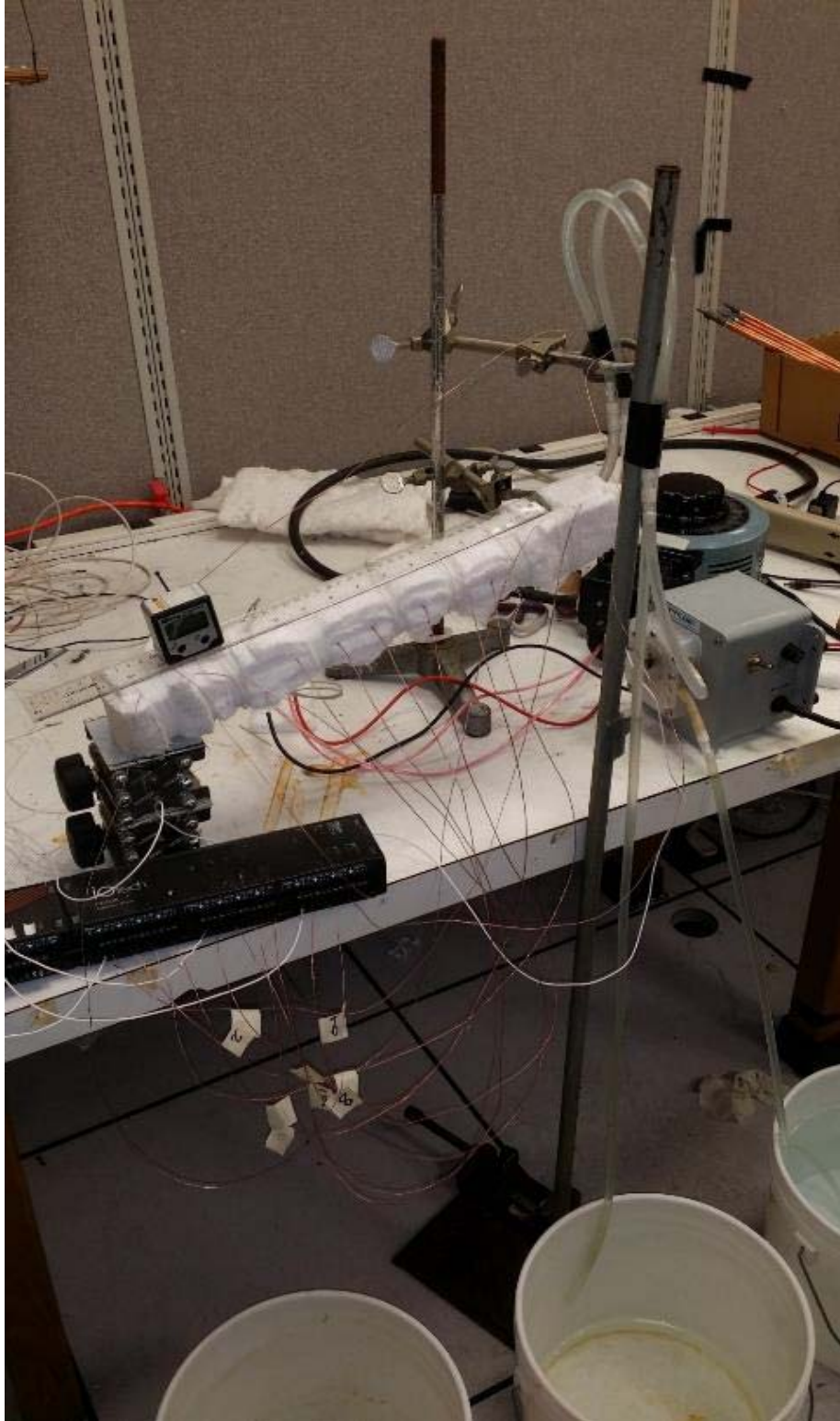


Figure 91: Thermo-syphon test

Approved for public release; distribution is unlimited.

4.5.2. Test results

There are two cartridge heaters in the heater blocks, and the electronic resistance of each is 73.6Ω . The maximum stable voltage that can be obtained from the variac is $110V$, so the maximum input power is 328.8 watts. The tests are initiated with an input power of 20 watts for 15 minutes to reach a steady state. Afterwards, the input power is increased 20 watts every 10 minutes until dry out or 320 watts is reached.

Based on the thermal fluid model in Section 4.2.1, the minimum fill amount of the working fluid is 0.87ml at 320 watts. In addition, Negishi and Sawada [36] found that the highest heat transfer rate was obtained when the filling ratio, the ratio of the volume of the working fluid to the volume of the evaporating region, was between 25% and 60% for water. As a result, about 1.47ml working fluid, 60% of the volume of the evaporating region, was charged in the thermo-syphon tests for the inclination angles of 90° and 30° from horizontal. However, with the inclination angle decreasing, the effect of the gravity decreases, and more and more working liquid stays in the liquid back flow in the adiabatic and condensing regions. In addition, the design of the thermo-syphon test has a relatively small ratio of the evaporating length and the total length, so the thermo-syphon charged with 1.47ml water is found dry out very early at an inclination angle smaller than 30° . Another rule of the filling ratio given by Faghri [34] says the optimal fill ratio of a thermo-syphon, the ratio of the liquid fill volume to the total volume, should be in the range of 0.10 - 0.20 . Therefore, about 3.60ml of the working fluid, 16% of the total volume, was charged in the thermo-syphon tests for the inclination angles of 20° , 10° , 5° , and 3° .

First, two copper thermo-syphons were tested with inclination angles of 90° and 30° . One was charged with 1.47 -gram of water, and the other one was charged with 1.54 -gram of UCLA

Approved for public release; distribution is unlimited.

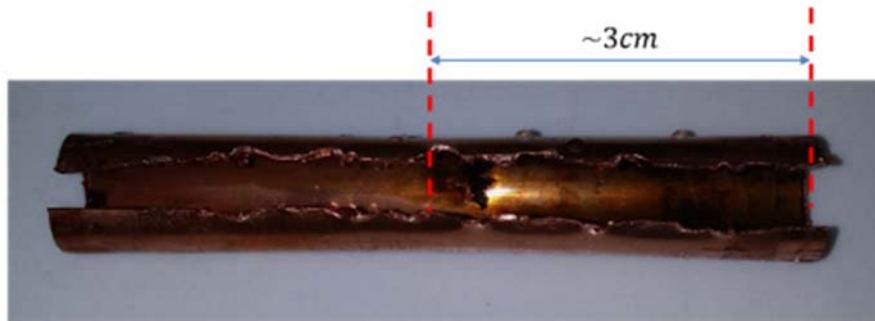
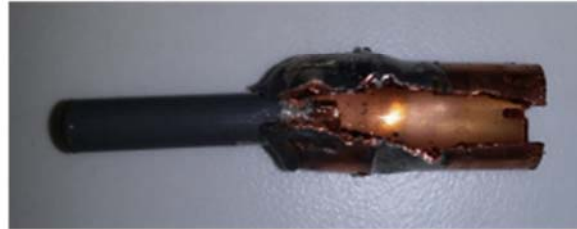
IAS #3.2. The J-B weld adhesive requires 24 hours to be fully cured, so all newly charged thermo-syphons are left overnight before testing. The water tests are not affected by the delay because there is no redox reaction occurring in it. How the IAS charged thermo-syphon is located during the 24 hours determines where the oxides coat. The IAS thermo-syphon was located vertically with the rod end (evaporator) at the bottom. Therefore, all the oxides coat the evaporating region, and they are irremovable.

A sample copper thermo-syphon was charged with UCLA IAS #3.2. After being sealed by the cold welder and the J-B weld adhesive, it was located vertically with the rod end at the bottom. Two hours later, it was cut open, and the liquid was collected. The liquid was completely decolorized to yellow indicating that the permanganate had been reacted out. Therefore, 2 hours is long enough for the redox reaction between copper and permanganate to be accomplished at the room temperature.

Approved for public release; distribution is unlimited.



(a)



(b)

Figure 92: Overview of a cut open IAS/copper thermo-syphon

After being tested, the evaporating and condensing regions of the IAS thermo-syphon were cut open to show where the oxides coating was to be found, see Figure 92 (a). There was no color change or black coating detected in the condensing region, but the 3cm length of the evaporating region changed colors and was coated by a black coating, see Figure 92 (b). The volume of a 3cm length tube is equal to the fill amount of 60% of the evaporating region.

Two runs were made for each thermo-syphon per inclination angle. Usually, the second run starts working stably at a smaller input power, see Figure 93. Therefore, the results of the

Approved for public release; distribution is unlimited.

second runs will be used for comparison. In addition, when the temperature difference between the evaporator and the condenser is larger than 70°C, the tube is assumed to dry out.

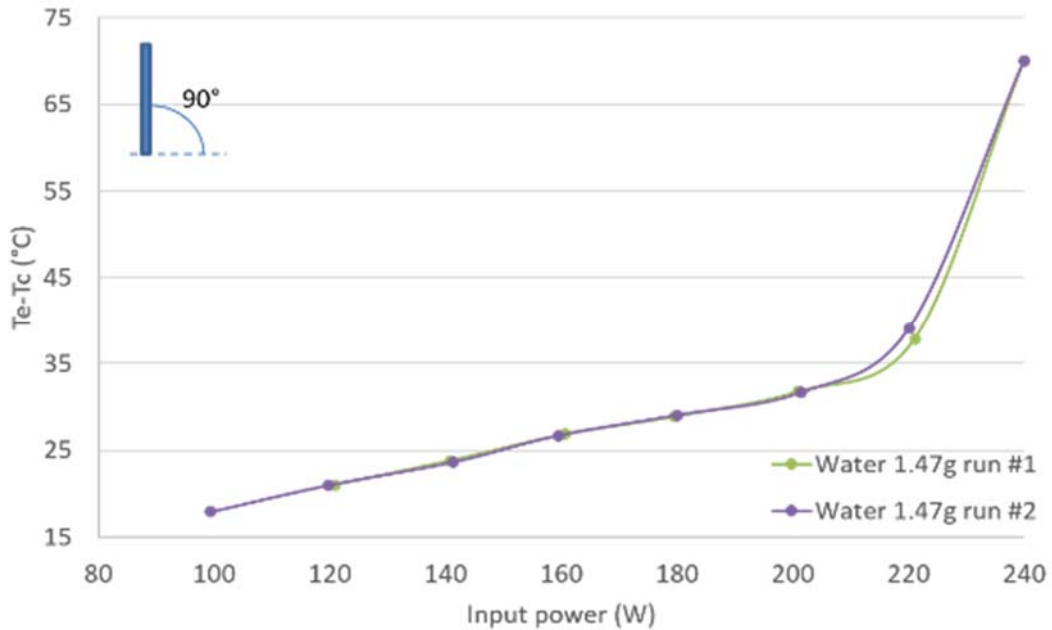


Figure 93: Test results of thermo-syphon with 1.47g water at inclination angle 90°

Figure 94 shows the performance comparison between water/copper and IAS/copper thermo-syphons at the inclination angle of 90°. The water filled tube starts working stably earlier and has a smaller temperature difference between the evaporator and the condenser below 220 watts. After 220 watts, the water filled tube dries out, but the IAS filled tube keeps working without drying out till the maximum input power 320 watts.

Approved for public release; distribution is unlimited.

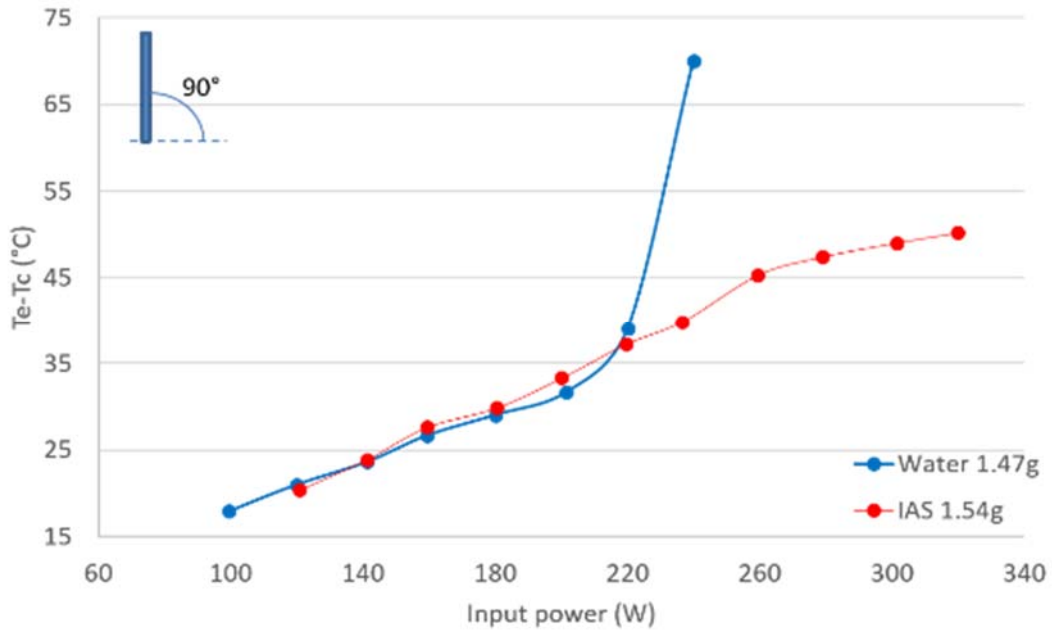


Figure 94: Performance comparison between water/copper and IAS/copper thermo-syphons at inclination angle 90°

Figure 95 shows the performance comparison between water/copper and IAS/copper thermo-syphons at the inclination angle of 30°. It is similar with that of 90°, but the water one dries out a lot earlier. The IAS one still keeps working without drying out till 320 watts.

Approved for public release; distribution is unlimited.

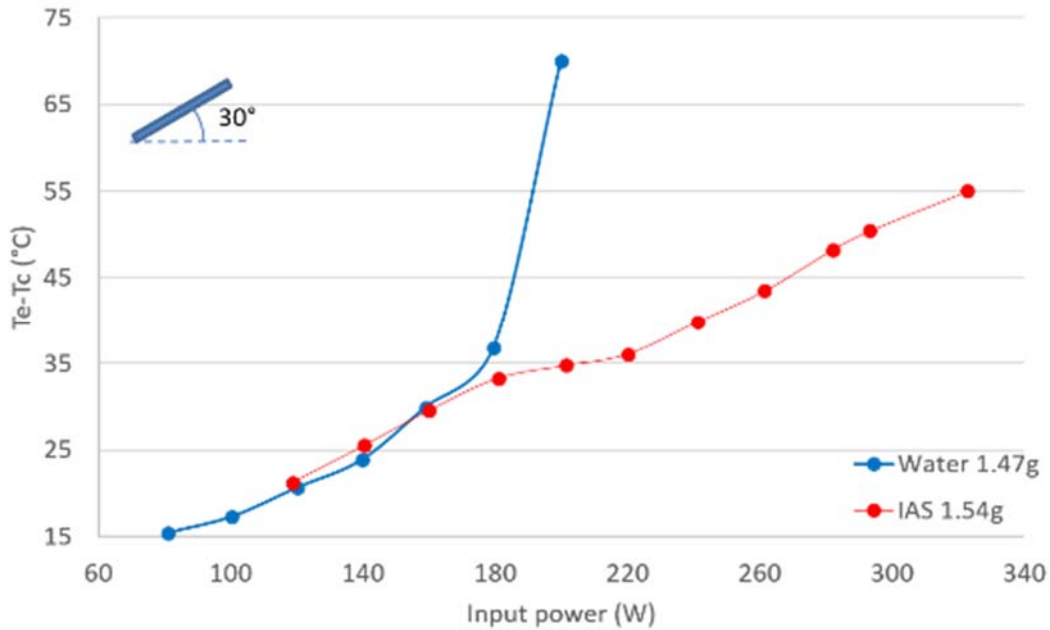


Figure 95: Performance comparison between water/copper and IAS/copper thermo-syphons at inclination angle 30°

The water thermo-syphon, charged with 1.47g water, was further tested at inclination angles of 15° and 10°. However, it dried out at low input powers when a stably working had not been reached. The thermo-syphon used in this test has a relatively small evaporating region. The length of the evaporating region is 5cm, which is 11.1% of the total length of the thermo-syphon. If the charge amount is 60% of the evaporating region, it will be only 6.7% of the total volume. With the inclination angle being smaller, there will be more liquid in the condensing and adiabatic regions flowing back to the evaporator. Based on the data given by Faghri [34], the optimal fill ratio of a thermo-syphon, the ratio of the liquid fill volume to the total volume, should be in the range of 0.10-0.20. Therefore, a larger charge amount 3.60ml, which is about 16% of the total volume, was used for the inclination angles of 20°, 10°, 5°, and 3°.

Approved for public release; distribution is unlimited.

The Bond number

$$Bo_D = \frac{gD^2(\rho_l - \rho_v)}{\sigma} \quad (72)$$

represents the ratio of the gravitational force to the surface tension force.

For the thermo-syphon tests, the Bond number should be larger than 1

$$Bo_D = \frac{g \sin \theta D_i^2 (\rho_l - \rho_v)}{\sigma} > 1 \quad (73)$$

which means that the gravitational force is dominant, and the condensed liquid in the condensing and adiabatic regions will flow back to the evaporator. For the temperature range of 5°C to 120°C, the inclination angle should be no smaller than 7.04°,

$$\theta \geq 7.04^\circ \quad (74)$$

Therefore, thermo-syphons with pure water cannot work at inclination angles that are smaller than 7.04°. This was demonstrated by the testing and the results are shown in Figure 96.

Three thermo-syphons, charged with DI-water, UCLA IAS #3.2, and UCLA Yellow #1, were tested at inclination angles of 20°, 10°, 5°, and 3°. UCLA Yellow #1 has the same chemical concentrations as UCLA IAS #3.2 but no potassium permanganate, see Appendix 0. Figure 96 shows the test results of inclination angles of 5° and 3°. The one with yellow fluid could not reach stable operation before drying out.

Approved for public release; distribution is unlimited.

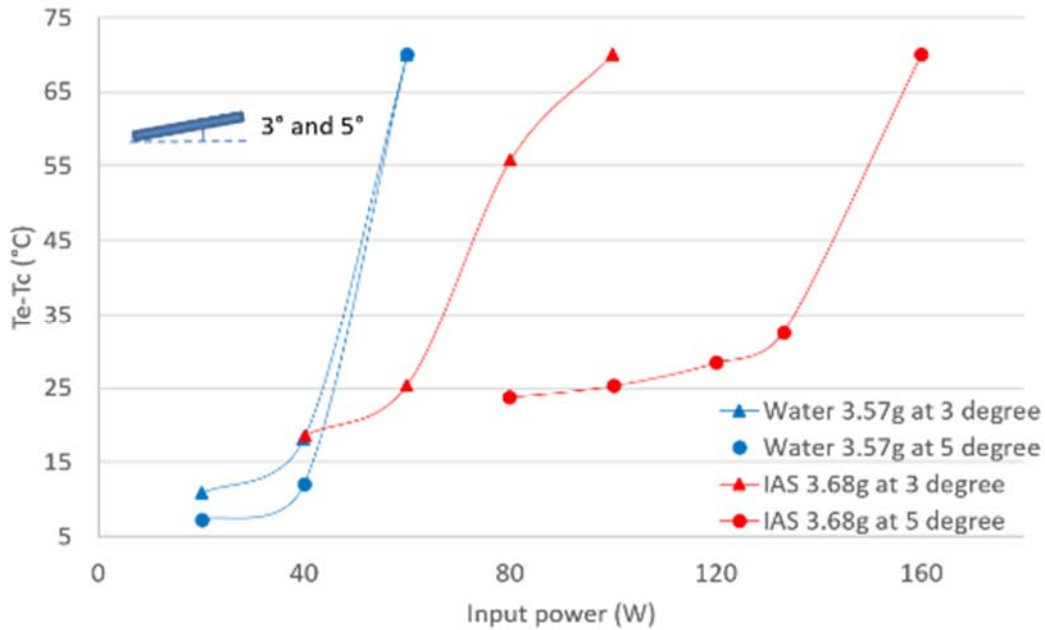


Figure 96: Performance comparison between water/copper and IAS/copper thermo-syphons at inclination angles of 3° and 5°

The water thermo-syphon dried out at 60 watts at both inclination angles of 3° and 5°. Actually, it appeared that all the water moved from the evaporator to the condenser, and then it dried out. The IAS filled tube dried out at around 80 watts, 20 watts above that of the water one at an inclination angle of 3°. However, it continued working well until 160 watts at an inclination angle of 5°.

Figure 97 shows the test results at an inclination angle of 10°. The water filled thermo-syphon started working stably at 20 watts, which was much earlier than the yellow and IAS filled tubes, but it dried out at 100 watts. The yellow filled tube started working stably at 80 watts, but it dried out at 140 watts. The IAS filled tube could not reach the stable operation until 100 watts, but it continued working without drying out until 260 watts.

Approved for public release; distribution is unlimited.

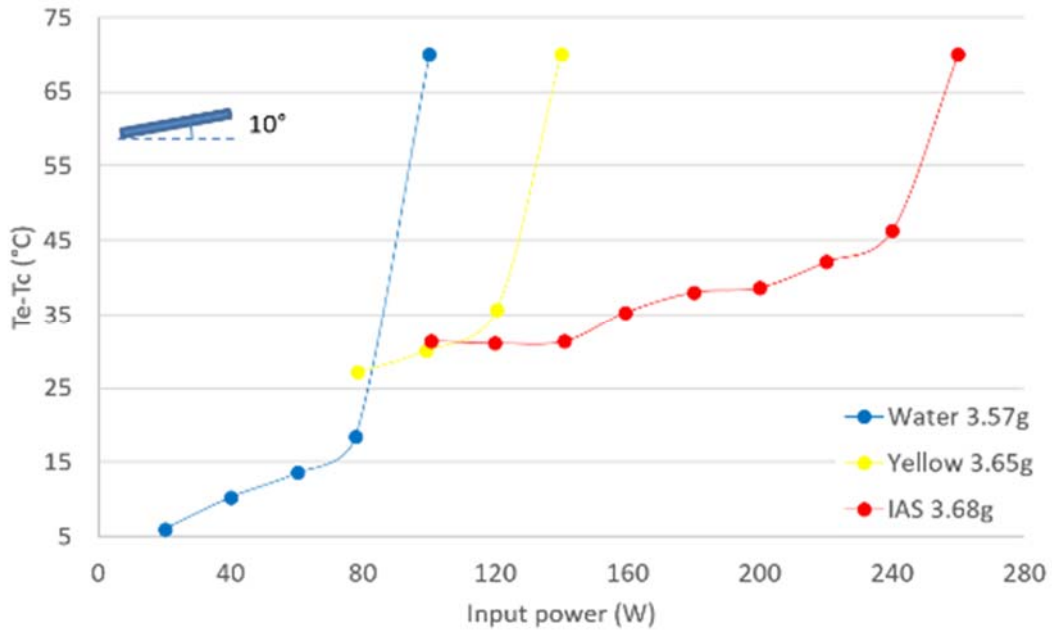


Figure 97: Performance comparison between water/copper, yellow/copper, and IAS/copper thermo-syphons at inclination angles 10°

Figure 98 shows the test results for an inclination angle of 20°. The water thermo-syphon began stable operation the earliest, but it dried out the earliest at 160 watts. The yellow filled tube dried out later than the water filled tube, but not by very much. The IAS filled tube began stable operation at 100 watts, and it had the same temperature difference between the evaporator and the condenser as the water filled tube at 100 watts. In addition, the IAS charged thermo-syphon did not dry out at the maximum input power, 320 watts.

Approved for public release; distribution is unlimited.

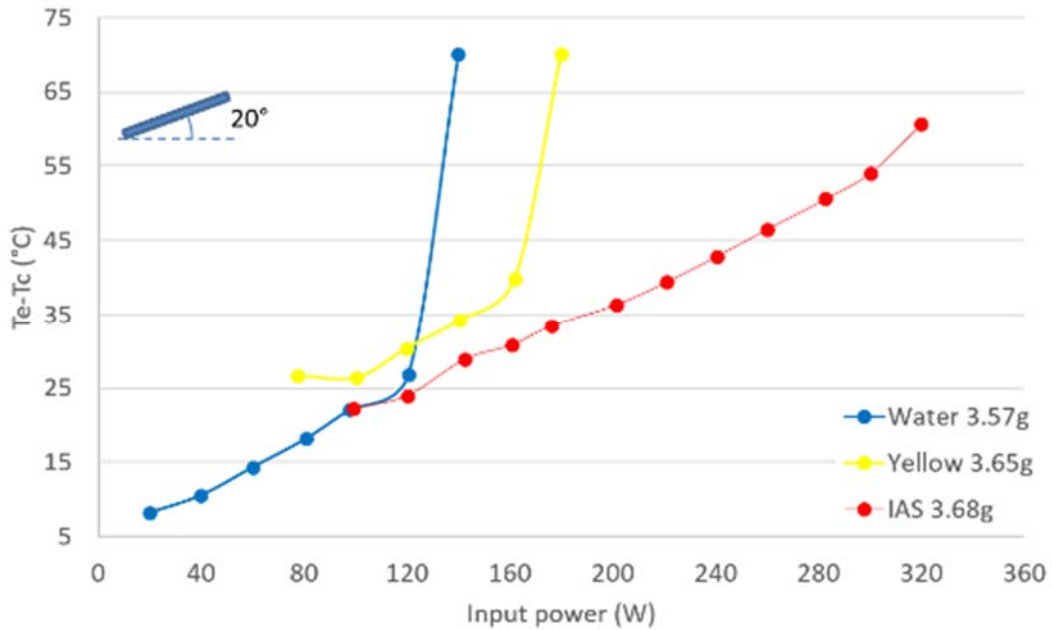


Figure 98: Performance comparison between water/copper, yellow/copper, and IAS/copper thermo-syphons at inclination angles 20°

4.5.3. Results and Discussion

Based on the results of the diffusion model and the capillary tests, IAS will coat the surface that is submerged with a layer of oxides that are permanent during the operation. Solid chromate salts are generated in the meniscus region because of the advection of the liquid flow. Both improve the surface wettability and enhance the bonding force between the liquid and the surface. The meniscus regions in vertical IAS/copper and water/copper thermo-syphons are shown in Figure 99 if the liquid back flow is not considered.

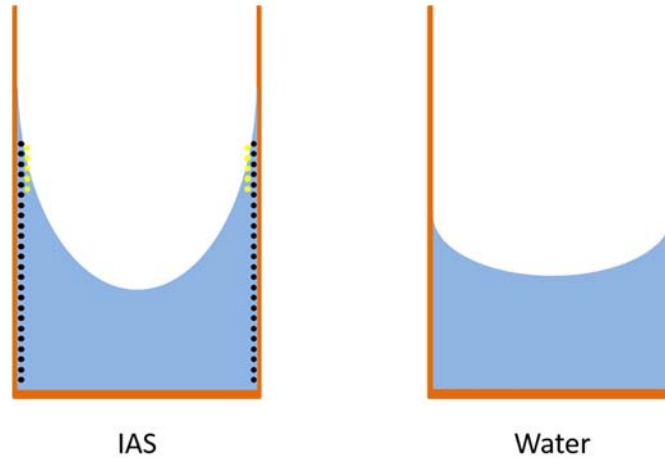


Figure 99: Meniscus regions in vertical IAS/copper and water/copper thermo-syphons, without liquid back flow

However, the thermo-syphon is a closed system, and the condensed liquid flows back to the evaporator along the tube wall. This makes the meniscus region of the IAS/copper thermo-syphon different. Figure 100 is the original test results of the 1.47g water/copper thermo-syphon at the inclination of 90°, and it can be divided into four working regions: not working, unstable operation, stable operation, and dry out.

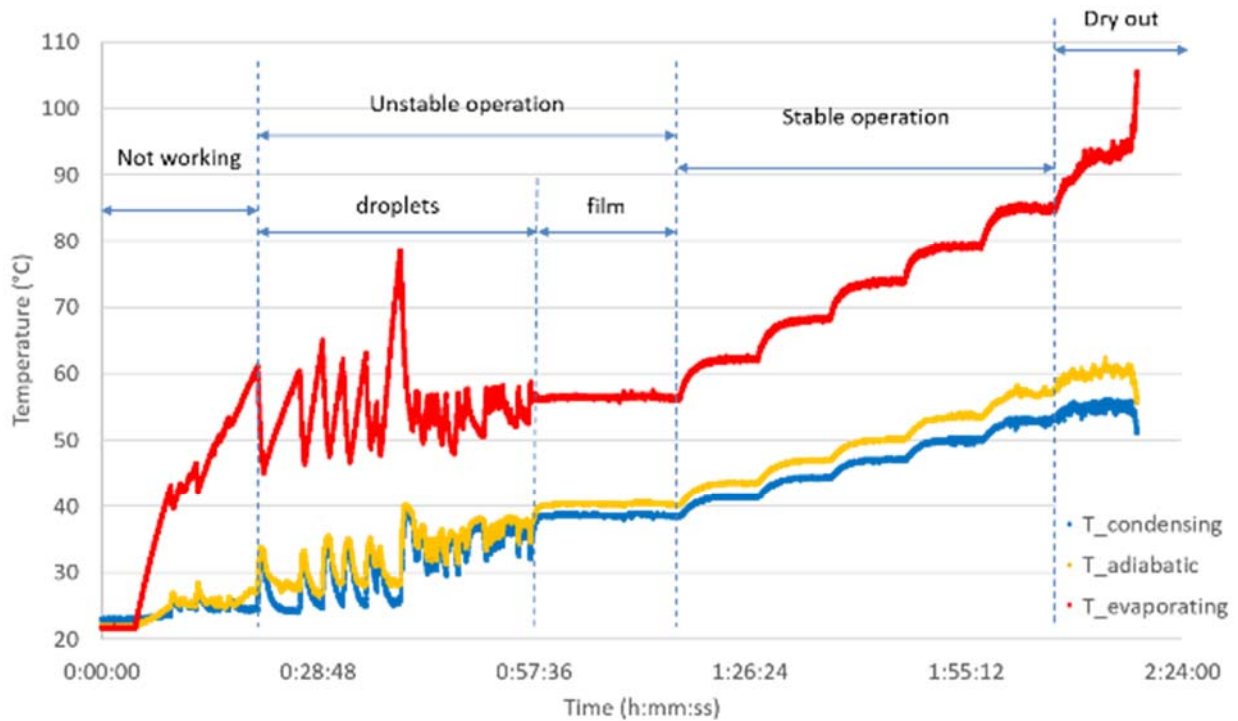


Figure 100: Working regions of a thermo-syphon

When the test is initiated, the liquid in the evaporator is heated up. The thermo-syphon will not start working until the vapor pressure difference between the evaporator and the condenser is large enough to pump the vapor flow. In addition, while the thermo-syphon is working at low input powers, the condensed liquid flows back to the evaporator by droplets. This causes the pulsatile temperature profiles in the unstable operation region. Moreover, the stable operation will not be reached until a stable film flow is formed. Last, when the boiling limit is reached, the thermo-syphon starts to dry out.

For a IAS/copper thermo-syphon, it follows the same working regions as the water one. While, the difference is that before a film flow is formed, chromate salts will be generated and coat the meniscus region, as shown in Figure 99. When a film flow is formed, it starts to wash off the previously generated chromate salts. The coatings bring extra resistance to the liquid flow and

Approved for public release; distribution is unlimited.

cause an extra instability, so the IAS/copper thermo-syphon reaches stable operation later than the water one. When the stable operation is reached, the chromate salts are washed off, and the film thickness of the liquid flow is large enough to submerge the oxides coating. In this case, the curvature of the liquid/vapor interface of the IAS thermo-syphon is the same as that of the water thermo-syphon, see Figure 101.

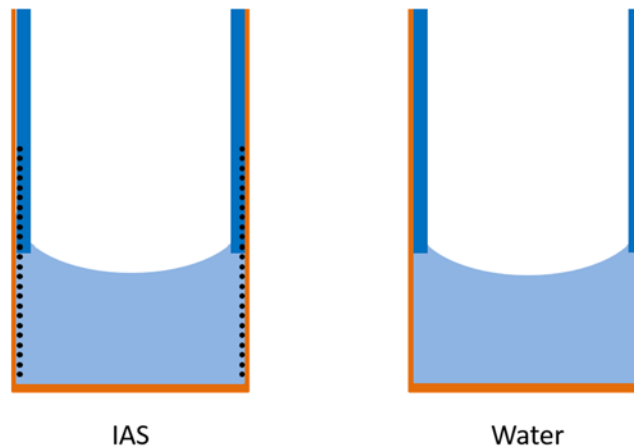


Figure 101: Meniscus regions in vertical IAS/copper and water/copper thermo-syphons, with liquid back flow

As a result, for a given input power, if both IAS/copper and water/copper thermo-syphons, at inclination angles of 90° and 30° , are operating in the stable operation region, they should have similar heat transfer performances. Because the thin oxides coating brings an extra thermal resistance to the IAS/copper thermo-syphon, the heat transfer performance of it should be a little worse than that of the water/copper thermo-syphon. This can be demonstrated by the test results in Figure 94 and Figure 95.

For small inclination angles, the condensed liquid flows back to the evaporator only along one side of the tube, see Figure 102. In region (1), where the meniscus is interrupted by the liquid back flow, the chromate salts are washed off, and the oxides coating is submerged by the liquid

Approved for public release; distribution is unlimited.

film, just like the case in Figure 101. However, in region (2), the meniscus is not interrupted by the liquid back flow, as the case in Figure 99, so both chromate salts and oxides coat the meniscus region and enhance the surface wettability. Therefore, an inclined IAS/copper thermo-syphon should have a better heat transfer performance than the water/copper one.

However, based on the test results in Figure 97 and Figure 98, the water/copper thermo-syphon dried out before the IAS/copper thermo-syphon reached stable operation, so the thermo-syphon test is not a good design to demonstrate the performance enhancement effect of IAS on a smaller thermal resistance. While, this effect of IAS has been demonstrated by Supowit [37] using a grooved flat heat pipe, which will be discussed in Section 4.6.

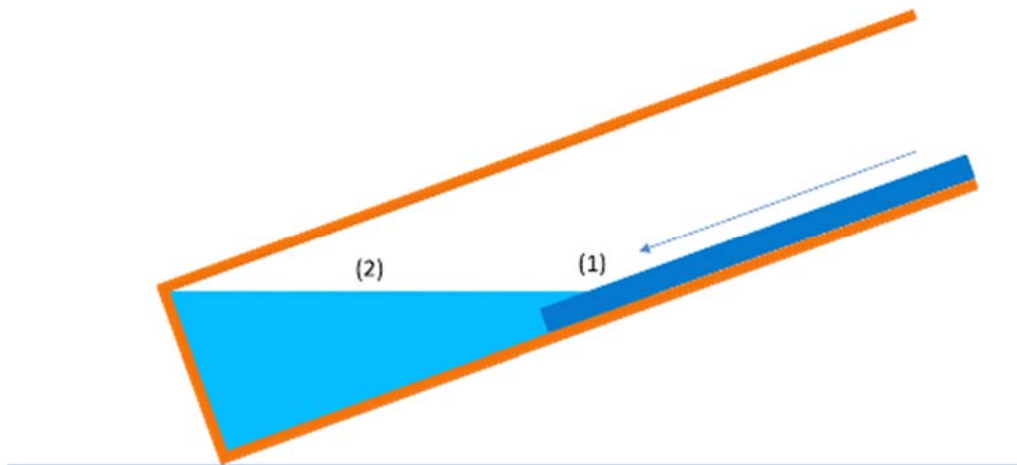


Figure 102: Meniscus regions in an inclined thermo-syphon, with liquid back flow

Nevertheless, the thermo-syphon tests demonstrated the performance enhancement effect of IAS on delaying dry out. First, as mentioned in Section 4.3, the combination effects of the chromate solution and oxides improve the surface wettability, and it makes the meniscus more difficult to retreat. Even in case if the meniscus retreats, a layer of large solubility chromate salts will be left on the dried surface, and it makes the surface much easier to be rewetted. As a result,

Approved for public release; distribution is unlimited.

when nucleation boiling occurs, there will not be large bubbles generated, and the dried surface, caused by bubbling, will be rewetted immediately after the bubble departs. All of these make boiling not a limit anymore to IAS/copper thermo-syphons.

4.6. Comparison Tests in Other Applications

The performance enhancement of different phase change devices was investigated to determine the value of IAS for different applications. The heat transfer performances of IAS in two applications: a grooved flat heat pipe and a sintered heat pipe, were tested. The results were compared to those of water.

4.6.1. Flat heat pipe test

Supowit [37] measured the heat transfer performance of IAS in a copper grooved flat heat pipe and compared it to the results for water at different inclination angles, see Figure 103. At an inclination angle of 3° , IAS has a smaller thermal resistance than water over the entire operation region. In addition, IAS has a much later dry out than water. Actually, the IAS did not dry out for the tests at inclination angles of 3° , 5° , and 6° .

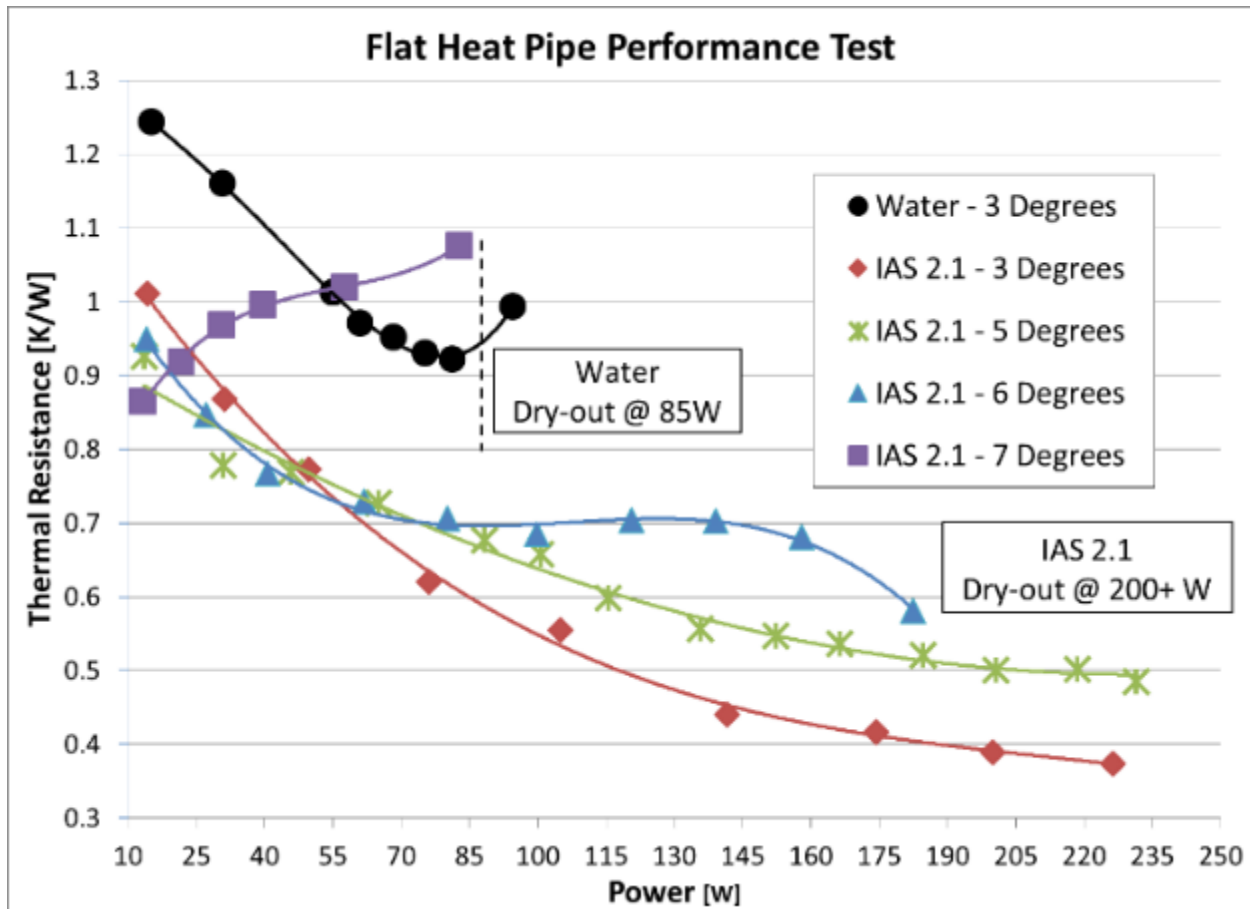


Figure 103: Flat heat pipe test results

Supowit's test results demonstrate the performance enhancement effect of IAS by achieving a lower thermal resistance. The reasons for this are explained in Section 4.5.3. Figure 104 shows the difference between water and IAS in the evaporating region of the grooved flat heat pipe. In flat heat pipe, meniscus regions are on the side walls of each groove. Because the chromate solution and oxides improve the surface wettability in the meniscus region, thinner liquid films are formed for IAS leading to the smaller thermal resistance of heat transfer.

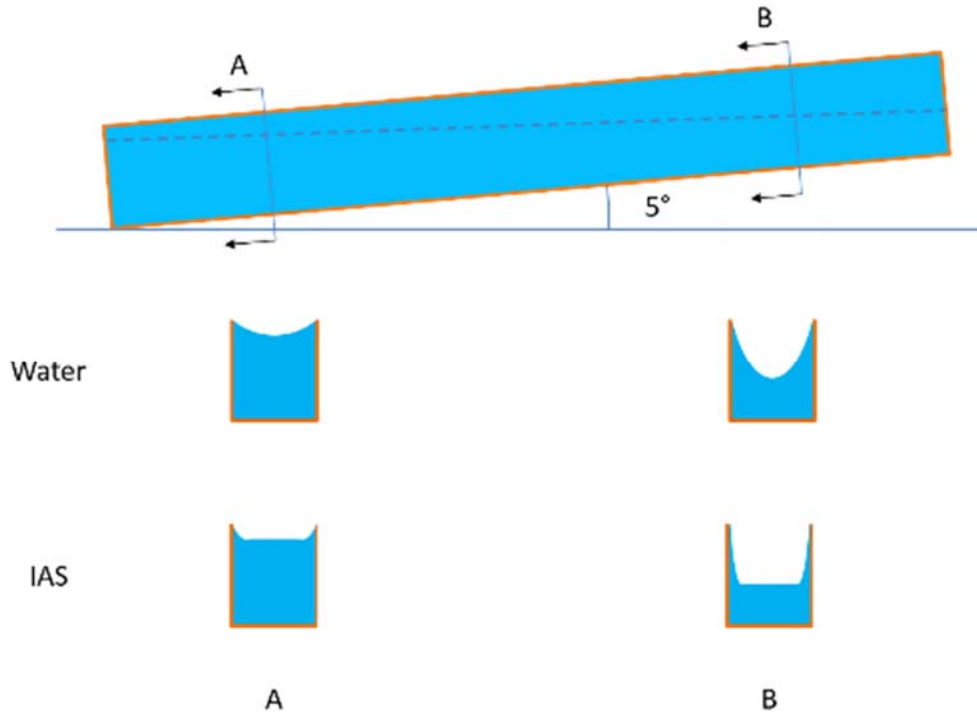


Figure 104: Difference between water and IAS in grooved flat heat pipe, evaporating region

4.6.2. Sintered heat pipe test

Copper sintered heat pipes, purchased from Enertron, were opened and recharged with DI-water and UCLA IAS #3.2. The heat transfer performance was tested, and the results were compared to those of the stock Enertron heat pipes. Table 33 shows the information of the Enertron heat pipes.

Table 33: Information of Enertron heat pipe

Length	30cm
OD	8mm
Tube thickness	~0.5mm
Wick thickness	~1mm
Particle size	60 μ m
Charge amount	2.6ml
Maximum workload	~40W

Approved for public release; distribution is unlimited.

The procedure for preparing heat pipes was to open the fill end of the heat pipe and install a joint end cap with a fill tube. JB-weld adhesive was used to seal the connections among the fill tube, the joint end cap, and the heat pipe. The original working fluid was vacuumed out at the room temperature, and then it was recharged with the same amount of DI-water or UCLA IAS #3.2. The fill tube was sealed by cold welding and then protected by an Epoxy adhesive, see Figure 105.



Figure 105: Original Enertron heat pipe and recharged heat pipe

Figure 106 is a schematic showing the thermocouple locations for the heat pipe tests. The heat pipe is located horizontally. It is heated by a heater block with two cartridge heaters and cooled by a cooling block with tap water at 20°C pumped by a peristaltic pump. A total of six thermocouples are located on the tube: two in the evaporating region, two in the adiabatic region, and two in the condensing region.

Approved for public release; distribution is unlimited.

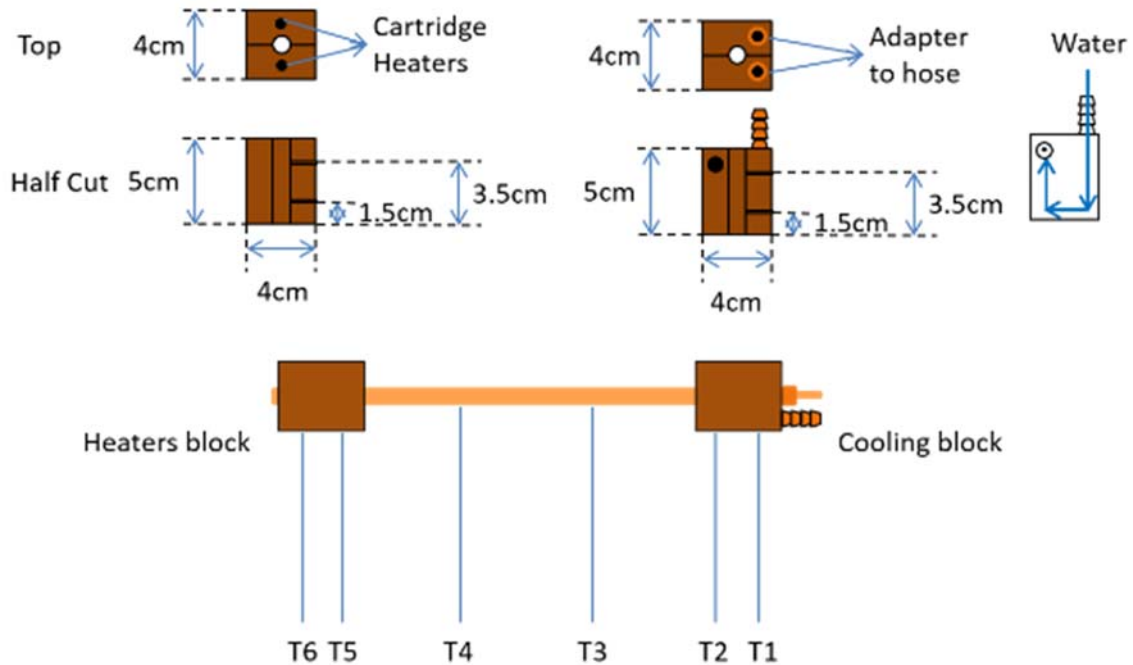


Figure 106: Schematic and thermocouple locations of heat pipe test

Each test was initiated with an input power of 10 watts for 15 minutes, and then the input power was increased 5 watts every 10 minutes until dry out. Once the temperature difference between the evaporator and the condenser was larger than 40°C, the heat pipe was assumed to dry out. Figure 107 shows the heat pipe test results.

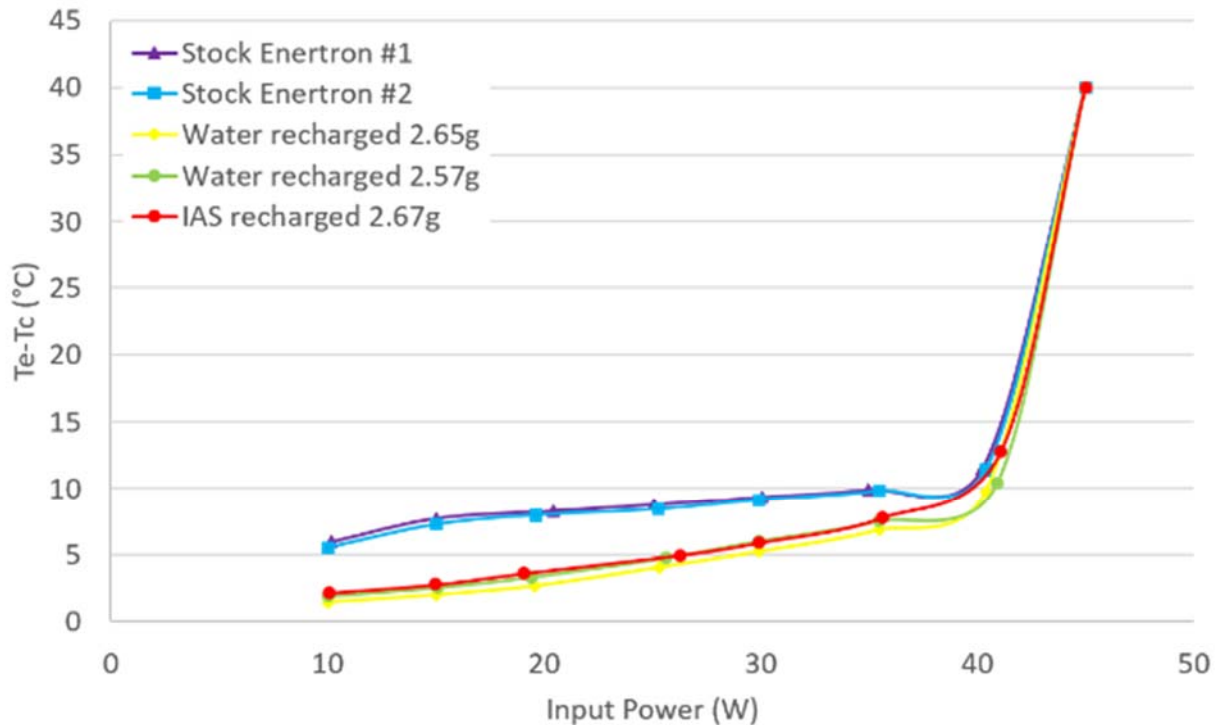


Figure 107: Heat pipe test results

First, two stock Enertron heat pipes were tested, and the performances were the same for both. Both of them dried out at 45 watts. Next, two recharged water heat pipes were tested. Their performances were identical to each other, but their performances were better than those of the stock Enertron heat pipes. This can be explained by the differences in the filling process. In industry, heat pipe manufacturers use a boil-off method to evacuate the air in heat pipes before sealing. This method is easy and fast, but it will leave a small amount of air inside of the heat pipe and an uncertainty in the actual fill amount. The recharged heat pipes were vacuumed by a powerful vacuum pump and then charged with a known amount of degassed DI-water, so the amount of air left in the recharged heat pipes is much smaller than those in the stock Enertron heat pipes.

Approved for public release; distribution is unlimited.

The heat pipes were then recharged with IAS and tested. The performance was found to be identical to the performance of the recharged water heat pipes. It had similar thermal resistance to the recharged water pipes, and it dried out at the same input power of 45 watts. Therefore, an IAS charged sintered heat pipe did not improve the heat transfer performance.

In an operating sintered heat pipe, the meniscus regions are at the outer layer of the spheres that are sintered to make the wick. As a result, because the advection is dominant, all the chemicals will be pushed out of the wick, and chromate salts will be generated and coat only the outer layer of spheres of the wick. The liquid flowing inside of the wick will be relatively pure water, see Figure 108.

For a sintered heat pipe, boiling limit is usually reached first because of the thick wick. Nucleation usually initiates inside of the wick and close to the tube wall, point A as shown in Figure 108, because it has the largest superheat. However, there is no chromate in the liquid at point A. Once bubbles are generated, the surface is dried out and will not be rewetted. As a result, IAS cannot delay the dry out of a sintered heat pipe with a thick wick in which boiling limit is dominant. However, for a thin wick, chemicals will be brought into the wick for a small distance while the meniscus recedes. If the small distance is on the order of the thickness of the wick, it will become similar to a thermo-syphon, and there will be dry out improvement. This area needs to be further explored.

Approved for public release; distribution is unlimited.

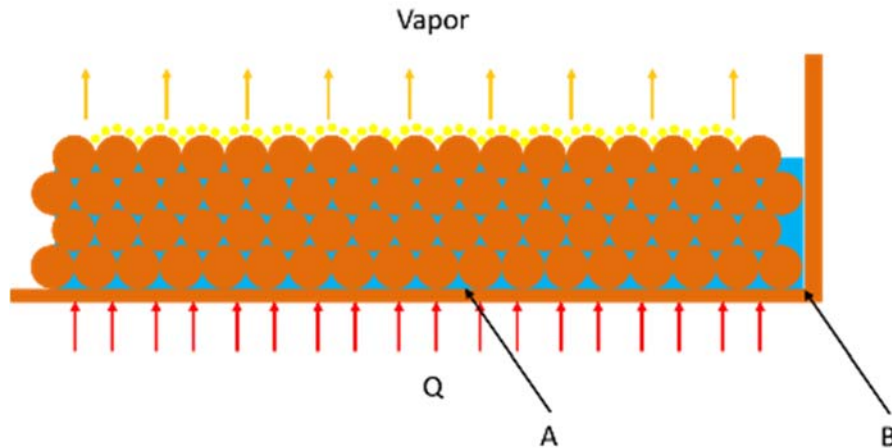


Figure 108: Schematic of the evaporating region of a heat pipe, with IAS as working fluid

Moreover, the thermal resistance of a heat pipe is dominated by the effective thermal resistance of the wick saturated with the working fluid. In an operating heat pipe, charged with IAS, the liquid flowing inside of the wick is pure water, so the effective thermal conductivity of the saturated wick is the same as a water heat pipe. IAS improves the surface wettability of the outer layer of spheres of the wick. To obtain the same capillary pressure, a lower liquid level of IAS is required, see Figure 109. A smaller effective wick thickness leads to a smaller effective thermal resistance. However, the performance enhancement is only noticeable when the diameter of the copper sphere and the thickness of the wick are on the same order, $\delta \leq 10d$. Otherwise, the decreased thermal resistance by IAS is too small compared to the total thermal resistance of a heat pipe. This means the wick design has to consider the improved capillarity and the thermal resistance of the deposits if a benefit is to be achieved.

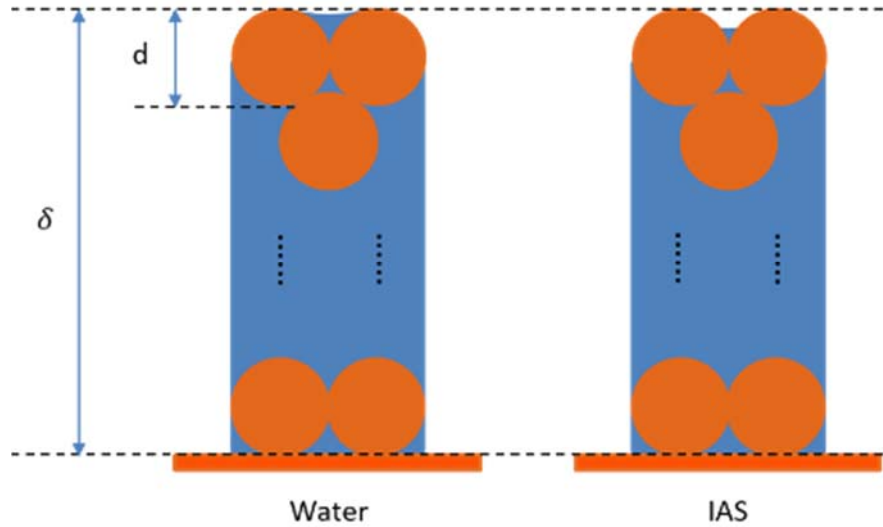


Figure 109: Comparison between water and IAS in sintered wicks

Based on the conclusions above, a smaller wick thickness in the evaporating region is required to use IAS in sintered heat pipes. In addition, a smaller charge amount is required while using IAS, which leads to a smaller effective thermal resistance. Moreover, a biporous wick, a large cluster diameter, will also be a good design for IAS.

4.7. Conclusion

In this chapter, the performance enhancement resulting from the use of IAS in copper phase change heat transfer devices has been demonstrated. The mechanisms that lead to an explanation of how IAS improves the surface wettability is revealed, and the limits of using IAS in different heat transfer applications are discussed.

Using diffusion model, advection is shown to dominate diffusion in phase change heat transfer devices. As a result, all the soluble chemicals will be pushed to the meniscus region in an operating phase change heat transfer device.

Approved for public release; distribution is unlimited.

The combined effect of chromate solution and oxides is the reason IAS improves the surface wettability. Copper (I) oxide and manganese (IV) oxide are generated by the reaction between IAS and the copper surface, and they will uniformly coat the surface submerged by IAS. Chromate solution has better wettability on oxide coated surfaces than that on clean copper surfaces, and the contact angle decreases with the concentration increasing. In addition, solid chromate salts are generated and coat the meniscus region because solubility limits are reached, which provides capillarity and prevents meniscus receding. All of above increase the surface wettability and delay the dry out.

In thermo-syphons, use of IAS becomes stable at higher heat fluxes than that of water but significantly increases the heat flux at dry out. Because of the liquid back flow merging with the meniscus region, IAS will not decrease the thermal resistance of vertical thermo-syphons. For inclined thermo-syphons, the use of IAS results in a much later dry out compared to those with water. In addition, the water filled thermo-syphons dry out at fluxes where the IAS based thermo-syphons have not yet to reach the stable operation. At the smaller angles of inclination, an IAS filled tube could operate whereas the water filled tube could not. The thermo-syphon tests demonstrate the performance enhancement effect of IAS on a later dry out, but it is not a good configuration to demonstrate the performance enhancement effect of IAS on a smaller thermal resistance.

The grooved heat pipe is an ideal application for IAS. Compared to water, IAS has a smaller thermal resistance and a much later dry out. The performance enhancement derived from the use of IAS is demonstrated by the significantly later dry out and a smaller thermal resistance.

Approved for public release; distribution is unlimited.

IAS did not improve the heat transfer performance in an existing sintered heat pipe as well as it did in other phase change heat transfer applications. The improvement depends on the thickness of the wick and the particles diameters. When using IAS in sintered heat pipes, a smaller wick thickness in the evaporating region and a smaller charge amount are required to delay the dry out and achieve a smaller thermal resistance.

Approved for public release; distribution is unlimited.

5. USING IAS IN ALUMINUM DEVICES

For ground-based phase change heat transfer devices, copper and water are the most commonly used casing material and working fluid. Water is the most common liquid because it has a large latent heat of evaporation. Copper is chosen because of its high thermal conductivity and excellent compatibility with water. However, for space applications, this combination is not perfect anymore. Because of the weight limit, aluminum is widely used because it is three times less dense than copper [38]. It is also much cheaper than copper. Aluminum is highly chemically active material, and it can reduce water and generate hydrogen gas, a non-condensable gas (NCG), which can fail the phase change heat transfer device in a few minutes. As a result, water is not compatible with aluminum made phase change heat transfer devices. For aluminum phase change heat transfer devices, fluids such as ammonia or methanol are used as the working fluid to avoid generating NCG. However, because of their low evaporation latent heats, the maximum load of such devices is limited.

IAS was shown to be compatible with aluminum phase change heat transfer devices by Reilly et al [23] and Stubblebine et al [24]. This chapter aims to develop an explanation of why IAS is compatible with aluminum phase change heat transfer devices and establish the limits on the use of IAS in different aluminum made heat transfer applications.

5.1. Aluminum Passivation Theory

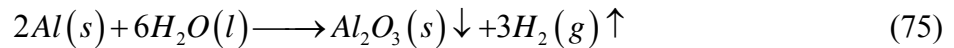
The chemicals in IAS can be classified into two groups, passivation and performance enhancement, as shown in Table 34. Passivation is the main concern in this chapter, so only the chemicals in the passivation group will be discussed.

Approved for public release; distribution is unlimited.

Table 34: Ion roles for IAS and aluminum

Passivation	Performance Enhancement
MnO_4^-	CrO_4^{2-}
$Cr(VI)$	Ca^{2+}
Ag^+	Sr^{2+}
pH number (H^+)	K^+
	Na^+

In general, aqueous solutions are not able to be used as the working fluid in aluminum phase change heat transfer devices. Aluminum metal is highly chemically active, and it is easily oxidized by water to become aluminum (III) compounds. In addition, the reaction generates hydrogen gas, a non-condensable gas (NCG),



which will be compressed and accumulated in the condenser of the device forming a NCG block. Over time, the gas block grows, reduces the effective condensing region, and eventually fails the heat transfer device.

However, aluminum has been shown to be passivated by several different methods. No matter which method is chosen, the final goal is generating a thin and compact layer of aluminum oxide to protect the surface and prevent further reactions. Such a layer can be generated in a strong oxidation environment, and the oxidizers in the IAS fluid are strong enough to make it happen.

Figure 110 is an E-pH diagram for pure aluminum at 25°C in an aqueous solution. Lines (a) and (b) are the boundaries corresponding to the stability of water. Above line (b), water will be oxidized, and oxygen gas will be generated. Below line (a), water will be reduced, and hydrogen gas will be generated. When aluminum is in contact with pure water, water will be reduced to generate hydrogen gas because the region of aluminum immunity is much lower than line (a).

Approved for public release; distribution is unlimited.

Moreover, when aluminum is in contact with an aqueous solution, if the solution is strong acidic or basic, aluminum (III) ion or aluminate ion will be generated separately, as seen in Figure 110. However, if the aqueous solution is neutral, aluminum (III) will be generated as aluminum oxide, a thin and compact layer of coating, which will protect the aluminum surface and prevent further reactions. In addition, if the aqueous solution is oxidative, above line (a), because of a soluble strong oxidizer, aluminum prefers to react with the oxidizer rather than water, which will prevent the generation of hydrogen gas.

Therefore, in order to make aqueous solutions compatible with aluminum phase change heat transfer devices, an approach can be given that the potential and pH number of the solution should locate in the region of passivation but bounded by line (a) and line (b) in Figure 110. There is no hydrogen gas or oxygen gas, both of which are NCGs, generated, and the corrosion of aluminum is greatly reduced because of the protection of aluminum oxide.

However, the lines move with temperature. For aluminum phase change heat transfer devices, the region in Figure 110 that guarantees passivation and NCG prevention, while both being stored and operating, will be smaller. Stubblebine [39] studied how the passivation region, for aluminum phase change heat transfer devices, changes with temperature.

Approved for public release; distribution is unlimited.

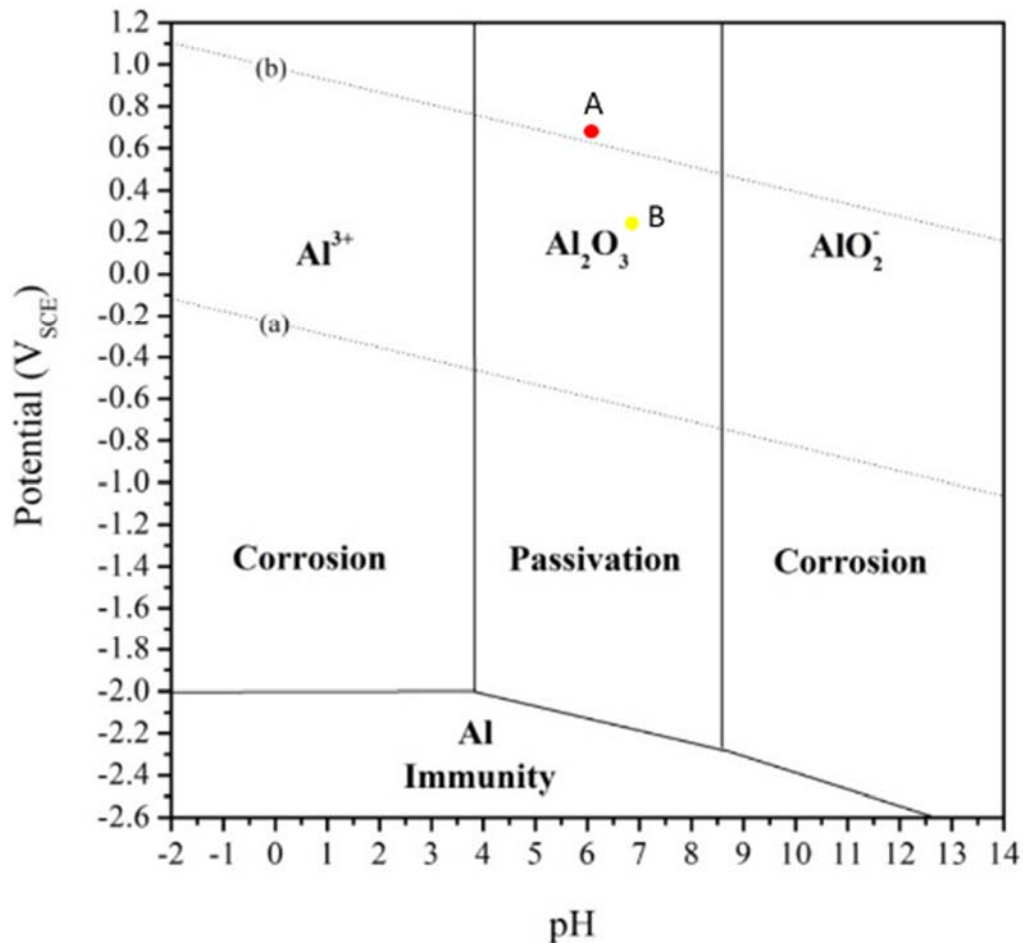
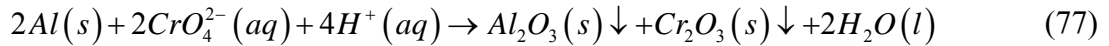
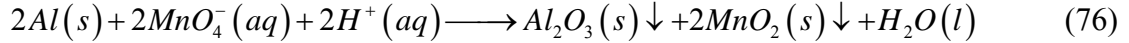


Figure 110: E-pH diagram for pure Al at 25°C in aqueous solution

IAS fluid is such an aqueous solution with the potential and pH number in the passivation region during the lifetime of the heat transfer devices. The electrode potential and pH number of the fresh IAS fluid are 0.910V (SCE) and 0.622, see point A in Figure 110, and the ones of the yellow fluid, used IAS, collected from used aluminum heat transfer devices, are 0.233-0.245V (SCE) and 0.665-7.03, see point B in Figure 110. If IAS is used as the working fluid in aluminum devices, because of the strong oxidizers in IAS fluid, aluminum prefers to react with the oxidizers first instead of hydrogen ions. The two reactions, (76) and (77), form a thin and compact layer of aluminum oxide that protects the surface and prevents further reactions.

Approved for public release; distribution is unlimited.



For aluminum, both permanganate and chromate are oxidizers. Permanganate is stronger and reacts faster, so it is useful in the initial passivation of the aluminum surface. However, the slower reacting but larger amount of chromate is available for the oxidation to heal the aluminum oxide layer and maintain the passivation over the lifetime of the device.

5.2. Passivation in Phase Change Heat Transfer Devices

IAS can passivate aluminum surfaces with no NCG generated while it is directly in contact with the surface. However, in an operating phase change heat transfer device, the vapor of IAS is pure water vapor, and all the chemicals are pushed to the evaporator because advection is dominant, see Section 4.3. As a result, the aluminum surfaces in the condensing and adiabatic regions are exposed to pure water.

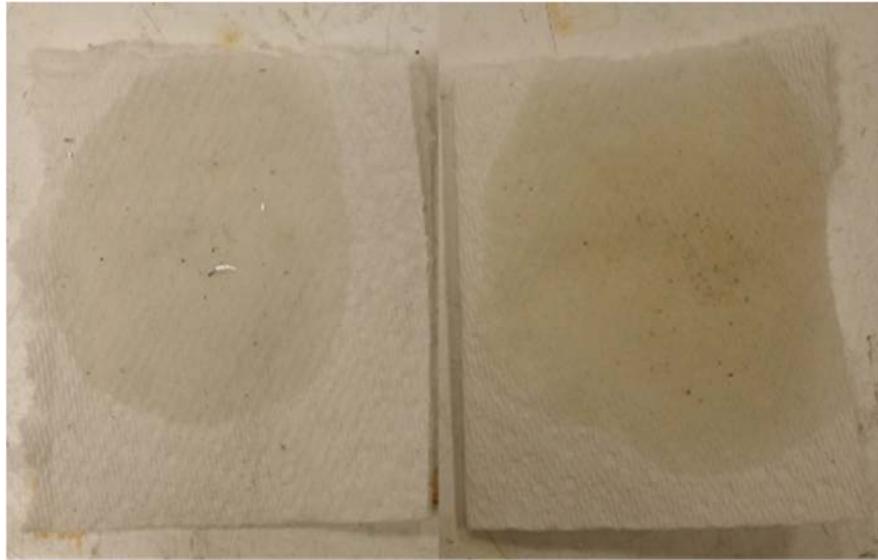
Figure 111 shows a cut open aluminum/IAS thermo-syphon. (a) is the condensing region, and (b) is the evaporating region. It can be seen that the surface of the condensing region is a clean aluminum surface, but the surface of the evaporating region is coated by a layer of yellow coating.



Figure 111: Cut open aluminum/IAS thermo-syphon: (a) condensing region; (b) evaporating region

Figure 112 shows the color of the DI-water after being used to rinse the surfaces of the condensing region and the evaporating region. It can be seen that the color of the DI-water used to rinse the evaporating region becomes yellow, but the one used to rinse the condensing region has no color. All above demonstrate that all the chemicals are in the evaporating region, and there is no chemical in the condensing region.

Approved for public release; distribution is unlimited.



(a)

(b)

Figure 112: DI-water after used to rinse (a) condensing region; (b) evaporating region

Aluminum oxide can protect the aluminum surface and prevent further reaction, but it is not generated as a single whole piece. For an aluminum surface pre-coated by aluminum oxide, ions can still be transported through the gap of two pieces of aluminum oxide and react with the aluminum surface, but the overall reaction rate is tremendously reduced. As a result, such an aluminum surface can be used directly in contact with water and has little corrosion. However, if the pre-treated aluminum surface is used in a phase change heat transfer device with water as the working fluid, a small amount of hydrogen gas will still be generated. Because of the low pressure in phase change heat transfer devices, the volume of the small amount of hydrogen gas is not negligible. This is why a pre-treated aluminum phase change heat transfer device is still not compatible with water.

How does IAS passivate the aluminum surface and prevent the generation of hydrogen gas in the condensing and adiabatic regions?

Approved for public release; distribution is unlimited.

5.2.1. Electrochemical cycle in aluminum passivation

The existence of an electrochemical cycle in an operating aluminum phase change heat transfer device can be used to explain how IAS passivates the aluminum surface and prevents the generation of hydrogen gas in the condensing and adiabatic regions, see Figure 113.

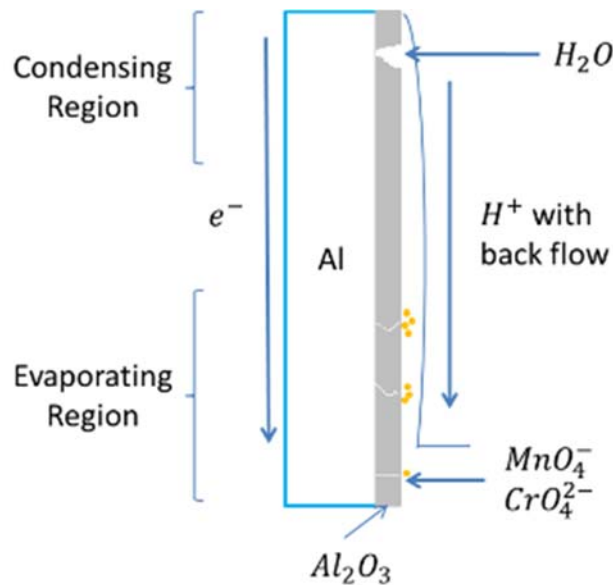


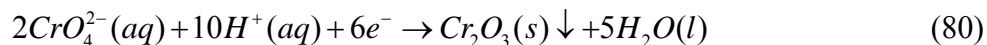
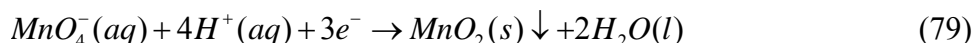
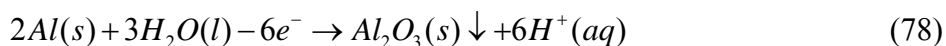
Figure 113: Electrochemical cycle in aluminum passivation

In the evaporating region, a thin and compact layer of aluminum oxide is generated to protect the surface. Aluminum oxide is an electronic insulator, but it is not generated as a single whole piece. Electrons and ions can be transported through the gap of two pieces of aluminum oxide, and it is also where all the redox reactions take place.

As a result, once a bare aluminum surface is exposed in the condensing or adiabatic region, one aluminum atom loses three electrons and then combines with three hydroxide ions to generate aluminum oxide, see reaction (78), which passivates the bare aluminum surface. The electrons are transported by the aluminum body of the device, go through the gap of the aluminum oxide, and then react with the oxidizers in the reservoir. On the liquid side, the residual hydrogen ions are

Approved for public release; distribution is unlimited.

transported back to the evaporating region by the liquid back flow to contribute to the reactions between the oxidizers and the electrons, as shown in reactions (79) and (80). As a result, in order to accomplish passivation of the whole device, a continuous liquid back flow is required to cover the whole internal surface.



The electrochemical cycle enables an aluminum surface to be passivated by IAS while not being in contact with it.

5.2.2. Aluminum thermo-syphon test

An aluminum thermo-syphon test was performed to demonstrate the existence of the electrochemical cycle. Figure 114 is a schematic of the aluminum thermo-syphon test. It is composed of a cartridge heater block, an ice water condensing reservoir, and an aluminum tube with one end welded with an aluminum joint end cap and the other end closed by a Swagelok bellows-sealed valve.

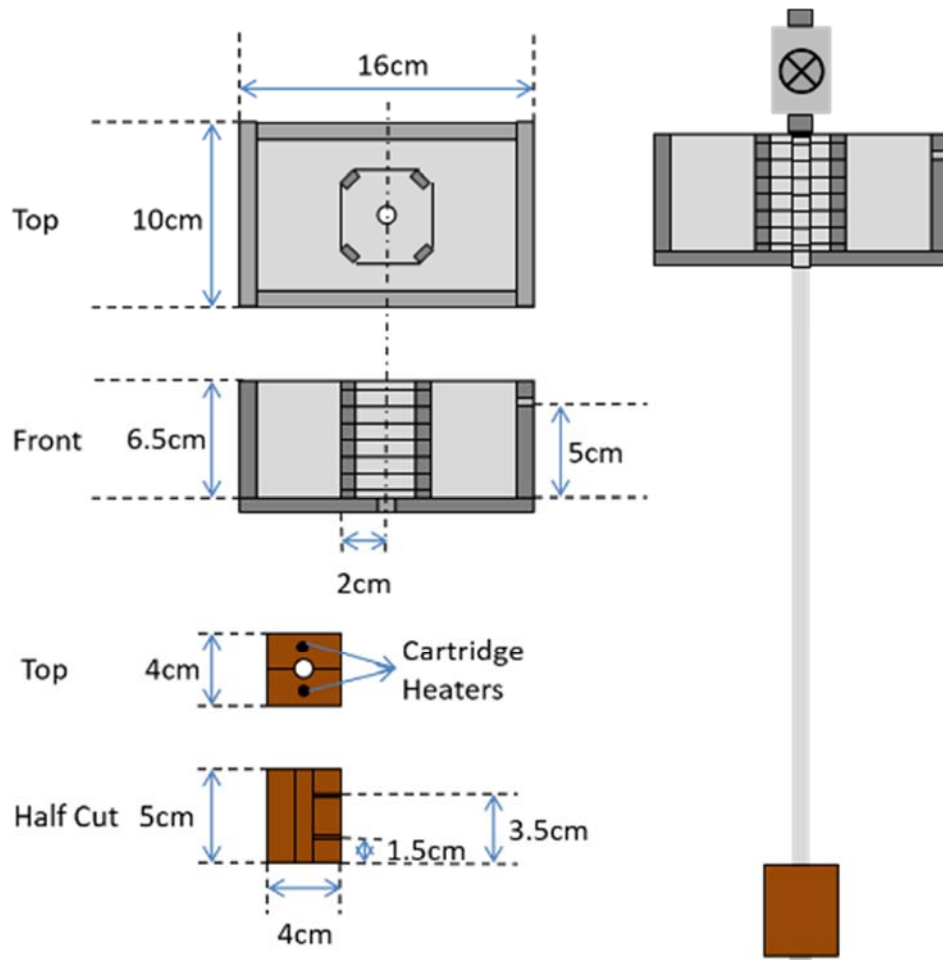


Figure 114: Schematic of the aluminum thermo-syphon test

Figure 115 shows the thermocouple locations in the aluminum thermo-syphon experiment. There are a total of ten type T thermocouples used to monitor the temperatures: two in the evaporating region, two in the condensing region, and six in the adiabatic region.

Approved for public release; distribution is unlimited.

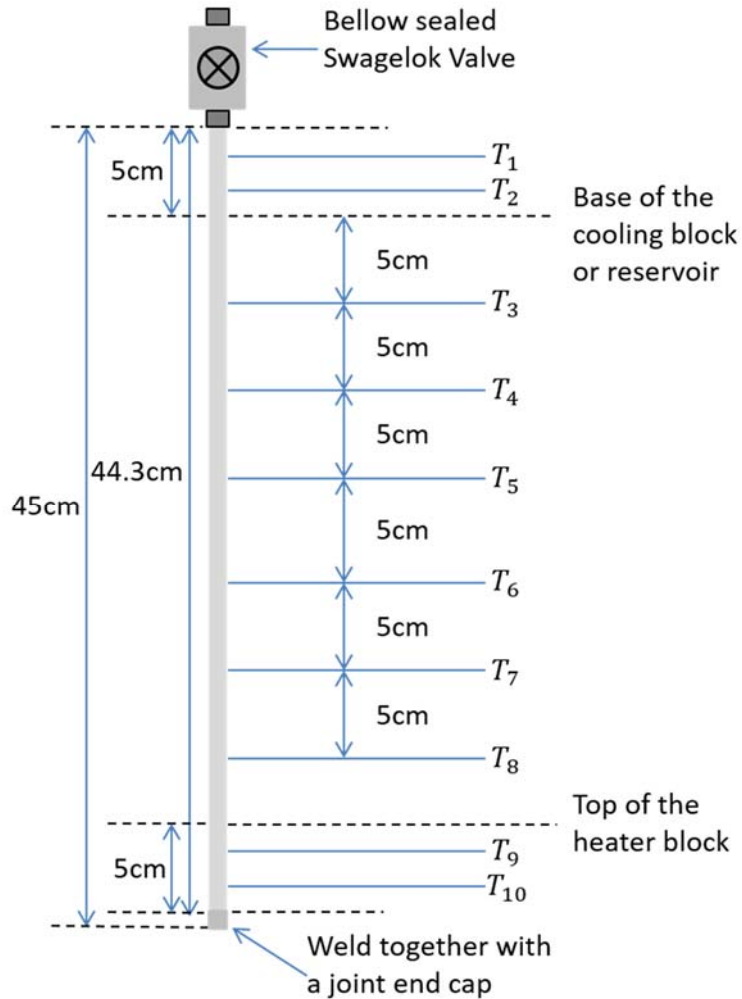


Figure 115: Thermocouple locations in the aluminum thermo-syphon experiment

Figure 116 shows the performance of water and UCLA IAS #1 in aluminum thermo-syphons. For each run, the test was initiated with an input power of 20W. Steady state was reached in 15 mins. The input power was then increased by 10W every ten minutes. After 85 mins, the input power of the water filled tube was maintained at 90W. However, the input power of the IAS tube continued being increased every ten minutes until a value of 160W was reached.

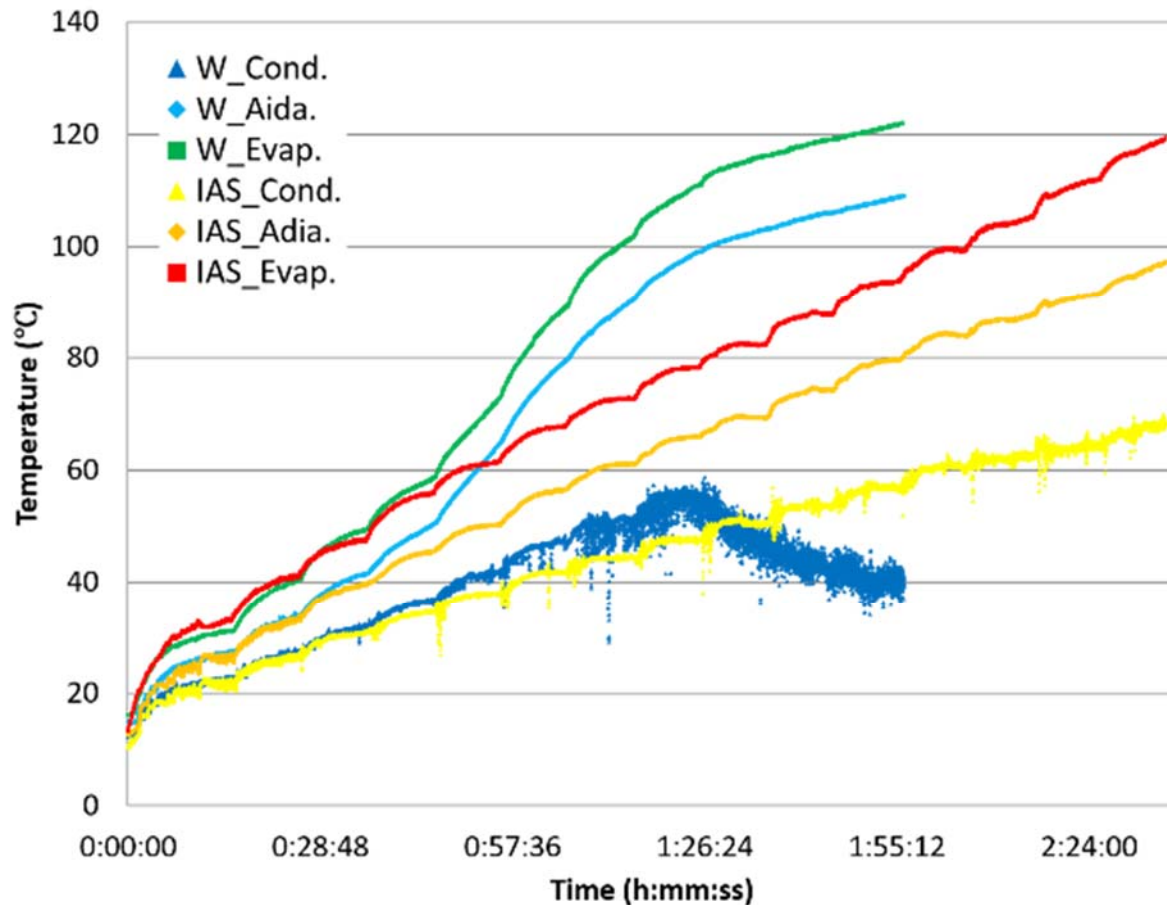


Figure 116: Performance comparison between water and IAS in aluminum thermo-syphons, temperatures at condensing, adiabatic, and evaporating regions

The result indicates that NCG was obviously generated in the water thermo-syphon when the evaporating temperature was greater than 60°C, and finally failed the test. Even after the input power stopped increasing, the temperature difference between the evaporating and the condensing regions still kept becoming larger. However, for IAS fluid, no NCG was generated. The test was stopped before the evaporating temperature reached 120°C because of a safety consideration of the welded cap. No dry out or other thermal limitation was noted. The test clearly demonstrates that IAS is compatible with aluminum heat transfer devices and that no NCG is generated. Moreover, the adiabatic temperature was as high as 90°C, which is much higher than 60°C. It means that hot

Approved for public release; distribution is unlimited.

water at 90°C was directly in contact with the aluminum surface in the adiabatic region, but there was no NCG generated. Therefore, the existence of the electrochemical cycle has been demonstrated.

A copper thermo-syphon, charged with water, was tested under the same conditions as the aluminum/IAS one. Figure 117 shows the comparison of the heat transfer performance between them. The temperature difference (ΔT) of the evaporating temperature and the condensing temperature was measured and compared.

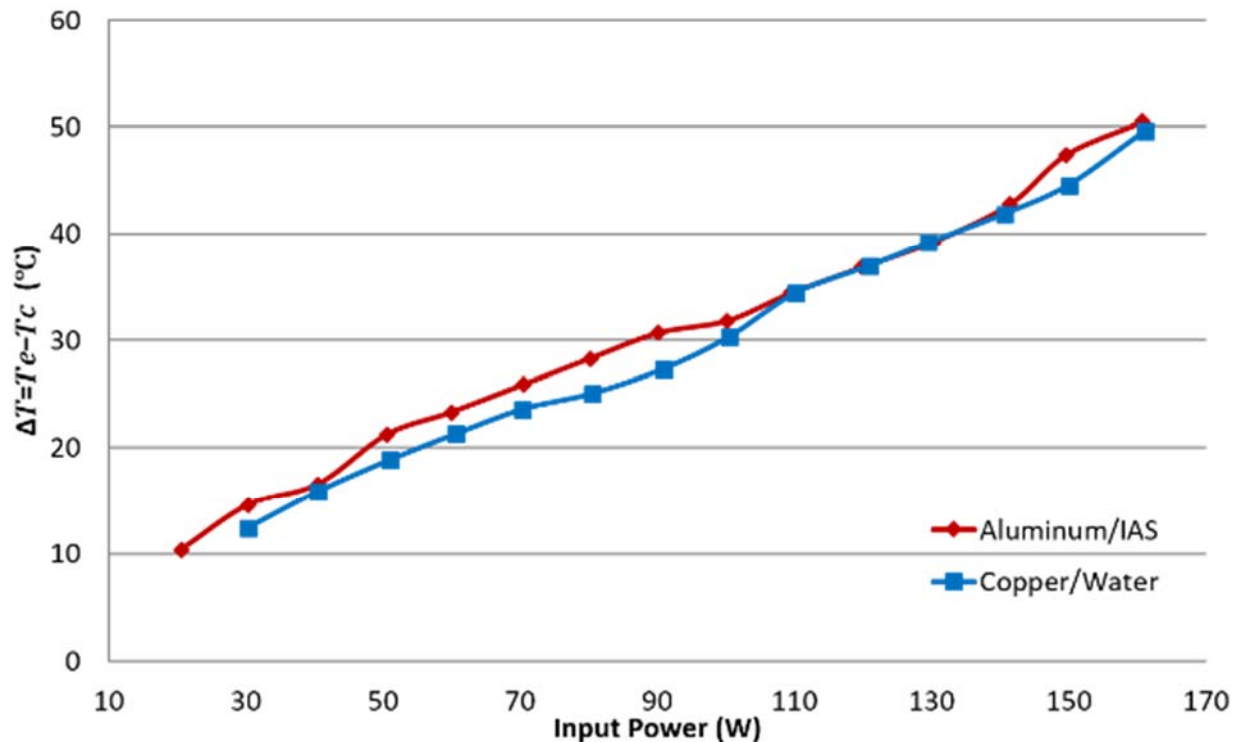


Figure 117: Performance comparison between copper/water and aluminum/IAS thermo-syphons, temperature difference of the evaporating temperature and the condensing temperature

It shows that the heat transfer performance of an aluminum/IAS thermo-syphon is close to the performance of a copper/water thermo-syphon. Therefore, aluminum/IAS thermo-syphons have the potential to replace copper/water thermo-syphons in the market.

Approved for public release; distribution is unlimited.

5.2.3. Silver effect

The IAS used in the aluminum thermo-syphon test was UCLA IAS #1, which had silver ions in it. In addition, silver was assumed to play an important role by acting as a bridge connecting the aluminum tube and the liquid over the aluminum oxide layer, see Figure 118, because silver metal was detected on an aluminum surface pre-treated by the original IAS 0. However, based on recent tests, this assumption is no longer considered to be correct.

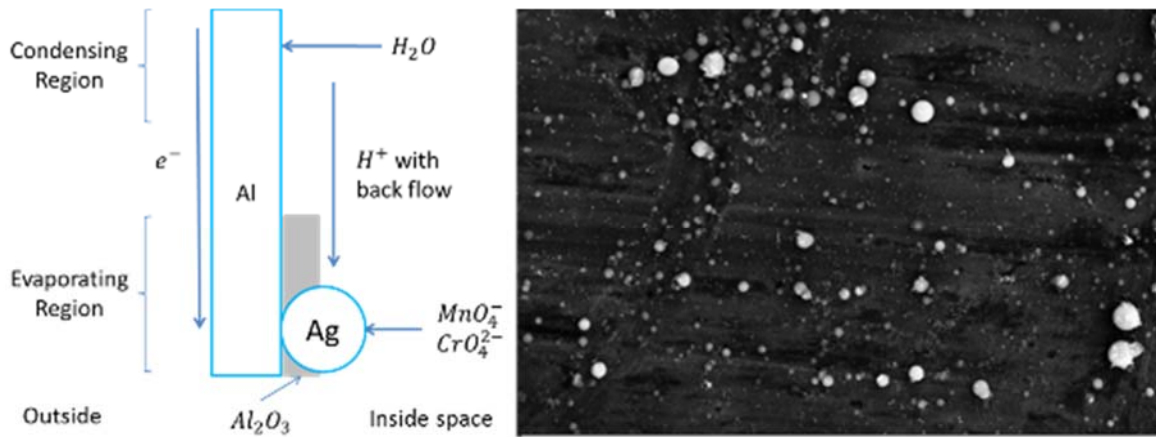


Figure 118: Effect of silver in electrochemistry circle and SEM result of aluminum surface cooked by IAS fluid with Mag=504X

A non-silver IAS was made with the concentrations of the other chemicals the same as UCLA IAS #1, called **UCLA IAS #2.1**. It was used in an aluminum thermo-syphon with the same geometries and then tested under the same conditions as before. The thermo-syphon, charged with 1.5ml IAS, was heated by a heater block at the bottom and cooled by an ice bath at the top. The test results, see Figure 119, show that there is no failure detected. As a result, the silver ion was determined to be unnecessary for the aluminum passivation, and it can be removed from the solution.

Approved for public release; distribution is unlimited.

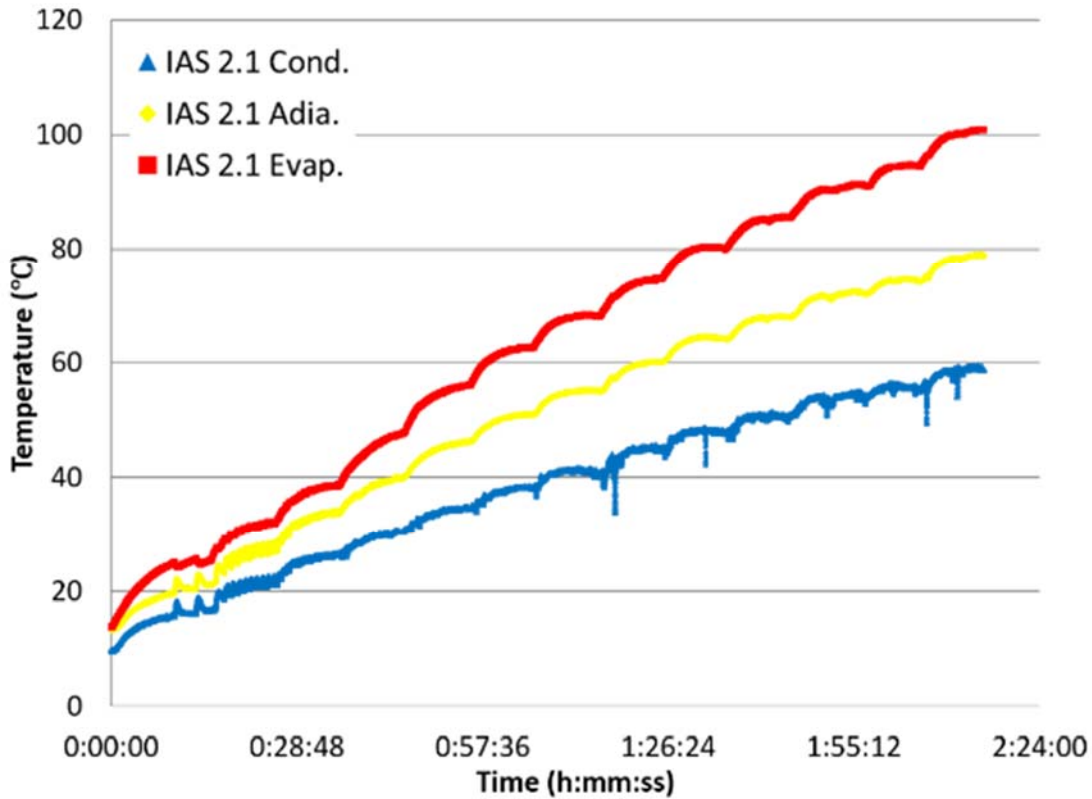


Figure 119: Test result of IAS 2.1 in aluminum thermo-syphon: temperatures of evaporating, adiabatic, and condensing regions

5.3. Importance of a Continuous Liquid Back Flow

For a thermo-syphon, if the condensation rate in the condenser is insufficient, the condensed liquid exists as droplets instead of a continuous liquid film, so a discontinuous liquid back flow appears, see Figure 120 [40]. In this case, residual hydrogen ions will be accumulated in the disconnected part, and an electronic force will be generated to prevent electrons from transporting away. If the concentration of the residual hydrogen ions surpasses a limit, electrons will choose to react with the hydrogen ions and generate hydrogen gas, an NCG which eventually fails the heat transfer device. With the input power increasing, the disconnected region will shrink and eventually disappear.

Approved for public release; distribution is unlimited.

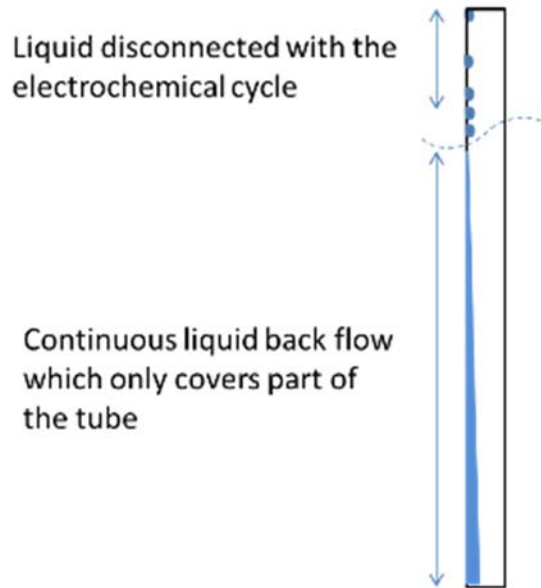


Figure 120: Discontinuous liquid back flow in a thermo-syphon

As a result, how a thermo-syphon is cooled is important to the existence of a discontinuous liquid back flow. Figure 121 shows three thermo-syphons with the same geometries but heated by different input powers or cooled by different methods. Only the condensing and adiabatic regions are shown. Tube (1) is cooled by a cooling block, and the rest part of the tube is adiabatic. Tube (2) and (3) are cooled by natural convection, and there is no adiabatic region. Tube (1) and (2) are heated with an input power Q , but tube (3) is heated with an input power $2Q$.

Approved for public release; distribution is unlimited.

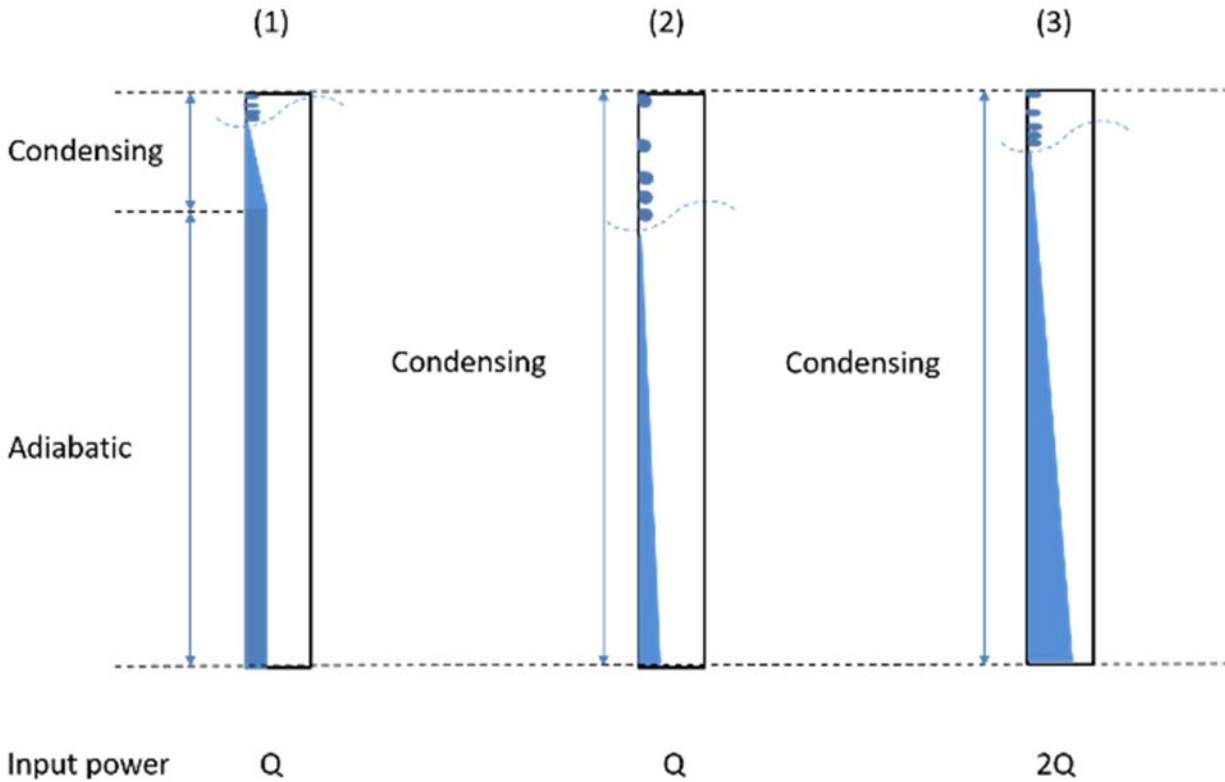


Figure 121: Comparison of thermo-syphons cooled by different methods

It can be seen that for a given Q , tube (2) has the largest discontinuous liquid flow region, in which liquid is disconnected with the electrochemical cycle and hydrogen gas will be generated. In addition, with Q increasing, all the disconnected regions shrink, and tube (1) will be the first one obtaining a continuous liquid back flow throughout the whole tube.

5.3.1. Aluminum thermo-syphon test with a natural convention cooling

An aluminum thermo-syphon experiment with a natural convention cooling is set up to demonstrate the continuous liquid back flow requirement. Figure 122 is a schematic of the experiment setup. An aluminum 6061 tube, with 0.375 inch OD and 0.311 inch ID, is selected as the body of the thermo-syphon. One end is welded with a joint end cap, and the other end is closed by a Swagelok bellows-sealed valve. A copper heater block with two cartridge heaters is used as

Approved for public release; distribution is unlimited.

the heat source, and the thermo-syphon is cooled by the natural air convection. Four tests were done with tube lengths of 1 foot, 2 feet, 3 feet, and 6 feet. All the thermo-syphons are charged with 1.4ml IAS fluid, which covers about 60% of the evaporating region.

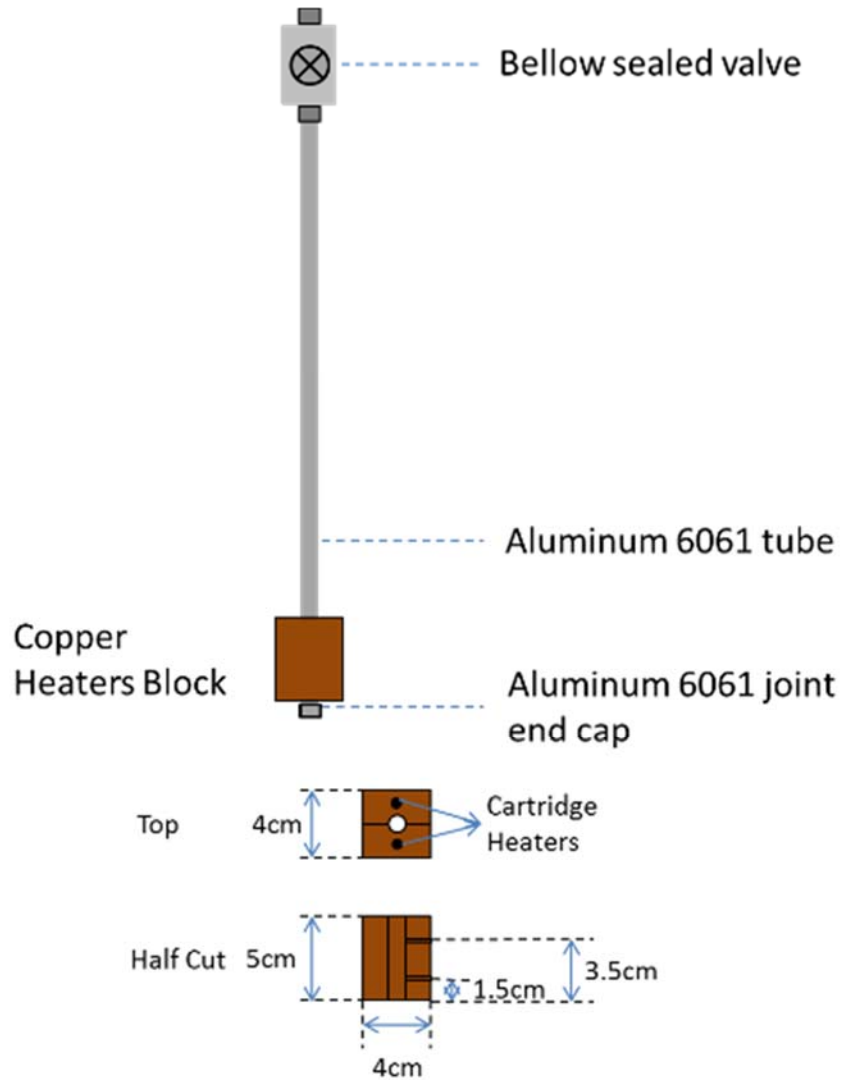


Figure 122: Aluminum thermo-syphon experiment setup

Figure 123 shows the thermocouple locations of the aluminum thermo-syphon experiment. Two thermocouples are located in the evaporating region. Six thermocouples are located in the first nine inches from the bellows-sealed valve, and additional thermocouples are added every nine

Approved for public release; distribution is unlimited.

inches. All the thermocouples are numbered from the top to the bottom. Because failure or not is the only concern in this test, the heat transfer performance will not be quantitatively discussed.

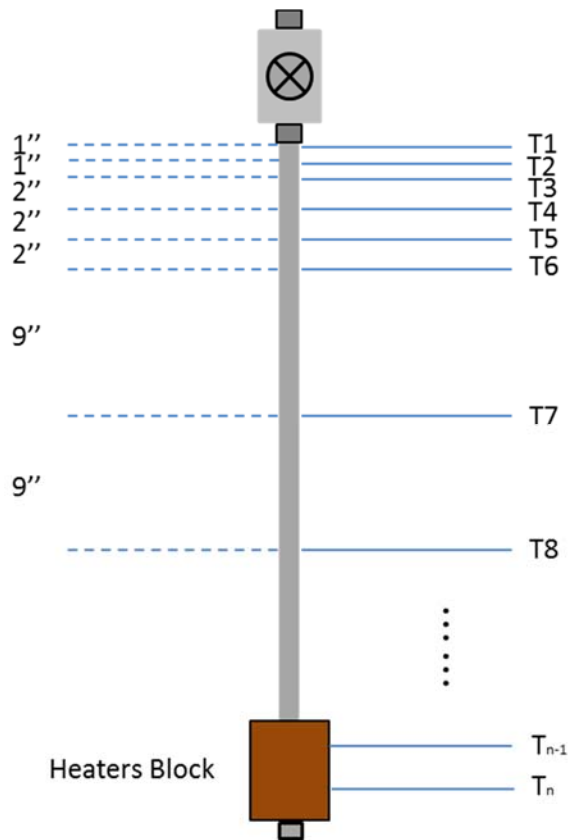


Figure 123: Thermocouple locations

Based on the continuous liquid back flow theory, for a fixed input power, with tube length increasing, discontinuous liquid back flow appears after a critical length. Moreover, with the tube length further increasing, the length of the discontinuous liquid back flow region increases. Therefore, if a 1-foot thermo-syphon can hold the aluminum passivation, with the tube length increasing, there must be a critical length that thermo-syphons with a smaller length than it will

Approved for public release; distribution is unlimited.

hold the passivation, but the ones with a larger length than it will fail. In addition, the longer tube length is than the critical one, the faster NCG is generated.

5.3.2. Results and Discussion

A 6-foot thermo-syphon was first tested. 50 watts were added for the first 20 minutes, and then increased to 100 watts. Figure 124 shows the test results of the 6-foot thermo-syphon.

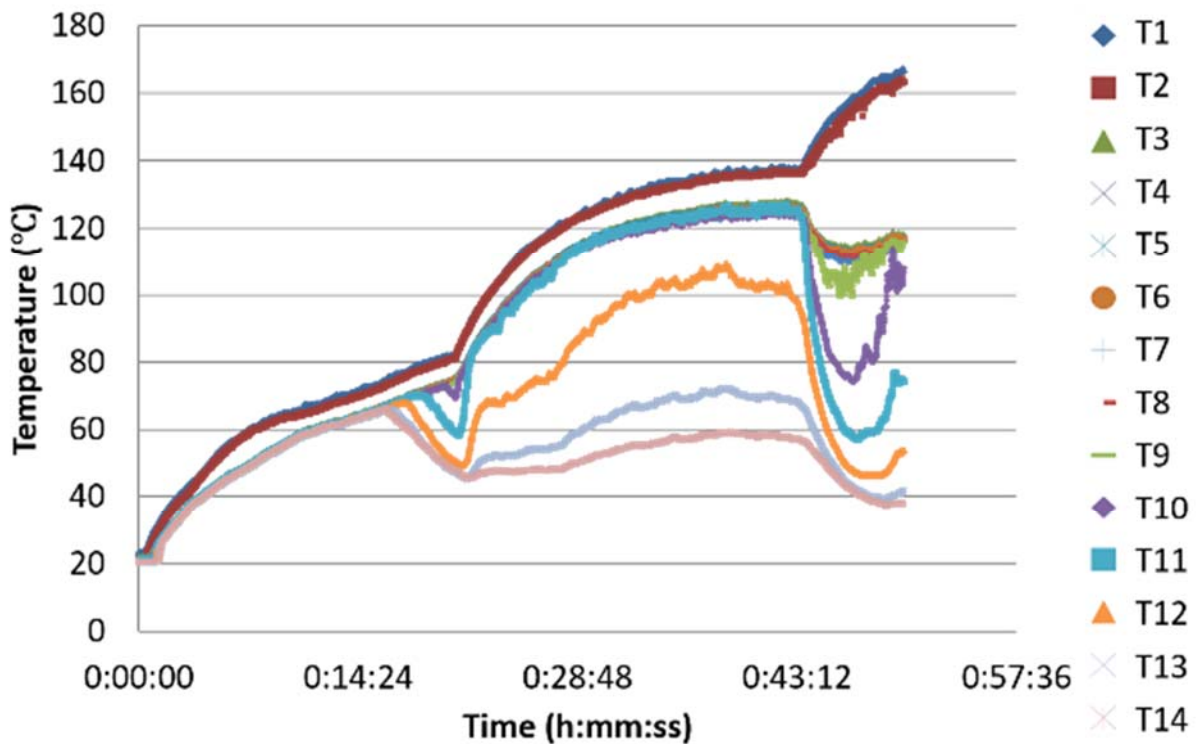


Figure 124: Test results of 6-foot thermo-syphon

After 16 minutes, T1 started to decrease. It was a sign of the NCG appearance. After 20 minutes, a total of five thermocouples were covered by NCG, and then the input power was increased to 100 watts, and T4 and T5 went back to normal, which is another sign of NCG generation, because a higher vapor pressure, caused by the higher temperature, compressed the NCG. With the tube length decreasing, the area of the condensing region decreases, so the surface

Approved for public release; distribution is unlimited.

temperature increases. In order to avoid the internal pressure being too high, the input power was limited at 50 watts in the later tests. For the set charge amount and input power (50 watts), 6 feet was found to be larger than the critical length.

3-foot and 2-foot long thermo-syphons were tested afterwards, and the input power was 50 watts. As shown in Figure 8, the 3-foot thermo-syphon is definitely a failing case, so it is still larger than the critical length. In Figure 9, T1 is the only one that is different with the other temperatures in the condensing region, but it is still close. As a result, 2 feet is still larger than the critical length, but the critical length is very close to 2 feet.

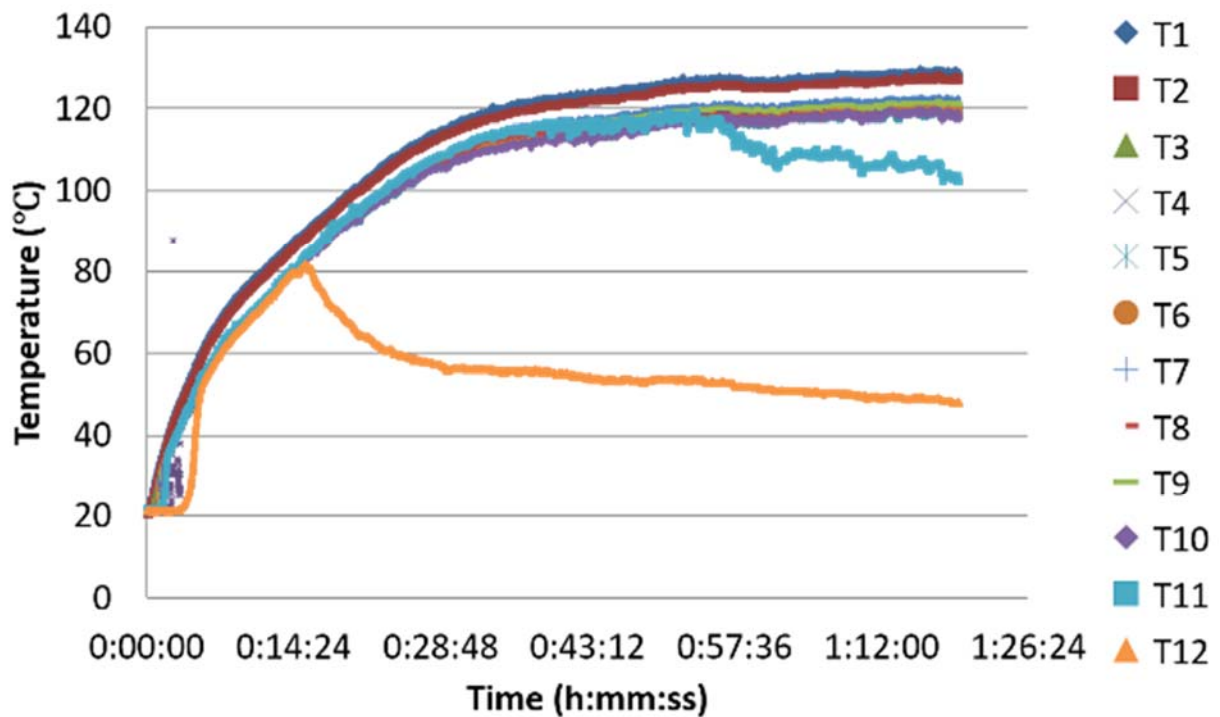


Figure 125: Test results of 3-foot thermo-syphon

Approved for public release; distribution is unlimited.

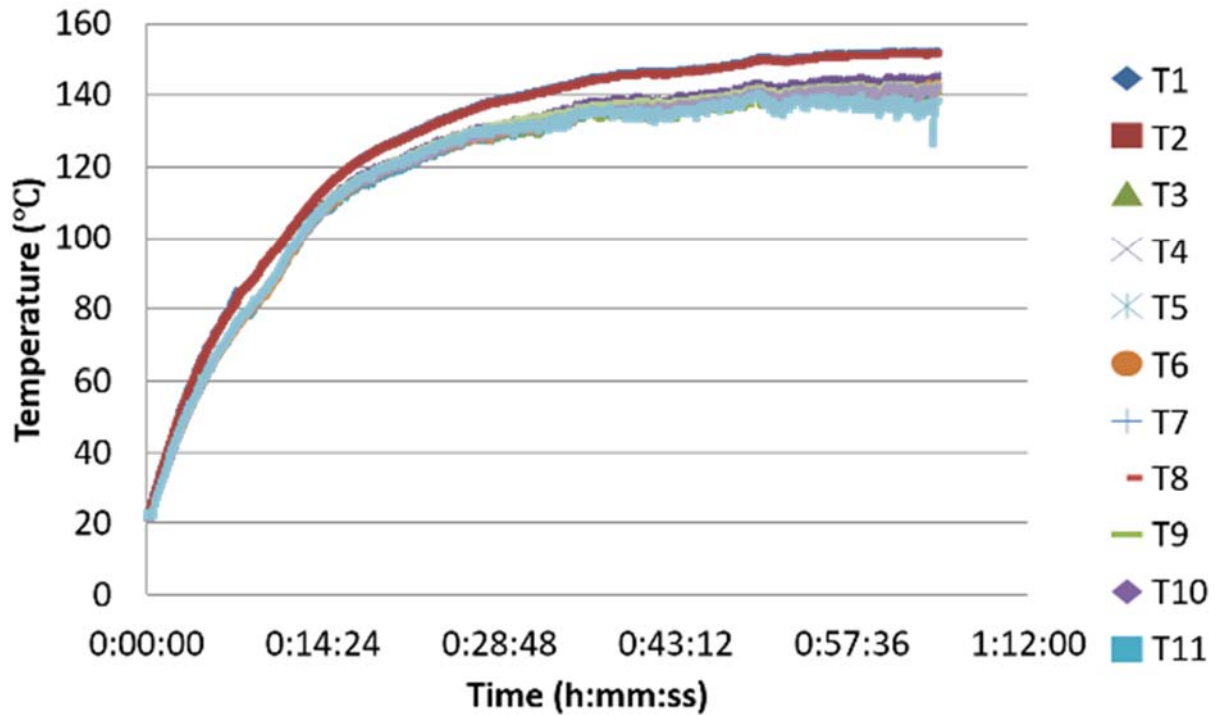


Figure 126: Test results of 2-foot thermo-syphon

Figure 127 shows the test result of a 1-foot aluminum thermo-syphon. The temperature difference of the seven thermocouples on the condensing region are within 1 degree, which within the accuracy of the thermocouple. Therefore, it is assumed that there is little to no NCG generated, and 1 foot is likely smaller than the critical length.

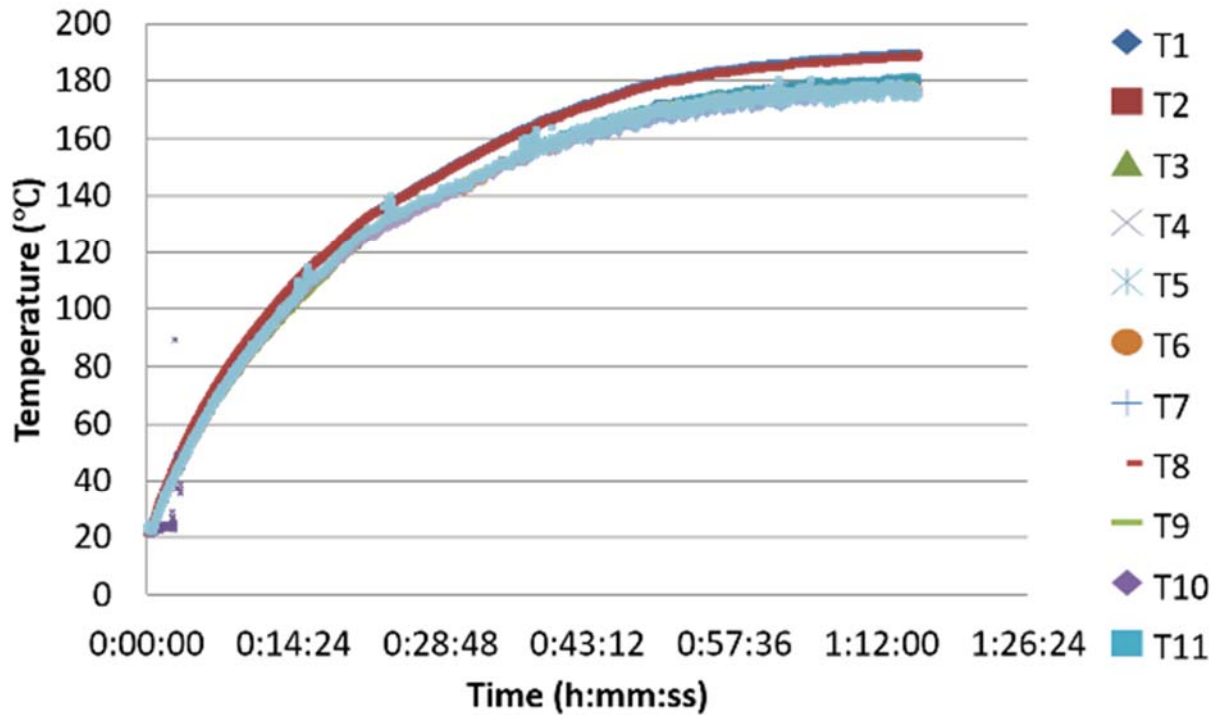


Figure 127: Test results of 1-foot thermo-syphon

The charge amount was fixed at 1.4ml for all the tests. With the tube length, and therefore the internal surface area, increasing, it definitely requires more oxidizers to finish the passivation process. Even though, in general aluminum passivation requires a very small amount of oxidizers because the required aluminum oxide layer is very thin, whether or not the oxidizers in 1.4ml IAS is enough to passivate a 6-foot aluminum thermo-syphon is still unknown. The failure might be a result of a discontinuous liquid back flow, the lack of oxidizers, or both. In order to eliminate the effect of the lack of oxidizers, another 6-foot aluminum thermo-syphon was charged with 2.6ml of a three times concentrated IAS fluid. It means that there are 5.6 times more oxidizers as the previous charge. It has been demonstrated that the previous charge is more than enough to accomplish the passivation process of a 1-foot aluminum thermo-syphon. Therefore, the new charge should have enough oxidizers to passivate a 6 feet aluminum thermo-syphon. At least, the

Approved for public release; distribution is unlimited.

generation rate of NCG should be sharply reduced if lack of oxidizers is the reason of the failure instead of the appearance of the discontinuous liquid back flow.

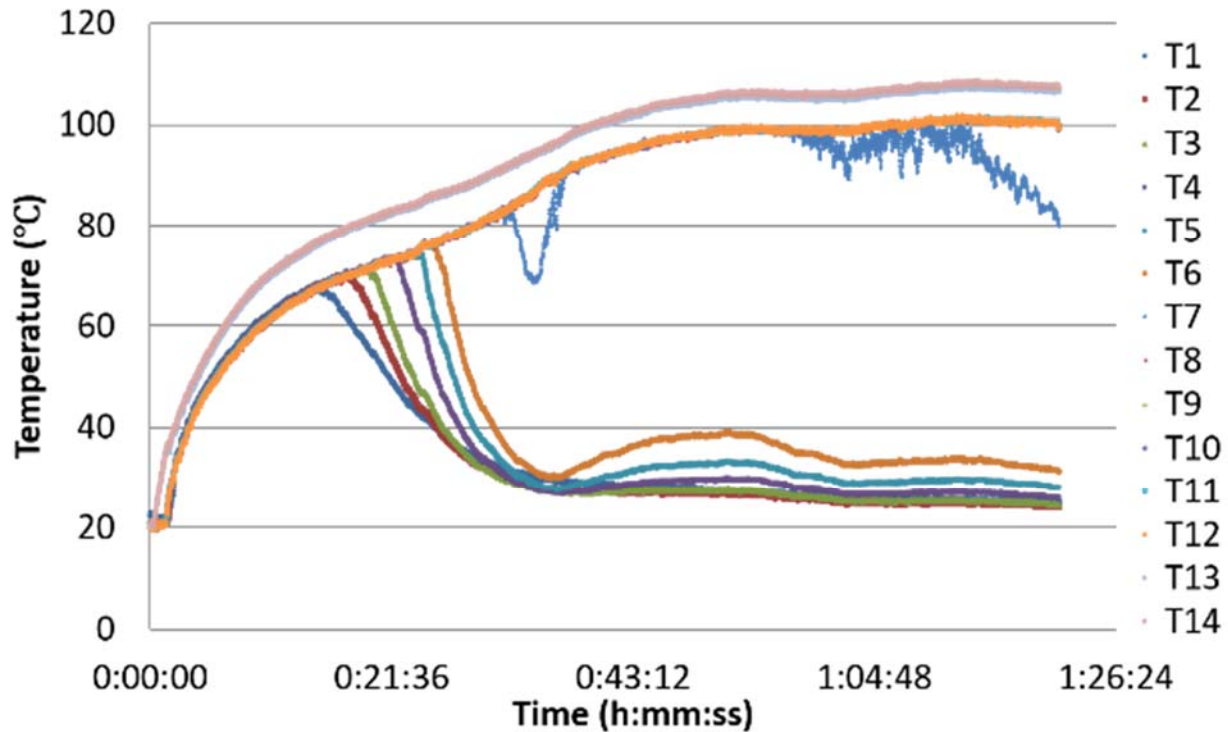


Figure 128: Test results of 6-foot thermo-syphon with 2.6ml three times concentrated IAS

As seen in Figure 128, 16 minutes after heating up, T1 started to decrease. It was a sign of the NCG appearance, and the time is about the same as the previous test. With time lasting, more and more NCG was generated, and T2-T6 fell down one by one. It shows that, a lack of oxidizers is not the reason for the failure of the 6-foot aluminum thermo-syphon, or at least it is not the dominant reason. Therefore, the discontinuous liquid back flow is a limit to be considered while using IAS fluid in aluminum made phase change heat transfer devices.

A continuous liquid back flow covering the whole internal surface is likely required while using IAS as the working fluid in aluminum phase change heat transfer devices. It is a function of

Approved for public release; distribution is unlimited.

the tube geometries, the input power, and the charge amount. For the specific case investigated, the critical length was found to be between 1 and 2 feet. Adding grooves, screens, or sintered wicks to provide capillary paths could benefit the formation of a continuous liquid back flow.

5.4. Conclusion

It is demonstrated that IAS is compatible with aluminum phase change heat transfer devices. The oxidizers in IAS can passivate aluminum surface, generating a thin and compact layer of aluminum oxide to protect the surface and prevent further reactions. In addition, an electrochemical cycle, formed by the device body and the liquid back flow, enables IAS to passivate the aluminum surface in the condensing and adiabatic regions without directly being in contact with it.

In addition, beside enough oxidizers are required to maintain the electrode potential and pH number of IAS in the passivation region of the Pourbaix diagram of aluminum during the lifetime, a continuous liquid back flow throughout the whole heat transfer device is required for the aluminum passivation. Adding wicks to provide capillary paths could benefit the formation of a continuous liquid back flow.

5.5. Discussion of Using IAS in Steel Devices

Using IAS in steel or stainless steel phase change heat transfer devices is similar to a combination case of using IAS in copper and aluminum devices.

Iron reacts with water and generates hydrogen gas too, and the electrochemical cycle is relevant for steel or stainless steel devices. However, iron (III) oxide, Fe_2O_3 , is not as compact as

Approved for public release; distribution is unlimited.

aluminum oxide, so it cannot prevent further reactions as well as aluminum oxide. Corrosion will continue slowly but faster than it does in aluminum heat transfer devices.

In addition, iron is less chemically reactive than aluminum, so it reacts with water slower and generates hydrogen gas slower. For example, a water/aluminum thermo-syphon fails in several minutes, but a water/stainless-steel thermo-syphon only loses 10% of the heat transfer performance per year. As a result, steel and stainless steel heat transfer devices are not sensitive to the discontinuous liquid back flow, which means that it will not be affected by an unstable liquid back flow a lot. All above make the life time of steel and stainless steel heat transfer devices easier to be increased by IAS. For instances, the lifetime of a water/aluminum thermo-syphon being increased by one thousand times is still not acceptable, while the lifetime of a water/steel or stainless steel thermo-syphon being increased by even ten times will be enough.

Further, steel or stainless steel surface is more hydrophilic than an aluminum surface, so steel or stainless steel wicks can help forming a continuous liquid back flow better.

Finally, iron (III) oxide is a better base for chromate salts to sit on than aluminum oxide, so the thermal resistance of steel or stainless steel heat transfer devices can be decreased by IAS, and the dry out can be delayed by IAS too.

Approved for public release; distribution is unlimited.

6. CONCLUSIONS

The objectives of this report are to understand what IAS is, how it contributes to the enhancement of the heat transfer performance, and how it passivates aluminum and is compatible with aluminum phase change heat transfer devices. These objectives have been met and are briefly summarized with some suggestions for future work.

6.1. Main Contributions

The Qu tube is well known for its superior heat transfer performance. However, how it was described and advertised was implausible, and others failed to reproduce the advertised performance even when following the procedure given by the developer. In addition, products using the Qu technology were tested and sometimes found to have a much better heat transfer performance compared to the similar size heat pipes whereas some of them had the same or worse heat transfer performance. This uncertainty was the result of the developer's lack of understanding of why and how the technology actually worked, and it made people not have the courage to use it. Since 1999, a lot of money and time have been spent investigating how the Qu tube works, and there is still not a clear conclusion. All of above make the Qu tube and the Qu technology remain a mystery.

The work done in this report uncovered the mystery of the Qu tube and the Qu technology. A new method of improving heat transfer performance of phase change heat transfer devices using chemical processes is introduced. A complete physical and chemical analysis was performed to understand what IAS is, what chemical reactions take place when IAS is used in copper and aluminum devices, and how these reactions contribute to the improvement of the heat transfer. In

Approved for public release; distribution is unlimited.

addition, using IAS in different copper phase change heat transfer devices is discussed. How IAS enhances performance, reduces thermal resistance, and higher critical heat flux or delays dry out are demonstrated, and the limitations associated with its use for performance enhancement purposes are introduced. Lastly, it is usually the case that aqueous solutions cannot be used as the working fluid in an aluminum phase change heat transfer device because water will be reduced by aluminum and generate hydrogen gas, a NCG, which will fail the device. However, IAS, an aqueous solution, is compatible with aluminum made phase change heat transfer devices because of chemical electrochemical processes that passivate the aluminum surface and prevent the generation of the hydrogen gas. A passivation theory is introduced in this report, and the primary requirement for using IAS in aluminum devices is discussed.

6.2. What is IAS

The original IAS was a dilute aqueous solution with some black solid suspensions. It had a dark red color and a pH number of 6.22. In the solution, the following chemical constituents were detected: sodium (I) ion, potassium (I) ion, silver (I) ion, magnesium (II) ion, calcium (II) ion, strontium (II) ion, permanganate ion, and chromium (VI) ions, and the black solid suspension was tested to be manganese (IV) oxide.

Magnesium (II) ions and silver (I) ions were in a very small amount and have been demonstrated to not contribute to performance enhancement or to aluminum passivation. As a result, they were eliminated from the list of constituents in IAS. In addition, the black solid suspension was demonstrated to be a byproduct during the storage. As a result of these observations, the UCLA made IAS is a clear aqueous solution with the following chemical

Approved for public release; distribution is unlimited.

constituents: sodium (I) ion, potassium (I) ion, calcium (II) ion, strontium (II) ion, permanganate ion, and chromium (VI) ions. It has a dark red color and a pH number of 6.22.

The bulk physical properties of IAS are very close to those of pure water. As a result, IAS does not improve the heat transfer performance by changes in any of its physical properties. However, while being used in copper or aluminum phase change heat transfer devices, the chemicals in IAS react with metal surfaces and generate solid compounds that coat them during the operation. The chemical reactions and the solid coatings are the reasons for performance enhancement and aluminum passivation.

6.3. IAS and copper

When IAS is used as the working fluid in copper phase change heat transfer devices, the copper (I) oxide and manganese (IV) oxide, generated by the redox reactions between the oxidizers in IAS and the copper surface, coat the entire submerged surface in the evaporator, and the oxides coating is permanent and cannot be washed off by liquid flow during its operation. Because convection dominates the diffusion of chemicals in the solution, all the soluble chemicals will be pushed to the meniscus region in an operating phase change heat transfer device. Hydrophilic chromate salts will be generated because solubility limits are exceeded and will coat the meniscus region. The combination of the oxides and the chromate solution improves the surface wettability in the meniscus region. This enhances heat transfer performance and increases the heat flux at which dry out of a copper phase change heat transfer device occurs.

However, there are limitations to the use of IAS in different copper applications. In thermosyphons, use of IAS achieves stable operation at a higher heat flux than that of water but

Approved for public release; distribution is unlimited.

significantly increases the heat flux at dry out. Because the liquid back flow merges with the meniscus region, IAS will not decrease the thermal resistance of vertical thermo-syphons. For the thermo-syphons tested in this report, the critical heat flux at dry out of water filled tubes was sharply decreased when the tubes were inclined. It makes water and IAS filled tubes work in different ranges of heat fluxes when stable operation is reached.

The grooved heat pipe is an ideal application for IAS. Compared to water, IAS has a smaller thermal resistance and a much greater dry out heat flux. Each groove can be seen as a smaller size inclined thermo-syphon. Because of the capillarity, both water and IAS can work in the same region of heat flux when stable operation is reached. The combination of the oxides and the chromate solution improves the surface wettability in the meniscus region, which makes the liquid film thinner than that of the water tube. As a result, IAS has a smaller thermal resistance than water in grooved heat pipes.

When tested in a traditional sintered heat pipe, however, it was found that IAS did not improve the heat transfer performance and sometimes decreased it because the evaporation takes place on the wick surface leading to deposits. The traditional heat pipe has a monoporous wick. Other wick designs like the biporous wick, done by Reilly [22], results in improvement. The improvement depends on the thickness of the wick and the particles diameters. A smaller wick thickness and a larger particle diameter are better to show the performance enhancement effect of IAS in sintered phase change heat transfer devices.

Approved for public release; distribution is unlimited.

6.4. IAS and aluminum

It has been demonstrated that IAS is compatible with aluminum made phase change heat transfer devices, see Chapter 5. When IAS is used as the working fluid in aluminum made phase change heat transfer devices, the oxidizers in IAS can passivate the aluminum surface by generating a thin and compact layer of aluminum oxide which protects the aluminum surface and prevents further reactions. In addition, an electrochemical circuit, formed by the body of the device and the liquid back flow, has been demonstrate to exist and thus enable the oxidizers in the evaporator to passivate the aluminum surface throughout the whole device without directly being in contact with it. Last, a continuous liquid back flow throughout the whole device has been demonstrated to be the key factor in maintaining the compatibility between IAS and aluminum made phase change heat transfer devices. An unstable or discontinuous liquid back flow will cause the generation and accumulation of hydrogen gas and eventually lead to the failure of the device. Adding a wick to help maintaining a continuous liquid flow during both storage and operation is important.

Approved for public release; distribution is unlimited.

7. RECOMMENDATIONS

Based on the work done in this report, a full understanding of what IAS is and how it works in copper and aluminum made phase change heat transfer devices is achieved. Future work can be done to optimize the performance of IAS and quantitatively relate device geometries and chemical molarities to the performance enhancement of heat transfer and the aluminum passivation.

7.1. Chemical optimization

First, there are chemicals in IAS having similar effects, such as calcium/strontium and potassium/sodium. Further researches are required to find if they are all required. If yes, what are the different roles they are playing? If no, which one or ones of them can be eliminated?

Next, the combination effect of oxides coating and chromate salts is the reason of the performance enhancement of heat transfer. However, over amount chemicals will cause an extra thermal resistance or lead to clogging of the wick. Therefore, an optimal amount of chemicals requires further researches to find. The optimal amount of permanganate should be a function of the surface area of the evaporating region or the entire internal surface of the device depending on the type of the heat transfer application. The optimal amount of chromate should be a function of the area of the meniscus region during operation and the type of the heat transfer application.

Third, the oxidizers in IAS is the key factor of the generation of aluminum oxide and the aluminum passivation. Permanganate is a stronger oxidizer than chromate, so it reacts with aluminum fast. It is used to form the initial aluminum oxide layer to protect the surface. However, permanganate is unstable, and an over amount of permanganate will lead to the generation of another NCG, oxygen gas. It is because of that the over amount of permanganate will self-

Approved for public release; distribution is unlimited.

disassociate and release oxygen gas. Chromate, a slower reactor to aluminum, cannot passivate a large area of aluminum surface fast enough to prevent the generation of the hydrogen gas, so it only contributes to the healing of the aluminum oxide during the lifetime of operation. Therefore, further work is required to find the optimal amount of permanganate and the minimum amount of chromate for aluminum phase change heat transfer devices. Both of them should be functions of the area of the total internal surface.

Last, chromium (VI) is carcinogenic, and it is accumulative in human's body. As a result, it is strictly restricted in some regions, such as Europe. Further researches are required to find another chemical constituent that can be used to replace the chromium (VI) in IAS. It should have a large solubility in water at a pH number range of 6 to 8. In addition, it should be an oxidizer having a similar oxidization ability with chromate at a pH number range of 6 to 8. When it reacts with metal surfaces, there should be no NCG generated as the product. Selenium (VI) might be a possible option.

7.2. Design of heat transfer applications

IAS cannot improve the heat transfer performance of monoporous sintered heat pipes with thick wicks. Further researches are required to find the critical wick thickness that if the wick thickness is smaller than it, IAS helps. Changing the structure of the wick might also help, such as a biporous wick.

A continuous liquid flow is required to maintain the aluminum passivation during both storage and operation. For aluminum thermo-syphons, further work is required to find the critical condensing heat flux, larger than which, a discontinuous liquid back flow can be avoided. In

Approved for public release; distribution is unlimited.

addition, adding a wick can help maintaining a continuous liquid flow. Further researches are required to find which type of wicks should be used and what material the wick should be made of.

Compared to an aluminum phase change heat transfer device, the lifetime of a steel or stainless-steel phase change heat transfer device will be increased more significantly by IAS. Both of the performance enhancement and passivation effects of IAS should be considered while being used in steel or stainless-steel phase change heat transfer devices. Further researches are required to investigate how IAS works in steel or stainless-steel phase change heat transfer devices.

Approved for public release; distribution is unlimited.

REFERENCES

- [1] Innovative Research and Products Inc., 2014, “*Electronic Thermal Management – Technology, Materials, Devices, New Developments, Industry Structure and Global Markets*,” Available at <https://irapinnoresearch.wordpress.com/category/electronic-thermal-management/>
- [2] Anon, 1882, “*Memoirs of Angier March Perkins*,” Proc. Inst. Civ. Eng., Vol. 67, Pt. 1, pp. 417-419.
- [3] Gaugler, R. S., 1944, “*Heat Transfer Device*,” U.S. Patent 2350348.
- [4] Grover, G. M., 1963, “*Evaporation-Condensation Heat Transfer Device*,” U.S. Patent 3229759.
- [5] Grover, G. M., Cotter, T. P., and Erickson, G. F., 1964, “*Structures of Very High Thermal Conductance*,” J. App. Phys., Vol. 35, p. 1990.
- [6] Korn, F., 2008, “*Heat Pipes and Its Applications*,” MVK160 Heat and Mass Transport, Lund, Sweden.
- [7] Peterson, G.P., 1994, “*An Introduction to Heat Pipes Modeling, Testing, and Applications*,” Wiley, ISBM: 0-471-30512-X.
- [8] Marcus, B. D., 1972, “*Theory and Design of Variable Conductance Heat Pipes*,” Report No. NASA CR, 2018, National Aeronautics and Space Administration, Washington, DC.
- [9] Cotter, T. P., 1967, “*Heat Pipe Startup Dynamics*,” Proc. SAE Thermionic Conversion Specialist Conference, Palo, CA.

Approved for public release; distribution is unlimited.

- [10] Peterson, G. P. and Bage, B., 1991, "*Entrainment Limitations in Thermo-syphons and Heat Pipes*," ASME Journal of Energy Resources Technology, Vol. 113, No. 3, September, pp. 147-154.
- [11] Reay, D. and Kew, P., 2010, "*Heat Pipes Theory, Design, and Applications*," Fifth Edition, ISBN-13: 978-0-7506-6754-8.
- [12] Chi, S. W., 1976, "*Heat Pipe Theory and Practice*," McGraw-Hill, New York.
- [13] Wayner, P. C., Kao, Y. K., and Lacroix, L. V., 1976, "*The Interline Heat-Transfer Coefficient of an Evaporating Wetting Film*," Int. J. Heat Mass Transfer, Vol. 19, pp. 487-492.
- [14] Solovyev, S. L. and Kovalev, S. A., 1984, "*Mechanism of Evaporation of a Liquid from a Porous Surface*," Proc. 5th Int. Heat Pipe Conf., Tsukuba, Japan, Preprints, II: 77-82.
- [15] Ibrahim, K., Abd Rabbo, M.F., Gambaryan-Roisman, T., and Stephan, P., 2010, "*Experimental Investigation of Evaporative Heat Transfer Characteristics at the 3-Phase Contact Line*," Experimental Thermal and Fluid Science, Vol. 34, pp. 1036-1041.
- [16] Miao, J., Wang, J., and Ma, T., 2001, "*Analysis of Evaporation Heat Transfer of Thin Liquid Film in a Capillary of Equilateral Triangular Cross-Section*," J. of Thermal Science, Vol. 10, No. 4.
- [17] Wasekar, V. M. and Manglik, R. M., 2000, "*Pool Boiling Heat Transfer in Aqueous Solution of an Anionic Surfactant*," Journal of Heat Transfer 122, No. 4: 708.
- [18] Wen, D. and Ding, Y., 2005, "*Experimental Investigation into the Pool Boiling Heat Transfer of Aqueous Based γ -Alumina Nanofluids*," Journal of Nanoparticle Research 7, No. 2-3 (June): 265-274.

Approved for public release; distribution is unlimited.

- [19] Das, S., 2003, “*Pool Boiling Characteristics of Nano-Fluids*,” International Journal of Heat and Mass Transfer 46, No. 5 (February): 851-862.
- [20] Kendig, M. and Buchheit, R., 2003, “*Corrosion Inhibition of Aluminum and Aluminum Alloys by Soluble Chromates, Chromate Coatings, and Chromate-Free Coatings*,” Corrosion, Vol. 59, No. 5.
- [21] Rocco, A. M., et al, 2004, “*Evaluation of Chromate Passivation and Chromate Conversion Coating on 55% Al-Zn Coated Steel*,” Surface and Coatings Technology, Vol. 179, pp. 135-144.
- [22] Reilly, S. and Catton, I., 2011, “*Application of Kovalev Type Modeling to Evaporation in Biporous Media*,” ASME 2011 International Mechanical Engineering Congress and Exhibition, IMECE 2011-64683, Denver, CO.
- [23] Reilly, S., Amouzegar, L., Tao, H. T., and Catton, I., 2011, “*Use of Inorganic Aqueous Solutions for Passivation of Heat Transfer Devices*,” 10th International Heat Pipe Symposium (IHPS), Taipei, Taiwan.
- [24] Stubblebine, M., Reilly, S., Yao, Q., and Catton, I., 2013, “*Use of an Inorganic Aqueous Solution to Prevent Non-Condensable Gas Formation in Aluminum Heat Pipes*,” ASME 2013 Summer Heat Transfer Conference, HT2013-17802, Minneapolis, MN.
- [25] Qu, Y., 1997, “*Superconducting Heat Transfer Medium*,” U.S. Patent 6132823.
- [26] Entrekin, S. F., 2008, “*Experimental Investigation of the Qu Tube Heat Pipe*,” M.S. Report, The University of Alabama in Huntsville, www.uah.edu/prc/research/theses-dissertations.

Approved for public release; distribution is unlimited.

- [27] Rao, P. R., 2009, "*Thermal Characterization Tests of the Qu Tube Heat Pipe*," M.S. Report, The University of Alabama in Huntsville, <http://gradworks.umi.com/14/78/1478462.html>.
- [28] Fu, X., Shen, W., and Yao, T., 1990, "*Physical Chemistry*," 4th Edition, Nanjing University, China, ISBN 7-04-002868.
- [29] Zaytsev, I. D. and Aseyev, G. G., 1992, "*Properties of Aqueous Solutions of Electrolytes*," Crc Press, Inc., ISBN 13:978-0-8493-9314-3.
- [30] Central China Normal University, Northeast Normal University, and Shaanxi Normal University, 1999, "*Analytical Chemistry*," China Higher Education Press, ISBN 7-07-000141-1.
- [31] Want, T. and Li, Z., 2004, "*Some Thermodynamic Properties of Calcium Chromate*," Journal of Chemical Engineering, 49, pp. 1300-1302.
- [32] Davis, T. W., 1942, "*Solubility of Strontium Chromate and Detection of Strontium*," Analytical Chemistry, 14(9), pp. 709-711.
- [33] Mills, A. F., 2001, "*Mass Transfer*," 1st ed., Prentiss Hall, ISBN 0-13-032829-4.
- [34] Faghri, A., 1995, "*Heat Pipe Science and Technology*," Global Digital Press, ISBN 1-56032-383-3.
- [35] Li, Y., 1974, "*Diffusion of Ions in Sea Water and in Deep-Sea Sediments*," Geochimica et Cosmochimica Acta, Vol. 88, pp. 703-714.
- [36] Negishi, K. and Sawada, T., 1983, "*Heat transfer performance of an ITPCT*," Int. J. Heat Mass Transfer, Vol. 26, No. 8, pp. 1207-1213.

Approved for public release; distribution is unlimited.

- [37] Supowit, J., Heflinger, T., Stubblebine, M., and Catton, I., 2015, “*Designer Fluid Performance and Inclination Angle Effects in Flat Grooved Heat Pipe*,” ASME-ATI-UIT Conference on Thermal Energy Systems: Production, Storage, Utilization and the Environment, Napoli, Italy.
- [38] Reay, D. and Kew, P., 2006, “*Heat Pipes: Theory, Design, and Applications*,” 5th ed., Elsevier, Oxford, UK.
- [39] Stubblebine, M. J., Yao, Q., Supowit, J., and Catton, I., 2015, “*A New Method for Evaluating Heat Pipe Fluid Compatibility*,” ASME-ATI-UIT Conference on Thermal Energy Systems: Production, Storage, Utilization and the Environment, Napoli, Italy.
- [40] Ghiaasiaan, S. M., 2007, “*Two-Phase Flow: Boiling and Condensation in Conventional and Miniature Systems*,” 1st ed., Cambridge University Press, ISBN: 978-0-521-88276-7.

Approved for public release; distribution is unlimited.

APPENDIX: Coding of 1-D Diffusion Model

```
#include "Header.h"
#include <stdio.h>
#include <conio.h>
#include <math.h>
#include <stdlib.h>
#define pi 3.141592654

void main()
{
    int n, N, count;
    double Tw_e, Tw_c, T, den, visc, tcond, hfg;
    double L, Le, La, Lc, Di, dT, Q;
    double *l, *delta, *V, *C_cr, *C_ca, *C_k, *vol;
    FILE *fp1, *fp2, *fp3;
    int a, b;
    int ztca, ztcaaa, ztcabb, zctk, zctkaa, zctkbb, zca, zcaaa, zcabb, zcr, zcraa, zcrbb, zk,
    zkaa, zkbb;
    double FT[601], Fden[601], Fvisc[601], Ftcond[601], Fhfg[601];
    double FTT[200], Fkspk[200], Fkspca[200], kspk, kspca;
    double Ct_cr, Ct_ca, Ct_k, coat_ca, coat_k, Ct_crt, Ct_cat, Ct_kt;
    double D_cr, D_ca, D_k, vol_t;
    double dca, dcr, dk, dctca, dctk;
    double pp, pp1, pp2;

    N = 100000;
    Tw_e = 103.69;
    Tw_c = 57.81;
    L = 0.45;
    Le = 0.05;
    Lc = 0.05;
    Di = 0.0079;
    Q = 241.28;
    Ct_k = 0.0612835;
    Ct_cr = 0.0776398;
    Ct_ca = 0.0132388;

    if ((fp1 = fopen("input.txt", "r")) == NULL)
    {
        printf("cannot open this file\n");
    }
}
```

Approved for public release; distribution is unlimited.

```

        exit(0);
    }

    T = (Tw_e + Tw_c) / 2;
    for (a = 0; a <= 600; a++)
    {
        fscanf(fp1, "%lf %lf %lf %lf %lf", &FT[a], &Fden[a], &Fvisc[a], &Ftcond[a],
&Fhfg[a]);
    }
    for (a = 0; a < 600; a++)
    {
        if ((T >= FT[a]) && (T <= FT[a + 1]))
        {
            den = Fden[a] + (Fden[a + 1] - Fden[a])*(T - FT[a]) / (FT[a + 1] - FT[a]);
            visc= Fvisc[a] + (Fvisc[a + 1] - Fvisc[a])*(T - FT[a]) / (FT[a + 1] - FT[a]);
            tcond= Ftcond[a] + (Ftcond[a + 1] - Ftcond[a])*(T - FT[a]) / (FT[a + 1] -
FT[a]);

            hfg= Fhfg[a] + (Fhfg[a + 1] - Fhfg[a])*(T - FT[a]) / (FT[a + 1] - FT[a]);
            break;
        }
    }

    La = L - Le - Lc;
    l = (double*)malloc((N + 1)*sizeof(double));
    delta = (double*)malloc((N + 1)*sizeof(double));
    V = (double*)malloc((N + 1)*sizeof(double));
    C_cr = (double*)malloc((N + 1)*sizeof(double));
    C_ca = (double*)malloc((N + 1)*sizeof(double));
    C_k = (double*)malloc((N + 1)*sizeof(double));
    vol= (double*)malloc(N*sizeof(double));

    dT = (Lc + Le) / Lc / Le*pow(pow(3 * Q / 4 / pi / Di, 4) * 4 * visc / (hfg*1000) / den / den
/ 9.8 / pow(tcond, 3), 1.0 / 3);

    for (n = 0; n <= N; n++)
    {
        l[n] = L*n / N;
        if (l[n] <= Lc)
        {
            delta[n]
pow(4*tcond*visc*dT*Le*l[n]/den/den/9.8/(hfg*1000)/(Lc+Le),0.25);
            if (n == 0)
            {
                V[n] = 0;
            }
        }
    }

```

Approved for public release; distribution is unlimited.

```

        }
        else
        {
            V[n] = 4 * (Q*I[n] / Lc) / pi / den / (hfg * 1000) / (Di*Di - pow(Di
- 2 * delta[n], 2));
        }
    }
    else
    {
        if (l[n] < L - Le)
        {
            delta[n] = pow(4 * tcond*visc*dT*Le*Lc / den / den / 9.8 / (hfg *
1000) / (Lc + Le), 0.25);
            V[n] = 4 * Q / pi / den / (hfg * 1000) / (Di*Di - pow(Di - 2 * delta[n],
2));
        }
        else
        {
            delta[n] = pow(4 * tcond*visc*dT*Lc*(L-l[n]) / den / den / 9.8 /
(hfg * 1000) / (Lc + Le), 0.25);
            if (n == N)
            {
                V[n] = 0;
            }
            else
            {
                V[n] = 4 * (Q*(L-l[n]) / Le) / pi / den / (hfg * 1000) / (Di*Di
- pow(Di - 2 * delta[n], 2));
            }
        }
    }
}

vol_t = 0;
for (n = 0; n < N; n++)
{
    vol[n] = 0.25*pi*(Di*Di - (Di - delta[n] - delta[n + 1])*(Di - delta[n] - delta[n +
1]))*L / N;
    vol_t = vol_t + vol[n];
}

if ((fp2 = fopen("ksp.txt", "r")) == NULL)
{
    printf("cannot open this file\n");
}

```

Approved for public release; distribution is unlimited.

```

        exit(0);
    }

    for (a = 0; a <= 199; a++)
    {
        fscanf(fp2, "%lf%lf%lf", &FTT[a], &Fkspk[a], &Fkspca[a]);
    }
    for (a = 0; a < 199; a++)
    {
        if ((Tw_e >= FTT[a]) && (Tw_e <= FTT[a + 1]))
        {
            kspk = Fkspk[a] + (Fkspk[a + 1] - Fkspk[a])*(Tw_e - FTT[a]) / (FTT[a +
1] - FTT[a]);
            kspca = Fkspca[a] + (Fkspca[a + 1] - Fkspca[a])*(Tw_e - FTT[a]) / (FTT[a
+ 1] - FTT[a]);
            break;
        }
    }

    D_cr = (0.2417*T + 5.0959)*pow(10, -10);
    D_ca = (0.1677*T + 3.7258)*pow(10,-10);
    D_k = (0.3877*T + 9.8297)*pow(10, -10);

    zctca = 0;
    zctcaaa = 0;
    zctcabb = 0;
    zctk = 0;
    zctkaa = 0;
    zctkbb = 0;
    coat_ca = 0;
    coat_k = 0;
    count = 0;
    dctca = 0.1;
    dctk = 0.1;

    if ((fp3 = fopen("output.txt", "w")) == NULL)
    {
        printf("cannot open this file\n");
        exit(0);
    }

    while (zctk*zctca == 0)
    {

```

Approved for public release; distribution is unlimited.

```

pp1 = 2 * pow(pow(10, -6.22), 2) / 1.044898e-15;
pp2 = 1 + pow(10, -6.22) / 3.2e-7;
Ct_crt = (sqrt(pp2*pp2+4*pp1*(Ct_cr- coat_ca - coat_k))-pp2) / 2 / pp1;
Ct_cat = Ct_ca - coat_ca;
Ct_kt = Ct_k - 2 * coat_k;

zca = 0;
zcaa = 0;
zcabb = 0;
C_ca[N] = Ct_cat;
dca = 0.1;
while (zca == 0)
{
    for (n = N - 1; n >= 0; n--)
    {
        C_ca[n] = C_ca[n + 1] / (exp((V[n] + V[n + 1])*L / N / 2 / D_ca));
    }
    pp = 0;
    for (n = 0; n < N; n++)
    {
        pp = pp + vol[n] * C_ca[n];
    }
    pp = pp / vol_t;
    if (pp >= Ct_cat)
    {
        zcaa = 1;
    }
    else
    {
        zcaa = -1;
    }
    if ((zcaa*zcabb == -1) && (dca < 0.000001))
    {
        zca = 1;
    }
    else
    {
        if (zcaa*zcabb == -1)
        {
            dca = dca / 10;
        }
        if (zcaa == 1)
        {
            C_ca[N] = C_ca[N] * (1 - dca);
        }
    }
}

```

Approved for public release; distribution is unlimited.

```

        }
        else
        {
            C_ca[N] = C_ca[N] * (1 + dca);
        }
        zcabb = zcaaa;
    }
}

zcr = 0;
zcraa = 0;
zcrbb = 0;
C_cr[N] = Ct_crt;
dcr = 0.1;
while (zcr == 0)
{
    for (n = N - 1; n >= 0; n--)
    {
        C_cr[n] = C_cr[n + 1] / (exp((V[n] + V[n + 1])*L / N / 2 / D_cr));
    }
    pp = 0;
    for (n = 0; n < N; n++)
    {
        pp = pp + vol[n] * C_cr[n];
    }
    pp = pp / vol_t;
    if (pp >= Ct_crt)
    {
        zcraa = 1;
    }
    else
    {
        zcraa = -1;
    }
    if ((zcraa*zcrbb == -1) && (dcr < 0.000001))
    {
        zcr = 1;
    }
    else
    {
        if (zcraa*zcrbb == -1)
        {
            dcr = dcr / 10;
        }
    }
}

```

Approved for public release; distribution is unlimited.

```

        if (zcraa == 1)
        {
            C_cr[N] = C_cr[N] * (1 - dcr);
        }
        else
        {
            C_cr[N] = C_cr[N] * (1 + dcr);
        }
        zcrbb = zcraa;
    }
}

zk = 0;
zkaa = 0;
zkbb = 0;
C_k[N] = Ct_kt;
dk = 0.1;
while (zk == 0)
{
    for (n = N - 1; n >= 0; n--)
    {
        C_k[n] = C_k[n + 1] / (exp((V[n] + V[n + 1])*L / N / 2 / D_k));
    }
    pp = 0;
    for (n = 0; n < N; n++)
    {
        pp = pp + vol[n] * C_k[n];
    }
    pp = pp / vol_t;
    if (pp >= Ct_kt)
    {
        zkaa = 1;
    }
    else
    {
        zkaa = -1;
    }
    if ((zkaa*zkbb == -1) && (dk < 0.000001))
    {
        zk = 1;
    }
    else
    {
        if (zkaa*zkbb == -1)

```

Approved for public release; distribution is unlimited.

```

        {
            dk = dk / 10;
        }
        if (zkaa == 1)
        {
            C_k[N] = C_k[N] * (1 - dk);
        }
        else
        {
            C_k[N] = C_k[N] * (1 + dk);
        }
        zkbb = zkaa;
    }
}

if (count == 0)
{
    for (n = 0; n <= N; n++)
    {
        fprintf(fp3, "%e %e %e %e %e %e\n", l[n], delta[n], V[n], C_ca[n],
C_cr[n], C_k[n]);
    }
    fprintf(fp3, "*****\n");
}

if (C_ca[N] * C_cr[N] > kspca)
{
    ztcaaa = 1;
}
else
{
    ztcaaa = -1;
}
if ((ztcaaa*ztcabb == -1) && (dctca < 0.000001))
{
    ztca = 1;
}
else
{
    if (ztcaaa*ztcabb == -1)
    {
        dctca = dctca / 10;
    }
    else

```

Approved for public release; distribution is unlimited.

```

    {
        zctca = 0;
    }
    if (zctcaaa == 1)
    {
        if (count == 0)
        {
            coat_ca = Ct_ca*0.1;
        }
        else
        {
            while (coat_ca*(1 + dctca) > Ct_ca)
            {
                dctca = dctca / 10;
            }
            coat_ca = coat_ca*(1 + dctca);
        }
    }
    else
    {
        coat_ca = coat_ca*(1 - dctca);
    }
}
zctcabb = zctcaaa;

if (C_k[N] * C_k[N] * C_cr[N] > kspk)
{
    zctkaa = 1;
}
else
{
    zctkaa = -1;
}
if ((zctkaa*zctkbb == -1) && (dctk < 0.000001))
{
    zctk = 1;
}
else
{
    if (zctkaa*zctkbb == -1)
    {
        dctk = dctk / 10;
    }
    else

```

Approved for public release; distribution is unlimited.

```

        {
            if (dctca > 0.0000001)
            {
                zctk = 0;
            }
        }
    if (zctkaa == 1)
    {
        if (count == 0)
        {
            coat_k = Ct_k*0.05;
        }
        else
        {
            while (2*coat_k*(1 + dctl) > Ct_k)
            {
                dctl = dctl / 10;
            }
            coat_k = coat_k*(1 + dctl);
        }
    }
    else
    {
        coat_k = coat_k*(1 - dctl);
    }
}
zctkbb = zctkaa;
printf("%e %e %e %e %e %d---%e %e %e %e %e %d\n",kspk, C_k[N] *C_k[N]*
C_cr[N],Ct_k,coat_k,dctl,zctkaa, kspca, C_ca[N] * C_cr[N], Ct_ca, coat_ca, dctca, zctcaaa);

    count++;
}
fprintf(fp3, "Potassium chromate: %10.8f%\n", 2 * coat_k / Ct_k);
fprintf(fp3, "Calcium chromate: %10.8f%\n", coat_ca / Ct_ca);

fclose(fp1);
fclose(fp2);
fclose(fp3);
}

```

Approved for public release; distribution is unlimited.

UCLA IAS Data Book

Table A1: UCLA IAS #1

UCLA IAS #1	Date	6/21/2012		
	pH	6.22	Vol. 1L	
	Chemical	Theoretical Concentration(gram/L)	Actual Concentration(gram/L)	Error
	Potassium Permanganate	0.44	0.4405	0.11%
	Potassium Dichromate	8.5338	8.5336	0.00%
	Chromium Trioxide	1.9058	1.9108	0.26%
	Silver Chromate	0.0065	0.0074	13.85%
	Strontium Hydroxide	0.1042	0.1058	1.54%
	Calcium Hydroxide	0.9751	0.9757	0.06%
	Magnesium Hydroxide	0.0335	0.0338	0.90%
	Sodium Hydroxide	0.2678	0.2699	0.78%

Table A2: UCLA IAS #2.1

UCLA IAS #2.1	Date	1/31/2015		
	pH	6.18	Vol. 1L	
	Chemical	Theoretical Concentration(gram/L)	Actual Concentration(gram/L)	Error
	Potassium Permanganate	0.44	0.442	0.45%
	Potassium Dichromate	8.5338	8.5385	0.06%
	Chromium Trioxide	1.9058	1.9163	0.55%
	Strontium Hydroxide	0.1042	0.1062	1.92%
	Calcium Hydroxide	0.9751	0.9801	0.51%
	Magnesium Hydroxide	0.0335	0.0367	9.55%
	Sodium Hydroxide	0.5508	0.5545	0.67%

Approved for public release; distribution is unlimited.

Table A3: UCLA IAS #3.2

UCLA IAS #3.2	Date	7/31/2015		
	pH	6.22	Vol. 1L	
	Chemical	Theoretical Concentration(gram/L)	Actual Concentration(gram/L)	Error
	Potassium Permanganate	0.44	0.4494	2.14%
	Potassium Dichromate	8.5338	8.5406	0.08%
	Chromium Trioxide	1.9058	1.9127	0.36%
	Strontium Hydroxide	0.1042	0.108	3.65%
	Calcium Hydroxide	0.9751	0.9799	0.49%
	Sodium Hydroxide	0.5508	0.5659	2.74%

Table A4: UCLA Yellow #1

UCLA Yellow #1	Date	10/10/2015		
	pH	6.22	Vol. 1L	
	Chemical	Theoretical Concentration(gram/L)	Actual Concentration(gram/L)	Error
	Potassium Dichromate	8.5338	8.5421	0.10%
	Chromium Trioxide	1.9058	1.9203	0.76%
	Strontium Hydroxide	0.1042	0.1066	2.30%
	Calcium Hydroxide	0.9751	0.9814	0.65%
	Sodium Hydroxide	0.5508	0.5656	2.69%

Approved for public release; distribution is unlimited.

List of Symbols, Abbreviations, and Acronyms

Acronym

EDS	Energyo-Dispersive X-ray Spectroscopy
HPLC	High Performance Liquid Chromatography
IAS	Inorganic Aqueous Solution
ICP-OES	Inductively Coupled Plasma-Optical Emission Spectrometry
ID	Inside Diameter
NCG	Non-Condensable Gas
NRL	Naval Research Laboratory
OD	Outside Diameter
SEM	Scanning Electron Microscope
SHE	Standard Hydrogen Electrode
SRI	Stanford Research Institute
TAMU	Texas A&M University
UCLA	University of California, Los Angeles
XRD	X-Ray Diffraction

Notation

P	Pressure
L	Length
x	Length variable; Concentration variable; Mole fraction
T	Temperature

Approved for public release; distribution is unlimited.

λ	Latent heat of vaporization
ρ	Density
k	Thermal conductivity
σ	Surface tension
r	Radius
q	Heat flux
N_l	Merit number
h_{fg}, H_{lv}	Latent heat of evaporation
μ	Dynamic viscosity
R	Thermal resistance
ν	Kinematic viscosity
θ	Contact angle
E	Electrode
G	Gibbs free energy
K	Chemical equilibrium constant
R	Ideal gas constant
c	Concentration
ϕ	Electrode potential
e	Electron
V	Velocity
N	Mole flux
D	Diffusion coefficient; Diameter

Approved for public release; distribution is unlimited.

A	Area
Q	Power
Pe	Peclet number
δ	Thickness
\forall	Volume
g	Gravity

8.

Superscripts and subscripts

c	Capillary; condenser
m	Max; Molar
v	Vapor
eff	Effective
l	Liquid
ph	Phase transition
e	Evaporator
+	Normal hydrostatic
	Axial hydrostatic
cr	Critical
sat	Saturated
i	Inner
b	Boiling

Approved for public release; distribution is unlimited.

s	Surface; Solid
g	Gas
w	Wall; Water
aq	Aqueous
θ	Standard condition
f	Formation; Film
max	Maximum
a	Adiabatic
p	Pool

Approved for public release; distribution is unlimited.

DISTRIBUTION LIST

DTIC/OCP 8725 John J. Kingman Rd, Suite 0944 Ft Belvoir, VA 22060-6218	1 cy
AFRL/RVIL Kirtland AFB, NM 87117-5776	2 cys
Official Record Copy AFRL/RVSV/Andrew Williams	1 cy

Approved for public release; distribution is unlimited.

(This page intentionally left blank)

Approved for public release; distribution is unlimited.